Department für Nanotechnologie

Institut für Biophysik

Vorstand: Univ. Prof. Dr. José Luis Toca-Herrera

Betreuer: a.o. Univ. Prof. DI Dr. Dietmar Pum (Boku)

Dr. Ursula Sauer (AIT)

DISSERTATION

"DEVELOPMENT OF A NEW DETECTION SYSTEM FOR THE HIGH THROUGHPUT SCREENING OF ENDOCRINE ACTIVE SUBSTANCES"

Dissertation zur Erlangung des Doktorgrades an der Universität für Bodenkultur Wien

Eingereicht von

M. Sc. Konstanze Gier

Wien, 09.03.2018

Acknowledgement

This work was part of the Marie Curie Innovative Training Network (FP7-PEOPLE-2013-ITN) Sample In - Answer Out Optochemical Sensing Systems (SAMOSS) and was financially supported by the European Commission. The development of the protein microarray and the establishment of the cell culture were made at the AIT (Austrian Institute of Technology), Health & Environment Department, Bioresources at the group of Dr. Claudia Preininger. The whole microfluidic work and the development of the devices were performed at the University of Groningen, The Netherlands, Faculty of Science and Engineering in the Pharmaceutical Analysis group of Prof. Sabeth Verpoorte. Immobilization work was rendered at Scienion AG, Berlin, Germany. I like to thank, my supervisor **Dr. Ursula Sauer** from the AIT for her support over the whole time of the doctoral project and for boosting me in the right moments, my supervisor **Prof. Dietmar Pum** from the University of Natural Resources and Life Sciences, Vienna for providing friendly and fast assistance with all organizational things of the work and for the final evaluation of my thesis, Prof. Elisabeth Verpoorte from the University of Groningen for giving me the opportunity to work in her lab and providing material as well as an office place, **Dr. Claudia Preininger** for her initial idea of a cell– and protein-based double chip system for toxicity measurements and the correction of the first publication, the **SAMOSS Network** for the interesting and hilarious gatherings in Europe and Israel and the possibility to meet people from different countries. I like to gratefully acknowledge the work of **Patty P.M.F.A Mulder** from the University of Groningen. She introduced me in the methods of the microfluidic device fabrication, extended her support in device production processes and took selflessly care of the publication and thesis proofreading. I like to acknowledge **Jean-Paul Mulder** from the University of Groningen for the production of 3D printed elements for the microfluidic system, the solid work images of the hanging drop device, his technical support and amusing meetings at the smoking area. **Jolanda Meindertsma** from the University of Groningen relieved my life due to her kind, fast, organized and conscientious processing of all bureaucratic documents, nice and informative talks and caring about the shipment of lab equipment. Likewise I like to give thanks to **Sara Doppler** from the AIT, for the introduction in the lab and method relevant processes and organizing the purchasing orders in Austria. Marten Hoekstra from the University of Groningen supported me with 3D prints, when J.P. was not around, thanks for that. Thanks a lot to the working group of Sabeth Verpoorte, especially to **Pim de Haan** for inspiring discussions about microfluidics and worldly problems. He took kindly care about my cells, when I was not around. You made my life in the group much easier. Last but not least I like to thank my **parents**, my **brother**, my partner in life **Patty**, my new **Dutch family** and all my **friends,** who supported me with love, friendship, advices, help and joyful days in every stage of my life. I would not have passed that without you.

Abstract

Endocrine disrupting chemicals (EDCs) are substances, which affect the hormone system in organisms through interference with different signalling pathways. They can act as agonists or antagonists on nuclear receptors at concentrations in the picomolar range and are associated with diseases such as cancer, Type 2 diabetes, obesity and developmental disorders. Existing analysis platforms for endocrine activity are generally inadequate, as they either require several methods to detect this activity, or cannot assess the complex interactions of hormone-active chemicals at all.

Therefore we developed a multi-chip microfluidic screening system to better assess the adverse effects of EDCs on organisms. The screening platform includes a microfluidic hanging-drop component to generate multi-cellular MCF (Michigan Cancer Foundation) -7 spheroids. 3D cell culture was used to better mimic *in vivo* tissue conditions and thus improve the *in vivo* predictability of our assay. The cells are cultured in serum-free, phenol red-free medium to ensure that no hormones or hormone-active substances are present, thus circumventing possible interferences by these compounds on experimental results. In order to avoid leaching of potential hormone-active components or additives from the plastics conventionally used in cell culture, we have developed the microfluidic spheroid-generation platform in glass.

The glass hanging drop platform allows through a parallel channel droplet well order a very stable generation of six spheroids in time. A hydrophobic ring out of a UV curable perfluoropolyether (PFPE) was introduced around the lower edge of each well onto the hydrophilic platform, to support droplet formation and avoid spreading of the liquid. A 3D printed incubation chamber with an integrated glass window was designed and constructed to minimize evaporation and to detect the generated spheroids under the microscope.

Once formed, the spheroids can be automatically transferred to integrated perfusion micro chambers for further cultivation. After incubation with known estrogen active substances such as ß-estradiol, bisphenol A, genistein, and nonylphenol, and antiestrogens such as fulvestrant and tamoxifen the system allows a protein-microarray to be coupled to it, to quantify ten biomarkers which are related to various endpoints of EDC action in organisms and are secreted by MCF-7. Exposure of 2D cultured MCF-7 cells with the test substances resulted in distinct protein secretion patterns. Stimulation of the cell line with Interleukin (IL)-1ß increased the secretion of low abundant proteins IL-6, Rantes and IL-8, which made them detectable within the working range of the microarray. In parallel, a resazurin proliferation assay determined the proliferating effect of these substances on the cancer cells.

The immobilization of Bisphenol A (BPA) in sciPOLY3D gel was investigated additionally, for the development of an on-chip BPA binding inhibition assay, to quantify BPA in applied samples in the screening platform.

The fluorescence-based microfluidic multi-chip screening platform for the analysis of estrogenic and anti-estrogenic substances is a new *in vitro* tool for the high throughput screening of endocrine active compounds in environmental and food samples, or their general effects on molecular or cellular level.

Keywords: endocrine disruptor, microfluidics, MCF-7 cells, hormones, proliferation, protein microarray, 3D cell culture, hanging drop system

Kurzfassung

Endokrin disruptive Chemikalien (EDCs) sind Substanzen die durch Störung unterschiedlichster Signalwege Einfluss auf das Hormonsystem von Organismen nehmen. Diese können als Agonisten oder Antagonisten, bereits in picomolaren Konzentrationen, an nuklearen Hormonrezeptoren agieren und werden assoziiert mit Krankheiten wie Krebs, Diabetes Typ 2, Obesitas und Reproduktionsstörungen. Bereits existierende analytische Plattformen zum Nachweis von hormonaktiven Substanzen sind generell inadäquat, da diese meist mehrere unterschiedliche Methoden erfordern oder nur partikulär die komplexen Interaktionen dieser Chemikalien erfassen.

Für eine bessere Beurteilung schädlicher Effekte auf Organismen durch EDCs haben wir ein, auf Mikrofluidik basierendes, Multi-Chip Screening System entwickelt. Das neue Screening System inkludiert eine mikrofluidische Hängetropfen Komponente zur Generierung von multizellulären MCF-7 Sphäroiden. 3D Zellkultur wurde benutzt um besser *in vivo* Konditionen nachahmen zu können und so die *in vivo* Aussagekraft unseres Assays zu verbessern. Die Zellen wurden in serum- und Phenol Rot-freiem Medium kultiviert um sicherzustellen dass keine Hormone oder hormonaktive Substanzen die experimentellen Ergebnisse beeinflussen. Um Auslaugen von potentiell hormonaktiven Komponenten oder Zusätzen aus Plastik welche konventionell in der Zellkultur benutzt wird zu verhindern, entwickelten wir eine Mikrofluidik basierende Sphäroid generierende Plattform aus Glas. Die gläserne Hängetropfen Plattform erlaubt durch eine parallele Anordnung der Kanäle und Tropfenwells eine sehr stabile Generation von sechs Sphäroiden auf einmal. Ein hydrophobischer Ring aus dem UV-härtenden Perfluoropolyether (PFPE) wurde an der unteren Kante jedes Wells in die hydrophile Plattform eingeführt, um die Tröpfchenformierung zu unterstützen und das Verlaufen der Flüssigkeit zu verhindern.

Eine 3D gedruckte Inkubationskammer mit einem integrierten Glasfenster wurde entworfen und produziert um die Evaporation des offenen Systems zu minimieren und eine Detektion von den Sphäroiden unter dem Mikroskop zu gewährleisten.

Einmal geformt, können die Sphäroide für die weitere Kultivierung automatisch in integrierte Mikroperfusionskammern transferiert werden. Nach Inkubation mit bekannten östrogen-aktiven Stoffen wie ß-Estradiol, Bisphenol A, Genistein und Nonylphenol und Antiöstrogenen wie Fulvestrant und Tamoxifen können zehn Biomarker welche von der hormonsensitiven humanen Brustkrebszelllinie sekretiert werden durch einen integrierten Proteinmikroarray quantifiziert werden. Die Exposition von MCF-7-Zell 2D Kultur mit den Testsubstanzen resultierte in deutlichen Sekretionsmustern. Eine Stimulation der Zelllinie mit dem Interleukin

(IL)-1 ß erhöhte die Sekretion von geringfügig exprimierten Proteinen wie IL-6 und IL-8 und machte sie dadurch innerhalb des Arbeitsbereichs des Mikroarrays detektierbar.

Ein auf Resazurin basierender Proliferationsassay determiniert parallel dazu die proliferierenden Effekte dieser Substanzen auf die Krebszellen.

Des Weiteren wurde die Immobilisierung von Bisphenol A in sciPOLY3D Gel getestet, für die Entwicklung eines On-Chip BPA Screeningassays, welcher als Erweiterung für die Screening Plattform dient und BPA in applizierten Proben quantifiziert.

Die Fluoreszenz basierende Mikrofluidik Multi-Chip Screening Plattform für die Analyse von östrogenen und antiöstrogenen Substanzen ist eine neue *in vitro* Methode für das Hochdurchsatz-Screening von endokrin aktiven Fremdstoffen in Umwelt- und Lebensmittelproben als auch für die Erforschung von generellen Effekten auf molekularem und zellulärem Level.

Schüsselwörter: endokrine Disruptoren, Mikrofluidik, MCF-7 Zellen, Hormone, Proliferation, Proteinmikroarray, 3D Zellkultur, Hänge Tropfen System

Content

Acknowledgement **1**
Abstract **2**
Kurzfassung **4**
Content **6**
1. General introduction **10**
1.1. Endocrine disruptors 10
1.1.1. The endocrine system 10
1.1.2. Exposure sources, and routes of EDCs, and their stability 11
1.1.3. Endogenous and exogenous estrogenic chemicals 14
1.1.4. Mechanism of action 18
1.1.5. Issues of EDCs action 20
1.1.6. State of the art of *in vitro* methods for investigating estrogenic action 21
1.2. Biomarkers 26
1.2.1. Biomarkers in toxicology 26
1.3. Microarrays 27
1.3.1. Assay principles of protein microarrays 28
1.3.2. Protein microarrays – from fabrication to analysis 30
1.3.3. Surface functionalization and strategies for probe immobilization 31
1.3.4. Immobilization of small molecules 32
1.3.5. Probe printing techniques 33
1.3.6. Recognition elements – The capture molecules in immunoassays 35
1.3.6.1. Antibodies 35
1.3.6.2. Recognition via small organic molecules 37
1.3.6.3. Bisphenol A as recognition element 37
1.3.7. Sample preparation, calibration and matrix effects 39
1.3.8. Parameters for evaluation of assay performance 40
1.3.9. Sensing methods 42
1.3.9.1. Label-based techniques: Fluorescence 43
1.3.10. Readout and image analysis of protein microarrays 45

1.4. Cell assays- *in vitro* test systems predicting human toxicology 47
1.4.1. Proliferation assays 48
1.4.2. Cell culture media 50
1.5. Microfluidics 51
1.5.1. Materials for microfluidic cell culture applications 52
1.5.2. Microfluidic device fabrication methods 54
1.5.3. 3D cell culture 57
1.5.4. Microfluidic spheroid culture 59
1.5.5. The hanging drop method 63
2. Aim of the thesis 65
3. Materials and Methods 66
3.1. Cell culture 66
3.1.1. Cell line and conventional cell culture conditions 66
3.1.2. Serum-free cell culture conditions 66
3.1.3. Collagen coating for serum-free cell culture 67
3.1.4. Growth curve 67
3.1.5. Culture conditions for biomarker secretion and proliferations assays 68
3.1.6. Cell treatment for biomarker and proliferation assays 68
3.2. Proliferation assay 68
3.2.1. Standard curve and single cell density proliferation assay 69
3.2.2. Proliferative response to estradiol treatment 69
3.2.3. Statistical analysis proliferation assay 70
3.3. Protein microarray: materials and reagents 70
3.3.1. Protein microarray fabrication, processing and scanning 71
3.4. Bisphenol A immobilization: hapten-protein conjugates 72
3.4.1. Hydrogel coating 73
3.4.2. Bisphenol A immobilization: SciPOLY3D 73
3.4.3. Validation of BPA immobilization 74
3.4.4. BPA binding inhibition assay 74
3.5. Statistical data analysis protein microarray and BPA immobilization 74

3.6. Microfluidics: Hanging drop device production and characterization 75
3.6.1. Fabrication of PDMS hanging drop devices 75
3.6.2. Fabrication of glass hanging drop devices 76
3.6.3. Contact angle and roll off angle measurements 77
3.6.4. Introducing of hydrophobic rings 77
3.6.5. Droplet formation and perfusion 78
3.6.6. Droplet evaporation 78
3.6.7. Rhodamine adsorption 78
3.6.8. Treatment of microfluidic devices for the usage in cell culture 79
3.6.9. Statistical data analysis 79
3.7. 3D cell culture conditions for flow and static experiments 79
3.7.1. 3D cell viability assessment 79
3.7.2. 3D-cell culture treatment with 17ß-estradiol 80
3.7.3. Image analysis of MCF-7 cell spheroids 80
3.7.4. Statistical data analysis for 3D cell culture 80
3.8. Perifusion chamber: production 80
3.8.1. Flow experiments 81
3.8.2. Integration of glass membrane 81
3.8.3. Glass coating 81
4. Results and discussion 82
4.1. Establishment of a serum-free and phenol-red-free MCF-7 cell culture 82
4.2. Establishment of a resazurin based cell proliferation assay 86
4.2.1. Proliferative response under hormone lacking conditions 89
4.3. Biomarker panel 92
4.3.1. Biomarker chip development and matrix effects 93
4.3.2. Quantification of MCF-7 cell protein secretion in cell medium 96
4.3.3. Influences of solvents on protein secretion 99
4.3.4. Specific secretion patterns 101
4.4. Immobilization of Bisphenol A 105
4.5. Channel assembly of the glass hanging drop system 110

4.5.1. Challenges of the glass hanging drop device fabrication....112
4.5.2. Droplet formation and stability....116
4.5.3. Introduction of a hydrophobic PFPE ring....119
4.5.4. Network stability, simultaneously filling and transfer of droplets....121
4.5.5. Incubation chamber against evaporation....123
4.5.6. Biocompatibility of the glass device materials....125
4.5.7. Effect of material and flow on experimental outcome and spheroid growth....128
4.6. Spheroid perifusion chamber....132
5. Summary and conclusions....139
6. List of references....143
7. Table index....171
8. Figure index....172
9. Appendix I....179
10. Appendix II....188
10.1. Conference contributions....189
10.2. Publications....196
11. Table of abbreviations....215
12. Curriculum Vitae....216

1. General introduction

1.1. Endocrine disruptors

Endocrine disrupting chemicals (EDCs) are described as “exogenous substances or mixtures that alter functions of the endocrine system and consequently cause adverse health effects in an intact organism, or its progeny, or (sub) populations” (Damstra et al., 2002). They are highly heterogeneous and can be classified as naturally occurring and synthesized chemicals (Kabir et al., 2015). Naturally occurring EDCs can be found in food as for instance phytoestrogens from soybean such as genistein or mycotoxins such as zearalenone. Synthesized EDCs are grouped as industrial used chemicals (solvents and lubricants) and their side products (e.g. dioxins, polychlorinated biphenyls), plastic additives (bisphenol A (BPA)), plasticizers (e.g. bis (2-ethylhexyl) benzene-1,2-dicarboxylate (DEHP)), pesticides (e.g. atrazine, 2,4-dichlorophenoxyacetic acid (2.4-D), dichlorodiphenyltrichloroethane (DDT)), fungicides (e.g. vinclozolin) and pharmaceutical products (e.g. diethylstilbestrol (DES), ethinyl estradiol) (Diamanti-Kandarakis et al., 2009b). The chemical structure of the less than 1000 Da small EDCs is quite diverse, and consequently they are able to affect different mechanism within an organism. Additionally some of the chemicals show endocrine activity only after being metabolized. Nevertheless some distinct structural features indicate estrogenic, thyroidogenic and glucocorticoid activities (Kidd et al., 2012).

1.1.1. The endocrine system

To better understand the mechanism of endocrine action, it is important to visualize and comprehend the complexity of the endocrine system. This system consists of several interacting organs and tissues, which are communicating with each other by signaling molecules, the so called hormones. By this, various processes in organisms such as cell differentiation in early developmental stages, bone formation and organ function are controlled. Figure 1 shows the human endocrine system with its main glands, organs and target tissues. Around 50 different hormones and hormone related molecules (e.g. cytokines) are secreted by glands or endocrine cell containing tissues and organs. Many organs and tissues are targeted by sex steroids and can thereby also be affected by EDCs. Among them are breast, uterus, cervix and vagina, organs which are directly connected to reproduction processes, but also the brain, the hypothalamic-pituitary-gonadal system, bones, muscles and skin (Marieb, 2015; Neave, 2007).

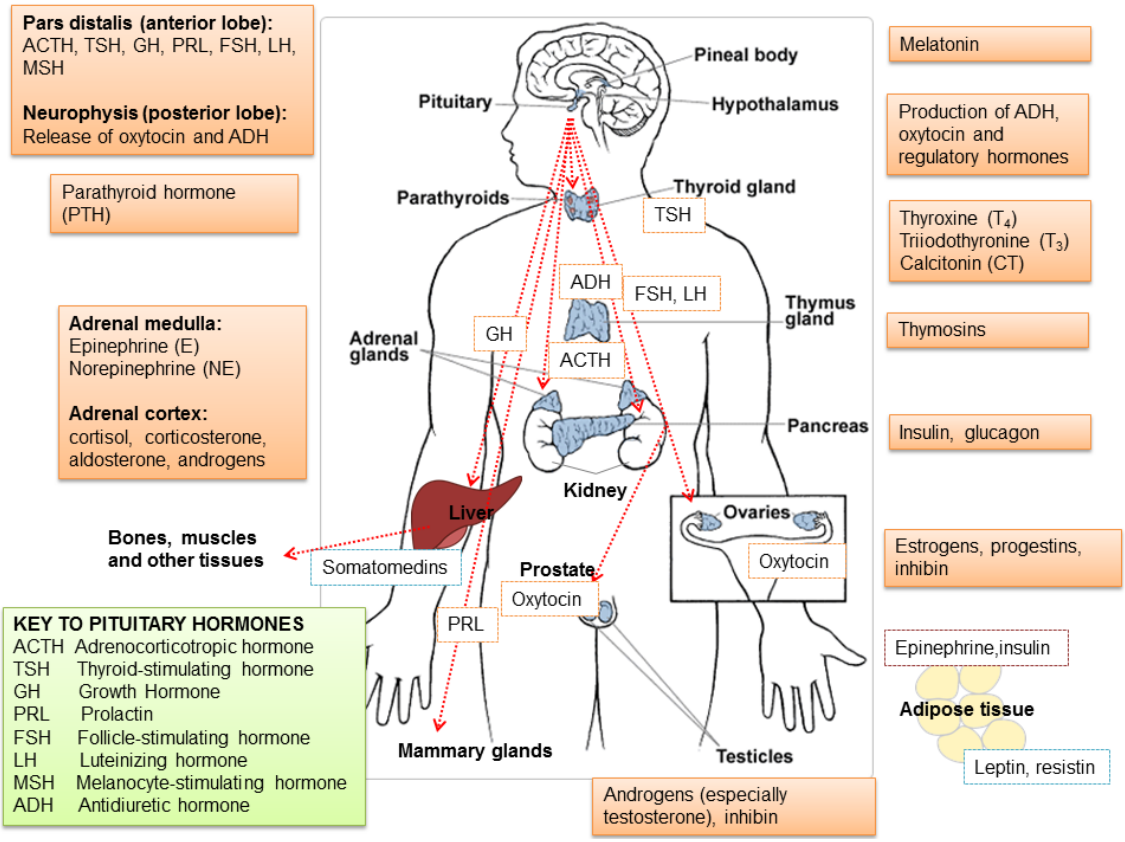

Figure 1: Section of the human endocrine system with the main endocrine glands (pituary, pineal, thyroid, parathyroid and adrenal glands), organs containing endocrine cells (pancreas, thymus, gonads (ovaries and testicles) and hypothalamus) and hormone targets (adipose tissue, bone, muscle, heart) (Hadley and Levine, 2006). Pictures of the endocrine system, liver and adipose tissue arrived from the clip art gallery of Microsoft Office Professional Plus PowerPoint 2010.

1.1.2. Exposure sources, and routes of EDCs, and their stability

The sources of exposure to EDCs are manifold and different in the world. The presence of different EDCs in the environment continuously changes due to legal restrictions or residue regulations in use, the introduction of new chemicals, and distribution of EDCs with substantial differences between countries (Kidd et al., 2012). Humans can be exposed for instance to bisphenol A (BPA) via food packaging, baby products and house dust. In the moment only the European Union and North America (USA, Canada) made regulations to ban BPA out of baby products, while BPA in food packing or other products with BPA content do not underlie any restrictions. The production and use of nonylphenol, a substance, which is not easily biologically degradable and so highly bioaccumulated in the environment is prohibited in the European Union, while the USA only recommends to decreases the use. For Asia and South America it is still widely available, due to little regulations (Baluka and Rumbeiha, 2016; Soares et al., 2008). The main exposure routes in humans are dermal contact, oral uptake or inhalation (Kidd et al., 2012; Yang et al., 2015). Once in the body

some, EDCs can accumulate in bones or fat tissue or they can be transferred to fetuses via the placenta (Yang et al., 2015).

Generally, naturally occurring or industrially manufactured chemicals with endocrine effects find their way to humans in direct or indirect manner (See: Figure 2). The major route of exposure for humans to EDCs is food. Next to direct exposure to natural food ingredients with endocrine potential such as genistein from soybean or hop from beer, the exposure to EDCs occur often via indirect paths such as contamination of food due to production processes, packaging material, residues of agrochemicals in food and feed (Karabín et al., 2016; Kidd et al., 2012; Patisaul and Jefferson, 2010; Yang et al., 2015).

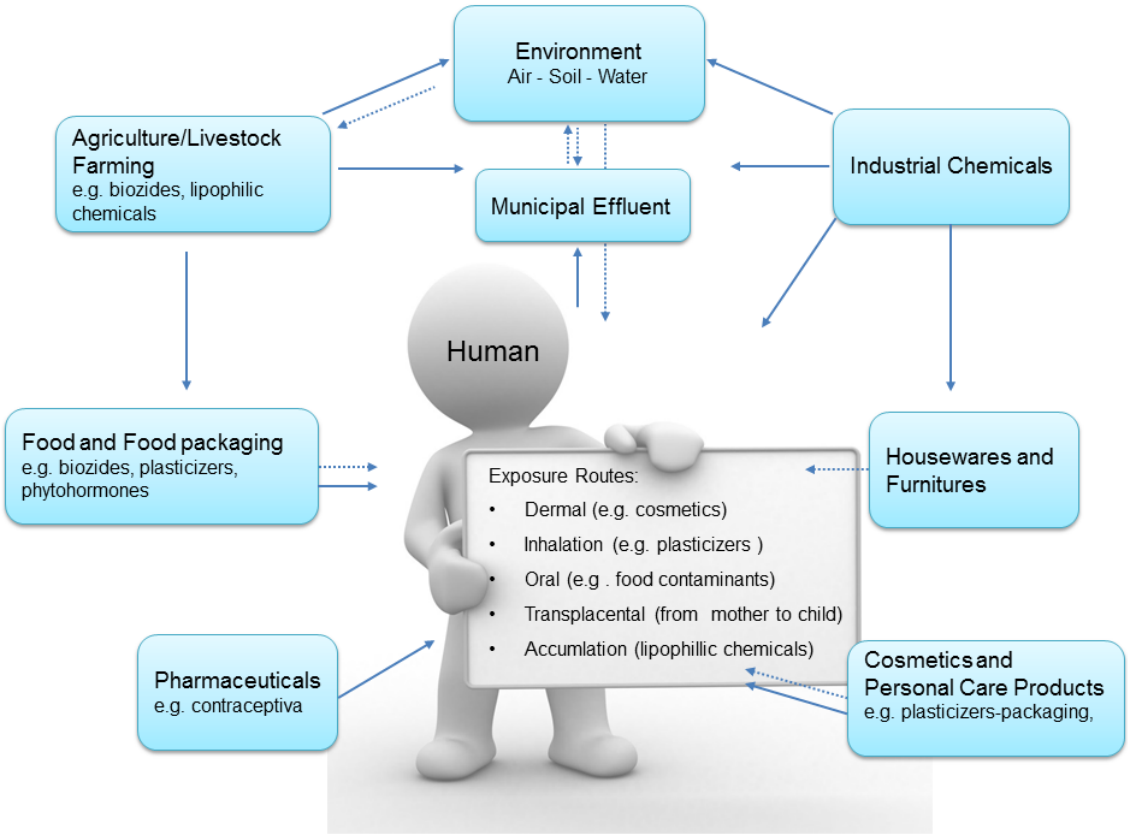

Figure 2: Exposure sources for humans and environment and major exposure routes of EDCs for humans. The exposure by EDCs can be direct (→) by the raw chemical or indirect (-->) by treatments or manufacture processes (Kidd et al., 2012; Yang et al., 2015). Free Stock Image 3D Human Character arrived from cute-pictures.blogspot.ro.

Other significant sources are housewares and personal care products. These contain endocrine active substances such as the volatile phthalates used as plasticizer in flooring and wallcovering and getting released fast into the environment or parabens which serve as preservatives in cosmetic or pharmaceutical products. In Table 1 sources are listed with

applications of the respective endocrine active substances and their chemical classes (Diamanti-Kandarakis et al., 2009a).

Table 1: Sources of exposure to EDCs and EDCs applications and characterizations (Dodson et al., 2012; Gore, A.C. et al., 2014). Abbreviations see: Table of abbreviations.

Sources	Application	Substance class	Substances
Agriculture	Pesticides	Organochlorides, triazine	DDT, Lindane, Atrazine
Cosmetics, personal care products	Preservatives, solvents, UV-filter	Parabens, phthalates, glycol ethers	Butylparaben, DEHP, 2-butoxyethanol
Food	Phytoestrogens	Isoflavone, coumestans	Genistein, daidzol
Food packaging	Plasticizer and plastic additives	Phthalates, bisphenols	DIDP, BPA, DINP
Housewares	Wallpaper, flooring	Phthalates	BBP, DEHP
Pharmaceuticals	Contraceptiva	Synthetic steroides	Ethinyl estradiol
Municipal effluent	Natural hormones (animals, human)	steroides	Estradiol, testosterone
Industrial effluent	Surfactants (removing oil), plasticizer	Alkylphenols, phthalates	Nonylphenol, dibutyl and butylbenzyl phthalates

Some EDCs are more persistent in the environment than others. By this they can accumulate in the food chains and reach high concentrations in humans and animals. BPA has a short half-life of 4-8 hours and is therefore not considered to be bioaccumulative, but still spread in the environment and persistent enough to find its way into the body of human and animals. Polychlorinated biphenols (PCBs) have to be numbered among the highly environmental persistent substances. They get globally distributed via water and air and accumulate due to their high lipid solubility in adipose tissue of humans and animals (Kidd et al., 2012). An US study in pregnant woman from 2003-2004 showed an high amount of endocrine active substances from many different chemical classes (See: Figure 3), whereas the highly persistent PCBs with 34 % and volatile organic compounds (VOCs) with 20 % represented the most prominent groups (Woodruff et al., 2012).

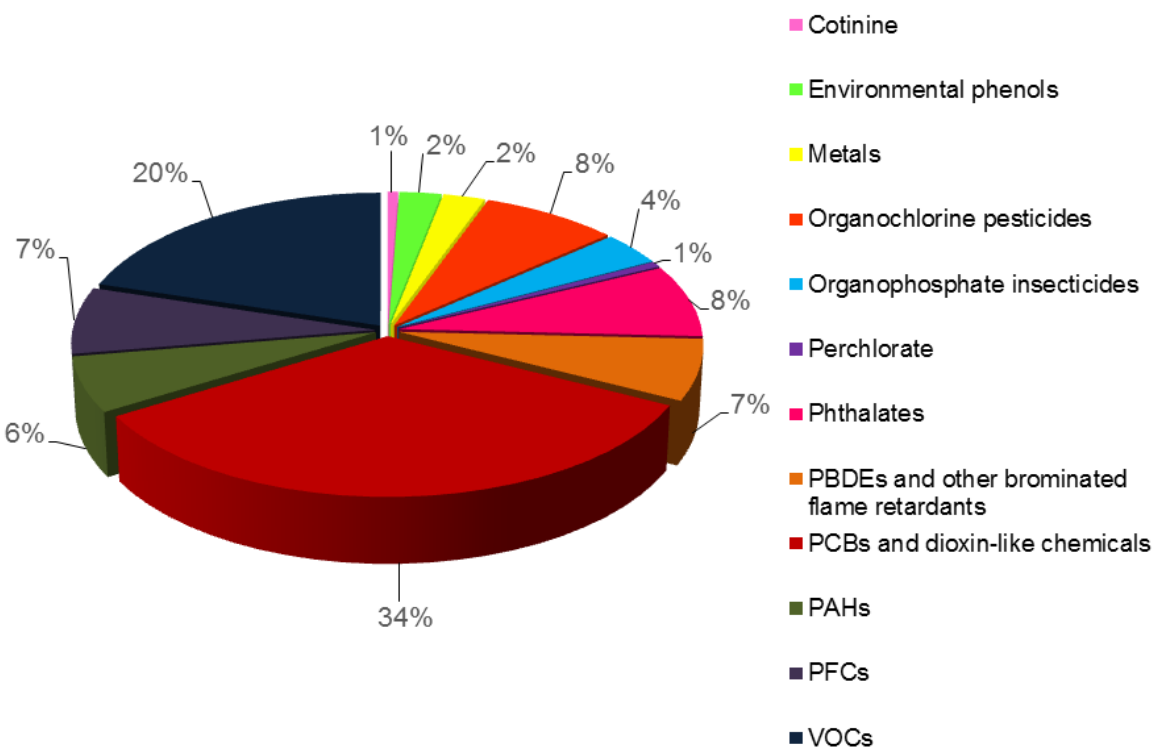

Figure 3: Endocrine relevant chemicals accumulated and measured in pregnant woman in the United States of America in the years 2003-2004 within the National health and Nutrition Examination Survey (NHANES) Data from Woodruff et al., (2012) (See: Table of abbreviations).

Natural steroidal EDCs such as estradiol, estrone, estriol and testosterone are described as endocrine substances with higher potency compared to non-steroidal anthropogenic generated EDCs. They are directly released from humans and mammals by excretion into the environment and found in significant amounts in sewage or treated waste water (Kidd et al., 2012).

1.1.3. Endogenous and exogenous estrogenic chemicals

The steroid hormones Estrone (E1), estradiol (E2), and estriol (E3) are the three major naturally occurring forms of estrogen, whereas estradiol is the most potent and affine endogenous ligand. Estrogens are produced in human in the ovaries, placenta, liver, adrenal glands and breasts within the steroidogenesis by conversion of androstenedione and testosterone. This reaction is catalyzed by key enzyme for estrogen synthesis, the aromatase (Nelson and Bulun, 2001) (See: Figure 4).

Estrogens have important functions in males and females and are involved in the development and regulation of the female reproductive system and secondary sex characteristics as well as in lipid metabolism, protein synthesis and the pathogenesis of

diseases (e.g., cancer, neurodegenerative/cardiovascular diseases) (Kiyama and Wada-Kiyama, 2015).

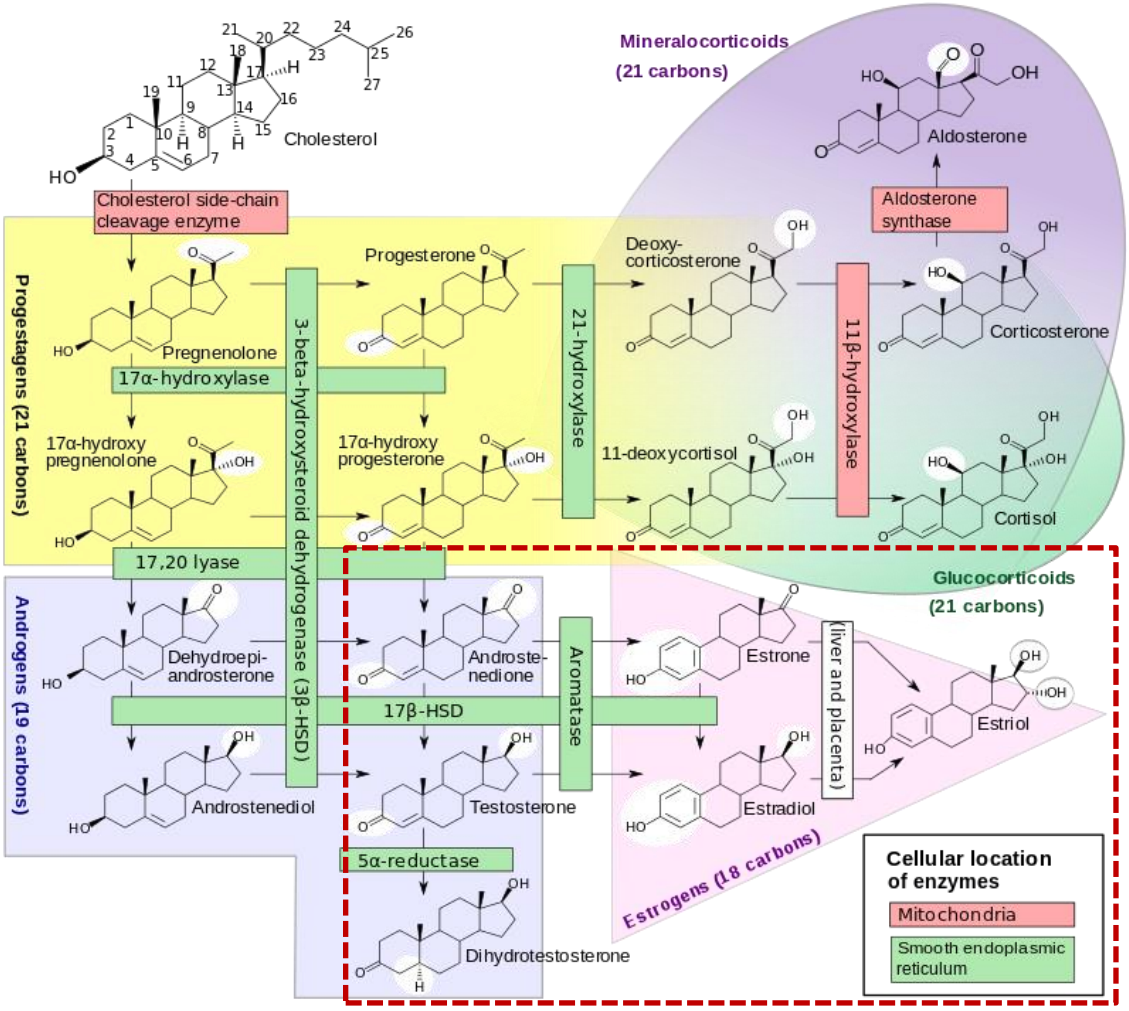

Figure 4: Overview of the human steroidogenesis. Major classes and subclasses of steroid hormones inclusive their enzymatically conversion are shown. Chemical changes are highlighted in white and estrogens in red (Häggström et al., 2014).

The chemical structure of estrogen compounds is divers, but they often consist of a phenol ring similar to the endogenous steroid hormone estrogen and do not contain halogens (Kidd et al., 2012) (See: Figure 5).

In general, estrogenic compounds show different binding preferences and binding affinities for both nuclear receptor subtypes with variation for animals and humans (Matthews et al., 2000). Table 2 contains a selection of endogenous and exogenous ligands of the human estrogen receptor and their binding affinity to the receptor. There are described due to their

relative binding affinity (RBA) to the estrogen receptor (ER) in relation to the most affine endogen ligand, 17ß-estradiol (RBA=100%) as weak (log RBA <–2), moderate (log RBA 0 to –2), or strong binder (log RBA > 0). Natural steroids, such as 17ß-estradiol, estriol and estrone, as well as synthetic steroids (diethylstilbestrol, ethynyl estradiol) exhibit strong affinities to the estrogen receptor with log RBA over zero. However, synthetic estrogens show with an RBA of 400 for diethylstilbestrol and 190 for ethynyl estradiol much greater affinities compared to 17ß-estradiol (See: Table 2) (Blair et al., 2000).

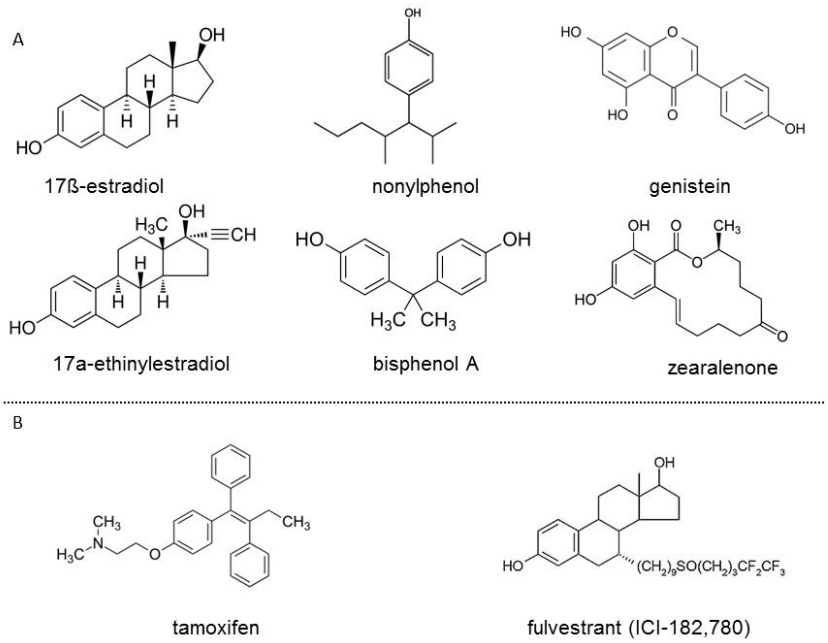

Figure 5: Chemical structures of some natural and synthesized estrogenic (A) and antiestrogenic (B) compounds and their structural similarity to the endogen steroid hormone 17ß-estradiol.

Table 2: Human estrogen receptors (ER), half maximal inhibitory concentration (IC50), relative binding affinities (RBA) and Log RBA values of selected ER agonists and antagonists arrived from a competitive ER binding assay. Binding affinities are relative to 17ß-estradiol and calculated by division of the IC50 of 17ß-estradiol by the one of the competitor (Blair et al., 2000).

Estrogenic compounds	IC50 (M)	ER RBA (%)	Log RBA
Agonists			
Diethylstilbestrol	$2.3 \pm 0.1 \times 10^{-10}$	400	2.60
Ethynyl estradiol	$4.7 \pm 0.6 \times 10^{-10}$	190	2.28
17ß-estradiol	$8.9 \pm 0.3 \times 10^{-10}$	100	2.00
Estriol	$9.3 \pm 1.8 \times 10^{-9}$	9.7	0.99
Estrone	$1.2 \pm 0.3 \times 10^{-8}$	7.3	0.86
Nonylphenol	$2.6 \pm 0.3 \times 10^{-6}$	0.035	-1.46
Bisphenol A	$1.7 \pm 0.6 \times 10^{-5}$	0.008	-2.11
Antagonists			
ICI-182,780 (Fulvestrant)	$2.4 \pm 1.1 \times 10^{-9}$	38	1.57
Tamoxifen	$5.6 \pm 0.1 \times 10^{-8}$	1.6	0.14

Synthetic chemicals modulate estrogenic action in a direct and indirect way and include estrogen as well as anti-estrogen active substances. Antiestrogens or estrogen antagonists prevent the action of estrogen agonist by blocking the estrogen receptor (ER) and/or inhibiting hormone production in individuals. They include selective estrogen receptor modulators (SERMs) such as tamoxifen and the selective estrogen receptor degrader (SERD) fulvestrant as well as aromatase inhibitors and antigonadotropins. However, aromatase inhibitors and antigonadotropins do not reduce the response to estrogen, they decrease hormone levels by suppressing the production and are therefore distinguished from antiestrogens (See: Figure 6) (Thiantanawat et al., 2003).

EDCs can even show, depending on the tissue, opposite effects of endocrine disrupting action. BPA and alkylphenols such as nonylphenol show for instance estrogenic as well as anti-androgenic effects by binding on estrogen and androgen receptor (H. J. Lee et al., 2003). Depending on the chemical structural element, they are receptor agonists or antagonists and are able to affect male and female reproduction, breast development, cancer, metabolism, obesity, neuroendocrinology and cardiovascular endocrinology (Kabir et al., 2015).

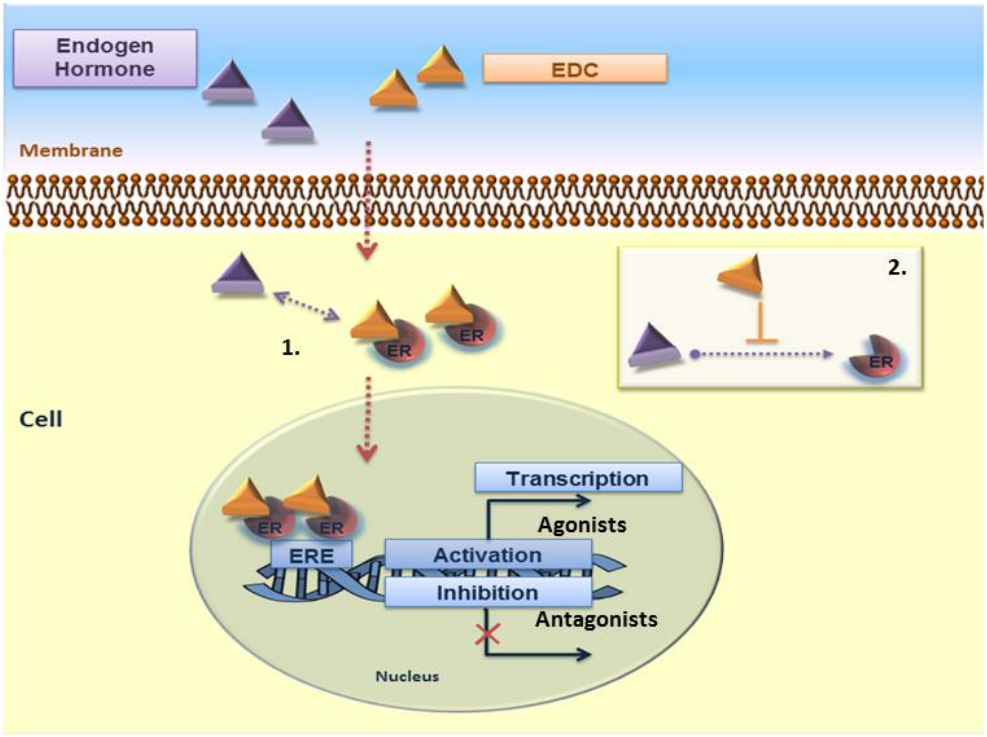

Figure 6: Estrogenic and antiestrogenic action. 1. Direct action via nuclear ER. Binding of antagonists can inhibit the transcription of downstream genes of the ER receptors, while agonists activate it. 2. Suppression of hormone synthesis, which result in no binding to the receptors.

1.1.4. Mechanism of action

The action of estrogenic active substances is categorized into genomic and non-genomic pathways, which belong to the intracellular network and the autocrine/paracrine signaling describing the extracellular network (See: Figure 7). The genomic pathway includes the binding of endogenous or exogenous estrogenic ligands such as 17β-estradiol and nonylphenol to the ER ligand binding domains. Due to activation by the ligand, the ER translocate into the nucleus where it binds to a specific estrogen response element (ERE) of the DNA. This event initiates the transcription of target genes, which results in cell signaling (Kiyama and Wada-Kiyama, 2015).

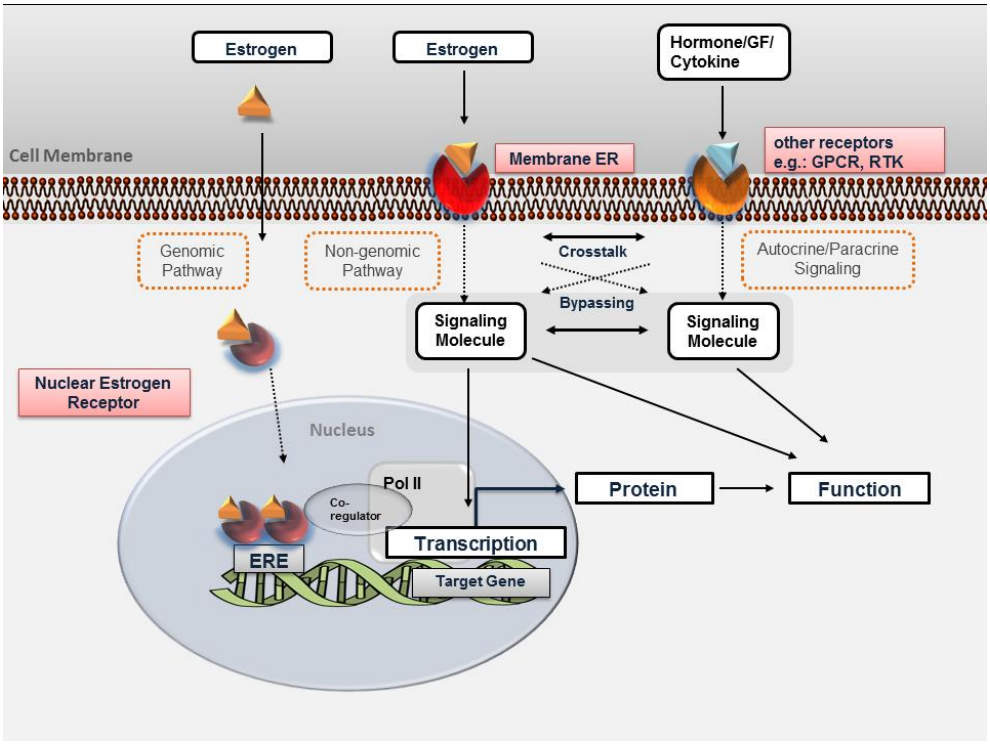

Figure 7: Genomic, non-genomic pathways and autocrine/paracrine signaling of estrogenic active substances. Adapted from Kiyama and Wada-Kiyama, 2015.

ERs are divided in two classes: intercellular nuclear estrogen receptors (ERα and ERβ) located in the cytosol and involved into the genomic pathway and membrane estrogen receptors (mERs). Membrane estrogen receptors include G-protein coupled receptors such as the G-protein coupled estrogen receptor (GPER (GPR30)), ER-X and ER-α36 which are variants of the nuclear ERs (Soltysik and Czekaj, 2013). The mERs and/or other non ER related receptors are part of the non-genomic pathway. They rapidly transduce signals after activation by estrogen through crosstalk and/or bypassing. In addition there are nuclear estrogen–related receptors (ERR) with their own response elements. They don't bind to estrogens but they do mediate their signaling by cooperation with different kinds of autocrine/paracrine signaling and affect therefore other hormones, tissues and the hormone synthesis itself (Kiyama and Wada-Kiyama, 2015; Misawa and Inoue, 2015; OECD, 2015). The signaling pathways linked to estrogenic active substances are manifold (e.g. phosphatidylinositol-4,5-bisphosphate 3-kinase (PI3K), mitogen-activated protein kinases/extracellular signal-regulated kinases (MAPK/ERK) pathway and nuclear factor kappa-light-chain-enhancer of activated B cells (NF-κB)). They are mostly associated to cell growth and proliferation, differentiation and development, apoptosis, metabolism, inflammation and carcinogenesis (Kiyama and Zhu, 2014) (See: Table 3).

Table 3: Examples of endogenous and exogenous estrogenic and antiestrogenic compounds and their involvement in signaling pathways (See: table of abbreviations) (Kiyama and Wada-Kiyama, 2015).

Estrogenic compounds	Signaling Pathway
Agonists	
Diethylstilbestrol	• ERRα • GPER/PKA/ERK/CREB/testis
Ethynyl estradiol	• ER/MAPK/cell growth
17ß estradiol	• mER/ERK/Ca2+/proliferation
Zearalenone	• ER/Wnt/anti-reproduction • ERα
Genistein	• GPER/ERK/c-Fos/cell growth • ERα, ERβ • GPER/IL-1β/MAPK /inflammation • ERα/IGF-1R/IRS-1/Akt/carcinogenesis • ERα/MAPK/NF-κB/AP-1/differentiation
Nonylphenol	• ER/NF-κB/NO/inflammation
Bisphenol A	• ERα • GPER/ERK/c-Fos/transcription
Antagonists	
ICI-182,780 (Fulvestrant)	• ERα/Wnt/β-catenin/carcinogenesis • ER/HER/c-Src/proliferation • GPER/TGF-β1/Smad/migration • GPER/ERK/calpain/cell adhesion
Tamoxifen	• Cell growth (ER-independent) • ER/apoptosis (ER-dependent/ independent) • ERα/IGF-1R/EGFR/MAPK/proliferation • ERα/Wnt3A/β-catenin/differentiation

The phytoestrogen genistein was reported to be involved in differentiation events, mediated by induction of ERα gene expression due to the activation of the MAPK (mitogen-activated protein kinase) /NF-κB/AP-1 (Activator protein 1) signaling pathway (Liao et al., 2014). In addition the phytoestrogen inhibits inflammation processes through the membrane receptor GPER by shifting the interleukin (IL)-1ß activation of MAPK (Luo et al., 2012) (See: Table 3).

1.1.5. Issues of EDCs action

EDCs´ action in organisms bring along different issues, which have to be considered in the course of their evaluation. First of all the age of exposure has to be taken into account

because of different effects on especially sensitive age groups, such as unborn, children or elderly persons, and the well-known higher risks in early developmental stages (Kabir et al., 2015). They may not only affect the exposed human but also following generations by epigenetic effects in the germline, due to modification in DNA methylation and histone acetylation. Latency due to EDCs exposure is most often a consequence of exposure in early developmental stages. Furthermore it is important to mention that individuals are exposed to mixtures of different EDCs with different potencies. These mixtures can show additive, i.e. a summing up of the effects of single EDCs or synergistic effects, which are even higher than the additive. EDCs are known to show higher potencies in low exposure levels compared to higher doses, the so-called low-dose effects. They even show a non-monotonic dose response (See: Figure 8). Low-dose effects as well as non-monotonic dose response were already known for hormone and neurotransmitter action and are lately also discussed for EDCs (Diamanti-Kandarakis et al., 2009a).

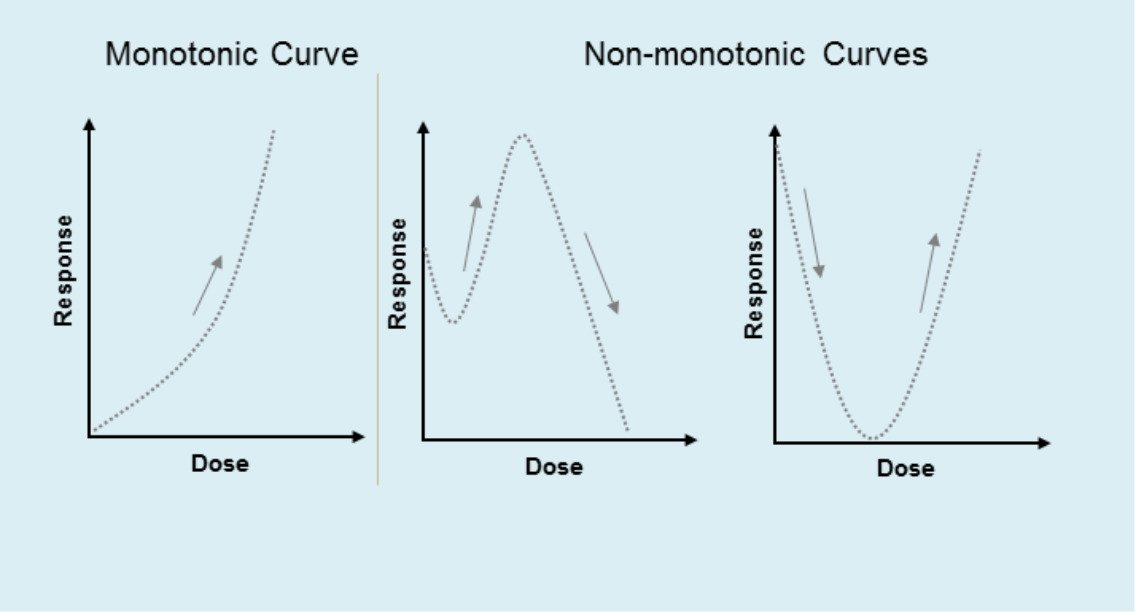

Figure 8: Comparison of monotonic and non-monotonic dose-response curves. Monotonic curves show a proportional increase or inversely proportional decrease of response with the dose. Non-monotonic curves are U-shaped, inverted U-shaped, or even more complex and characterized by different responses for intermediate or low and high doses, but with potential higher effects for low doses. Figure adapted from Fagin, 2012.

1.1.6. State of the art of *in vitro* methods for investigating estrogenic action

The evaluation of estrogenic chemicals and their action in organisms is performed with various methods, such as ligand-binding assay, reporter-gene assay, transcription assay, protein assay, signaling pathways analysis, cell assay and animal tests (See: Figure 9) (Kiyama and Wada-Kiyama, 2015). Table 4 gives an overview of assigning methods with

assay principles, endpoints, advantages and disadvantages. However, internationally accepted standard methods assessing potential endocrine effects on chemicals for human health and environment, the so called OECD Test Guidelines (TG), provide an *in vitro* test battery with focus on endocrine mechanisms and pathways such as ER binding affinity (OECD TG 493), ER transactivation (OECD TG 455, 457), steroidogenesis (OECD TG 456) and MCF-7 cell proliferation assays (OECD, 2017; Soto et al., 1995).

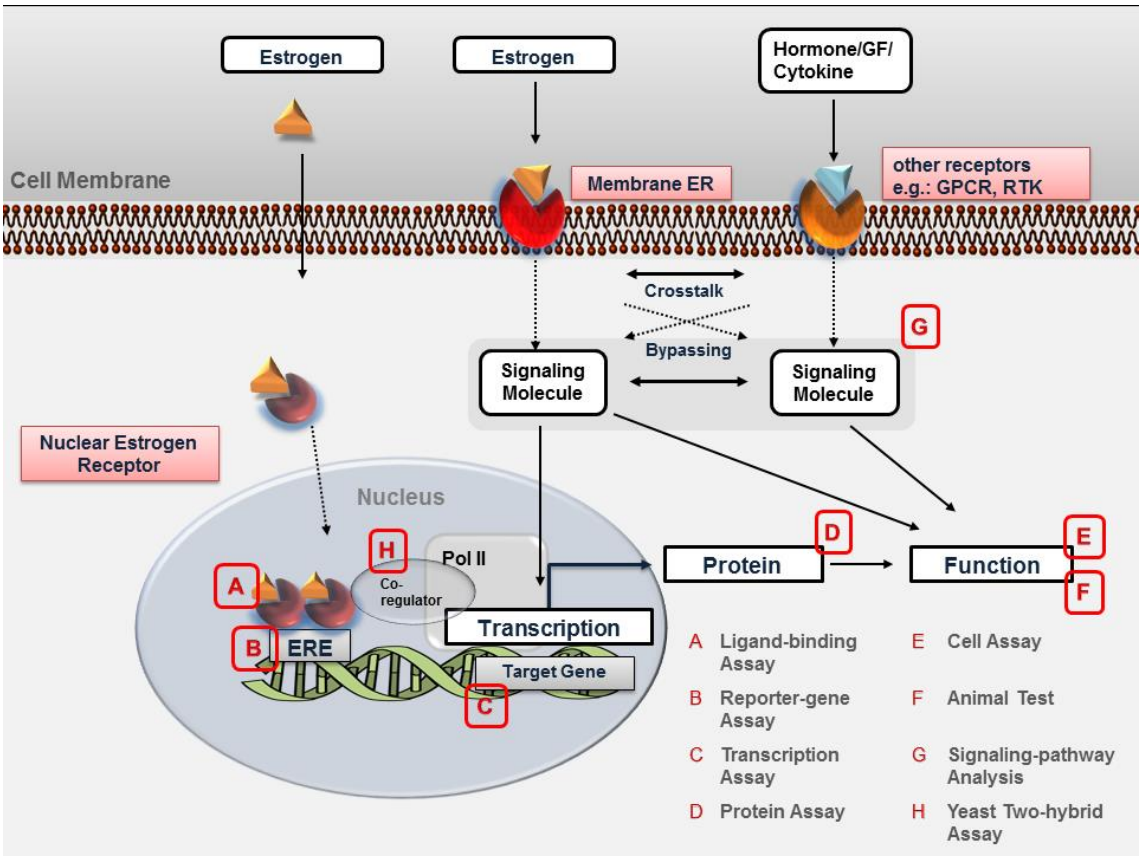

Figure 9: Overview of methods used to detect estrogenic activity by determination of the signaling network of estrogen and estrogen like chemicals. The red letters indicate the methods used to evaluate the corresponding action. Adapted from Kiyama and Wada-Kiyama, 2015.

Ligand-binding assays focus on the binding of a test substance in competition with radiolabeled 17ß-E2 to the ERs and can evaluate therefore the relative binding affinity of the substance to the receptors (See: Table: 4). Differentiation between agonists and antagonist was not possible in the first assays (Kiyama and Wada-Kiyama, 2015). The assay was further developed by introduction of a split Venus fluorescent protein, which produces a fluorescence signal after conformational changes of the receptor ligand binding domain through binding of an estrogenic chemical which is able to distinguish agonistic and antagonistic action (Mclachlan et al., 2011). Results of ligand binding assays cannot be

extrapolated to the complex mechanism of the endocrine system *in vivo* and test substances can influence the assay performance by pH changes or denaturation of the receptor protein and they do not provide more information on further gene transcription (OECD, 2015).

Reporter or transactivation assays investigate the transcription of a downstream reporter gene after binding of the receptor-ligand-complex to the specific DNA response element (See: Table: 4). Different reporters such as ß-galactosidase (lacZ), chloramphenicol acetyltransferase (CAT), luciferase and green fluorescent protein (GFP), different cell systems (mammalian cells, yeast cells) and different receptor/reporter constructs are applied (Kiyama and Wada-Kiyama, 2015). A famous representative is the CALUX (Chemically Activated Luciferase expression) bioassay from Sonneveld et al., (2005) for the detection of androgenic, estrogenic, progesterone and glucocorticoid action via quantification of the luciferase protein in different assays using stable transformed human osteosarcoma cells (US-OS). Cells which do not express endogenous receptors have to be transfected with two plasmids for receptor or reporter gene. These assays are robust and sensitive, but exhibit artefactual or off-target interferences which desire internal controls (Gasparri and Galvani, 2010). Yeast cells are frequently used for this assay formats, due to a fast performance. The Yeast Estrogen Screen (YES) assay uses fluorescence–based reporters (Bovee et al., 2004; Leskinen et al., 2005). However the discrimination of agonistic and antagonistic action is not possible in the yeast system and due to a bad membrane permeability of lipophilic substances and differences in enzymes, transport proteins and signaling pathways leads to divergent responses compared to human cells (Kiyama and Wada-Kiyama, 2015).

Analysis of the transcriptome is described as one of the most effective methods to predict estrogenic activity (See: Table: 4). Techniques such as DNA microarrays, real time polymerase chain reaction (PCR) or next-generation sequencing are applied to quantify ER downstream genes or specific marker genes for instance trefoil factor (TFF) -1 (pS2), progesterone receptor (PGR, PR), breast cancer 2 (BRCA2) or apolipoprotein (APOA1, ApoA-1) (Kiyama and Wada-Kiyama, 2015). An advantage of this analysis is that it provides expression profiles of the individual chemical, which can be correlated to genes with importance for cell functions. However, while being useful for pre-screens to identify potential candidates it is hard to correlate gene expression levels to protein levels which are reflecting cell functions (Vogel and Marcotte, 2012).

Protein assays like enzyme linked immunosorbent assay (ELISA), western blotting or mass spectrometry are only applied for single ER proteins or protein biomarkers such as TFF1 (pS2), PGR (PR), cyclin D1 (CCDN1), APOA1 (ApoA-1), stromal cell-derived factor 1 (SDF-1, CXCL12) or vitellogenin, whereas proteome microarrays for analysis of estrogenic action not exist (See: Table: 4). Techniques such as ELISA are additionally applied as screening

systems for endocrine chemicals in the environment or in food matrices (Habauzit et al., 2010; Kiyama and Wada-Kiyama, 2015).

Cell assays used for prediction of estrogenic action are mostly based on cell growth and proliferation (See: Table: 4). One prominent representative is the E-Screen developed by Soto et al., (1995). Common cell lines used in cell assays are estrogen receptor positive breast cancer cell lines, such as the breast cancer cell lines MCF-7 and T-47D. These cell lines are hormone sensitive and proliferate in presence of estrogen active substances (Al-Bader et al., 2011). For the determination of the proliferation by live/dead stains or metabolic activity, colorimetric or fluorometric methods are applied (Riss et al., 2013).

Table 4: Overview of test battery for estrogenic substances with assay principles, advantages and limitations

Assay class	Assay principle /Endpoint	Advantages	Limitation	Reference
Ligand binding assays (e.g. ELRA, QSAR)	Nuclear receptor-ligand interactions (relative binding affinity), detection via antibodies or bimolecular fluorescence complementation	• Easy and fast to perform • High throughput	• no discrimination between agonists and antagonists (c.a.) • poor sensitivity	(Li and Gramatica, 2010; Mclachlan et al., 2011; Seifert et al., 1999)
Reporter-gene assay (e.g. CALUX®, YES/YAS)	Quantification of e.g. luciferase, GFP expression due to transcription of target genes	• Initiating transcription of target genes by ligands • Higher sensitivity than e.g. ELRA	• Interferences by other receptors • Yeast systems: no discrimination agonists and antagonists; limit in membrane permeability for lipophilic substances, different proteins and pathways	(Sonneveld et al., 2005)(Routledge and Sumpter, 1996)
Yeast two-hybrid assay	β-galactosidase activity	• Determination of endocrine active substances	• Not be accurate enough to represent mammalian or human systems	(Nishikawa et al., 1999)
Transcription assay (e..g. microarrays, PCR)	Quantification of DNA/RNA expression of ER genes, specific marker genes or genes responding to estrogen	• Gene-expression profiles according to the chemicals • Fast and effective	• Dependent on concentrations within linear range • Assay interference related genes	(Francois et al., 2003; Kiyama and Zhu, 2014)
Protein assay (e.g. ELISA, Western blot)	Qualitative and quantitative of protein screening	• Verification of estrogenic potential • Sensitive • Direct screening of EDCs	• Sets of protein markers for proteomic profiling seldom used • Focus on single biomarkers like	(Sumpter and Jobling, 1995)
Cell assay (e.g. EScreen, Steroidogenisis assay(S.A.))	Cell Proliferation after substance exposure (MCF-7 cells/) Detection of modulators of steroidogenesis by quantification of E2/T (H295R cells)	• EScreen: easy to use, high throughput, fast screening tool • S.A.: investigation of effects on steroid hormone synthesis and cell viability, cell line expresses all the key enzymes for steroidogenesis	• EScreen: cells from different sources give different responses, lack of xenobiotic metabolism • S.A.: Metabolic capability of cells unknown, Interference with mineral and glucocorticoid pathway	(Hecker and Giesy, 2008; Odum et al., 1998; OECD, 2011; Soto et al., 1995)
Signaling pathway assay (e.g. microarray, cytometry)	Signaling pathways relating to e.g. apoptosis, cancer, cell growth, differentiation, development, inflammation	• Information about the mechanism of chemical action and involvement in different pathways	• Using of various assay formats	(Totta et al., 2004)
Enzyme assay (aromatase assay)	Determination of $^{3}H_20$ deveoloped during the conversion of ^{3}H-ASDN to estrone in presence of test chemical quantified by liquid scintillation counting - measure of aromatase activity	• High sensitivity and reproducibility • Easy to use	• Limited to inhibitory effects • No answer for mechanisms • Interaction of test compound with other enzymes; changes on aromatase activity • Use of radioactive material	(EPA, 2011)

1.2. Biomarkers

Biomarkers were first defined as “cellular, biochemical or molecular alterations that are measureable in biological media such as human tissues, cells or fluids” by Hulka et al., 1990. Thirteen years later the definition was extended to “a biomarker is a characteristic that can be objectively measured and evaluated as an indicator of normal biological processes, pathogenic processes or pharmacological responses to therapeutic intervention” (Naylor, 2003). In general biomarkers are classified as prognostic, predictive and pharmacodynamic biomarkers, and can be further subdivided depending on their clinical application as molecular (genomic, transcriptomic, proteomic, metabolomic), cellular or imaging biomarker (Gainor et al., 2014; Mayeux, 2004; Muller and Dieterle, 2009).

Prognostic biomarkers give indications about the status of a disease by measuring the increase or decrease of e.g. the secretion of disease specific proteins in blood. They can be directly (as a main factor within the disease) or indirectly (as effect of exposure/disease dependent change) associated with a disease. Predictive biomarkers detect the response to a drug or toxin and its activity. They are highly sensitive and specific. Pharmacodynamic biomarkers are used to analyze the effect of a drug to its target. Additionally they give further information about dosing, proof of mechanism and concept and further understanding of responsive or resistant action (Gainor et al., 2014). Biomarkers are used in clinical and basic research and clinical practice as well as in the close related field of toxicology (Strimbu and Tavel, 2010).

1.2.1. Biomarkers in toxicology

In toxicology research, particularly biomonitoring, biomarkers are used for the exposure assessment of humans/organisms to drugs or chemicals and they are classified as biomarker of exposure, effect and susceptibility (Nordberg, 2010). The exposure to a chemical substance or its metabolites for instance measurements of bisphenol A concentrations can be measured in body fluids or tissues such as blood, urine and saliva. Quantifiable changes of the health of an organism including the early stages of a disease, picture the effect of an exposure. These types of biomarkers are mainly used because they provide additional information about uptake, metabolism or distribution of a substance. Different individuals respond differently to the effects of an exposure to one specific chemical. They own individual natural characteristics such as polymorphisms of the cytochrome P450 genes, which can affect the function of the identically named enzymes involved in xenobiotic metabolism in humans or animals. This makes the organism more or less susceptible to the effects of an exposure (Nordberg, 2010; Zhou, 2009).

The characteristics for a biomarker of drug safety assessment were defined by the European Commission in 2005. A new biomarker: ”i) should be specific for certain types of injury; ii) indicates injury in a variety of experimental species as well as humans; iii) can be used to bridge across nonclinical/preclinical studies to clinical and surveillance types of studies; iv) should be more effective at indicating injury than other biomarker currently used; v) used instead of classic biomarkers, not in addition; vi) can be easily measured (in real time) even at a later stage (measurement is not strongly time dependent); vii) more reproducible and sensitive than the original toxicity endpoint it would replace and viii) reduces the number of individuals tested (animals or humans)” (Campion et al., 2013). These characteristics can also be applied to exposures to hazardous compounds by food or through the environment (Swenberg et al., 2008).

1.3. Microarrays

Microarrays are generic terms for miniaturization of molecular biology techniques on a solid substrate and arose from Roger Erkins ambient analyte immunoassay in the year 1989. This method allows the parallel quantification of thousands of probes with low material input in a very sensitive way. In general microarrays are classified as biochips generated of biological molecules for instance: DNA, proteins or cells, or chemical microarrays which is based on arraying of small organic molecules, peptides or sugars (Xu and Lam, 2003). The concept of Roger and Erkins (1989) was successfully converted into DNA microarrays for gene expression profiling (Schena et al., 1995; Sutandy et al., 2013). The further development of the DNA microarrays was based on their limitations such as the often missing correlation between gene and protein expression (Kopf and Zhahary, 2007; Zhu and Snyder, 2001) and the increasing request for more insights into the function of biological processes and research of complex biological samples. Proteins as the central functional unit in cellular processes can be detected with protein microarrays. The principle of protein microarrays is based on highly specific antigen-antibody interactions for the detection of an entire set of proteins in parallel using a small sample volume by providing a good reproducibility (Haab, 2005; Kopf and Zharhary, 2007). Protein microarrays are nowadays used for biomarker discovery, antibody characterization, the determination of protein expression, evaluation of protein-protein interactions, drug development and disease diagnostics (Stoevesandt et al., 2009). Over the time different microarray techniques, utilized also artificial recognition elements such as MIPs and aptamers and were expanded to cell, cell lysate and tissue based systems (Hong et al., 2017; Menger et al., 2016; Rothbauer et al., 2015; Witt et al., 2015). Current advancements in the field were made by functional integration of microfluidics. The so called microfluidic based micromosaic technology overcomes the challenges of bulk dependence and diffusion limitation for transcriptome, genome, proteome

and cell based applications. Existing microfluidic platforms are microbead-based, centrifugal system-based or merged systems, for instance combined protein and cell arrays measuring protein secretion of cells utilizing a microfluidic delivery system for reagents or samples (Dixit and Aguirre, 2014; Nahavandi et al., 2014; Tourovskaia et al., 2005).

1.3.1. Assay principles of protein microarrays

In general, protein microarrays can be classified into three main classes the analytical, functional and reverse phase protein assays (Kricka et al., 2006; Sutandy et al., 2013). The immobilized capture molecules, for instance antibodies catch the corresponding analytes from a single sample in analytical assays (Hartmann, 2009; Chen and Zhu, 2006). In reverse-phase microarrays cell or tissue lysates or antigen targets are immobilized for simultaneous analysis of single proteins via antibody recognition (Boellner and Becker, 2015). Functional assays are based on the analysis of functional activity of one or more proteins. Analysis of protein-protein binding, biochemical activity or immune responses are possible with these platforms making them a valuable tool for high throughput in drug and biomarker discovery (Hu et al., 2011). Analytical protein arrays are mainly used for medical screening within the diagnosis and pathogenesis of diseases (Greenbaum et al., 2002; Lee et al., 2008).

Different assay formats are applied for analytical protein microarrays. Direct, competitive, binding inhibition and sandwich assays (See: Figure 10) are performed in a microarray format, the choice of one of them depends on the availability of reagents and the assay requirements. The sensitivity of the assay format is mainly determined by the binding affinity of the antibodies (Cox, 2012; Darwish, 2006; Sauer et al., 2011).

A direct assay format involves the immobilization of the antigen to the surface (See: Figure 10). The antigen interacts directly with the target molecules such as antibodies. A species specific labeled antibody is added for the detection resulting in direct proportional relationship between target concentration and signal (See: Figure 10 (1)) (Cox, 2012; Kingsmore, 2006).

In a sandwich assay, two antibodies bind to two different specific epitopes of the antigen or target (See: Figure 10 (1)). The capture antibody is immobilized onto a surface. After binding the antigen, the detection antibody is added to sandwich the antigen. The detection can be performed with a single antibody or an antibody pair containing a primary antibody for the binding to the antigen and a secondary antibody, which binds species specific to the primary antibody. The detection antibody is directly conjugated to a reporter (fluorophore, biotin, enzymes) for quantification. In consequence of increasing antigen concentrations, the amount of bound detection antibody increases, as well as the signal intensity. The

concentration of analytes in the sample is therefore proportional to the signal intensity (Sittampalam et al., 2016).

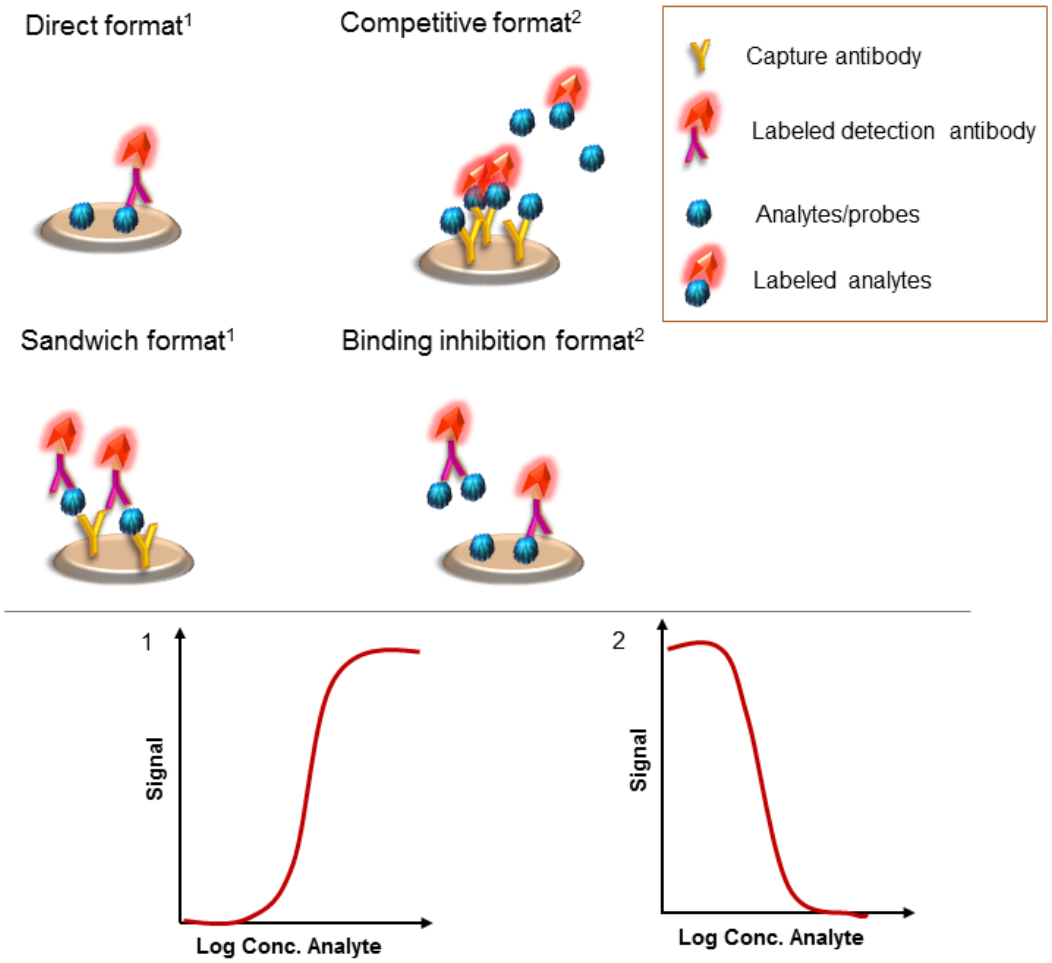

Figure 10: Direct, sandwich competitive and binding inhibition immunoassay formats with corresponding calibration curves are shown (1 and 2). Direct and sandwich formats show a direct proportional relationship of analyte concentration and signal (1), and competitive and binding inhibition formats an inversely proportional analyte-signal correlation (2) (Cox, 2012).

In the competitive format, defined amounts of antibody are immobilized. They capture added labeled or unlabeled analytes from the sample. The analytes compete with each other for binding to the limited binding sites. In case of less unlabeled analytes in a sample, a high amount of labeled analytes bind to the antibody and results in high signal intensities (See: Figure 10 (2)) (Sittampalam et al., 2016).

In binding inhibition assays the analytes are immobilized on the surface, whereas labeled detection antibodies, first incubated with analytes in the sample, are applied on the immobilized probes. The more analyte in the sample the less antibodies are free to bind to

the immobilized probes. As a result, signals generated via binding of labeled molecules are inversely proportional to the analyte concentration (See: Figure 10, (2)) (Sauer et al., 2011).

The binding inhibition and competitive formats are frequently applied for the determination of high abundance proteins, as they show less assay sensitivity compared to a sandwich format. In addition they are performed for small molecules (<10kDa) assays due to less binding sites on the molecule, steric hindrance for antibodies and antibody availability (Ekins, 1987; Self et al., 2013; Slagle and Ghosn, 1996). Different assay formats can be perfectly combined on one chip for instance for the detection of low and high abundant proteins (Sauer et al., 2011).

1.3.2. Protein microarrays – from fabrication to analysis

From the fabrication to the analysis of a protein microarray, five main steps are involved: surface functionalization, probe immobilization, assay or chip processing, detection of targets and the data analysis (See: Figure 11). In order to get protein microarrays with a high sensitivity and specificity, each of these steps has to be optimized. The following chapters (1.3.3 – 1.3.10) explain more in detail which techniques are applied for the whole procedure.

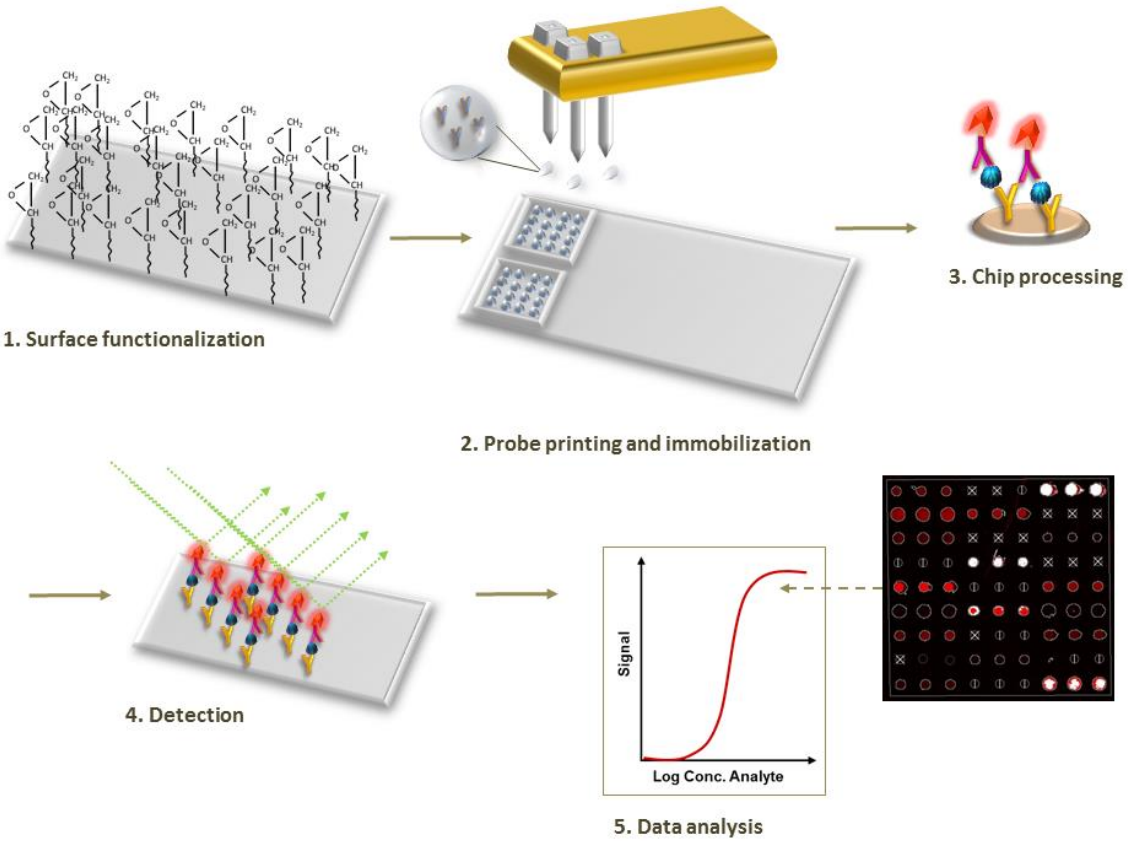

Figure 11: Scheme of the five main steps of a protein microarray. From fabrication to analysis.

1.3.3. Surface functionalization and strategies for probe immobilization

To ensure activity and proper orientation of the probes on surfaces, an efficient immobilization strategy is important. In order to achieve a good assay performance, the accessibility of binding sites of the probes in their conserved native structure is crucial (Rusmini et al., 2007). To fulfill the requirements, several immobilization strategies were employed: physical (adsorption, electrostatic), affinity- and covalent- binding. Which one to choose depends on chemical and structural properties of the probe molecule and required orientation and density of the probes on substrates (Rusmini et al., 2007).

The functionality of a substrate can be established by coating with reactive polymers or direct activation of the substrate. Coatings of reactive polymers can be applied with several techniques such as dip-coating and spin-coating. The functionalization of the substrate decides about the binding strength of the probe to the surface. It is further important to gain an optimized density of functional groups for the immobilization of an adequate amount of probes with a good accessibility to the target, whereas low non-specific binding is required (Choi and Lee, 2011).

Glasses, plastics and metals are the most frequently applied substrates. Glass such as borosilicate, soda-lime or quartz, are chemical resistant, thermally stable, and show a low autofluorescence, which is important when working with fluorescence (Tao et al., 2007).

Electrostatic immobilization and adsorption belong to the group of physical immobilization techniques, which are based on intermolecular interactions of proteins with the surface such as electrostatic forces and hydrophobic or polar interactions (Rusmini et al., 2007). Physical immobilization is frequently applied for ELISA, western blot and protein microarray methods due to its simple implementation. In protein microarrays physical adsorption is especially used for the immobilization of large proteins. Nitrocellulose (Stillman and Tonkinson, 2000), poly-L-lysine (Haab et al., 2001) or hydrogels (Wang et al., 2002; Xu and Lam, 2003) are often used for this immobilization technique. Physically immobilized molecules are randomly or statistically oriented on the surface. Physically adsorbed molecules often suffer from weak binding and therefore an easy detachment from surfaces and finally a decrease in signal intensity (Liddel, 2005; Sutandy et al., 2013). Especially adsorption of molecules in randomly orientation can result in blocked binding sites or denaturation of proteins, due to hydrophobic interaction and loss of biological functionality (Gong and Grainger, 2007).

Immobilization of molecules using affinity is a chemically mild and reversible process especially for sensitive proteins such as receptors, and molecules are highly oriented. In nature the strongest affine and high resistant binding known is biotin-streptavidin with a KD

of 10^{14} M^{-1} and therefore often used in protein arrays (Narang et al., 1997). For instance (strept-)avidin is coated on the substrate, while biotin is conjugated to the recognition element/probe. Immobilization takes place after applying the probe complex on the substrate by interaction of biotin and streptavidin. Protein A and G (Anderson et al., 1997), chelators, calixarenes and DNA directed orientation and immobilization of molecules are other options (Xu and Lam, 2003).

Covalent immobilization of molecules to surfaces via binding between accessible side groups of amino acids of proteins and the functional groups presented at the surface. Table 5 shows the variety of functional groups, when dealing with proteins and their appropriate reaction partner. Glutaraldehyde- and epoxy- functionalized substrates are highly reactive against amines and form strong and stable bonds over wide temperature- and pH-ranges (Huy et al., 2011; Mateo et al., 2000a). Furthermore, epoxy reacts with sulfhydryl- and hydroxyl-groups. Its binding to the functional amino acids groups influences minimal the chemical structure of proteins (Mateo et al., 2000b). Covalent immobilized molecules are statistically oriented and can be even partly controlled by considering the surface pKa, the isoelectric point of proteins and the pH of the immobilization buffer (Hernandez and Fernandez-Lafuente, 2011). This immobilization strategy is preferentially used for small molecules and peptide microarrays (Xu and Lam, 2003).

Table 5: Functional groups of amino acids with interaction partner for probe immobilization (Rusmini et al., 2007).

Functional groups of amino acids	Surface functionalization
Amines-NH2	Epoxy Carboxylic acid Aldehyde Active ester (NHS)
Sylfhydryl-SH	Maleimide Epoxy
Carboxyl-COOH	Amine
Hydroxyl-OH	Epoxy

1.3.4. Immobilization of small molecules

There are a number of strategies for the immobilization of small molecules on solid supports such as glass. Low molecular weight probes are frequently conjugated to large macromolecules for instance bovine serum albumin (BSA) (Sun et al., 2009), oligonucleotides (Zuo and Ye, 2008), polypeptides (Baltzer, 2011) or polymer dendrimers

(Heegaard et al., 2009) to increase the access to the small molecule for the detection molecule by surface area enlargement.

In addition, molecules can be direct covalently bound to the surfaces via functional moieties. To conjugate the molecules to their carrier, functional groups such as amine (-NH_2), carboxyl (-COOH), sulfhydryl (-SH) or carbonyl (-CHO) are required (Köhn et al., 2003).

The coupling between large proteins and small molecules is frequently mediated by crosslinkers. 1-ethyl-3-(3-dimethylaminopropyl)carbodiimide hydrochloride (EDC) is one of the most frequently used. It forms active intermediates with COOH-groups and spontaneously reacts in a second step with primary amines. It is water soluble, which allows direct bioconjugation without preliminary organic solvent dissolution (Kluger and Alagic, 2004; Thermo Fischer, 2009). The choice of an efficient cross-linker is important due to its influence on the final binding behavior. There is a variety of cross-linkers on the market, with different spacer arm lengths or functional end groups (Kluger and Alagic, 2004). However, the choice is limited for small molecules with few functional groups especially molecules containing only hydroxyl- and hydrocarbyl-groups such as estradiol or bisphenol A. Annunziato et al., (1993) conjugated small molecules such as estradiol and progesterone to proteins using the heterobifunctional cross-linker p-maleimidophenyl isocyanate (PMPI). PMPI connects hydroxyl-containing molecules such as haptens via isocyanate groups to proteins with its sulfhydryl-reacting maleimide group. In addition hydrogels were used for the immobilization of small molecules such polyethylene glycol (PEG) with active esters for the immobilization or sol-gel (Ahn et al., 2012; Marsden et al., 2009).

1.3.5. Probe printing techniques

Protein microarray probes are transferred onto solid surfaces such as glass, plastic or metal by printing. The printing techniques are generally divided in non-contact and contact methods. Printing has to guarantee the transfer of hundreds of probes in pico- to nanoliter volumes onto the substrate with high reproducibility (Kricka et al., 2006).

Inkjet printing, aerosol jet printing, electro-hydrodynamic jet printing and dispensing printing belong to the group of non-contact printing techniques (Shin et al., 2015). These techniques are used for a variety of materials to replace expensive photolithographic processes or as non-surface-destructive technique for printing of sensitive molecules. A widely used printing method for delivery of biological molecules or cells is the piezoelectric inkjet printing technique. Droplets getting ejected through an applied current on a piezo element, which flexes and forces a droplet from a liquid reservoir out of a nozzle (Shin et al., 2015) (See: Figure 12A). These nozzles are most often made of glass or ceramic with different coatings,

to adapt to each probe viscosity or chemical properties of solutions. This printing type needs complex equipment and prints with high precision in micrometer range (5-150 µM), it is independent of surface material characteristics and most suitable for hydrogel and nitrocellulose surfaces (Ru et al., 2014a).

In contrast, contact printing deposits the probes on the substrate by direct contact. For this technique pins made of metal or silicon are used. The pins can be solid and require re-dipping after each print. Quilt and split pins contain a small probe reservoir allowing the deposition of several spots without re-dipping, whereas the pin determines spot volume and size (See: Figure 12 B). The split makes them also more susceptible for clogging. Between 50 µm and 500 µm spots can be printed with this technique by using smaller volumes than the non-contact printers. The spot size depends on the wettability of the surface, the print buffer composition, printing humidity and of course the size of the pin itself (Austin and Holway, 2011).

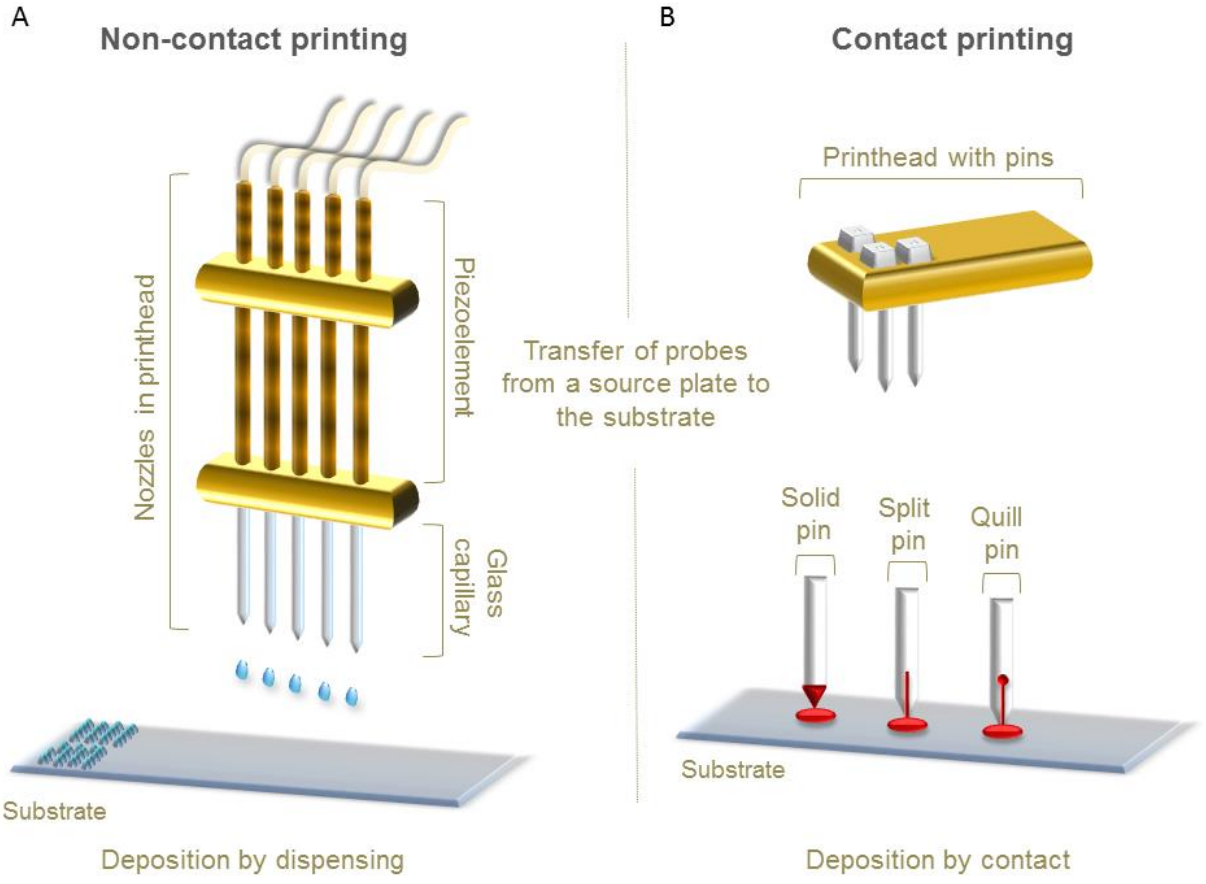

Figure 12: Principles of non-contact and contact printing. Non-contact printers dispense the probes without contact to the surface using nozzles. The dispensing of the probe is supported by a piezoelement contained in the nozzle (A). Contact printers despose the probe via contact to the surface using solid, split or quilled pins (B) (Austin and Holway, 2011; Ru et al., 2014b).

In consequence of a large surface-to-volume ratio, evaporation occurs during printing which influences the stability and activity of proteins by changes in concentration or pH (Wu and Grainger, 2006). In order to protect and stabilize the proteins on the chip, different print buffer compositions were developed. Components such as trehalose, sucrose or glycerol are hydroxylated and are therefore able to increase the stability of proteins by building of hydrogen bonds with water molecules (Lee and Kim, 2002). Detergents such as Tween 20, CHAPS or sodium deoxycholate are added in the print solution to avoid protein aggregation and to minimize denaturation or prohibit intermolecular interactions and enhance wetting of the chip surface (Choi et al., 2007; Domnanich et al., 2009).

1.3.6. Recognition elements – The capture molecules in immunoassays

Classic biological recognition elements such as antibodies, aptamers, proteins, peptides and small organic molecules, but also synthesized biomimetic probes such as molecularly imprinted polymers (MIPs) are used for the specific recognition of analytes in immunoassays (Hoff et al., 2010; Kricka et al., 2006; Menger et al., 2016; Rusmini et al., 2007; Witt et al., 2015). The decision for a recognition element depends on the research question and also on the availability on the market.

1.3.6.1. Antibodies

Antibodies, also known as immunoglobulins (Ig), are 150 kDa Y-shaped glycoproteins produced by immune cells as key proteins within the immune response of the body (Liddel, 2005).

They belong to the immunoglobulin superfamily and are made of structural units consisting of two large heavy and two small light chains (See: Figure 13). Due to their type of heavy chain, they define five different fragment constant (Fc) regions and therefore five isotypes in mammals. The main mammal isotypes are IgA, IgD, IGE, IgG and IgM with different locations and roles within the immune response (Maverakis et al., 2015). The structure of the different antibodies is quite similar. A small region of the light chains at the Y-tip is very variable, allowing millions of different antibodies to exist.

Antibodies recognize specific sequences of molecules, named the antigen, via their fragment antigen binding (Fab) region. The Fab region contains a paratope at each end of the y-shaped protein, which specifically recognizes and binds a particular epitope of the antigen (Schroeder and Cavacini, 2010). Due to their high affinity and specificity, they are applied as recognition elements in analytical methods such as enzyme linked immunosorbent assay

(ELISA) or protein microarray, in which monoclonal, polyclonal antibodies or antibody fragments are used (Leca-Bouvier and Blum, 2005).

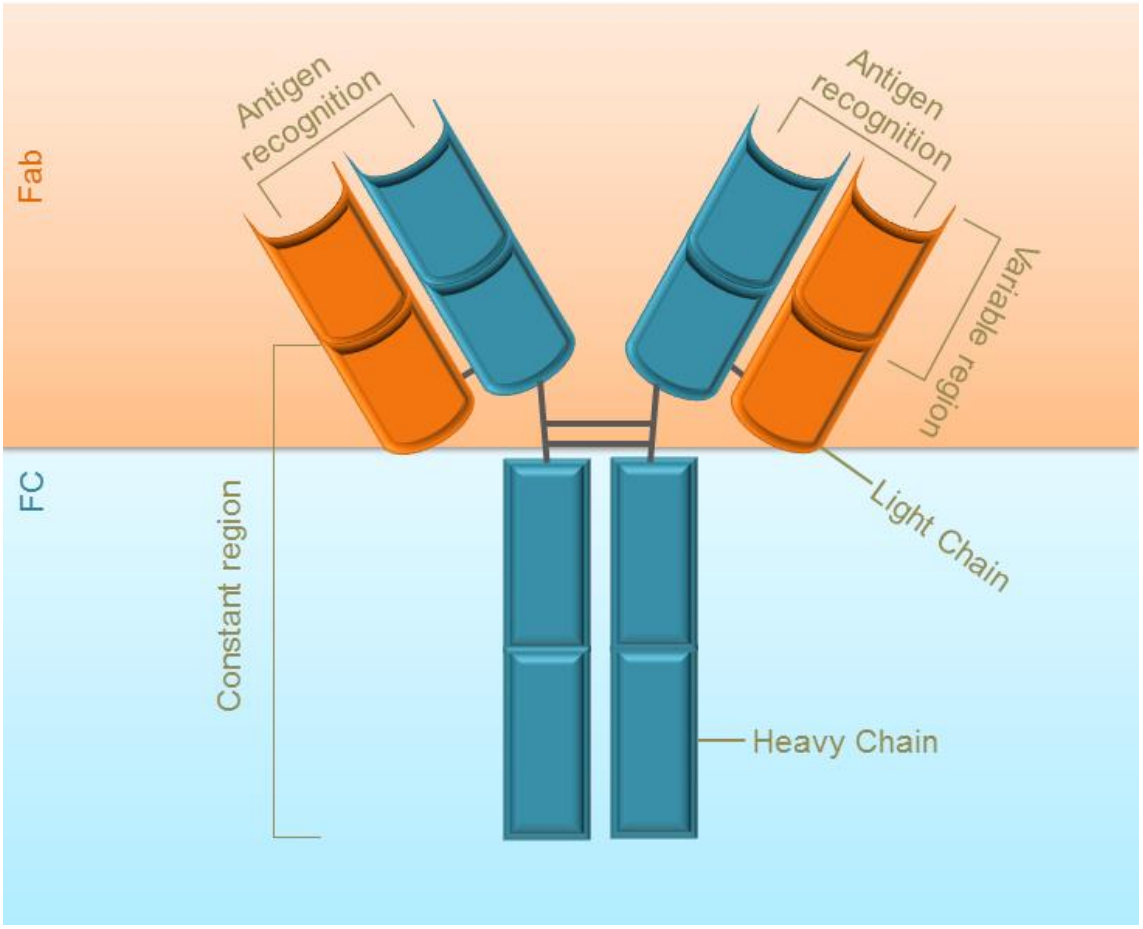

Figure 13: Structure of an IgG antibody. In general antibody monomers are divided into a Fab (fragment antigen binding) (orange) region with antigen binding sites and FC (fragment, crystallizable) region (blue) for cell interactions. They build of heavy (blue) and light (orange) chains, whereas the heavy chain defines the antibody class. Both consist of a variable (upper part) and a constant region (Schroeder and Cavacini, 2010).

The communication of the antibody with other immune cells is mediated via the Fc region, which is located at the base of the antibodies. The Fc region binds to specific Fc receptors on for instance immune cells, which are mediated by the glycan structure within the Fc region (Maverakis et al., 2015). The ability of binding to a specific receptor leads to a specific immune response. IgGs are the most common immunoglobulins in the body. They are highly abundant after immunization, have target affinities in the lower nM range and are very stable within the isolation and purification process. IgGs can bind two identical antigens to their two paratopes (Liddel, 2005).

Antibodies arrive via immunization of animals by an injected immunogen. Size and nature of the immunogen, exposure time and the recognition by the host as external molecule affect

the immunogenicity. Most potent immunogens are proteins and polysaccharides. Proteins with a molecular mass of 2000 g/mol or bigger are immunogenic, while smaller molecules, the haptens, have to be conjugated to carriers such as bovine serum albumin (BSA). Antigen-specific antibodies will then be produced by B-cells and secreted in the blood stream. The antibodies are afterwards isolated from the serum and purified mainly with Protein A or G (Liddel, 2005) .

Polyclonal antibodies derive from a heterogeneous mixture of antibodies, the polyclonal antisera, with varying binding affinities, specificities and isotopes. They recognize not only the epitopes of the immunogen, but also foreign matter. Polyclonal antibodies are fast and inexpensive to produce, whereas the purity of the immunogen and the purification of the serum influence the specificity of them (Liddel, 2005).

Monoclonal antibodies are produced by fusion of isolated B-cells from the spleen of an immunized animal and immortal myeloma cells, a technique developed by Köhler and Milstein (1975). As a result hybrid cells, the so called hybridomas are generated which have the ability to produce and secrete highly specific antibodies. After cultivation, the antibodies are obtained from the cell supernatant and can be further purified using the technique mentioned earlier. Due to their high specificity, monoclonal antibodies are usually preferred for immunoassays (Liddel, 2005).

1.3.6.2. Recognition via small organic molecules

Small organic molecules with a low molecular weight such as hormones, pharmaceuticals or toxins are not used very frequently as recognition elements for analytical protein arrays. They have typical lower binding affinities compared to the already mentioned capture elements, the antibodies. These low molecular weight molecules are normally more often implemented in functional assays to study molecule-protein interactions or drug target identification (Uttamchandani et al., 2005).

However, existing immunoassays for small molecules detection, especially estrogenic active substances such as bisphenol A (BPA), nonylphenol and atrazine are commonly based on competitive, binding inhibition or direct assay formats and are frequently applied for food or environmental samples (Feng et al., 2009; Ju et al., 2011; Lu et al., 2012).

1.3.6.3. Bisphenol A as recognition element

The organic synthetic compound bisphenol A (4,4'-(propane-2,2-diyl)diphenol, BPA) is a 228.29 g/mol big molecule and belongs to the group dimethylmethane derivates and bisphenols. It contains two hydroxyphenyl groups (See: Figure 5, Page 17) and is soluble in

organic solvents and less in water. BPA is used as a plasticizer for polycarbonate and epoxy resins and can be found in customer products such as water bottles, CDs, sports equipment or as coatings in cans containing food or beverages. Heat treatment of especially food or beverage packing material can result in leaching of BPA into the food or beverages (Geens et al., 2012). BPA attracted the attention, because of its estrogen-mimicking characteristics. It can bind to the estrogen receptor, due to structural similarities to estrogen and disrupt the function of the natural hormone (Vandenberg et al., 2009). It affects thyroid, pancreas, immune system, reproductive tract and brain function and is associated with diseases such as obesity, diabetes, cardiovascular dysfunction as well as with hepatotoxicity and neurotoxicity (Rubin, 2011). The reference dose, a recommended benchmark for BPA uptake per day and kilogram body mass is 0.005 mg. This level of exposure was defined by the European Food Safety Authority (EFSA, 2014) as dose without adverse health risks (Sun et al., 2016).

Due to its estrogenic and health affecting properties, several analytical methods for the detection of BPA in food and environmental samples have been developed for instance chemical-based and biologically-molecule based sensors (Ragavan et al., 2013). Especially a number of immunoassay techniques (e.g. ELISA and immunochromatographic assays) were applied because of high specificity and sensitivity, simple sample preparations and the possibility for high throughput (Sun et al., 2016).

Existing immunoassay techniques for the detection of low molecular weight molecules such as BPA and other EDCs are mainly based on competitive formats, because of low amounts of epitopes compared to macromolecules. This assay format is based on antigen or antibody based immobilization on a solid surface. The antigen is commonly immobilized hapten-protein complex. Large proteins such as BSA and ovalbumin (OVA) are conjugated to the hapten to ensure better epitope presentation at the surface and prevent sterically hindrance (See: Table 6) (Feng et al., 2009; Lu et al., 2012). Feng et al., (2009) could show that they achieved better assay performance with direct immobilization of the Bisphenol A derivate 4,4-bis(4-hydroxyphenyl) valeric acid compared to the hapten-protein conjugates. They concluded that conformational changes of the protein resulted in lower sensitivities (Feng et al., 2009).

Conjugation can be a very expensive process and parts of the hapten-protein conjugate can cross-react with the antibodies used in the assay, due to similarities in the antibody production, what lead to false positive results(Tijssen, 1985; Van Weemen and Schuurs, 1975).However, recently Ahn et al., (2012) used sol-gel for the immobilization of BPA on a solid surface and verified it by specifically interaction with a labeled aptamer.

Table 6: Overview of indirect competitive ELISAs for the detection of bisphenol A with immobilized conjugates, LODs and detection range of the assay (indirect refers to detection via primary and secondary antibody).

Immobilization of BPA	LOD [ng/mL]	Detection range [ng/mL]	Reference/ Company
BPA (not specified)	10	1000–10	(Antibodies-online, n.d.)
4,4-bis (4-hydroxy phenyl) valeric acid	0.27	157.60 -2.30	(Feng et al., 2009)
BPA-valerate-BSA conjugate BPA-acetate-BSA	0.10	10-0.1	(Lu et al., 2012)

1.3.7. Sample preparation, calibration and matrix effects

Several analytical techniques require sample preparation such as purification, filtration, and concentration of analytes especially for food or environmental matrices. Depending on the matrix, protein microarray sample preparation can be avoided or reduced even by for instance dilution with assay buffer (Sauer et al., 2012).

Serial dilutions of analytes, with a known dilution factor are the basis for the quantification of the analyte in the unknown sample. By this the generation of an external calibration curve can be performed, where the curve shows the relationship between signal and concentration of the analyte. Assays based on ligand binding are often described by a nonlinear correlation using a 4-Parameter-Logistic-Fit, which results in a sigmoidal shape of the calibration curve (Findlay and Dillard, 2007). The following equation describes the 4-Parameter–Logistic-Fit:

$$Y = D + \frac{A - D}{1 + \left(\frac{X}{C}\right)^{B}}$$

The Y displays the signal, D and A the signals for lower and upper plateau, B the slope factor, X the concentration and C the inflection point described as half maximal effective concentration (EC)50 or inhibitory concentration (IC)50 (See: Figure 14).

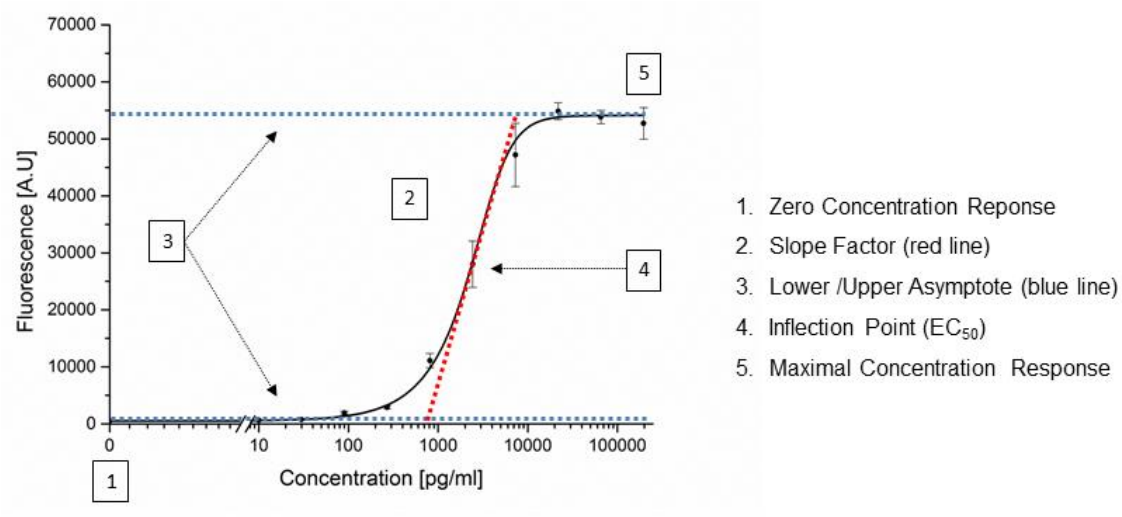

Figure 14: Sigmoidal calibration curve using the 4-parameter logistic fit is shown. Here the curve of a sandwich immunoassay is pictured and is characterized by a positive correlation between fluorescence signal and concentration (Davies, 2013).

For complex matrices such as blood, plasma, salvia and tissue extracts, this calibration type can be inaccurate due to effects appearing by the matrix (Skoog et al., 2007; Wood, 1991). These so called matrix effects are caused by changes of antibody binding, extent of non-specific binding or alterations of analyte concentration (Davies, 2013). Sources of interference for tissue and cell culture based application involve: enzymes, denatured analyte and medium components. However, in immunoassays impurities of detergents in assay buffers as well as buffer additives such as proteins may also show unwanted interferences on the assay performance (Wood, 1991).

1.3.8. Parameters for evaluation of assay performance

The evaluation of assay performance under different conditions can be determined by different parameters and calculated via a calibration curve and raw data. Coefficient of variation (CV), recovery rates, limit of detection (LOD), limit of quantification (LOQ) and cross-reactivity are common parameters used for that (See: Table 7) (Armbruster and Pry, 2008; Davies, 2013).

The calculation of CVs and recovery rates assess assay precision and accuracy, whereas precision is interpreted as inter-assay repeatability and accuracy as inner-assay recovery of a reference standard (See: Figure 15). Recovery rates are obtained by quantification with calibration curves and should be in a range of 70-130% (Sittampalam et al., 2016).

Table 7: Parameter for the evaluation of assay performance with description and equations (Armbruster and Pry, 2008; Davies, 2013).

Assay parameter	Evaluation	Description	Equations
LOD /LLOD	Analytical Sensitivity /Detection Limit	Lowest analyte concentration to reliably distinguish from blank values	LLOD=mean blank+(3xSD)
LOQ/LLOQ	Functional Sensitivity/ Quantification Limit	Lowest analyte concentration for reliable quantification	LLOQ=mean blank+(10xSD)
Recovery	Accuracy	Spiked concentration vs. measured values	$\%Recovery=\frac{Calibrated\ Concentration}{Nominal\ Concentration}x100$
CV	Precision	Reproducibility	$\%CV=\frac{SD\ mean}{mean\ signal}x100$
Cross-reactivity	Selectivity	Distinguish between analytes	$\%\ cross\text{-}reactivity=\frac{Concentration\ of\ analyte}{Concentration\ of\ cross-reactant}x100$

LOD and LOQ describe analytical and functional sensitivity of an immunoassay. The LOD is the lowest concentration measured that can be reliably distinguished from a blank signal and the LOQ the lowest concentration that can be reliably quantified. They are calculated via the mean of signals measured from blank value and its standard deviation.

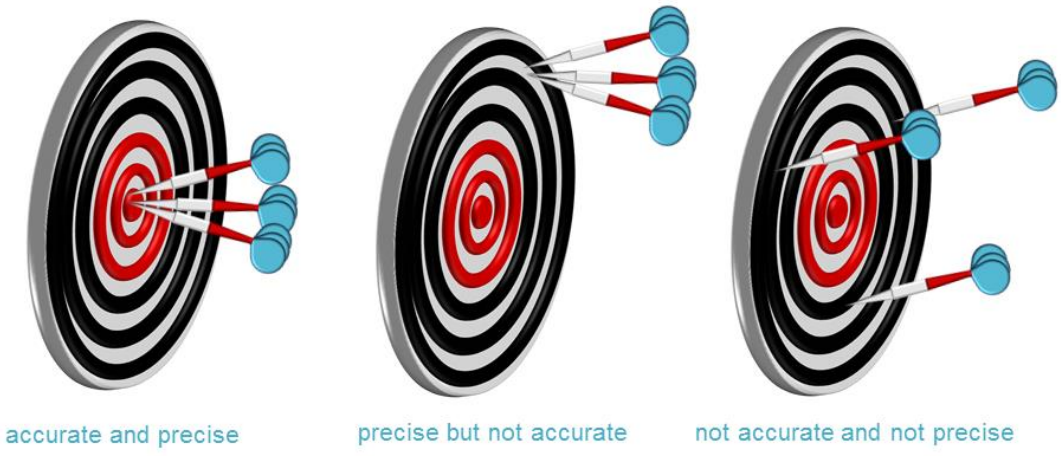

Figure 15: Accuracy versus precision. Accuracy describes how close the measured value to the spiked value is. Precision how reducible the measurement is. Pictured adapted from https://apchemcyhs.wikispaces.com.

Another important parameter in the evaluation of immunoassays is the cross-reactivity of antibodies interacting with other molecules then the analytes due to structure similarities. It characterizes the selectivity of an assay and can be examined and expressed in different ways. One method for determining the cross-reactivity is spiking of structure related molecules in the chosen matrix containing the analyte and measuring the binding to both, capture and detection antibody. The binding of the cross-reactant can interfere therefore in a positive way, resulting in increase or in a negative way by a decrease of signal (See: Figure 16). However the cross-reactivity can vary over the concentration range of an assay. This can be seen especially for polyclonal antibodies (Davies, 2013).

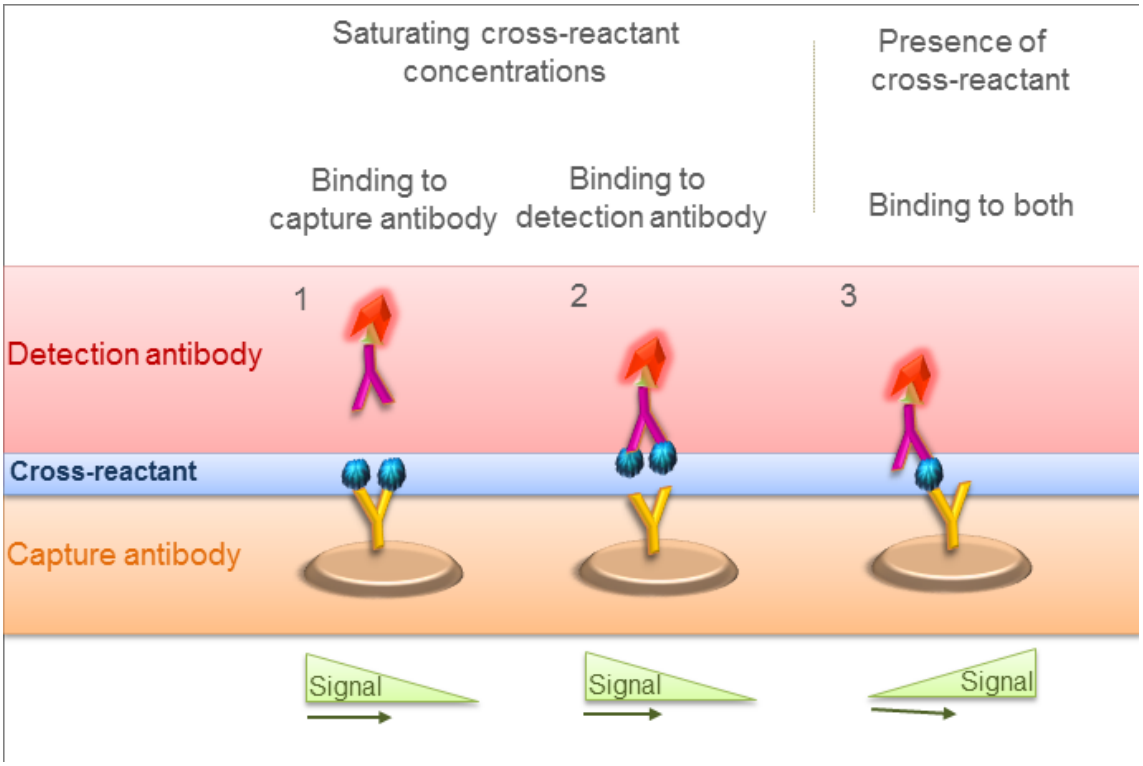

Figure 16: Ways of cross-reactivity in sandwich immunoassays. 1) Binding of cross-reactant to capture antibody blocks detection antibody binding. Decrease of signal intensities. 2) Binding of cross-reactant to the detection antibody blocks binding to endogenous analyte on capture antibody which result in a decrease of signal intensities. 3) Binding of cross-reactant to capture and detection antibody shows an increase of signal intensities.

1.3.9. Sensing methods

The interaction of antibody-antigen complexes can be measured via label–free or label based techniques. They differ in sensitivity, applicability, costs and instrumental equipment (Syahir et al., 2015).

A label describes a molecule which depending on the detection method, is reversibly or irreversibly conjugated to the sensing molecule for detection of molecular interaction or

presence. Prominent representatives for label containing methods are: fluorescence, colorimetry, chemiluminescence or radioactivity. Labeled especially optical methods are commonly used for protein microarrays, because there are more suitable for high throughput and more sensitive (Syahir et al., 2015).

Label-free sensing methods measure molecular biophysical properties for instance molecular weight or refractive index. Surface plasmon resonances (SPR), quartz crystal microbalances (QCM) or microcantilevers are frequently used. Furthermore label-free techniques are applied for real time monitoring of binding events or molecular kinetics and provide therefore additional information compared to the labeling. However they are described to be less sensitive or specific (Ray et al., 2010) and to some extent not suitable for high throughput (Syahir et al., 2015).

1.3.9.1. Label-based techniques: Fluorescence

Fluorescence is the most frequently used detection method in the field of microarrays. The labels for fluorescence detection are fluorophores, quantum dots or fluorescent proteins such as the green fluorescent protein (GFP) and its derivatives. They can be attached to the detection element in a direct or indirect way. Direct labeling refers to the covalent conjugation of the label to the antibody. Indirect labeling techniques using a tag on the antibody such as biotin, which mediates the interaction with the streptavidin conjugated fluorophores (Giepmans et al., 2006). Fluorescent labels are stable, easily to manipulate and ensure good sensitivity and resolution (De Silva et al., 1997).

Fluorescence, a subtype from luminescence occurs when an atom or molecule adsorbs light with a specific wavelength and emits it with a longer wavelength. Through the absorption of photons, an electron of the molecule gets promoted from the ground state (S_0) to a singlet short-lived (fluorescence: 10^{-9}-10^{-7}s) excited state (S_1). While returning of the excited electron to the ground state, it emits a photon of lower energy. The electron loses energy due to vibrational relaxation under excited conditions (See: Figure 17A). Therefore the emission of the photon corresponds to longer wavelengths and lower energy levels compared to the adsorbed one. The shift to longer wavelengths is defined as Stokes shift (See: Figure 17B), larger shifts result in better distinction of the peaks (Jabłoński, 1933; Williams and Bridges, 1964).

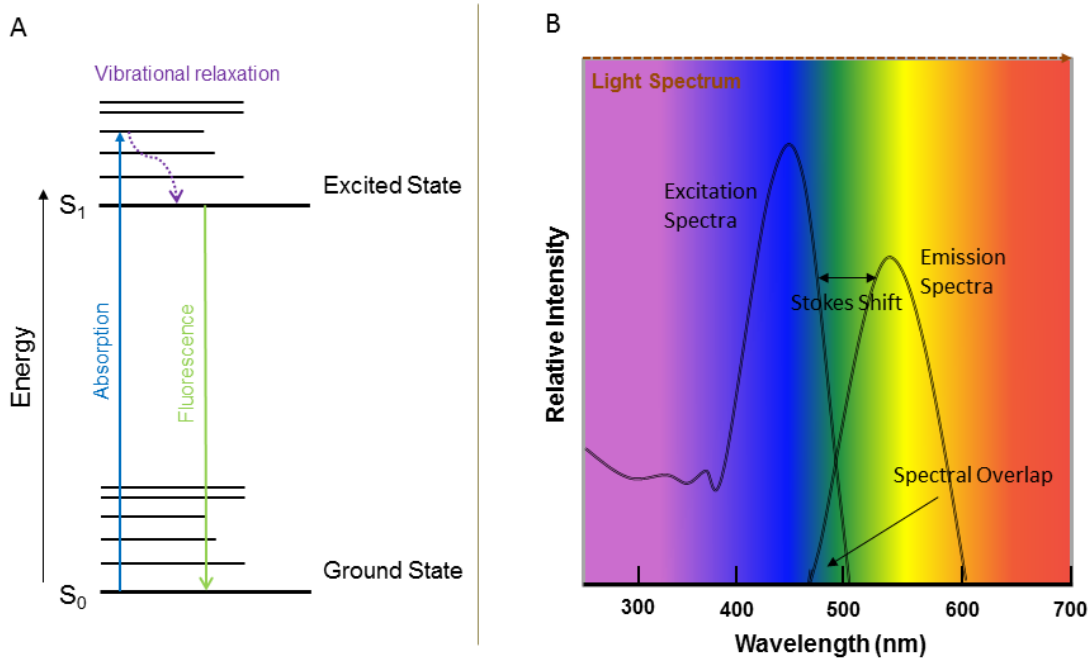

Figure 17: Jablonski diagram ((Jabłoński, 1933) picture adapeted) of fluorescence pictures the shift of an electron from the ground to an excited state due to absorption. The electron loses energy due to vibrational relaxation in the excited state and returns back to the ground state. There it emits photons (Fluorescence) with lower energy and longer wavelengths (A). The shift is called Stokes shift (B).

The emission efficiency of a fluorescent molecule is the quantum yield (Φ). It is defined as ratio of emitted to adsorbed photons and can give therefore additional information about the fluorophore brightness and the efficiencies about energy transfer processes (Würth et al., 2013). A spectrum of fluorophores from blue-violet to infrared wavelengths is commercially available. The specific excitation and emission wavelengths are molecule or atom dependent. Fluorescent molecules are normally conjugated systems. In protein microarrays organic fluorescent probes such as the sulfoindocyanines Cy3 (Lamda $(\lambda)_{ex}$ 552 nm/ λ_{em} 570; Φ = 0.15) and Cy5 (λ_{ex} 650 nm/ λ_{em} 670; Φ = 0.28) are preferred due to their high stability over pH ranges and their biocompatibility, but suffer from photobleaching and quenching (Delon et al., 2010; Ekins and Chu, 1991).

Modulation of fluorescence emission occurs due to various factors like pH, specific chemical environments and temperature. This modulation process is called quenching. It is characterized as static and dynamic quenching. Static quenching describes the reaction of a fluorophore and a quencher to a non-fluorescent complex. Dynamic quenching refers to the interaction of the fluorophore such as collisions with other atoms in the excited state. Next to quenching, also photobleaching can influence the fluorescence by irreversible destruction of the fluorescent probe. It is caused for instance by too high or long excitation times. In protein

microarrays quenching can be triggered by short-range interactions of fluorophores, due to too high densities of fluorescent labels (Ogawa et al., 2009).

1.3.10. Readout and image analysis of protein microarrays

There are several readout devices, the so called microarray readers from different companies commercially available, such as the GenePix™ 4000 B array scanner from Axon Instruments or the confocal laser scanner LS100 from the Tecan Group Ltd..

There are either confocal and non-confocal scanners or imagers such as CCD cameras. In general, scanners contain one or more lasers for different excitation wavelengths and sequential or simultaneous dual-fluorophore scanning. Furthermore these scanners consist of an optical system with objective and detector lenses and mirrors for high quality imaging, appropriate emission filters for particular fluorophores and a photo multiplier tube (PMT) as a detector for conversion of optical to electrical signals and for amplification of the signal (See: Figure 18) (Cheung et al., 1999; Dixon and Damaskinos, 2001).

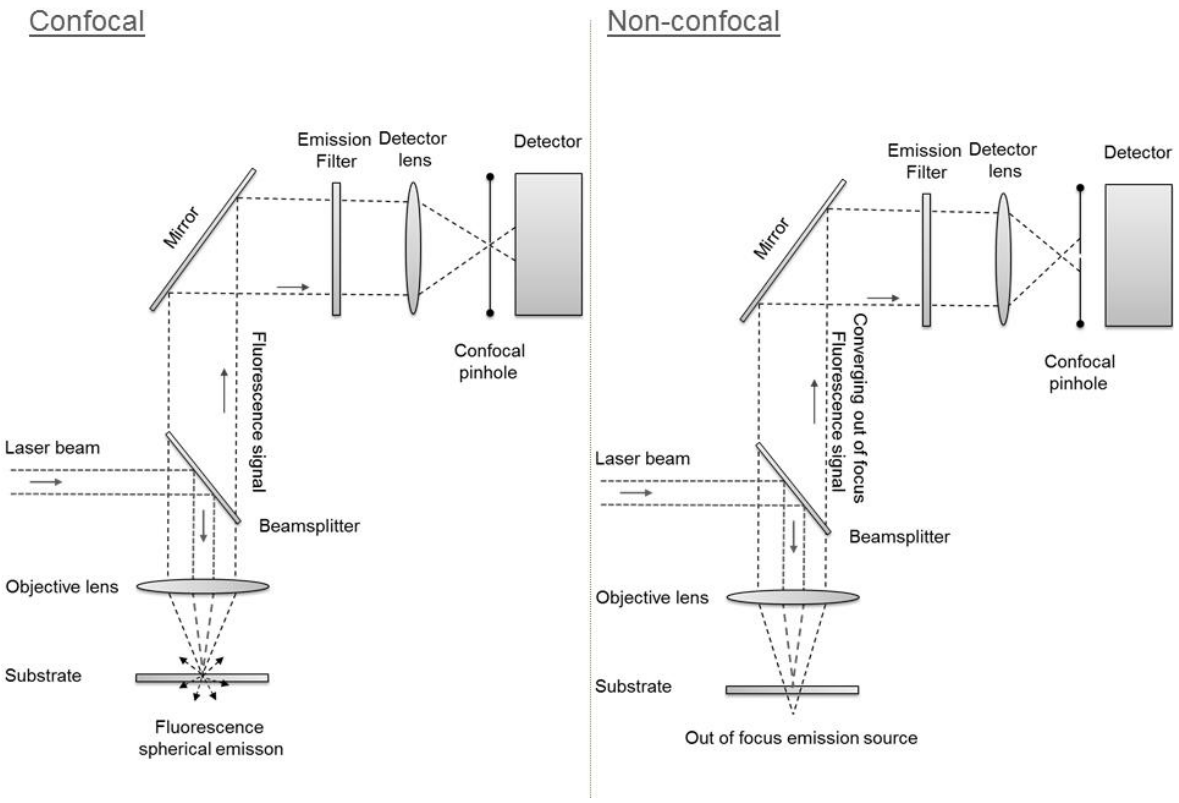

Figure 18: Principles of confocal (right) and non-confocal (left) laser designs. Confocal systems reject signals from out of plane, whereas non-confocal all signals get captured. Therefore non-confocal images contain more information from outside the focus plane. Picture adapted from (Core Life Science, 2012).

The advantage of confocal scanning is the reduction of out-of-focus fluorescent light through a pinhole, which results in an increase of the optical resolution and the contrast of images. However, the correct plane of focus may be difficult to find. Only thin focal depths can be reached with confocal scanners, which limit the light collection. In non-confocal scanning, all photons get captured. The entire sample gets irradiated evenly with light and excited at the same time, which result in high signal quality and good signals. However it also creates background noise in the image of the array. Since, specifically and un-specifically bound molecules are in one plane, confocal detection within microarray readout is not necessary (Cheung et al., 1999).

After readout, the generated images get analyzed by image analysis software, such as GenePix® (Axon Instruments, Inc., CA, United States). Via alignment and segmentation of each spot in the array, the spot location, the quality (flags), the spot intensity as well as the background intensity can be numerically determined (See: Figure 19). For the alignment, GenePix® Array List (GAL) files are used which contain printing parameters and probe positions. The obtained raw data are further analyzed with statistical software (Díez et al., 2012; Inc, 2010).

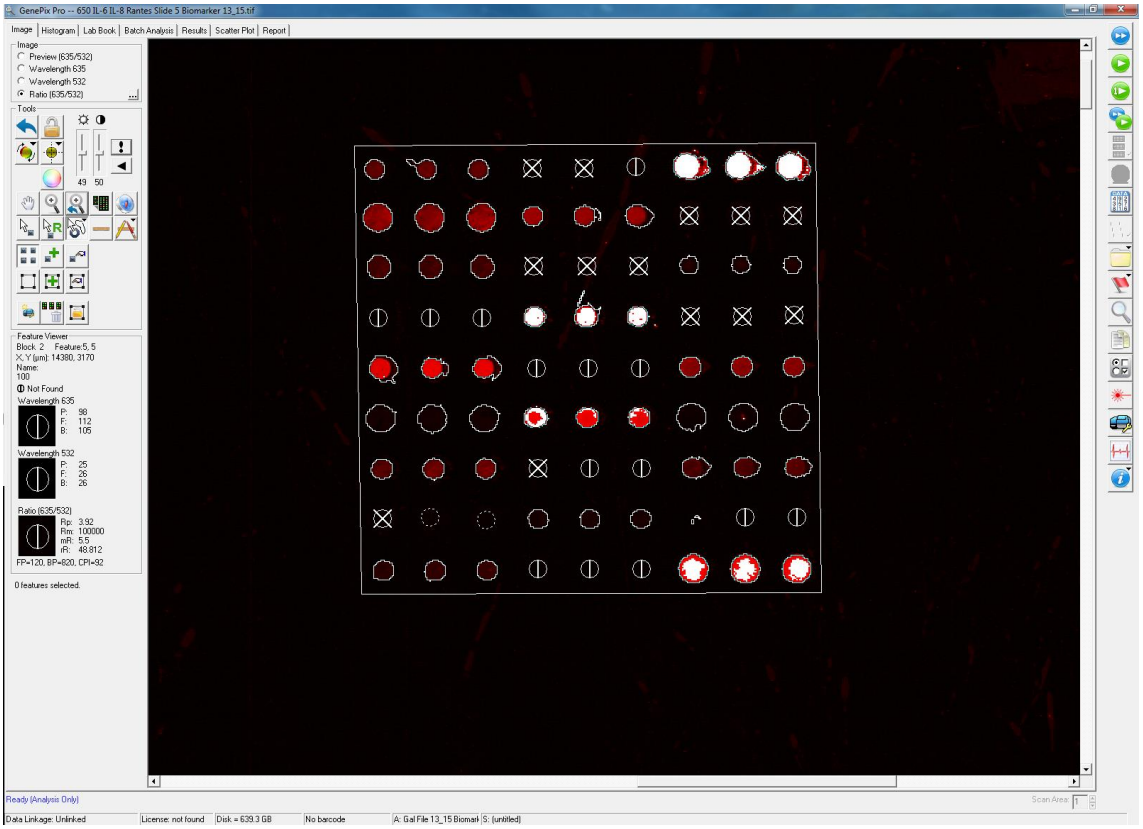

Figure 19: Alignment and spot segmentation of a protein microarray using GenePix®. Each spot can be evaluated with different flags (white surroundings, stripes or crosses). Flags decsribe the quality (presence, absence, bad) of the spot signal and are consequently used for analysis.

1.4. Cell assays- *in vitro* test systems predicting human toxicology

The importance of *in vitro* toxicity test systems increased over the last decades, especially to reduce and replace *in vivo* methods (McKim Jr., 2010). *In vitro* cell based methods were first limited to genotoxic properties of a substance and were further expanded to *in vitro* screening tools for the early assessment of potential hazardous chemicals or drugs, affecting several specific biological functions in cell and in tissue culture. The culturing of cells arriving from different organs is the most frequent method in toxicology (Ekwall et al., 1990).

General toxicity studies which focus on the determination of the biological activity of xenobiotica such as viability, proliferation and cytosolic enzyme release can be executed with a broad range of cells (e.g. HeLa, fibroblasts, hepatoma cells). Specialized cells are recommended when organ-specific effects are tested (e.g. substances with effect on adipocytes differentiation, hepatocytes for liver metabolism, macrophages phagocytosis) (Ekwall et al., 1990).

Primary cells are freshly isolated cells for instance from sections or surgeries. Primary cells offer properties which are close to original tissue and in general more sensitive to toxic effects by substances, due to adaption on culture conditions. However they are more heterogeneous compared to cell lines, have a short lifespan, are more susceptible to contamination and it is difficult to obtain reproducibility, but they should be applied when cell lines are not available. In contrast to primary cells, cell lines such as cancer cell lines are spontaneously or specifically immortalized for permanent passaging. Cell lines are more standardized, well characterized, easy to cultivate and homogenous what results in higher reproducibility. Through the high number of passages cell lines can differ strongly from the original tissue, due to genotypic and phenotypic changes. However, which cell culturing model to apply depends on the specific scientific question (Pan et al., 2009; Roggen, 2011).

A lot of *in vitro* test systems used for toxicological hazard assessment are tests for the acute toxicity, so the adverse effect arriving by single or multiple exposures to a substance in a short period. A prominent cell based method to evaluate acute toxicology is the measurement of cytotoxicity. Measurements of cytotoxicity can give additional information about membrane integrity, cell metabolism, ATP content, cell number or cell proliferation depending on the technique used. These test systems are recommended as pre-screening tools for the determination of initial doses for reduction of the number of animals taken in *in vivo* experiments (NAS, 2015).

However, monoculture assays show limitations in the determination of bioacculmulation, adsorption, distribution, metabolism and excretion (ADME). They give no information about

developmental stages or cannot show tissue specific effects when they rely on transfected receptors. Actually a test battery of multiple cells types, co- and 3D cultures with the priority on primary cell lines are needed to replace or reduce *in vivo* experiments (Roggen, 2011; Schug et al., 2013).

1.4.1. Proliferation assays

There are several methods predicting cell viability, such as protease activity, detection of ATP content and metabolic salt reduction. These assays are used to screen for cytotoxic effects of compounds, effects on the proliferation and the viability of cells**.** The reduction of salts for instance tetrazolium and resazurin as well as the measurement of protease activity display cell metabolism or the activity of enzymes for estimation of cell viability and proliferation (Riss et al., 2013).

This chapter will focus especially on proliferation assays based on metabolic resazurin reduction and its advantages and disadvantages compared to the related and commonly used tetrazolium assays.

The 3-(4,5-dimethylthiazol-2yl)-2,5-diphenyl tetrazolium bromide (MTT) assay was a long time the state of art within cell proliferation and cytotoxicity assays. However, due to several drawbacks such as cell death caused by the intracellular formed formazan crystals, cell lysis and dissolving of the formazan crystals before measurements, new reagents or tetrazolium salt derivates (e.g. WST, XXT, MTS) were applied (Präbst et al., 2017).

The blue non-fluorescent redox indicator resazurin (7-hydroxy-10-oxidophenoxazin-10-ium-3-one), also known as, Almar blue, Vybrant or UptiBlue is cell membrane permeable and gets intracellularly reduced to the pink colored and red fluorescent resorufin. The conversion to resorufin by the mitochondrial NADH/NADPH dehydrogenase requires the reductants NADH or NADPH (See: Figure 20). Compared to tetrazolium salt assays which allow only less sensitive colorimetric detection, resazurin assays enable additional fluorescence measurements at 560 nm excitation and 590 nm emission wavelengths using a conventional plate reader (Vega-Avila and Pugsley, 2011).

In general, resazurin based assays are easy to perform, inexpensive, suitable for high throughput, applied for cells growing in suspension, adherent cells and 3D cell culture and show low inter-well variability (Präbst et al., 2017; Squatrito et al., 1995; Uzarski et al., 2017). Furthermore resazurin was described being nontoxic and does not destroy the cells to receive results, as in all other tetrazolium variants (O'Brien et al., 2000; Präbst et al., 2017; Vega-Avila and Pugsley, 2011). This enables a reuse of the cells and therefore in addition

simultaneously measurements of other cell parameters (Präbst et al., 2017). However, Squatrito et al., (1995) reported that incubation times over several days were cytotoxic for ovarian cancer cells.

Through its solubility in physiological buffers, this reagent is more suitable for cell experiments compared to the often used tetrazolium salt based MTT assay. MTT has to be solved in organic solutions such as dimethyl sulfoxide (DMSO) and can affect therefore the cells (Vega-Avila and Pugsley, 2011). However, new derivates of the MTT salt such as XXT, MTS or WST are water soluble but need extra electron carriers for their reduction due to their large cell impermeability (Präbst et al., 2017). Resazurin assays show higher sensitivity than the similar reported tetrazolium based variants. Already 50 cells per well can be detected using resazurin. In order to generate distinguishable signals, the stain has to incubate one to four hours in the cell medium (Niles et al., 2008). The sensitivity is depending on the metabolic activity of the cell type and experimental parameter (e.g. pH, resazurin concentration, temperature) (Präbst et al., 2017) . The generated signal is proportional to the number of viable cells, whereas dead cells are not able to convert it any longer. The reduced form of resazurin stays up to ten days very stable in CO_2 buffered cell medium (O'Brien et al., 2000), and little concentrations are needed to obtain detectable signals compared to other related methods (Vega-Avila and Pugsley, 2011).

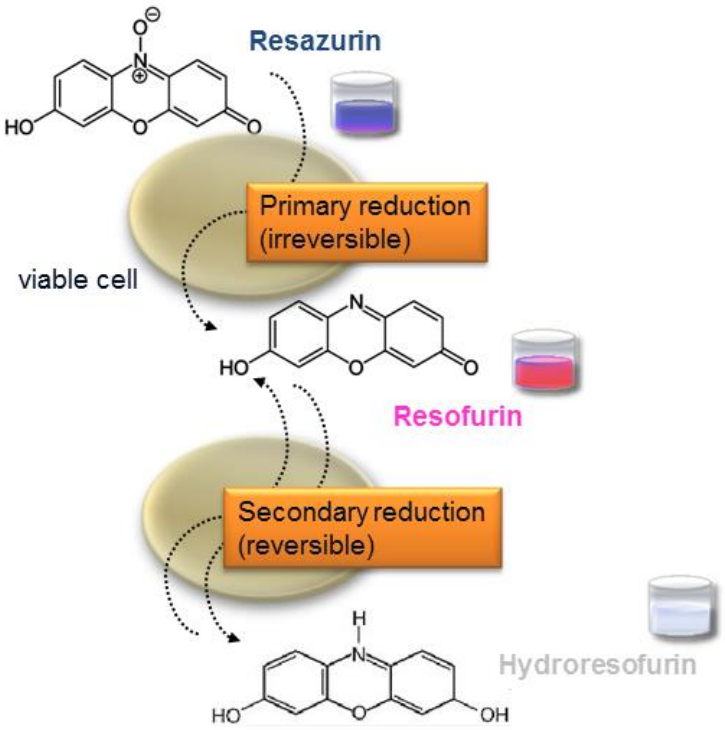

Figure 20: Intracellular reduction of the sodium salt resazurin to resofurin and finally hydroresofurin. Picture adapted and changed from Gier et al., (2017).

Resofurin can be further reduced to the colorless non-fluorescent and toxic hydroresofurin, which leads to false negative results. In order to avoid over-reduction of the substance, the reduction rate of the cells should be controlled and stain concentration and incubation time have to be optimized for experimental conditions (O'Brien et al., 2000; Präbst et al., 2017). Furthermore cross-reactivity of resazurin with test compounds, especially direct effects on the fluorescent signal was reported, which can result in overestimation of survival or underestimation of toxicity. Therefore it was recommended to add the stain after the incubation with a test substance (O'Brien et al., 2000).

1.4.2. Cell culture media

Human or animals cells can be cultured in naturally biological fluids such as plasma or artificial basal media (Dulbecco´s Minimum Essential Medium (DMEM), Roswell Park Memorial Institute (RPMI) medium) supplemented with cell type specific growth factors. The usage of natural media results often in poor reproducibility, because of unknown or different media compositions. Artificial media containing nutrients, salts, O_2 and CO_2 gas phases, serum proteins, carbohydrates and other cofactors in different specified amounts to maintain survival, growth and specialized functions of the cells (Arora, 2013; Kerbel and Blakeslee, 2006).

Artificial media can be divided into four groups: i) Serum containing media, ii) serum-free media, iii) chemically defined media and iii) protein-free media. Serum containing and serum-free media are the most frequently applied media (Arora, 2013).

The addition of serum mostly from animals such as fetal bovine serum (FBS) in media is very common for cell culture applications. The serum contains chelators or carriers for nutrients, hormones, protease inhibitors and growth factors for optimal culture conditions. Depending on the type of cells, 5-20% serum in the media is used (Arora, 2013).

However, the components of serum are very complex, undefined and show lot-to-lot differences (See: Table 8). To avoid the disadvantages such as misinterpretations of cell studies for hormone active substances of serum containing media, several serum-free media were developed. These media are cell type specific formulated with defined amounts of different purified growth factors like the epidermal growth factor (EGF) and fibroblast growth factor (FGF), lipoproteins, attachment factors and other supplements normally provided by the serum (Barnes and Sato, 1980a).

Commonly commercially available media contain the pH-indicator phenol red for continuously surveillance of the pH in the medium during cell growth. Due to differences in

pH in the medium, the color can change from yellow for low acidic pH to lilac for high basic pH. However, the optimum for cell growth, pH 7.4 is appearing in red. There are disadvantages using phenol red in the cell culture: i) it is known to act as a weak estrogen active substance, what makes it unsuitable for experiments with hormone sensitive cells such as MCF-7 (Berthois et al., 1986), ii) it can interfere the sodium-potassium homeostasis in serum-free media and 3) it affects flow cytometric detection (Arora, 2013).

The choice of the right cell culture medium and its composition is very important for the optimal growth of cells and for successful cell culture experiments. Its composition has to be experimental determined for each cell type (Arora, 2013).

Table 8: Advantages and disadvantages of serum-supplemented cell culture (Arora, 2013).

Advantages serum supplemented media	Disadvantages serum supplemented media
Variation of growth factors, nutrients and co factors for optimal cell growth	Lot-to-lot composition differences
Cell attachment factors (e.g. fibronectin)	Lot-to-lot testing to ensure same quality
Spreading factor	Possibly contains inhibition factors for growth
Buffering agent	Risk of contamination
Binding and transport proteins	Interference of purification and isolation of secreted proteins
Decrease damage by mechanical perturbation through viscosity	Contents (e.g. hormones) interfere in cell studies

1.5. Microfluidics

Microfluidics is a multidisciplinary research area involving chemistry, physics, biotechnology, biochemistry, engineering and nanotechnology and already exists since the early nineties. The main idea of microfluidics is to implement several analysis tools in one chip, which require normally an entire lab and therefore it refers to micro total analysis systems (µTAS) or lab-on-a-chip (LoC) technologies (Manz et al., 1990; Reyes et al., 2002; Sackmann et al., 2014). The basis of microfluidics is the manipulation of fluidics in volume ranges from micro-

to femtoliter in chips containing micrometer-sized channels (Whitesides, 2006). The fundamental physics of fluidics at the microscale differ from the macroscale. For example, gravity forces are strongly reduced at microscale whereas surface tension, fluidic resistance and capillary forces dominate. A very important parameter is the flow regime in micro channels (Beebe et al., 2002). The flow regime of a fluidic in a channel is defined by the Reynolds number and can be either laminar or turbulent. The Reynolds number, a dimensionless quantity, is the ratio of inertial- to viscous forces and defined by the following equation:

$$R_e = \frac{\rho v L}{\mu} = \frac{v L}{\nu}$$

where:

ρ = fluid density [kg/m³]

v = velocity [m/s]

L= the characteristic dimension [m]

μ = dynamic viscosity [Pa/s or Ns/m^2 or kg/ms]

ν = kinematic viscosity [m²/s].

Reynolds numbers lower than 2000 indicate laminar flow and above 3000 turbulent flow. The laminar flow dominates in microfluidic systems, due to micrometer dimensions of the channels and is characterized by mass transport via diffusion due to no convective mixing (Sackmann et al., 2014).

1.5.1. Materials for microfluidic cell culture applications

Common materials used to produce microfluidic devices are categorized into three groups: polymers, inorganic materials (glass, silicon, ceramic) and paper. Polymers are further subdivided into thermal or UV curable thermosets and thermoformable materials (Roy et al., 2016). All materials mentioned below are biocompatible and so far used for cell culture applications. The choice of the most suitable substrate is always depending on the respective application or method used (Halldorsson et al., 2015; Paul M. van Midwoud et al., 2012).

Within the thermal curable polymers, polydimethylsiloxane (PDMS) is the most used one. It is biocompatible, transparent, elastic, gas permeable, easy to use for fast fabrication of high numbers of chips at low costs (Whitesides, 2006). However this material ages which limits its performance over years. It is not compatible with a number of organic solvents, it recovers

hydrophobicity, un-crosslinked oligomers can leach out and it can adsorb small hydrophobic molecules and water vapor which can be released during experiments and makes this material inapplicable for some applications (Berthier et al., 2012; J. N. Lee et al., 2003; Regehr et al., 2009; Toepke and Beebe, 2006). Modifications of PDMS with paraffin waxes, parlyene or glass coatings can enable adsorption of molecules and increase chemical resistance (Abate et al., 2008; Berthier et al., 2012; Regehr et al., 2009; Ren et al., 2010).

The negative epoxy-based photoresist SU-8 is mostly applied for making molds, but additionally taken as adhesive and cell growth platform (Nemani et al., 2013; Yu et al., 2006a). It becomes a very mechanically, chemical and thermally stable material after UV exposure due to the very strong binding of the epoxy group network. However it is a quite brittle material once it is cured and so hard to handle and transfer (Roy et al., 2016).

Rolland et al.,(2004) developed a UV curable perfluoropolyether (PFPE) with low toxicity, low surface energy and high chemical resistance. This long-term stable perfluorinated polymer is oleophobic as well as hydrophobic and highly inert. PFPE microfluidic devices can be easily produced by photolithography (Roy et al., 2016). Schulte et al., (2010) additional showed that PFPE is a suitable material for cell culture and tissue engineering.

Polystyrene (PS), polymethylmethacrylate (PMMA) and polycarbonate (PC) belong to the thermoformable polymers and are increasingly used for microfluidic applications as well as for conventional cell culture dishes (PS/PC). They are especially used when rigidity or thermal resistance are required. These polymers are moldable after heating and therefore also recyclable, deformable and offer optical transparency (Roy et al., 2016). However bioactive compounds can leach out of the materials and strongly effect experimental outcomes (Grzeskowiak and Gerke, 2015; Watson et al., 2009) by for instance inhibition of human enzymes as shown by McDonald et al., (2008).

Silicon, one of the first materials used for microfluidic applications, is thermal conductive, not transparent and solvent compatible. In contrast to silicon, glass is additionally chemically inert, hydrophilic, high-pressure resistant, has a superior optical transparency and allows sufficient coatings. Its properties make it the most appropriate material for many applications (Hou et al., 2017). Besides this the introduction of valves is difficult to achieve in glass devices, when compared with materials such as PDMS (Ren et al., 2013; Sackmann et al., 2014). The raw material of glass is rather high cost than the other materials and the chip production is time-consuming (Ren et al., 2013; Sackmann et al., 2014).

One of the cheapest materials used in microfluidics is paper. It provides advantages such as its thinness, lightweight, it is easy to manipulate and to transport, but it is difficult to introduce

channel patterns, applicable detection methods are limited to the matrix properties and it is not suitable for large sample volumes (Akyazi et al., 2018).

1.5.2. Microfluidic device fabrication methods

Several techniques are applied for the production of microfluidic devices like soft lithography, micromachining (laser based techniques, etching, micromilling) injection molding, hot embossing, and the quite new and still progressing technique 3D-printing. Each technique shows limitations and advantages over the other. The choice of the appropriate fabrication method depends on the subsequent application and the material used (Beebe et al., 2002; Chen et al., 2016; Faustino et al., 2016). Table 9 shows an overview of the fabrication methods and suitable materials for each technique.

Table 9: Microfluidic device fabrication methods with appropriate materials for each technique (Beebe et al., 2002; Chen et al., 2016; Faustino et al., 2016).

Fabrication Method	Materials
Micromachining	
Mechanical: e.g. micromilling	Ceramics, metals, silicon, polymers
Ablation: e.g. laser based techniques	Ceramics, polymers, glass
Dissolution: etching	Glass, quartz silicon, ceramics, polymers
Soft Lithography	UV- and thermo-curable polymers
Hot embossing	Thermoformable polymers
Injection molding	Thermoformable polymers
3D-printing	Thermoformable polymers

However, one of the most prominent and common used method is soft lithography, due to fast and inexpensive fabrication of devices. Soft Lithography was developed in the year 1974 at Bell Labs is based on molding of soft materials such as the two-part polymer PDMS (elastomer and curing agent) from photolithographic masters. In general, it was used to pattern surfaces by elastomeric stamps (micro-contact printing) or fabrication microstructures by molding or embossing (Abdelgawad et al., 2008; Beebe et al., 2002; Faustino et al., 2016; McDonald and Whitesides, 2002).

Typically it refers to master production by photolithography and replication molding using PDMS (Beebe et al., 2002; Duffy et al., 1998; Wolfe and Whitesides, 2005). The master is produced by spin-coating of photoresist onto a glass wafer. Most commonly layers of the negative photoresist SU-8 are applied for PDMS applications (Del Campo and Greiner, 2007). Channels and other structures are introduced by UV exposure of the master using a mask containing the desired structures. As a consequence of the UV treatment the exposed parts get cross-linked, whereas the rest remains soluble and will be washed away while developing (Duffy et al., 1998). The resolution of the structures is dependent on the mask and can reach nanometer ranges (Faustino et al., 2016; McDonald and Whitesides, 2002).

Figure 21 pictures a typical microfluidic device production process using PDMS. Liquid PDMS is cast onto a master and cured by heat. The PDMS replicas are easily to remove from the master and can be bond to each other or materials such as glass by plasma treatment. Soft lithography is described as more suitable technique for most biological applications compared to micromachining. However, the mold production usual needs cleanroom facilities and can be quite cost intensive (Beebe et al., 2002; Faustino et al., 2016; Whitesides et al., 2001).

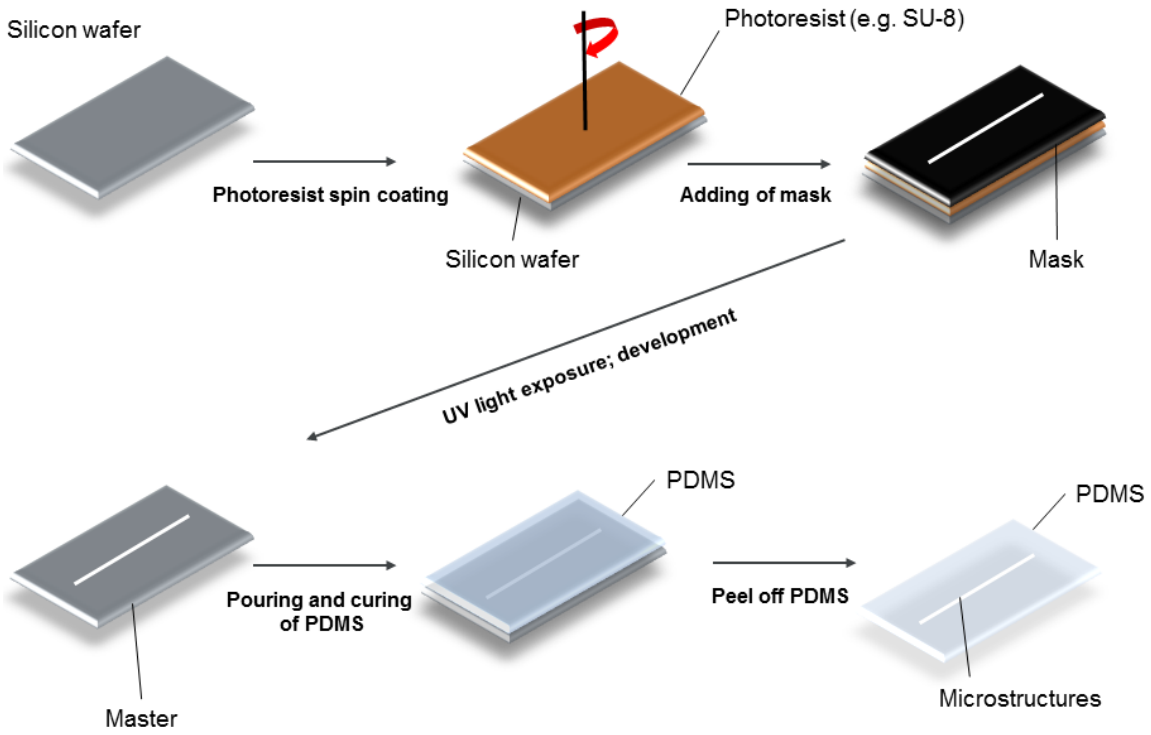

Figure 21: Scheme of production of a microfluidic device out of PDMS using soft-lithography.

Glass microfluidic devices are fabricated by micromachining techniques such as wet etching, laser based techniques or micromilling. These techniques are costly and require specialized skills and equipment but providing higher precision compared to other techniques (Faustino et al., 2016). Especially hard materials such as glass, silicon, metals and stiff polymers are used within micromachining (Faustino et al., 2016; Iliescu et al., 2012).

To pattern the substrate, photolithography in combination with etching (wet or dry) or laser ablation is used. Frequently borosilicate or soda lime glasses are applied. The production of a glass device requires a photolithographic mask, which is coated with for instance a chromium layer to enhance the adhesion and gold or an alternative photoresist such as AZ®. Due to UV-exposure, the positive photoresists form indene carboxylic acid at the exposed parts which can be washed away by alkaline solutions within the development (See: Figure 22) (Iliescu et al., 2012; Leester-Schädel et al., 2016; Lin et al., 2001).

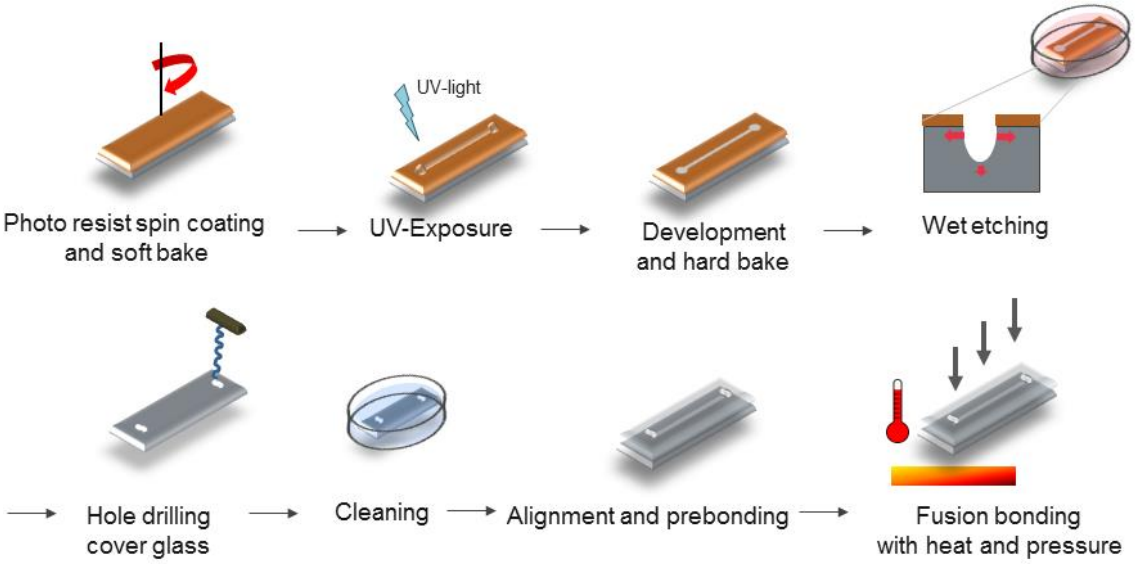

Figure 22: Production process of microfluidic devices made of glass using a positive photoresist, wet etching and fusion bonding.

In order to introduce structures in the glass surface, the developed wafers get etched. Pattering by wet etching is isotropic and commonly done with hydrofluoric (HF) solutions. Depending on the glass composition used, the etching behavior differs (C. Iliescu et al., 2008). Especially glasses with high oxide content affect the etching process through reaction with HF to insoluble products such as CaO, MgO, and Al_2O_3. However, HCL or H_3PO_4 can be added to the etching solution to remove them (Berthold et al., 2002; Iliescu et al., 2005). Additional, the etch rate differs with the glass composition (for Corning 7740 around 8 µm/min) and can be increased by heat, ultrasonic agitation or by annealing of the wafers and

reduced by dilution of the HF solution (Williams et al., 2003). Dry etching is used, when anisotropic etching profiles are needed. Compared to wet etching, dry etching is slower with etching rates of 0.5–0.7 µm/min (Iliescu et al., 2012). Laser ablation (with e.g. high-intensity femtosecond laser) describes the removal of the material based on absorption of photons, which is depending on the material specific wavelength. For this method pulse duration and energy, as well as translation speed, and repetition rate are relevant parameters. They can affect the quality of the generated structures (Giridhar et al., 2004; Leester-Schädel et al., 2016; Sugioka and Cheng, 2011; Tiggelaar et al., 2007).

Glass slides can be bonded via directly (fusion and plasma activated bonding) or indirectly via aniodic and adhesive bonding (e.g. SU-8, parlyene), whereas direct bonding is more advantageous due to the compatibility for medical and chemical application without influences of other substances (Iliescu et al., 2012; Leester-Schädel et al., 2016).

For the direct bonding the glass surface has to be very clean. The bonding process is based on intermolecular interactions. In order to bind glass with glass the substrates have to be aligned and pre-bond. The pre-bonding is reversible and is based on Van der Waals forces and the binding of OH-groups. The glass substrates become irreversible bonded after application of heat (above 800 °C for BOROFLOAT® 644 (Jellema et al., 2009)) and pressure under formation of silicon-silicon and silicon- oxygen bonds (Leester-Schädel et al., 2016).

1.5.3. 3D cell culture

Compared to the conventional 2D monolayer cell culture, 3D cell culture pictures better the morphological and functional properties of real tissues. *In vivo,* cells interact in a complex network with neighboring cells and with components of the extracellular matrix (ECM) via chemical and mechanical signals. These interactions are important for normal cell functionality, while cells grown in 2D cultures can lose tissue-specific properties (Pampaloni et al., 2007).

In the last decades numerous 3D cell culture models have been develop to overcome the disadvantages of 2D cell based assays and reduce therefore the number and costs of animal experiments within drug screening processes. One of the most frequently applied 3D Model in biomedical research is a freshly dissected tissue explant from animals, which is maintained *in vitro*. However, its acquisition is difficult and ethical approval is needed for removal and use. The specimen samples are several millimeter in size, which influences strongly the mass and gas transport to the center of the tissue and results in a transitory nature of them. As alternative to tissue explants, simple to prepare 3D culture models can be

used with tissue dimensions of 100-500 µm to improve mass and gas transport (Lin and Chang, 2008; Pampaloni et al., 2007). Several mammalian cells are able to self-assemble into 3D multicellular spheroids (MCS) through culturing in suspension or on non-adhesive surfaces, which was first demonstrated by Holtfreter, (1944) and Moscona and Moscona, (1952).

The spheroid formation was described by Lin and Chang, (2008) for hepatoma cells as a three-step process (See: Figure 23) and can be further applied to other cell types. A rapid aggregation of cells via integrin-ECM binding to form loose cell aggregates is the initial step. The second phase, the delay phase, is characterized by an increased E-cadherin expression and accumulation. The cell adhesion molecules bind to each other in the last phase with the result of tightly bonded cells and compact MCSs (Lin et al., 2006).

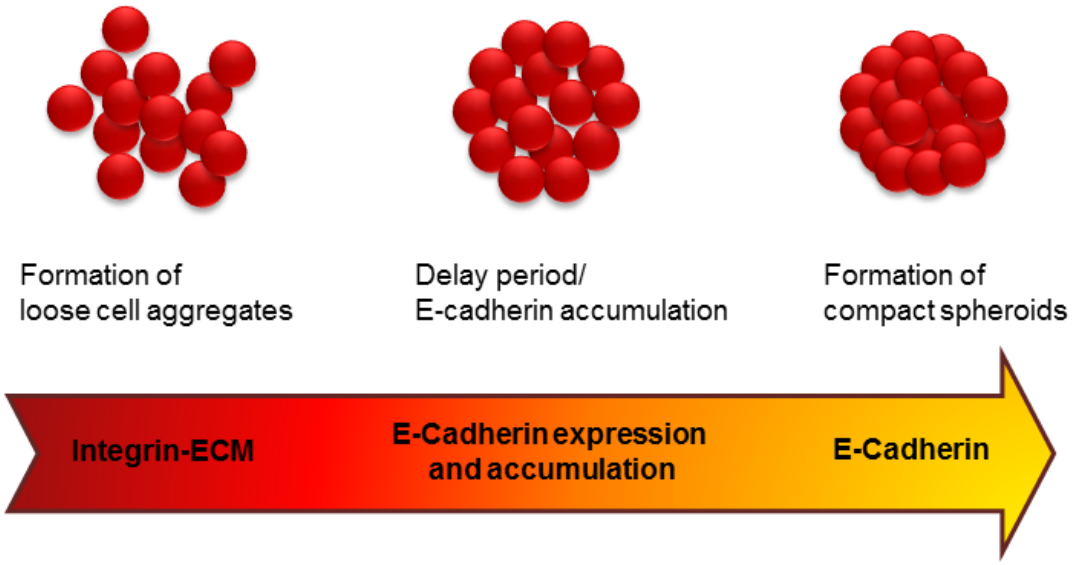

Figure 23: Spheroid formation process proceeds in three steps (Lin and Chang, 2008).

A MCS shows similar properties as avascular cell tissue. The bigger the dimensions, the more the diffusion for many molecules is limited. The inefficient transport of nutrients and O_2 results in accumulation of metabolic waste in the MCSs. MCSs with diameters above 200-500 µm are characterized by layer-like structures (See: Figure 24). The center is composed of a necrotic core surrounded by a layer of viable quiescent cells, which is in turn surrounded by a layer of proliferating cells (Alvarez-Pérez et al., 2005; Moshksayan et al., 2018).

Droplets of 15-30 µL volume with a density of approximately 300-3000 cells are mostly used. Depending on the cell type used, the MSC formation can differ. Some cells only form loose

aggregates. Therefore medium components such as collagen and fibronectin can be used to improve and strengthen the MSC formation (Lin and Chang, 2008).

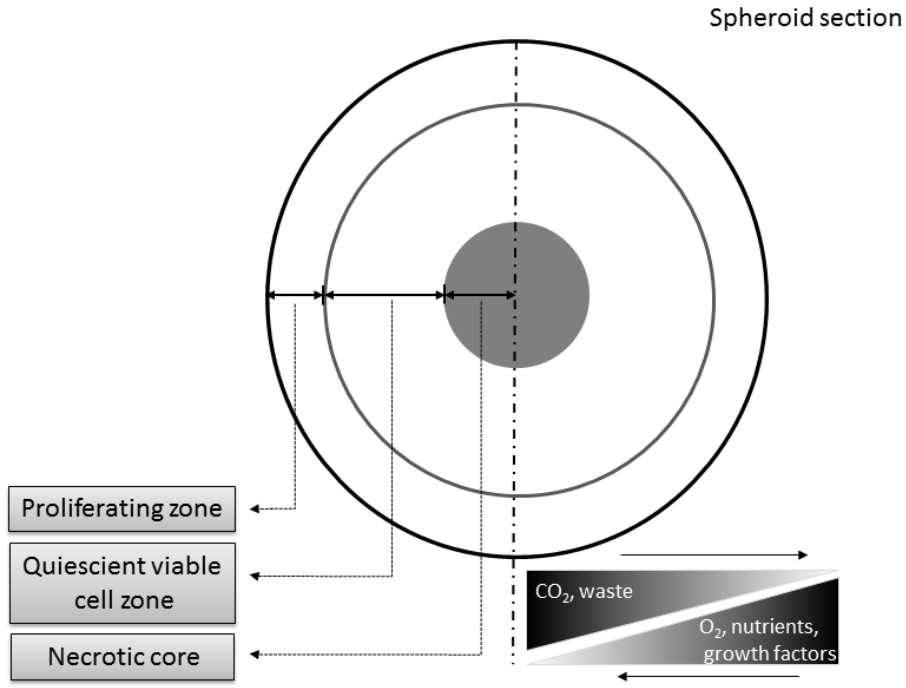

Figure 24: Microenvironments inside a spheroid according Lin and Chang, (2008). The layer like structure results in insufficient transport of CO_2 and waste out of the MCS and an inadequate supply of O_2, nutrients and growth factors.

Once formed, the MCSs are used in cancer research as avascular tumor models for the determination of metastasis and invasion processes or for dose-response studies. Through the 3D assembly viability and functional performance can increase, what makes them also ideal for tissue reconstruction (Achilli et al., 2012).

1.5.4. Microfluidic spheroid culture

The implementation of microfluidic techniques revolutionized 3D cell culture, which is frequently used for biomedical applications such as drug discovery and development, toxicity, protein studies or tissue engineering (Gupta et al., 2016). The flexibility in the production of micro-fabricated structures or devices allows mimicking microenvironments close to *in vivo* conditions by microscale dimensions equals the human body and creates the possibility to supply chemical gradients. In addition, gas permeable materials are used to support cell growth and proliferation. The possibility of microscale device production and the integration of several techniques in one chip lead to a high automatization of lab applications

from controlled cell seeding to continuously medium perfusion, sampling and finally direct real-time, on-chip analysis (Gupta et al., 2016; Halldorsson et al., 2015).

Different methods for the generation of microfluidic multi-cellular spheroids have been developed over the years. All of them own advantages and disadvantages with respect to production, cellular physiology and application field (Achilli et al., 2012; Cui et al., 2017; Lin and Chang, 2008). General criteria for selection of the most suitable method were described by Lin and Chang, (2008) and include: ”production efficiency, MSC size uniformity, possible damage or influences on cellular physiology, convenience and suitability for subsequent applications”, being the prevention of cell adhesion to the culture substrate as the main requirement. In general, microfluidic 3D cell generation platforms are categorized by the substrate used for production such as glass/silicon-based, polymer-based and paper based systems (Gupta et al., 2016). However, developed microfluidic spheroid culture techniques are grouped in structure-, physical- and chemical-based generation techniques, such as microwell structures, emulsions, gravity, rotation, digital microfluidics and porous membranes, whereas microwell structures are the commonest used (See: Table 10) (Moshksayan et al., 2018).

The frequently applied microwell technique utilizes U-, concave- or flat-shaped geometries to enable single and compact spheroid generation of uniform size in a short period (Moshksayan et al., 2018) with exception for flat bottom wells (Ruppen et al., 2014). Therefore cells get trapped out of the cell suspension in these structures. Cells, which do not got trapped, are rinsed out of the chip to avoid clogging (Chen et al., 2015; Lei et al., 2013; Patra et al., 2016). Micro molding or soft lithography can be used to produce microstructures with defined forms and dimensions from non-adhesive materials such as polyethylene glycol (PEG) or PDMS (Gupta et al., 2016; Moshksayan et al., 2018). This technique provides simple and easy to use platforms (Anada et al., 2012; Fukuda and Nakazawa, 2005; Okuyama et al., 2010).

Droplet flow generators are used within the emulsion approach. The technique provides a high throughput generation of uniform sized cell droplets with frequencies of 50 droplets per second, but long formation times (Kim et al., 2011; Moshksayan et al., 2018; Tomasi et al., 2013). Droplet generation frequency and diameter can be adjusted by the flow rate. Different liquids are applied for the cell encapsulation such as cell suspension in oil emulsion and cell-hydrogel (e.g. collagen, alginate) solution in oil (Hong et al., 2012; Sabhachandani et al., 2016; Schmitz et al., 2009; Wang and Wang, 2014; Yoon et al., 2013). Hydrogels create a protect zone for the encapsulated cells against shear stress. Generated cell containing droplets are trapped in microwells for spheroid formation under medium supplementation.

The trapping process was reported to be insufficient, as only half of the generated droplets were caught and they coalesced and clogged the channels (Moshksayan et al., 2018).

In addition, porous non-adhesive membranes in microfluidic devices were applied for the generation of spheroids in mono- and co-cultures (Hsiao et al., 2009; Kuo et al., 2012). The membranes are positioned between two channels and the introduced cells self-assemble to spheroids through the non-adhesive nature of the membrane. The spheroid size can be controlled by adjustment of the channel size or their geometry. However, generated spheroids vary in size (Torisawa et al., 2007).

The technique for the fastest formation of spheroids is the micro rotation flow method. Therefore, cells rotate in a cylindrical micro chamber with two tangential positioned in- and outlets to mediated the formation of spheroids within 120 seconds, but with high size variations (Ota et al., 2011).

The hanging drop method is based on spheroid formation by gravity in a medium droplet on the bottom edge of a microwell (Frey et al., 2014). In comparison to the mentioned techniques the hanging drop method shows the smallest size distribution with short spheroid formation times (Moshksayan et al., 2018). In addition, it is more sufficient for high throughput screenings than the other methods mentioned (Frey et al., 2014; Moshksayan et al., 2018; Wu et al., 2016).

The state of the art technique is digital microfluidics. Pico- to microliter droplets are handled by magnetic fields, electrostatic forces or optical actuation with negligible consequences on the viability, morphology and gene expression of cells (Abdelgawad and Wheeler, 2009; Au et al., 2014; Bogojevic et al., 2012; Choi et al., 2012; García et al., 2007; Yoon et al., 2013). However, this technique suffers from evaporation, discontinuous perfusion, complexity in control and fabrication as well as in biofouling (Choi et al., 2012; Ng et al., 2015).

In general, the growth of spheroids larger than 300-500 µm in diameter over long periods is limited by insufficient oxygen and nutrient supply to the center of the spheroid, which subsequently influences experimental outcomes (Inamdar and Borenstein, 2011; Wan et al., 2016). The implementation of micro-bioreactors or perifusion chambers with automated oxygen-triggered feedback loops or gas permeable membranes for spheroids as well as tissue culture improved the oxygen supply and therefore decreased the necrotic core. This enabled culturing of spheroids up to 17 days and spheroid sizes of 600 µm (Anada et al., 2012; Cui et al., 2007; Van Midwoud et al., 2010; Volkmer et al., 2012; Wan et al., 2016).

Table 10: Microfluidic spheroid culture techniques (Achilli et al., 2012; Cui et al., 2017; Lin and Chang, 2008).

Generation method	Advantages	Disadvantages
Microwells (U-, concave-, flat-bottom)	Simple to perform Well-controlled spheroid size Designed aggregate geometry Co-cultures	Limitation for high throughput Trapping efficiency depending on configuration of microwells Spheroid escape off the wells
Emulsion based	Well-controlled spheroid size High throughput droplet formation	Long formation times Partly gelation necessary Clogging at low flow rates Droplet coalescence Droplet anchorage insufficient
Porous membranes	Well-controlled spheroid size Good cell trapping Enable biological studies Co-cultures	Treatment of membranes Size variation of spheroids
Micro rotation	Fast spheroid formation	Variation in size and shape Large volume flow rates
Hanging drop	Simple to perform Well-controlled spheroid size Fast spheroid formation High reproducibility Controlled environment Co-cultures Easy to trace spheroid assembly High throughput	High evaporation
Digital microfluidics	No valves or pumps Droplet merging, mixing Dilutions	Biofouling Evaporation Discontinuous flow Complex fabrication and control

After formation, spheroids are analyzed on- or off-chip. Frequently used methods are the microscopy techniques such as confocal or fluorescence for the discrimination of death or viable cells by cell stains and for the evaluation of spheroid morphology and size. In addition, the collected cell supernatant is used for the evaluation of metabolic activity after treatment using colorimetry or luminescence based assays and measured in plate readers. Image

processing software (e.g. ImageJ) can be used for size measurements and evaluation of viable and death cells (Moshksayan et al., 2018). The size and shape of spheroids can be described by different parameters such as diameter, circularity, roundness, aspect ratio or volume (Aijian and Garrell, 2015; Chen et al., 2014; Frey et al., 2014; Takashimizu and Iiyoshi, 2016).

1.5.5. The hanging drop method

The hanging drop method was first established for the cultivation of embryoid bodies and is based on spheroid formation by gravity and surface tension in a medium droplet deposited at the bottom of a culture dish. The gravity pushes the cells to the bottom of the droplet and single MCSs are formed in each droplet at the liquid-air interface, reaching 100% size reproducibility (Gupta et al., 2016; Kelm et al., 2003). Hanging drop devices without microfluidic liquid support are limited by lab intensive exchange of cell medium from each droplet. The change of the medium is difficult and can affect the spheroid formation (de Groot et al., 2016). Channel-well networks, on the other hand, enable automatized cell perfusion and high throughput organoid culture without effects on its formation (Wu et al., 2016). Furthermore, they offer access on spheroids with the focus on further sampling due to the open network. Spheroids can be transferred by pipettes or by surface tension via contact to a flat surface for further analysis (Frey et al., 2014). Besides that, these platforms can be used to control cell co-cultures in their chip allowing screening of tissue–tissue interactions (Frey et al., 2014).

Frey et al., (2014) were the first, who developed a microfluidic supported hanging drop network made of PDMS and glass with an integrated concentration generator suitable for high throughput screening of spheroids up to 300 µM in diameter after drug exposure. This network contains 4 parallel positioned rows of channels where up to 6 droplet wells are connected in series via one open-bottom channel to the inlet and outlet. Through that design, they were able to prevent cell adhesion and avoid bubble formation. Nevertheless, this design is limited by droplet radii, channel resistance and mechanical perturbations (Frey et al., 2014). Later also Wu et al., (2016) and Saeed R Yazdi et al., (2015) presented interconnected droplet networks, which differ in design, well number and perfusion type (See: Table 11).

Materials used for hanging drop devices are polystyrene, glass with or without coatings and PDMS, whereas the latter predominates (See: Table 11). Perfusion of the droplet was applied by pressure driven, pneumatically driven, surface tension driven, hydrostatic pressure driven flow and by capillary forces (Aijian and Garrell, 2015; de Groot et al., 2016; Frey et al., 2014; Wu et al., 2016; Saeed R Yazdi et al., 2015). Depending on the way of

perfusion and the channel-well design chosen, the droplet volumes and flow rates vary. Systems with single channel-well designs are capable of working with volumes up to 60 µL per well and flow rates of 1 mL/min compared to channel-well networks with volumes between 0.26 to 14 µL per well and 0.8-5 µL/min (See: Table 11) (de Groot et al., 2016; Frey et al., 2014; Wu et al., 2016). Due to lower droplet volumes, the shear stress, provided by the medium perfusion at the spheroid, is higher and limits thereby the flow rate (Frey et al., 2014).

Table 11: Overview of microfluidic hanging drop platforms and their characteristics.

Material	No. droplet well	Well diameter [mm]	Channel design	Perfusion	Single drop volume [µL]	Flow rate	Ref
PDMS-glass	≥24	3.5	Serial	Pressure driven	14	1-5 µL min^{-1}	(Frey et al., 2014)
PDMS	10	3.5	Serial in a loop	Pneumatically driven	14	~0.8-2.2 µL min^{-1}	(Saeed Rismani Yazdi et al., 2015)
PDMS-glass	72	1	Serial	Hydrostatic pressure	~0.26	≥147 N/m²	(Wu et al., 2016)
Glass-silicone-coating	≥8	2.5	Single wells	Capillary forces	7-55	100-115 V_{pp}AC/ 18.5 kHz	(Aijian and Garrell, 2015)
Polystyrene	8	4.25 (4)	Well pairs	Surface tension driven	~60	1 mL min^{-1}	(de Groot et al., 2016)

2. Aim of the thesis

The main aim of the work herein was to develop high throughput tools for detecting and analysing EDCs and its action in environmental samples with a special focus on estrogen active substances. The following steps are included in the thesis:

- the establishment of serum-free MCF-7 cell culture as a central part of the tool. Analysing the effects of hormone active substances asks for a hormone free environment.

- the integration and establishment of a proliferation assay based on metabolically conversion of resazurin for the discrimination of agonistic and antagonistic action at the estrogen receptor. Due to agonistic action MCF-7 cells proliferate, whereas antagonistic action blocks this response.

- the development of a protein microarray for the detection of biomarkers secreted by MCF-7 cells challenged with EDCs. We hypothesized that, distinct secretion patterns of a set of biomolecules result from exposure of the cells to estrogen receptor agonists and antagonists reflecting their mode of action.

- the investigation of bisphenol A immobilization for on-chip EDC detection in applied samples within a binding inhibition format as an additional screening tool for the platform.

- the production and establishment of a microfluidic glass hanging drop device for the generation of multicellular spheroids. 3D cell culture creates conditions closer to *in vivo* and the hanging drop method may be ensures unique sized spheroids. The device material glass was chosen to provide an inert cell culture material, which do not suffer from leaching of substances in the cell culture or from adsorption of test substances into the platform and finally do not manipulate the assay outcomes.

- the development of open glass-coated microfluidic spheroid perifusion chambers, for continuously nutrient and oxygen supply and long-term growth of larger spheroids. The chambers will serve as an experimental platform for proliferation assays and shall be directly coupled to the protein microarray to quantify the secreted proteins, based on fluorescence detection using plate readers or microscopes.

3. Materials and Methods

3.1. Cell culture

3.1.1. Cell line and conventional cell culture conditions

The hormone sensitive breast cancer cell line MCF-7 (HTB-22) was obtained from American Type Culture Collection (ATCC, Manassas, VA, USA). The cells were cultivated routinely in low glucose Dulbecco´s modified Eagle´s Medium (DMEM) (Sigma Aldrich, St. Louis, MO, USA) supplemented with 10% heat inactivated fetal bovine serum (FBS), 1% non-essential amino acids (NEAA), 2 mM L-glutamine and 1% penicillin/streptomycin (Gibco® Thermo Fischer Scientific, Waltham, MA, USA) at 37 °C, 5% CO_2 and a humidity of 95% (Incubator: Memmert, Schwabach, Germany) in cell culture flasks (Falcon® Corning Inc., Corning, NY, USA).

Cells were grown for five days to 80% confluence and trypsinated by a 10% dilution of a 0.5% trypsinethylenediaminetetraacetic acid (EDTA) mixture (Gibco® Thermo Fischer Scientific, Waltham, MA, USA) in phosphate buffered saline (PBS) without magnesium and calcium (Sigma Aldrich, St. Louis, MO, USA).

After detaching, cells were stained with Trypan blue (Gibco® Thermo Fischer Scientific, Waltham, MA, USA) and counted in Bürker-Türk-counting chambers (Paul Marienfeld GmbH & Co. KG, Lauda Königshofen, Germany) using an inverted Bresser light microscope (Bresser GmbH, Rhede, Germany) for experiments and passaging. The total amount of the cells was calculated with the following quotation:

$$total\ cell\ number =$$
$$cell\ mean\ (4\ \text{counting quadrates}) \times 10^4 \times\ \text{dilution factor} \times \text{volume medium}\ [\text{mL}]$$

3.1.2. Serum-free cell culture conditions

MCF-7 cells were seeded on collagen I (10 µg/cm²) coated surfaces (See: Chapter 3.2.1.) and cultured in phenol-red free Dulbecco's Modified Eagle Medium/Nutrient Mixture F-12 (DMEM/F-12) medium (Thermo Fisher Scientific(Gibco®), Waltham, MA, USA)) containing 15 mM Hepes, L-glutamine, 0.03% (v/v) insulin/transferrin/selenite (ITS) (Thermo Fisher Scientific(Gibco®), Waltham, MA, USA), 1% penicillin/streptomycin and 10 mg/mL Bovine Serum Albumin Fraction V (7.5% solution) (BSA) (Thermo Fisher Scientific(Gibco®),

Waltham, MA, USA)) at 37 °C, 5% CO_2 and a humidity of 95%. The medium was changed every day.

3.1.3. Collagen coating for serum-free cell culture

A 4.55 mg/mL collagen type I solution (Sigma Aldrich, St. Louis, MO, USA) was diluted in autoclaved MilliQ water and coated in a density of 10 µg/cm² in cell culture dishes and incubated for two hours under sterile conditions. The coating concentrations were calculated using following equations (Freshney, 2010):

$$Conc.collagen\ solution\ [\mu g/\mu L] = \frac{Growth\ area\ [cm^2]\ x\ collagen\ density\ on\ surface\ [\mu g/cm^2]}{volume\ of\ collagen\ solution\ [\mu L]}$$

$$collagen\ weight\ [mg] = \text{Volume [mL] x conc. collagen solution } \left[\frac{\text{mg}}{\text{mL}}\right]$$

$$\text{volume stock solution } [mL] = \frac{\text{weight collagen [mg]}}{\text{stock conc. collagen [mg/mL]}}$$

After discarding of the solution, the dishes were dried and sterilized overnight by UV–light in the cell culture hood. The coated dishes were stored at 4 °C until usage.

3.1.4. Growth curve

1x10^4 or 5x10^4 cells per well were seeded in 48-well Nunclon Surface plates (Nalgene® NUNC™, Rochester, New York, USA) with three replicates per condition. Cells were cultured over seven days in DMEM with10% FBS and the phenol-red free DMEM/F-12 and counted every day. Image acquisition was made with a Bresser MikroCam 1.3 camera (Bresser, Rhede, Germany) using the software MicroCamLab7 under an inverted microscope (Bresser, Rhede, Germany). Mean and standard deviation of the cell numbers were calculated in Excel. Graphs were designed with Graph Pad Prism 5.0. The doubling times of the cells in the exponential growth phase were calculated with the following equations:

$$growth\ rate\ (gr\ [h]) = \frac{\ln\left(\frac{N(t)}{N(0)}\right)}{t[h]}$$

$$doubling\ time\ [h] = \frac{\ln(2)}{\text{gr[h]}}$$

where:

N(*t*) = the number of cells at time *t;* *N*(*0*) = the number of cells at time *0*

gr = growth rate; *t* = time [h].

3.1.5. Culture conditions for biomarker secretion and proliferations assays

$5x10^4$ cells per well were seeded in Costar® cell culture plates, 96 well, flat bottom (Corning Incorporated, Corning, NY, USA). MCF-7 cells were cultured on the first day in 200 µL DMEM with 10% FBS (Supplements see: 3.1.) at 37 °C, 95% humidity and 5% CO_2, allowing them to attach for 24 hours. After 24 hours, the medium was changed to DMEM/F-12 (Supplements see: 3.2.). The next day, the medium was changed again to DMEM/F-12 without insulin with 5.5 µg/mL transferrin (Thermo Fischer Scientific, Waltham, MA), 5 ng/mL sodium selenite (Sigma- Aldrich, St. Louis, MO), 10 mg/mL BSA solution and 1% pen/strep to enhance the proliferative response (Payne et al., 2000) and for cell acclimatization in the serum-free environment. Before changing to the new medium, the cells were washed with 300 µL PBS (-Ca/-Mg). Method according Gier et al., (2017).

3.1.6. Cell treatment for biomarker and proliferation assays

The cells were treated after 72 hours with 1 nM ß-estradiol, 1 nM tamoxifen, 10 nM fulvestrant, 1 µM nonylphenol, 1 µM bisphenol A (BPA) and 1 µM genistein (Sigma- Aldrich, St. Louis, MO, USA) in 200 µL DMEM/F-12 without insulin for 48 hours. Half of the cells were stimulated by 10 ng/mL human recombinant IL-1ß (eBioscience, San Diego, CA, USA). After 48 hours, 200 µL supernatant was removed and transferred into 96 well plates for centrifugation at 0.3 (x 1000) rpm for 1 minute. While processing of the protein microarray the supernatants were stored on ice. The solvents of the test substances dimethyl sulfoxide (DMSO) (Sigma- Aldrich, St. Louis, MO, USA) or 99.9% ethanol absolute (EtOH) (EmsureR Merck Millipore, Darmstadt, Germany) were sterilized and used in a final concentration of 0.1% in the assay. Cells were washed with 300 µL PBS (-Mg/-Ca) before application of the resazurin solution. Method according to Gier et al., (2017).

3.2. Proliferation assay

$1x10^4$ or $5x10^4$ MCF-7 cells were seeded per well in Nunclon surface microtiter plates with 200 µL medium. After cell acclimatization, cells were challenged according to chapter 3.1.6.. for 48 hours. The supernatant was removed and cell layers were washed with 300 µL of PBS (-Mg/-Ca). 200 µL DMEM/F-12 medium containing resazurin (Sigma- Aldrich, St. Louis, MO, USA) in a final concentration of 120 µM was applied per well, including resazurin blank controls and incubated for 4 hours. The plates were covered with aluminum foil for the incubation at 37 °C, 5% CO_2, and 95% humidity. 150 µL of the solution was removed for each treatment and transferred into white Falcon™ White Opaque 96 Well Tissue Culture Plates (Corning, Corning, NY, USA) plates. The readout were made at λex= 560 nm and

λem= 590 nm on a Synergy HTX plate reader (BioTek Instruments Inc., Vermont, USA). Method according to Gier et al., (2017).

3.2.1. Standard curve and single cell density proliferation assay

For the generation of the standard curves, cell densities of 200, 400, 800, 1600, 3200, 6400, 12800, 25600, 51200, 102400, 204800 cells per well and for the single cell density, cell densities of 100, 200, 400, 800, 1600, 3200, 6400, 12800, 25600, 51200, 102400, 204800 cells per well with three replicates for each density were seeded in 200 µL DMEM with 10% FBS or DMEM/F-12 in a 96-well plate. Cell attachment was performed at 37°C, 95% humidity and 5% CO_2 overnight. Afterwards the supernatant was removed and cell layers were washed with 300 µL of PBS (-Mg/-Ca). 200 µL DMEM/F-12 or DMEM with 10% FBS containing 120 µM resazurin was applied at per well, including resazurin controls (without cells) and incubated for 3, 4, 5 and 6 hours for the standard curves and for the single cell density. The plates were incubated for 0-6 hours (37°C, 95% humidity and 5% CO_2). After each hour, 150 µL of the solution was removed for each treatment and transferred into white Falcon™ White Opaque 96 Well Tissue Culture Plates (Corning, Corning, NY, USA) plates. The readout were made at λex= 560 nm and λem= 590 nm on a Synergy HTX plate reader (BioTek Instruments Inc., Vermont, USA). LOD-, LOQ- values and recovery rates were calculated according to chapter 3.5..

3.2.2. Proliferative response to estradiol treatment

$1x10^4$ or $5x10^4$ MCF-7 cells were seeded per well in 200 µL DMEM with 10% FBS. After 24 hours, the medium was changed to DMEM/F-12 with insulin, followed by a second change after additional 24 hours to DMEM/F-12. The second change was only applied for insulin lacking conditions. For the evaluation of the incubation time under estradiol lacking conditions, cells were treated immediately after seeding or after 48 hours with 1 pM to 100 µM estradiol (10-times dilution steps), in 200 µL DMEM/F-12 without insulin for 48 hours. For the comparison under insulin lacking conditions, the control medium contained insulin and the cells were treated with the before mentioned concentrations of estradiol 72 hours after seeding for 48 hours. The supernatant was removed and cell layers were washed with 300 µL of PBS (-Mg/-Ca). 200 µL DMEM/F-12 medium containing resazurin (Sigma- Aldrich, St. Louis, MO, USA) in a final concentration of 120 µM was applied per well, including resazurin blank controls and incubated for 4 hours. The plates were covered with aluminum foil for the incubation at 37 °C, 5% CO_2 and 95% humidity. 150 µL of the solution was removed for each treatment and transferred into white Falcon™ White Opaque 96 Well Tissue Culture Plates (Corning, Corning, NY, USA) plates. The readout were made at λex= 560 nm and λem= 590 nm on a Synergy HTX plate reader (BioTek Instruments Inc., Vermont, USA).

3.2.3. Statistical analysis proliferation assay

The fluorescence signals measured in the proliferation assays were subtracted by the average of the intensities of the resazurin control and plotted as mean with SEM. The fluorescence intensity values of the proliferation assay were baseline corrected to the estradiol treatment and medium control (C0). The bar graphs and curves were set up with Graph Pad Prism 5.0.. The data of the solvent experiment were log transformed (Y=Log(Y)). Test for normal distribution was made with the Kolmogorov-Smirnov test. Statistical significance against the medium control was tested with one way ANOVA and Bonferroni multiple comparison test (alpha=0.05).

3.3. Protein microarray: materials and reagents

As platform for protein immobilization, the proprietary ARChip Epoxy (Preininger et al., 2004) was applied. All materials and reagents according Gier et al., (2017) (See: Table 12 and 13).

Table 12: Reagents with provider used in the protein microarray.

Reagent	Company
Anti-human IL-6 (MQ2-13A5)	eBioscience (San Diego, CA, USA)
Recombinant IL-6 protein	eBioscience (San Diego, CA, USA)
Biotinylated anti-human IL-6 (MQ2-39C3)	eBioscience (San Diego, CA, USA)
Anti-human MCP-1 (5D3-F7)	eBioscience (San Diego, CA, USA)
Recombinant MCP-1	eBioscience (San Diego, CA, USA)
Biotinylated anti-human MCP-1 (2H5)	eBioscience (San Diego, CA, USA)
Anti-human IL-8 (H8A5)	Biolegend (San Diego, CA, USA)
Recombinant protein IL-8	Biolegend (San Diego, CA, USA)
Biotinylated anti-human IL-8 (E8N1)	Biolegend (San Diego, CA, USA)
Anti-human CXCL10 (IP-10) (J036G3)	Biolegend (San Diego, CA, USA)
Recombinant protein CXCL10 (IP-10)	Biolegend (San Diego, CA, USA)
Biotinylated anti-human CXCL10 (IP-10) (Poly5194)	Biolegend (San Diego, CA, USA)
Anti-human Rantes (J047C5)	Biolegend (San Diego, CA, USA)
Recombinant protein Rantes	Biolegend (San Diego, CA, USA)
Biotinylated anti-human Rantes (Poly5197)	Biolegend (San Diego, CA, USA)
Human IGFBP-3 Antibody (E8N1)	R&D Systems (Minneapolis, MN, USA)
Recombinant Human IGFBP-3	R&D Systems (Minneapolis, MN, USA)
Biotinylated Antihuman IGFBP-3	R&D Systems (Minneapolis, MN, USA)
Antibody Human IGF-I (MAb56408)	R&D Systems (Minneapolis, MN, USA)

Recombinant Human IGF-I	R&D Systems (Minneapolis, MN, USA)
Human IGF-I Biotinylated Affinity Purified PAb	R&D Systems (Minneapolis, MN, USA)
Monoclonal Anti-human IL-11 Antibody	R&D Systems (Minneapolis, MN, USA)
Recombinant Human IL-11	R&D Systems (Minneapolis, MN, USA)
Biotinylated Anti-human IL-11(22616)	R&D Systems (Minneapolis, MN, USA)
Anti hVEGF 165 (26503)	R&D Systems (Minneapolis, MN, USA)
Recombinant Human VEGF 165	R&D Systems (Minneapolis, MN, USA)
Anti-hVEGF biotinylated	R&D Systems (Minneapolis, MN, USA)
Human Anti-hMMP-9 (36020)	R&D Systems (Minneapolis, MN, USA)
Recombinant Human MMP-9	R&D Systems (Minneapolis, MN, USA)
Biotinylated Anti-human MMP-9	R&D Systems (Minneapolis, MN, USA)
IL-1ß	eBioscience (San Diego, CA, USA)
Streptavidin Dy647	Dyomics (Jena, TH, Germany)

Table 13 Chemicals and their provider applied in the protein microarray.

Chemicals	**Company**
Polysorbate 20 (Tween 20)	Sigma (St. Louis, MO, USA)
Sodium deoxycholate ($C_{24}H_{40}O_4$)	Sigma (St. Louis, MO, USA)
Sodium chloride (NaCl)	Sigma (St. Louis, MO, USA)
Calcium chloride (CaCl)	Sigma (St. Louis, MO, USA)
Phosphate buffered saline (PBS, pH 7.2, 10X)	Thermo Fischer Scientific (Waltham, MA, USA)
Tris(hydroxymethyl)aminomethane (Tris)	AMRESCO (Cleveland, OH, USA)

3.3.1. Protein microarray fabrication, processing and scanning

Sterile 1x PBS (pH 7.2)/0.01% sodium deoxycholate was used as spotting buffer and for dilution of the biomarkers in concentrations of 0.4 µg/mL for IL-6, IL-8, IL-11, CXCL10, Rantes, VEGF, MCP-1, IGF-1, IGFBP-3, MMP-9 and 0.5 µg/mL for VEGF. Triplicates of the capture antibodies were arrayed onto ARChip Epoxy using an Arrayit Nanoprint contact spotter. The array was spotted twelve times with a SMP3 and a spot-to-spot distance of 350 µm split pin on each slide at a relative humidity of 50%. The slides were stored for at least 3 days at 4 °C for complete immobilization. Spotting conditions (e.g. print buffer, humidity, antibody concentration) were applied according to Domnanich et al., (2009). After storage the slides were blocked in 1× PBS (pH 7.2)/0.1% Tween 20 for half an hour. Slides were washed two times in 1x PBS (pH 7.2) and dried with compressed air. Hybridization cassettes (Arrayit) holding four slides for 4 × 12 separated arrays were used for processing of the chip.

At least 10 standards were used in the quantitative assays for retaining the calibration curves. The dilution series of biomarker mixtures were prepared in DMEM/F-12-BSA (without insulin). For the semi-quantitative procedures, 3 calibration standards (linear range) and the medium blanks were used. Each calibration standard was made in nine replicates with different distribution on the array fields of three slides as well as 6 biological replicates of the cell culture samples (each with three technical replicates). The samples were incubated for 2.5 hours. After incubation, the slides were washed 3 times. 50 µL of mixtures of biotinylated detection antibodies in buffer J (100 mM TRIS, 100 mM NaCl, 10 mM $CaCl_2$ and 0.1% Tween 20; pH 7.4) with final concentrations of 1 µg/mL each, were applied and incubated for 45 minutes. Subsequently to an additional washing step, Dy647 streptavidin (in buffer J) in a concentration of 2 µg/mL was added and incubated for 45 minutes. After a final washing cycle with PBS-Tween (2 times) and with 1x PBS (2 times), slides were removed of the hybridization cassettes and dried with compressed air. The ready processed slides were stored in the dark until scanning. The whole chip processing was performed at room temperature, incubation steps were made on a rotary shaker. A confocal laser scanner (LS100, Tecan Group Ltd, Switzerland) was used for the readout at λex= 635 nm, λem= 670 nm at optimal photomultiplier tube (PMTs) voltages for each analyte. Cross-reactivity experiments were performed for each single biomarker under application of all nonspecific capture antibodies of the biomarker panel. The reactivity was calculated in percent as a ratio of specific to unspecific fluorescence signal of an intermediate concentration within the linear range. Method was performed according to Gier et al., (2017).

3.4. Bisphenol A immobilization: hapten-protein conjugates

The conjugation of bisphenol A to the isocyanate group of the cross linker p-maleimidophenyl isocyanate (PMPI) was performed according to the protocol of the manufacturer (Thermo Fisher, Waltham, Ma, USA) and to Annunziato et al., (1993). Therefore, 2 mg (9.34 mM) PMPI and 2.13 mg (8.76 mM) BPA were mixed in DMSO in a 1:1 ratio and incubated in the dark for 4 hours on a rotational shaker.

The SH-groups of the protein carriers including the keyhole limpet protein (KLH) (Thermo Fisher, Waltham, Ma, USA), the human serum albumin (HSA) (Sigma Aldrich, St. Louis, MA, USA), the horseradish peroxidase (HRP) (Thermo Fisher, Waltham, MA, USA) and BSA (Sigma Aldrich, St. Louis, MA, USA) were first dissolved in milliQ water and then reduced using 10 mM dithiothreitol (DTT) in 1x PBS (pH 6.7). The mixture was incubated in the dark for 1 hour at RT on a rotational shaker. 1 to 2 mg of reduced and unreduced proteins was used for the conjugation to BPA-PMPI. After mixing, the solution was incubated in the dark for 2 hours at RT on a rotational shaker. The hapten-conjugates were stored at -20 °C before printing. The conjugate stocks were diluted 1:1 with sodium deoxycholate buffer and were

spotted on different functionalized surfaces ARChip Epoxy, ARChip Gel, super aldehyde, amine (Arrayit, Sunnyvale, Ca, USA), poly-L-lysine (Anopoli Biomedical Systems, Eichgraben, Austria) slides in one big array in triplicates. In addition BPA, BPA-PMPI conjugate as well as the reduced and unreduced protein carriers were spotted (See: Table 14).Prior to processing the slides were stored at 4 °C for three days.

Table 14: Hapten-protein conjugates, proteins (reduce/unreduced) and reagents were tested.

Probes
BPA-PMPI-Protein (HRP, KLH, BSA, HSA)
BPA-Protein (HRP, KLH, BSA, HSA)
Protein (HRP, KLH, BSA, HSA)
BPA-PMPI
BPA

3.4.1. Hydrogel coating

HistoBond® slides (Paul Marienfeld GmbH & Co. KG, Lauda-Königshofen Germany) were dip-coated with 2% ARChip Gel (polyurethane D1) solved in 95% EtOH/5% H_2O. The slides were dipped in the solution for 1 min and dried vertically at RT.

3.4.2. Bisphenol A immobilization: SciPOLY3D

0.4, 0.5, 1, 2, 3, 4 mg/mL bisphenol A dissolved in DMSO were immobilized in 1 mg/mL SciPOLY3D (Scienion AG, Dortmund, Germany) solution (See: Table 15) with or without 200 mM trehalose. As immobilization matrix, ARChip Epoxy slides were used. The probes were spotted in triplicates in each of the twelve arrays with a PDC 80 Type 3 nozzle (Scienion AG, Dortmund, Germany) and a Scienion SciFlex printer (Scienion AG, Dortmund, Germany). The gel was crosslinked with UV-light at 1 J/cm^2 (245 nm) (Stratalinker 2400, Stratagene, San Diego, CA, US). The slides could be immediately used.

Table 15: Mastermix printing solution.

Reagents	**Stock concentration**	**Volume**
SciPOLY3D	10 mg/mL	5 µL
sodium phosphate buffer	500 mM	20 µL
BPA (DMSO)	Different concentrations	15 µL
H_2O (+/-trehalose)	200 mM trehalose	10 µL
Total		**50 µL**

3.4.3. Validation of BPA immobilization

Successful immobilization of BPA as conjugate or in sciPOLY3D was tested in a direct binding assay with different concentrations of Dy647-labeled BPA antibodies (0.1, 0.5, 1, 2 µg/mL) (Dyomics, Jena, TH, Germany). Assay buffer, blocking reagent and washing solution used for the BPA-protein conjugates were according to chapter 3.3.1. For the SciPOLY3D immobilization, 1x PBS plus 0.1% Tween was applied. Incubation times for the bisphenol A detection antibody were according to chapter 3.3.1..

3.4.4. BPA binding inhibition assay

1-4 mg/mL BPA in SciPOLY3D with and without 20 mM trehalose was printed in triplets in each of the 12 arrays on one slide and crosslinked. Assay performance of the BPA binding inhibition assay was tested for a concentration range of 0-3936.60 ng/mL BPA in 1:3 dilution steps. Each BPA standard was incubated with 0.75 µg/mL labelled BPA antibody 10 minutes before the samples were applied on the arrays and incubated there for 2 hours (Sauer et al., 2011). Fluorescence measurements were according to chapter 3.3.1.

3.5. Statistical data analysis protein microarray and BPA immobilization

The segmentation of spots and analysis of the biomarker array data were performed in GenePixR Pro 7.0 software (Molecular Devices, LLC Sunnyvale, CA, USA). The mean signals of nine technical and six biological replicates of the cell supernatant samples were background corrected under exclusion of out of mean signal values ± standard deviation (SD) data points. Calibration curves were generated with mean +/-SD values, using a four parameter fit in Origin Pro 8G. The bar graphs were set up with Graph Pad Prism 5.0. The LOD was calculated as mean zero concentration plus three SDs and LOQ plus ten SDs of the measured intensities of the blank (MacDougall and Crummett et al., 1980). The relative values of the recovery rates are given in %, displaying the relation between measured and spiked concentrations. Secretion data are baseline corrected to the medium control (C0). Test for normal distribution was made with the Kolmogorov-Smirnov test. The data of the stimulation experiment were log transformed (Y=Log(Y)). Statistical significance was tested with one way ANOVA and Bonferroni multiple comparison test (alpha=0.05) between antagonists and agonists.

The bar graphs for the BPA immobilization were made in Graph Pad Prism 5.0 and curves in Origin Pro 8G. Mean of fluorescence intensities with standard deviation were plotted. LOD-, LOQ- and EC50 values were calculated as mentioned above. Coefficients of variation represent the standard deviation divided by the mean of the same probe.

3.6. Microfluidics: Hanging drop device production and characterization

3.6.1. Fabrication of PDMS hanging drop devices

The chip design was made with the mask layout editor CleWin 3.0.11 (WieWeb, Hengelo, The Netherlands). Microfluidic structures (channel and hydrophobic rim structures) were created by casting of poly (dimethylsiloxane) (PDMS, Sylgard 184, Dow Corning Corp., USA) using a SU-8 mold. The molds were produced by soft lithography according to the manufacturer Microchem (reference datasheet). BOROFLOAT® (100 mm) wafers (Handelsagentur Helmut Teller, Jena, Germany) were cleaned with acetone, isopropanol (Sigma Aldrich, St. Louis, MO, USA) and milliQ water (Reinstwasseranlage, Wilhelm Werner GmbH, Leverkusen, Germany). The following heating step was performed for 5 minutes at 150 ^{o}C. 4.5 mL SU-8 50 photoresist (Microchem, Corp. Newton, MA, USA) was coated onto the cleaned wafers using a CEE^{TM} –100 - spin coater (Brewer Science, Rolla, MO, USA) to achieve a structure depth of 100 µm. After leveling for 30 minutes (RT), the temperature was ramped to 65 ^{o}C in temperature steps of 1 ^{o}C/min and heated for 10 minutes at this temperature. A further increase of the temperature to 95 ^{o}C (temperature steps: 1 ^{o}C/min) with a heating time of 30 minutes was performed before the wafers were cooled down to RT. The wafers were covered with transparency masks (Pro-Art BV Groningen, The Netherlands) and exposed to 300 mJ/cm^2 UV–light using a collimated UV-light source (OAI, San Jose, CA, USA). The wafers were heated again to 65 °C (temperature steps: 1 ^{o}C/min) and kept at this temperature for one minute. Further ramping to 95 ^{o}C (temperature steps: 1 ^{o}C/min) was performed with a baking time of 10 minutes at this temperature and a final cool down step. Development of the wafers was made in SU-8 developer (Microchem, Corp. Newton, MA, USA) for 10 minutes under shaking followed by an additional development step for 5 minutes with fresh developing solution. Afterwards a hard bake step at 150 °C for 20 minutes was performed. The structures were treated with 98% HDMS (Sigma Aldrich, St. Louis, MO, USA) for 30 minutes under vacuum.

PDMS was casted onto the masters with a thickness of 1 mm and cured for 2 hours at 70 °C. Drop well holes were made with Biopsy punchers (Kai Corporation, Tokyo, Japan) in both PDMS layers (ø 3 mm). A soda lime glass slide (26 mm x76 mm, 1 mm thick) (Menzel-Gläser, Fisher Scientific, Landsmeer, The Netherlands) was taken as an additional layer. In- and outlet holes for the glass layer were sandblasted with a powder-blaster (Wulsag, Zofingen, Switzerland) using 22 µm AL_2O_3 particles (Straaltechniek International BV, Dordrecht, The Netherlands) and a metal mask with drilled holes containing the desired diameter of 2 mm. To avoid damage of the glass during sandblasting, the slide was covered on the metal side with Scotch™ tape. Bonding was performed by oxygen plasma activation

for 30 seconds at 300-320 mTorr using an Harrick plasma cleaner (Harrick Scientific Products Inc., NY, USA).

3.6.2. Fabrication of glass hanging drop devices

The glass device was produced using two BOROFLOAT® 33 (Nexterion® glass B) glass slides (25 mm x 75 mm, 1 mm thick) (Schott, Jena, Germany). The drop well holes and in- and outlet holes were generated by sandblasting using a metal mask with the desired design and diameters (See: Chapter 3.6.1.). Prior to the sandblasting, both slides were coated on one side with AZ4562 (MicroChemicals GmbH, Ulm, Germany) to protect the glass and prebaked for 2 minutes at 125 °C. The opposite side was covered with Scotch™ tape. After the Scotch™ tape was removed the slides were pre-cleaned with tap water after sandblasting. Acetone was used to remove the AZ4562 layer. Then the slides were rinsed with acetone, isopropanol and milliQ, followed by drying with nitrogen. The lower layer containing the droplet well was dehydrated at 125 °C for 10 minutes and followed by HMDS treatment for at least 30 minutes under vacuum. Desorption of H_2O at 125 °C was performed for 2 minutes. The backside of this slide was covered with HF tape (provided by M. Skolimowski, Micronit, Enschede, The Netherlands) followed by a spin coating step (700 rpm; 700 rpm/s; 3 sec) with 2 mL AZ4562 photoresist. To avoid removal of the photoresist, the holes were filled with AZ4562. The slide was leveled for 15 minutes. After 2 hours prebaking at 100 °C (starting at 60 °C), the slide was kept for rehydration overnight on the bench. The slide was exposed to 3000 mJ/cm^2 UV-light using a transparency mask with the desired channel design. Development was made in AZ400K solution (1:3 dilution with milliQ) (MicroChemicals GmbH, Ulm, Germany) in two steps each 20 minutes. The developer was changed during these steps. The slide was rinsed with water and plasma activated for 20 sec at 320 mTorr.

Isotropic etched structures in glass were achieved with a hydrogen fluoride solution (49% HF:70% HNO_3:H_2O) in a ratio of 100:28:72 at a rate of 2 µm min^{-1} for 25 minutes. The slide was rinsed with milliQ for 5 minutes, dried and the photoresist was removed with acetone. Isopropanol and water were used for cleaning before both slides were dried with nitrogen. The pre-cleaned slides were treated with piranha solution (H_2SO_4:H_2O_2 3:1) at around 110 °C for 10 minutes, placed in a petri dish with milliQ water and finally in a water bath to a conductivity of 3.5 MΩ/cm (Jellema et al., 2009). The two glass slides were aligned and pre-bonded under water. They were pressed together to remove most of the water in between the glass slides and transferred in a furnace (Nabertherm, New Castle, DE, USA) among two ceramic plates (“Glass Microfluidic Device Fabrication SOP,” 2015).

Bonding pressure was applied by a 2 kg of a squared steel weight on top of the ceramic. The glass slides were bonded in different temperature steps. The slides were heated to 500 °C and kept there for 30 min, to 644 °C for 18 hours and finally cooled down to room temperature (~ 24 hours) (Jellema et al., 2009).

3.6.3. Contact angle and roll off angle measurements

BOROFLOAT® 33 and soda lime glasses as well as freshly cured PDMS and PFPE were used for the measurement of the contact angles of DMEM/F-12 medium and water. The PFPE slabs were prepared out of a mixture of Fluorolink® perfluoropolyether (Fluorolink® PFPE; MD700; Solvay Solexis, Bruxelles, Belgium) with 4% of 97% 2-Hydroxy-2-methylpropiophenone (Sigma-Aldrich, Zwijndrecht, The Netherlands). The BOROFLOAT® 33 glass slides were coated with Rain-X® (RainX®, Gouda, The Netherlands) by applying the solution on the slide. After 1 minute, the glass slide was polished. Glass rims were introduced using Scotch® tape and Biopsy punchers of 4 and 6 mm for the generation of a round mold by sandblasting. The glass rims were generated by 10 min treatment with HF. In order to etch a round rim into the glass slide, the surface was covered by HF paper and the rim was punched into the paper (inner diameter: 4 mm, outer: 6 mm). Another rim was made with a diamond pen. All non-coated glass surfaces were cleaned with acetone, isopropanol and MilliQ water and dried with air before a droplet of water or medium was applied. Images (Canon EOS 700D; Canon Nederland N.V., `s-Hertogenbosch, The Netherlands) of contact and roll off angles of 20 µL (for HF treated glass rims) and 40 µL droplets were measured in Image J software for n = 3 medium droplets compared to water.

3.6.4. Introducing of hydrophobic rings

The glass hanging drop device was first cleaned with acetone, isopropanol and miliQ water and dried. The dried chip was heated for 5 minutes at 150 °C (hotplate) and slowly cooled down. Approximately 5 µL SU-8 10 was coated on the glass chips around the drop wells by using a PDMS microstamp. The chip was leveled for 15 min and transferred to a 35 °C hotplate for the soft bake. The temperature was increased to 65 °C in 10 minutes (10% ramp temperature). After 3 minutes of incubation at 65 °C, the chip was heated to 95 °C in 10 minutes (30% ramp temperature) and incubated for 5 minutes and slowly cooled down to room temperature. PFPE was prepared according to chapter 3.6.3. A PDMS-glass mold was used for the preparation of Fluorolink® PFPE-rings. Approximately 20 µL PFPE mixture was pipetted in each ring mold, UV cured at 2 J/cm^2 (Dymax RediCure,Dymax Corp., Torrington, CT, USA) in a nitrogen atmosphere. A droplet of PFPE solution was used to bind the ring to the SU-8 coated glass chip within a second UV-curing step at 2 J/cm^2. The glass chip with the bonded rings was post baked with a weight of 584 g on top. The post bake was

performed at 65 °C for 3 minutes, followed by five minutes at 95 °C with 10% temperature ramps and slowly cooled down to room temperature.

3.6.5. Droplet formation and perfusion

Droplet formation experiments were performed in glass and PDMS hanging drop devices applying pressure driven flow at flow rates of 20, 80 and 150 µL/min. Detection of liquid distribution inside the droplets was performed with 30 µL MilliQ water, which was filled in the droplet wells. Afterwards blue food dye was applied with a 1 mL Omnifix®-F solo syringe (B.Braun Medical, The Netherlands) placed in a syringe pump (NE1000; Prosense B.V., Oosterhout, The Netherlands) connected to the device via 0.8 x 1.6 mm PTFE-tubing (Polyfluor Plastics bv, Breda, The Netherlands). Filling of the droplets were tested at flow rates of 20, 80 and 150 µL/min. The image acquisition was made at ~45° and 90° angles with a DigiMicro Scale 2.0 camera (dnt® Drahtlose Nachrichtentechnik, Dietzenbach, Germany) and the open source software MicroManager 1.4.22 (Edelstein et al., 2010, 2014) and analyzed with Image J.

3.6.6. Droplet evaporation

Evaporation was tested for PDMS slabs bonded to a glass slide with six droplet wells and compared with glass slides with six attached PFPE rings under static conditions with DMEM/F-12 medium in an incubator at 37 °C, 5% CO_2 and a humidity of 95% over 24 hours. Experiments were performed in wetted plastic boxes to mimic 95% humidity. The droplet devices were transferred to the incubator in the plastic boxes or the boxes were pre-warmed in the incubator for 15 minutes before the droplet devices were added. Experiments were performed with and without 3D printed incubation chambers, which differed in height. The 3D printed incubation chambers containing a soda lime glass bottom for detection were designed in Solidworks 2015. They were printed with a FELIX 3.0 3D printer (FELIXprinters, IJsselstein, The Netherlands) using 1.75 mm polylactic acid filament (PLA) (Formfutura VOF, Nijmegen, The Netherlands). For the determination of the evaporation, empty and filled devices were weighted with a micro scale before and after incubation as well as the six droplets. The droplets were transferred with a pipette for measurement.

3.6.7. Rhodamine adsorption

30 µL rhodamine B solution (50 µM rhodamine B in distilled water) (Sigma Aldrich, St. Louis, MO, USA) was pipetted in PDMS and PFPE rings, which were bonded to glass. They were placed into an incubator for 24 hours at 37 °C, 5% CO_2 and a humidity of 95%. The rhodamine solution was removed and the devices were cleaned with water before detection of red fluorescence using an inverted fluorescence microscope with filter Y3 (535/50 nm (ex)/

610/75 nm (em)). The acquired images were evaluated for rhodamine adsorption via fluorescence intensities analyzed in Image J.

3.6.8. Treatment of microfluidic devices for the usage in cell culture

PDMS devices were treated with oxygen plasma (300-320 mTorr) for 30 sec. The channels were filled with 70% EtOH and incubated for 15 minutes. The EtOH was removed and sterile H_2O was added for additional 15 minutes. Afterwards, cell medium was applied.

The glass devices were cleaned in an ultrasonic bath containing 70% EtOH and afterwards autoclaved. The PMDS connectors and PFPE rings were introduced, followed by an oxygen plasma (300-320 mTorr) treatment for 30 sec and an UV treatment at 2 J/ cm^2. The final cleaning step with EtOH and H_2O was performed according to the PDMS treatment, before the cell medium was applied.

3.6.9. Statistical data analysis

Graphs and statistical analysis were made in Graph Pad PRISM® 5.0. The evaporation data were tested for significance with the nonparametric the Mann-Whitney- U-Test and a confidence interval of 95%.

3.7. 3D cell culture conditions for flow and static experiments

300, 325, 750 or 1500 cells were seeded in 30 µL droplets with serum free DMEM/F-12 medium containing 10 ng/mL EGF (Pepro Tech EC, Ltd., London, UK), 10 ng/mL FGF (Pepro Tech EC, Ltd., London, UK), 0.03% (v/v) ITS (Thermo Fischer Scientific, Waltham, MA, USA), 0.5 µg/mL hydrocortisone (Sigma, St. Louis, Missouri, USA), 10 mg/mL bovine serum albumin solution (BSA), 2% Gibco® B27, 1% Pen/strep (Thermo Fischer Scientific, Waltham, MA,USA) and incubated at 37 °C, 95% humidity and 5% CO_2. MCF-7 spheroids grew for 3 to 7 days. After 24 hours, half of the medium was changed for static and flow conditions, followed by a media change every second day. Pressure driven flow was applied with a rate of 10 µL/min using syringe pumps.

3.7.1. 3D cell viability assessment

Cellular viability was assessed using Calcein acetomethoxy (CAAM) (Enzo Life Science, NY, USA) for viable and propidium iodide (PI) (Enzo Life Science, NY, USA) for dead cells. The spheroids were washed two times with PBS (- Ca, - Mg). 2 µM CAAM staining solution (DMEM/F-12 plus supplements) was applied. After 10 minutes of incubation at 37 °C, 95% humidity and 5% CO_2, 1 µM PI (PBS) solution was added and incubated for additional 5 minutes. The cells were washed two times with PBS. Images acquisition was made

immediately after the staining using a fluorescence microscope (Leica microsystems, Rijswijk, The Netherlands) in combination with an external light source (EL6000; Leica microsystems, Rijswijk, The Netherlands) with filter I3 (450-490 nm (ex)/ 515 nm (em)) for the detection of CAAM in viable and dead cells and filter Y3 (535/50 nm (ex)/ 610/75 nm (em)) for determination of PI in dead cells.

3.7.2. 3D-cell culture treatment with 17ß-estradiol

Spheroids were grown according to chapter 3.7 for 24 hours in DMEM/F-12 before the medium was changed to DMEM/F-12 supplemented with 0.03% ITS, 1% pen/strep, 10 ng/mL EGF, 10 ng/mL FGF and 10 mg/mL BSA for additional 24 hours. A further medium changed was made after 48 hours. The new hormone lacking DMEM/F-12 medium was enriched with 1% pen/strep, 10 ng/mL EGF, 10 ng/mL FGF, 5.5 µg/mL transferrin, 5 ng/mL sodium selenite and 10 mg/mL BSA. After 72 hours, the spheroids were challenged with 100 pM and 1 nM 17ß-estradiol in the hormone lacking DMEM/F-12. DMSO, the solvent of 17ß-estradiol was added in a concentration of 0.01% to the formulation. The spheroids were treated over 4 days. The medium containing 17ß-estradiol was changed every second day.

3.7.3. Image analysis of MCF-7 cell spheroids

Diameters, circularity and aspect ratios of treated and untreated MCF-7 cell spheroids as well as the fluorescence intensities of stained cells were measured and calculated using ImageJ software version 1.51 j8.

3.7.4. Statistical data analysis for 3D cell culture

Graphs and statistical analysis were made in Graph Pad PRISM® 5.01. Test for normal distribution was made with the Kolmogorov-Smirnov test. Significance was tested with a unpaired t-test for alpha=0.05. Corrected total cell fluorescence was calculated according to (McCloy et al., 2014).

3.8. Perifusion chamber: production

Before introduction of PDMS into the screwed molds, 4 µL drops of glycerol (98%) (Sigma Aldrich, St.Louis, MO, USA) were placed on each chamber mold to prevent clogging of the polycarbonate membrane and to create an open chamber. Cut parts of a polycarbonate membrane (8.0 µm, Isopore Membrane TETP04700, Merck Millipore Corporation)) were placed on the glycerol droplets over all three chambers. Stainless steel pins (Ø 1.5 mm channels) were placed into the molds to create the channels for inlet and outlet. Approximately 4 mL PDMS was added, using a 10 mL syringe with a 10 µL pipette tip inside,

into two matching micromilled molds (provided from Prof. Sabeth Verpoorte, University of Groningen /Pharmaceutical analysis) (Van Midwoud et al., 2010). After filling, the accesses were closed with stainless steel pins (ø 2.0 mm). PDMS was cured at 70 °C in an oven for 2 hours. A PDMS cover slab was produced by casting a 2 mm thick layer of PDMS (25 g) in a squared plastic petri dish and cured at 70 °C for 1 hour. The matching PDMS chamber parts and the cover slab were bonded to each other using oxygen plasma for 30 sec. The bonding was improved by a heating step at 70 °C on a heating plate and pressure for 30 minutes.

3.8.1. Flow experiments

Flow experiments were performed by hand with 1 mL syringes, filled each inlet and outlet with food dye stained water.

3.8.2. Integration of glass membrane

The microporous membrane chips (size 5.4 x 5.4 mm; 0.3 mm thickness) with 2x2 mm G-FLAT™ silicon oxide membrane (20% porosity, 3.0 µm pores) (SiMPore Inc., West Henrietta, NY, USA) were introduced after the glass coating process. For the introduction, 3D printed PLA clamps (6.5 x 6.5 mm, inner diameter 5.5 mm, height 1.80 mm) were used. The clamps were fixed in the molds around the perifusion chamber and removed after PDMS curing leaving a mold for the membrane. Three membrane chips were integrated for each chamber and the perifusion platform was closed with the cover PDMS slab using oxygen plasma for 30 sec.

3.8.3. Glass coating

The glass coating solution containing tetraethyl orthosilicate (TEOS), methyltrietoxysilane (MTES) (Sigma Aldrich, St. Louis, MO, USA), EtOH, and milliQ water pH 4.5 adjusted with HCl was mixed in a volumetric ratio of 1 : 1 : 1 : 1 under stirring at 65 °C on a hotplate until it became homogeneous (Abate et al., 2008). The solution was stored overnight at RT. In front of the coating process, the already bonded PDMS parts of the perifusion chamber were treated with oxygen plasma for 30 sec at 310-320 mTorr and heated on the hot plate for 5 minutes at 80 °C. The PDMS chambers were added into a bath filled with the precursor mixture of the glass coating mixture and incubated under movement for 30 minutes at 80 °C. The device inclusive channels were flushed with air using a 50 mL syringe to avoid clogging. Afterwards, there were transferred to a 100 °C hotplate, to initiate the gelation reaction. The validation of the consistence of the glass coating was made with 50 µM rhodamine solution over at least 24 hours. Therefore, the solution was applied into coated and non-coated PDMS chambers and incubated at RT in the dark. Evaluation of consistence and image analysis was made according to chapter 3.6.7.

4. Results and discussion

4.1. Establishment of a serum-free and phenol-red-free MCF-7 cell culture

Poorly defined serum ingredients, with lot to lot differences, such as hormones can affect the outcome of experiments researching influences of endocrine-active substances on cells (Barnes and Sato, 1980b). The well characterized breast cancer cell line MCF-7 was chosen as a model for our system. The cells require hormones such as estradiol to grow and retained properties expressed by breast epithelium *in vivo* such as expression of receptors for estrogen, androgen, progesterone, glucocorticoid, insulin and L-3, 3´, 5-triiodothyronine (T3) (Barnes and Sato, 1979a; Soule et al., 1973). In addition to the conventional added pH-indicator phenol red, used for detecting changes of medium pH by for instance bacteria contamination, had to be removed due to estrogenic action (Berthois et al., 1986). Therefore, the establishment of a serum- and phenol red-free MCF-7 cell culture is a necessary step in the development of our EDC screening platform.

The conventional cell medium DMEM with 10% FBS was replaced by the nutrient enriched phenol red-free DMEM/F-12 supplemented with an insulin-, transferrin-, selenite mixture (ITS), Hepes and L-glutamine. 6 µg/cm² collagen I was used for the attachment of the cells. For the adaption of the MCF-7 cells to the serum-free conditions, different approaches were investigated: inner adaption (immediate change of media), sequential media change (75% DMEM FBS/25% DMEM/F-12, 50%/50%, 25%/75% and 100% DMEM/F-12) and a stepwise decrease of FBS (5%, 2%, 1%, 0%). The approaches were compared to cell growth in conventional medium DMEM with 10% FBS and to the growth in DMEM/F-12 on uncoated surfaces and under ITS omission. The adaption was evaluated by cell counting, cell spreading, attachment and morphological changes. The cells were grown under the particular conditions for four days before media conditions were changed. Every second day the media was renewed.

Cells in DMEM/F-12 with decreased serum concentrations (< 2% FBS), grew slower and reached 30 to 50% of the cell numbers compared to the serum containing cell culture (Appendix I see: Figure A 1A-B, F). Growth with ITS supplement on collagen coated and uncoated surfaces supported the formation of large, compact and widely spread spheroid-like cell clusters (Appendix I See: Figure A 1B, D). Less attachment and a rounded cell morphology was seen for ITS or both ITS and collagen I omission. Similar changes in growth, cell morphology were observed for cells grown under sequential changed media conditions (Appendix I see: Figure A 2A-B, F). Cluster development was detected even for cells lacking ITS as well as collagen I. Improvement in cell spreading and growth of MCF-7

cells was detected after the immediate change of media in comparison to the stepwise decrease of FBS, the sequential media change and the conventional cell culture. When grown on collagen I coated surface and with ITS supplementation, cells spread over the whole surface and showed an elongated morphology. Equal cell quantities were detected compared to the conventional serum supplemented growth medium (See. Figure 25B; 26).

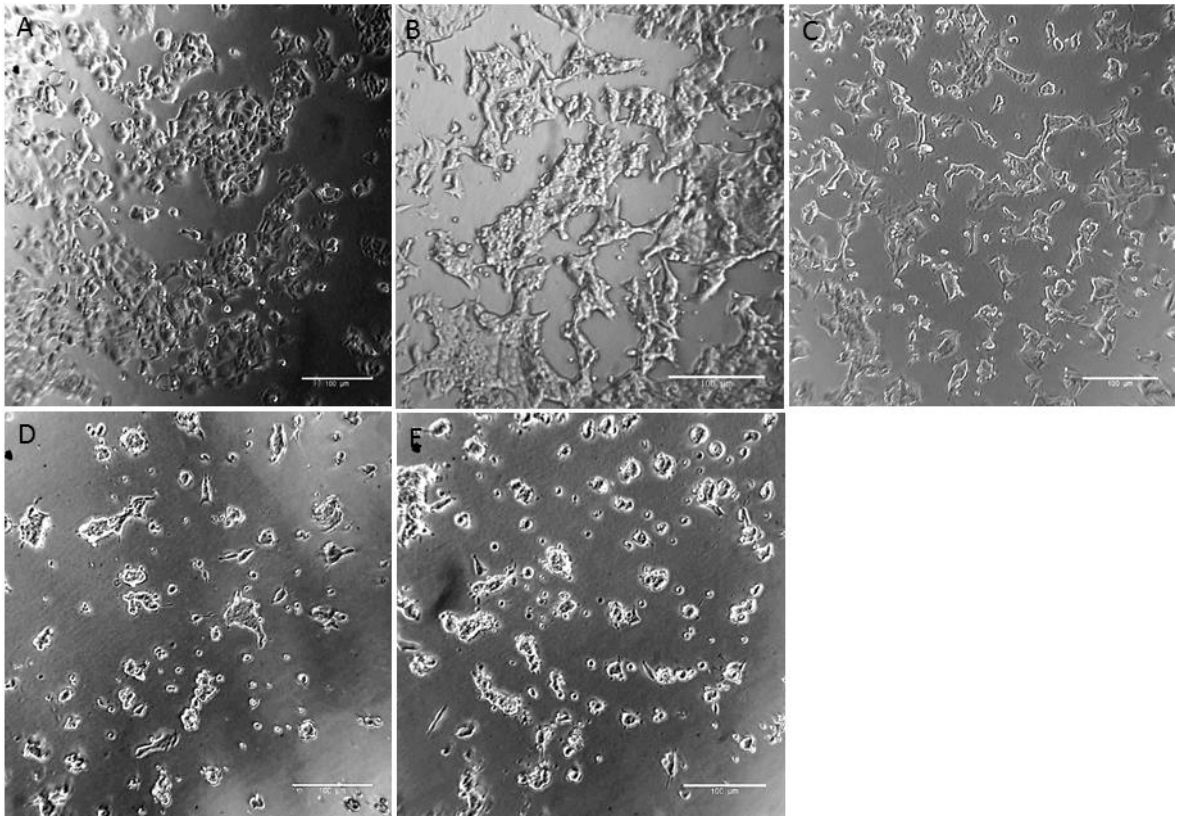

Figure 25: Cell morphology of MCF-7 cells after inner adaption of serum-free medium on day four. Comparison of cell growth in DMEM supplemented with 10 % FBS (A) to DMEM/F-12 serum-free cell culture conditions with collagen coating (B) as well as to ITS lacking conditions (C), no collagen I coating (D) or both (E).

The attachment factor collagen I and the insulin mixture were crucial for cell growth. Cells were stressed, died or formed small three-dimensional clusters under omission of these factors (See: 25C-E; Appendix I see: 1C-E, 2C-E). The cell growth in serum free medium was further improved by increase of the collagen density to 10 µg/cm² and a daily media change. As result, MCF-7 cells were strongly attached to the surface and the cell spreading was increased. Cells grew exponentially over seven days with doubling times of 40 (±24) hours under serum-free conditions. The doubling time were slightly higher compared to the conventional cultured cells with 38 (±18) hours. Cells reached growth stagnation at day five under serum supplemented conditions and under serum-free conditions on day seven of cell culture, with in average 2 fold less cell numbers in the exponential growth phase (day 4 and 5) (Appendix I see: Figure A 3).

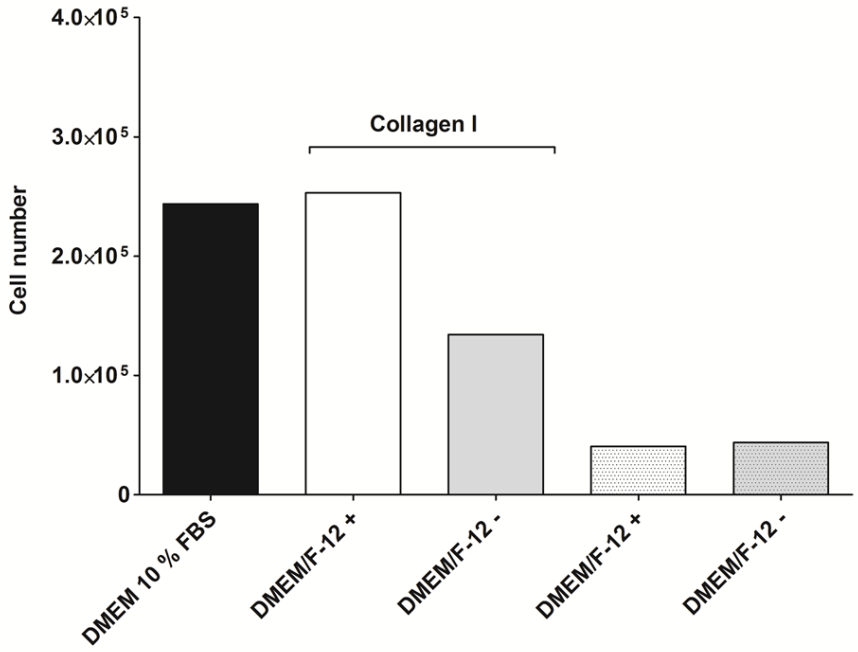

Figure 26: Total cell numbers after inner adaption of serum-free medium by MCF-7 cells on day four. Comparison of cell growth in serum-free DMEM/F-12 with collagen I coating compared to DMEM with 10% FBS. Additionally under lacking of ITS, collagen I or both. Total cell numbers were counted for n=2 and given as mean. ITS omission is coded by minus (-) and adding by plus (+). 1x10^4 cells were seeded on day 0.

Upon adding of 10 mg/mL BSA solution to the serum-free medium, equal cell morphologies compared to serum supplemented culture conditions were determined (See: Figure 27). No significant change of doubling time was determined. Under serum-free conditions, cells doubled in average after 47(±22) hours compared to serum supplemented with 35 (±14) hours. Exponential growth under serum-free conditions was determined over seven days (See: Figure 28).

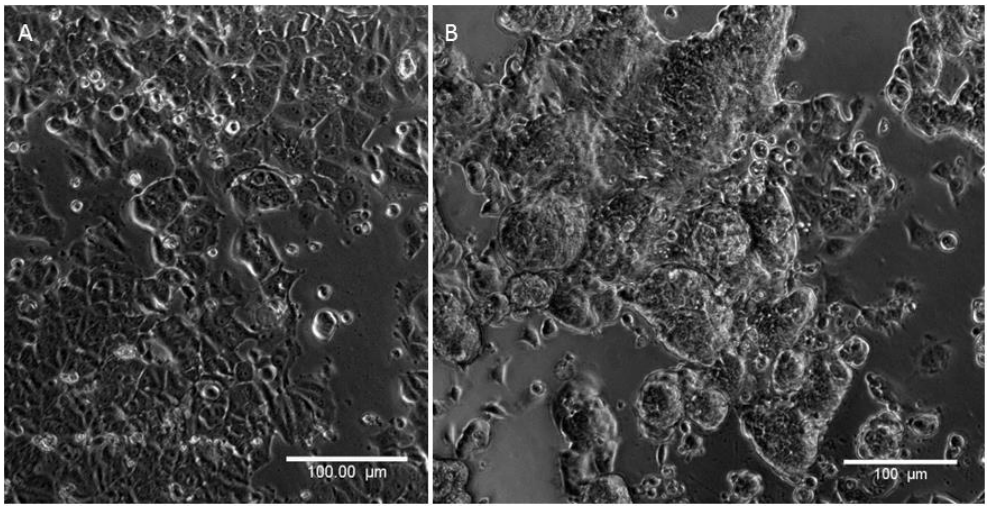

Figure 27: Morphology of MCF-7 cells after three days of growth in the conventional FBS supplemented medium (A) or in serum-free medium (B) on collagen I coated surfaces.

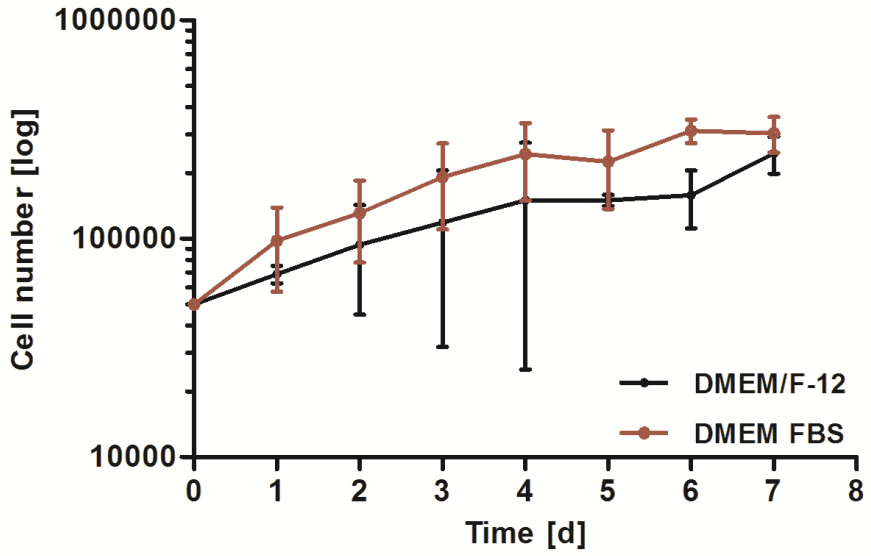

Figure 28: MCF-7 cell growth in the serum-free medium DMEM/F-12 supplemented with Hepes, L-glutamine, insulin/transferrin/selenium and 1 mg/mL BSA over seven days compared to the conventional DMEM with 10% FBS. 5x10^4 cells were seeded on day 0. Cells in serum-free medium were grown on collagen I (10 µg/cm²) coated surfaces. Data are shown as mean of triplicates with standard deviation.

A serum free MCF-7 cell culture was established on collagen type I coated surfaces in DMEM/F-12 supplemented with Hepes, L-glutamine, insulin/transferrin/selenium and BSA without an adaption phase to the new media conditions. Similar medium supplementations were reported by Barnes and Sato, (1979) and Briand and Lykkesfeldt, (1983). In addition, they added epidermal growth factor (EGF), prostaglandin $F_{2\alpha}$ ($PGF_{2\alpha}$), Holmes α-1 protein, fibronectin or collagen IV for the growth and spreading of MCF-7 cells. Thereby they supported identical cell numbers and morphology compared to cells grown under serum supplementation. Different attachment factors such as fibronectin or collagen IV or combinations of extracellular matrix proteins were used for growth enhancement, spreading and attachment of epithelial cells (Badaoui et al., 2017; Barnes and Sato, 1979b; Briand and Lykkesfeldt, 1983; Gstraunthaler and Lindl, 2013; Terranova et al., 1983). Medium adaption by the MCF-7 cells was implemented in different ways, by sequentially serum decrease or immediately change to the new conditions (Barnes and Sato, 1979; Briand and Lykkesfeldt, 1984). Longer doubling times of MCF-7 cell in serum-free medium compared to serum supplemented medium were reported before. Briand and Lykkesfeldt, (1983), described MCF-7 cell doubling times of 70 hours, with exponential growth to day seven. The growth regression can be probably ascribed to the omission of estradiol (Allegra and Lippman, 1978; Barnes and Sato, 1979). In addition insulin, transferrin and sodium selenite omission results in decreased cell populations compared to the serum supplemented medium (Allegra and

Lippman, 1978; Barnes and Sato, 1979). We did not add estradiol to the medium to avoid bias within the EDC treatment. However, long-term maintenance with insulin in the absence of estradiol results in higher expression of estrogen receptor-alpha (ERα) and development of hypersensitivity for estradiol, without losing the growth response to estrogen (Darbre, 2014). BSA was originally added to our serum-free cell medium, because it increased the sensitivity of our biomarker assays. Upon adding BSA solution in the cell culture medium, morphological changes to the serum supplemented culture changed. Barnes and Sato, (1979) added Holmes α-1 protein to eliminate morphological variances. However, Karey and Sirbasku, (1988) investigated that BSA supplementation of minimal 25 µg/mL, was absolute required for growth factor activities. Spheroid formation seen under growth factor or attachment factor lacking conditions can be a result of the lack of epidermal growth factor (EGF). Kim et al. (2012) reported that growth factor (GF)-free culture enhanced the formation of MCF-7 spheres compared to GF-containing culture.

4.2. Establishment of a resazurin based cell proliferation assay

In presence of hormones especially estrogen and estrogen-like substances, MCF-7 cells proliferate (Soto et al., 1995). The resazurin based assay was developed to detect proliferation differences of hormone sensitive MCF-7 cells after exposure to estrogen-active substances and as validation for the biomarker secretion. The assay was developed in parallel to the establishment of the serum-free cell culture and the biomarker chip and was first established for cells in conventional DMEM with 10% FBS and later compared to the serum-free cultured cells. In order to determine the appropriate assay conditions, the conversion of resazurin to resofurin due to the proliferation of cells was analysed for different incubation times, dye concentrations and cell numbers. Resazurin concentrations ranging from 40 µM to 2 mM were tested with the focus on short incubation times at a cell number of $1x10^5$ via colour change. The blue resazurin stain was not completely converted after 4.5 hours incubation in a 2 mM resazurin solution to the pink resofurin, when compared to the resazurin solution without cells (blank). In addition, a decrease of metabolic activity by a drop in fluorescence intensity of 20% from 76,300 [A.U.] to 62,200 [A.U.] for cells cultured in DMEM with 10% FBS and of 30% from 7,600 [A.U.] to 5,300 [A.U.] for the serum-free conditions was observed after 4.5 hours. Under serum-free conditions, the maximal fluorescence intensity was 8400 [A.U.] after 1.5 hours followed by a 10% decrease of signal to 7,600 [A.U.] after 3 hours at the same concentration (Appendix I see: Figure A 4). Similar results were obtained for resazurin concentrations of 1.6 and 1.2 mM. A steady increase of signal was determined with 0.8 mM resazurin. However, incubation times of 24 hours were needed for the complete conversion to resofurin (Data not shown). Dilution of the resazurin solution to 120 µM resulted in total conversion of resazurin to resofurin within 6 hours for a

cell density of $1x10^5$ cells in serum supplemented medium, whereas fluorescence intensities for cells densities starting from approximately 200 cells could be reliably distinguished (See Figure: 29). Lower resazurin concentrations were not sufficient to saturate the capacity of the resazurin conversion due to lower fluorescence intensities compared to 120 µM (Data not shown).

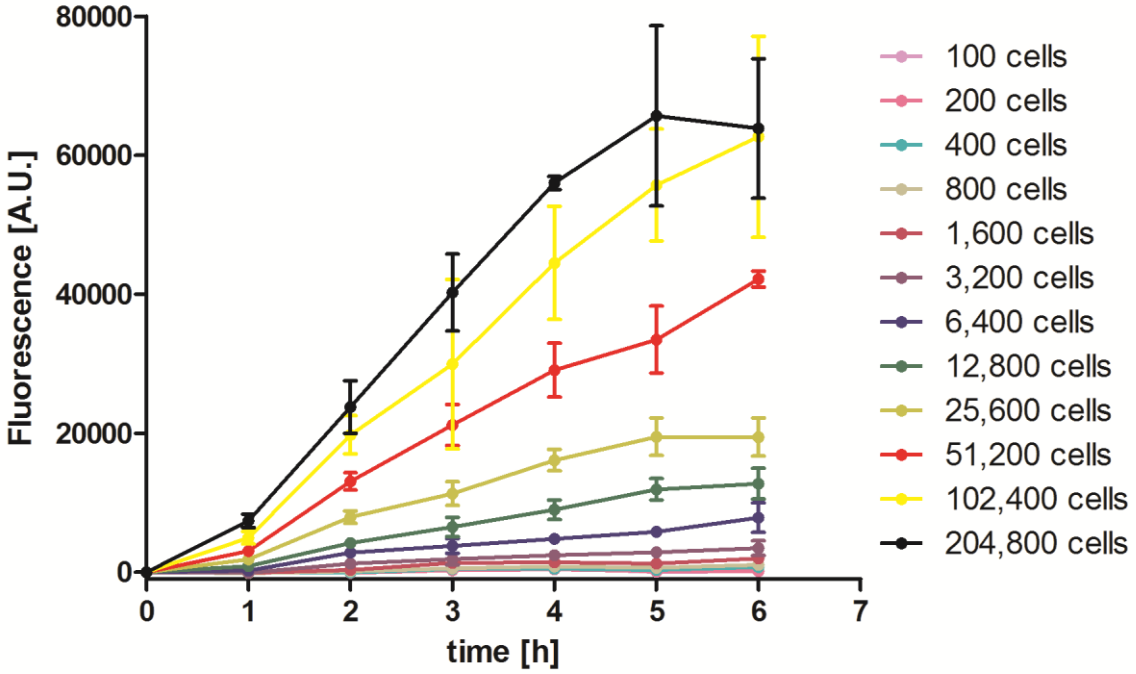

Figure 29: Dependency of incubation time at the single cell densitiy on resazurin conversion in DMEM with 10% FBS. Cells were incubated in 120 µM resazurin solution for 1 to 6 hours. Data are background corrected and shown as mean with SD for n=3.

Signal intensities of resazurin for serum-free and serum supplemented cells increased proportionally to the cell density after 4 hours. In comparison to the serum supplemented cell culture, the cell cultured in serum-free medium showed 40% lower signal intensities for the highest cell density after 4 hours of incubation in resazurin (See: Figure 30). The LOD and LOQ values of cells cultivated with serum-free medium are with 175 and 593 cells insignificant higher than cells cultivated with DMEM 10% FBS medium with 142 and 484 cells. Recovery rates of 102 to 116% were obtained for the conventional cell culture for cell densities in the lower, middle and upper part of the linear range. In comparison to cells cultured in DMEM with 10% FBS, the serum-free approach exhibited recovery rates ranging from 108-74%, whereas higher cell densities showed a lower recovery (See: Table 16).

Table 16: Recovery rates of the established resazurin proliferations assay for serum-free and serum supplemented cell culture.

Cell number	Recovery rates [%] DMEM 10% FBS	Recovery rates [%] DMEM /F-12
250	102	108
1000	116	99
4000	102	90
16000	105	74

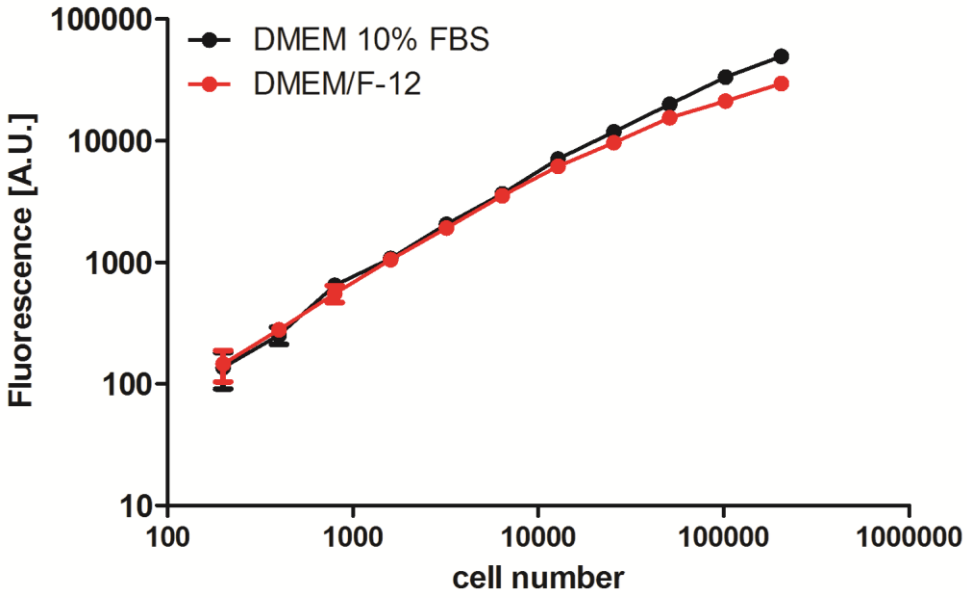

Figure 30: Comparison of resazurin reduction in serum-free cultured cells (red) and conventionally cultured cells (black). Cells were incubated for 4 hours in 120 µM resazurin solution. Data are background corrected and shown as mean with SEM for n=4.

DMEM with 10% FBS was taken for the establishment of the assay to estimate the proliferative response in presence of hormones. The implementation of the assay was focused on measuring the MCF-7 proliferation with a high sensitivity after short incubation times, in order to ensure a parallel determination of proliferation and biomarker secretion after exposure to EDCs. Nevertheless, long incubation times can result in inaccurate measurements, due to resofurin conversion to the non-fluorescent colourless and cytotoxic hydroresofurin (Vega-Avila and Pugsley, 2011). 120 µM resazurin and an incubation time of four hours was sufficient for the proliferation measurements of 200 to 204800 cells in a linear range, in both serum-free and serum supplemented MCF-7 cell culture, whereas 5 hours were needed to completely convert the stain to resofurin at the highest cell density. The assay concentration of resazurin reported in literature is divers and ranges depending on the application and cell line taken from ~ 40 µM to 4 mM (Borra et al., 2009; Magnani and Bettini, 2000; Perrot et al., 2003). Three hours incubation time was described for MCF-7 cells, when applying resazurin concentrations of 44 µM or 88 µM (Pace and Burg, 2013; Uzunoglu et al., 2010). The linear range and lower limit of detection are dependent on the cell type, the ability

to reduce resazurin, the resazurin concentration and the incubation time. Longer incubation periods expand the detectable range of the assay by increasing sensitivity (Vega-Avila and Pugsley, 2011). Low fluorescence signals seen for the conversion of 2 mM resazurin in serum-free cultured MCF-7 cells indicate a lower metabolic activity, due to serum-free culture conditions. Prior experiments showed that MCF-7 cell doubling times in serum-free medium were longer compared to the serum supplemented cells, what would be an argument for a lower metabolic activity. However, the drop in fluorescence for serum-free and serum-supplemented cell culture indicates a direct influence of resazurin on the cell viability. In general, viable cells retain the ability to reduce resazurin into resorufin, which is highly fluorescent. Nonviable cells rapidly lose metabolic capacity and do not reduce the indicator dye, thus do not generate a fluorescent signal (Vega-Avila and Pugsley, 2011). We exclude an influence by hydroresofurin due to short incubation times and no conversion of the stain. Pace and Burg, (2013) reported cytoxic effects on MCF-7 cells by 20% almarBlue® (Company brand, also known under resazurin), which is equivalent to 88 µM (O'Brien et al., 2000), after two to eight days incubation time. Additionally it was shown that resazurin triggers reactive oxygen species (ROS) production in Jukat and HL-60 cancer cells and thereby it direct initiates stress responses in the cells, which results in mitochondrial dysfunction, reduced proliferation of cells as well as autophagy and cell degradation, already 15 min after incubation of the stain in a concentration of 44 µM (Erikstein et al., 2010). However, this was not reported for MCF-7 cells.

4.2.1. Proliferative response under hormone lacking conditions

The proliferative response of MCF-7 cells to hormones can be enhanced under estrogen lacking conditions and by lowering of cell seeding densities (Payne et al., 2000). In order to achieve distinguishable intensities for different concentrations of various estrogen-active substances with different binding affinities to the estrogen receptor after 48 hours, the proliferation of cells were investigated for insulin omission, different incubation times in estrogen lacking medium and different cell densities prior to ß-estradiol exposure.

The effect of insulin and estrogen omission on the proliferation of MCF-7 cells was examined by different incubation times before estradiol treatment with the resazurin proliferation assay. Therefore, 1x104 cells were seeded in DMEM with 10% FBS to ensure cell attachment in presence of estrogen. After 24 hours, the medium was changed to DMEM/F-12 with insulin, followed by a second change to DMEM/F-12 without insulin only for the insulin lacking conditions after 48 hours of seeding. After 72 hours the cells were exposed to 1 pM to 100 µM ß-estradiol (10 times dilution steps) over 48 hours (See: Figure 31C). DMSO was taken as solvent for estradiol and applied in the assay in a concentration of 0.1%. The response to

the treatment was tested against the untreated cells, depending on the approach with or without insulin. Cells under insulin lacking conditions showed significantly higher responses to the estradiol treatment over the untreated cells, especially for concentrations of 1 pM to 1 nM, than cells cultured with insulin. Response variations of 25 to 50% were detected (See: Figure: 31 A). For the investigation of incubation under estrogen lacking conditions, cells were cultured equal to the insulin omission approach, whereas insulin was removed from the medium 24 hours prior treatment. MCF-7 cell were treated after 72 hours and challenged with same estradiol concentrations as mentioned before over two days and compared to cells, which were challenged immediately 24 hours after seeding (See: Figure 31 D).

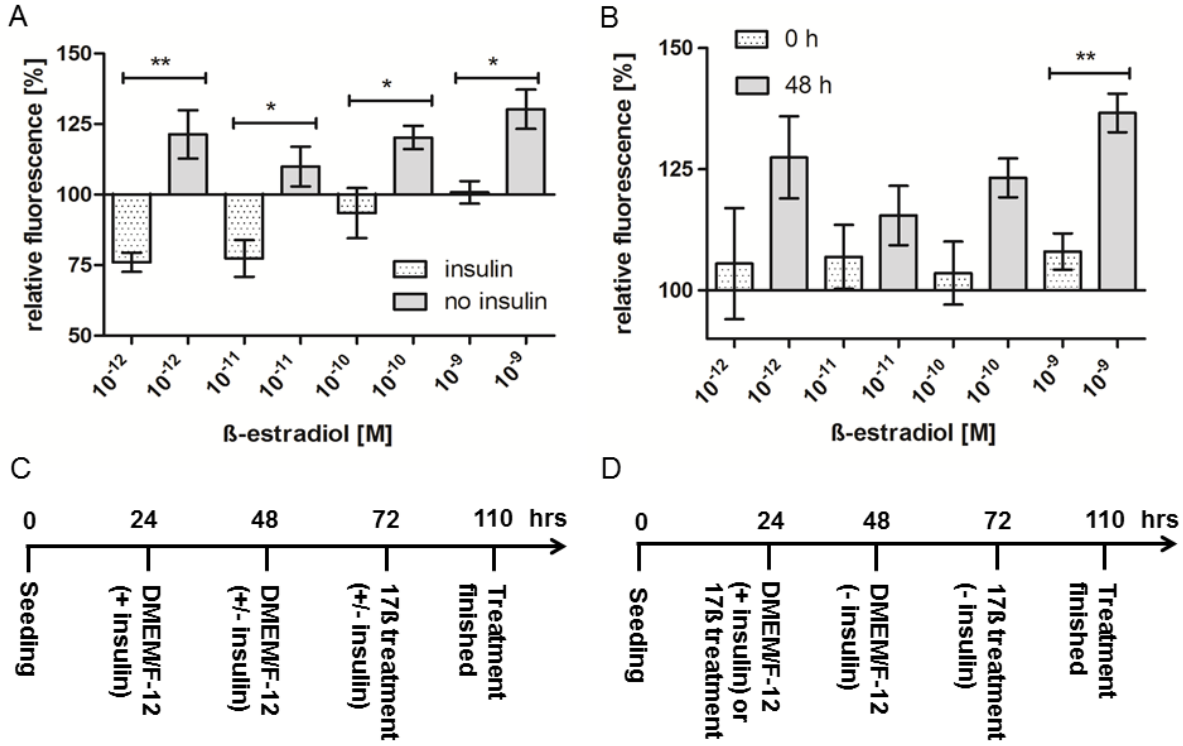

Figure 31: Influence of insulin omission (A) and incubation time in estrogen-free medium (B) on the proliferative response of 1x10^4 MCF-7 cells prior to and during treatment with estradiol (estradiol concentrations: 10^{-12}-10^{-9} M). Timeline for the insulin omission approach (C). Timeline for incubation under estrogen lacking conditions (D). Data are corrected to the fluorescence signals of the untreated cells and shown as mean of relative fluorescence intensities with SEM for n=3. Significance was tested for matching concentrations and treatments with an unpaired t-test for alpha=0.05. Estradiol was solved in DMSO (0.1 % was used in the assay).

Cells with a 48 hour incubation time in serum-free medium due to estradiol exposure, yielded a significantly higher response for the 1 nM estradiol treatment compared to cells, which were treated immediately after 24 hours. A 1.3 fold higher intensities were detected for cells which were incubated for 48 hours in hormone lacking medium compared to cells which were immediately treated (See: Figure 31B). For the comparison of different cell densities, 1x10^4 and 5x10^4 cells per well (densities within the linear range of the proliferation assay) were seeded, cultured and treated equal to the estradiol omission after 72 hours. The proliferative

response of $1x10^4$ cells over the medium control was slightly higher, but not significantly compared to $5x10^4$ cells. In general, the strongest proliferation was determined for 1 nM estradiol treatment compared to the untreated cells (See: Figure: 31A, B). In addition, an up to 1.25 fold decrease of signal was observed for 10 nM to 100 µM compared to the 1 nM treatment, but not over the untreated cells (Data not shown).

In agreement with Payne et al., (2000), MCF-7 cells with 48 hours incubation in estrogen-free medium prior to estradiol treatment showed an increased proliferative response compared to cells cultured in presence of estrogen. The enhanced response was explained by the increase of estrogen receptor expression in response to estradiol deprivation (Katzenellenbogen et al., 1987; Payne et al., 2000). Further enhancement was detected by insulin omission prior to and during estradiol treatment. Insulin is known to reinforce the action of the estrogen receptor (Gaben et al., 2012; Garnier et al., 2003) as well as to modulate MCF-7 cell responses to drugs or drug uptake by altering of cell membrane permeability (Agrawal et al., 2017), what would be an argument against our findings. However, (Stewart et al., 1990) reported that insulin like growth factor (IGF)-1, a protein secreted by MCF-7 cells, with a similar molecular structure as insulin and with the ability to bind to the insulin receptor (Huff et al., 1986), also promotes the proliferation of MCF-7 cells under estradiol treatment in a synergistic way in absence of insulin. In addition, Gupta and Tikoo, (2013) demonstrated that high glucose medium conditions in combination with insulin prevented MCF-7 cell proliferation, due to oxidative stress induced by the high glucose conditions. Our experiments were performed in high glucose medium, what perfectly supports the fact of a lower proliferation in the presence of insulin in comparison to insulin absence. 10 pM and 100 pM estradiol concentrations were reported to achieve the highest proliferative response of MCF-7 cells, significant to the untreated controls after 4 days, whereas concentrations above are in the saturating level of the estrogen receptor (Soto et al., 1995). We observed the highest response for 1 nM estradiol after two days. However, variances did not differ significantly against the pM-concentrations. In addition, the response to estradiol treatment can vary dependently with the applied MCF-7 cell stock and culture conditions (Hamelers et al., 2003; Payne et al., 2000; Soto et al., 1995; Villalobos et al., 1995). The decrease in proliferation for concentration above 1 nM indicates inhibition of proliferation or even cytotoxic effects at these concentrations. Cytotoxic effects of estradiol on cells were described for µM-concentrations, starting at 1 µM and initiated through oxidative stress (Yedjou et al., 2015). The solvent DMSO in a concentration of 0.1 % was taken for the experiments, because it neither showed effects on cell proliferation nor on biomarker secretion (See: Chapter 4.2.3.).

4.3. Biomarker panel

26 proteins, which are secreted by MCF-7 cells, were chosen from the literature as an initial panel for the biomarker chip. They showed to be secreted after estrogen exposure and are linked to toxicological and pathological endpoints of estrogen action within the human body such as reproductive and developmental toxicity, cancer and the metabolic syndrome The initial panel included: 24k -, 52 k- protein, amphiregulin, C-X-C motif chemokine 10 (CXCL10, IP-10), endothelin (ET) -1, gross cystic disease fluid protein (GCDFP) -24 (PBCP), GCDFP-15 (PIP), Insulin like growth factor (IGF)-1, Insulin like growth factor binding protein (IGFBP) -3 and -4, interleukin (IL) -6, IL-11, monocyte chemotactic protein (MCP) -1, matrix metalloproteinase (MMP)-9 and -2, Prostaglandin E2 (PGE2), estrogen-induced pS2 protein (pS2, TFF-1), Chemokine (C-C motif) ligand 5 (RANTES, CCL5), vascular endothelial growth factor (VEGF), transforming growth factor beta (TGF-ß), IL-8, IL-18, Stem cell factor (SCF), Platelet-Derived Growth Factor (PDGF), epidermal growth factor (EGF) and endostatin.

Due to insufficient performance of some commercially available antibodies in our assays (Appendix I see: Figure A 5) and limited availability on the market, we had to exclude biomarkers such as endostatin, an angiogenesis inhibitor, the platelet-derived growth factor (PDGF) involved in embryonic development and differentiation and the estrogen-induced protein pS2, which expression is directly induced by estrogens in MCF-7 cells (Bronzert et al., 1987; Kida et al., 1989; O ’reilly et al., 1997). Ten of the initial 26 biomarkers reached the final panel: VEGF, MMP-9, the cytokines IL-6, IL-8, and IL-11, Rantes, CXCL10, IGF-1, IGFBP-3 and MCP-1.

Several of the chosen biomarker (VEGF, MMP-9, IL-6, IL-8, IL-11, IGF-1, MCP-1 and Rantes) are connected to various developmental stages of cancer. IL-11 and MCP-1 stimulate the breast cancer development and progression. IL-6 is involved in survival, cell migration and proliferation (Chiu et al., 1996; Johnstone et al., 2015; Schafer and Brugge, 2007; Soria and Ben-Baruch, 2008). IL-8 and VEGF are linked to breast cancer metastasis and angiogenesis, whereas MMP-9 is responsible for ECM degradation and thereby invasion of tumor cells (Bendrik and Dabrosin, 2009; Garvin et al., 2005; Nilsson et al., 2007; Roomi et al., 2009). The main cell invasion inducer Rantes by contrast is related to advanced cancer stages, when co-expressed with MCP-1 (Soria and Ben-Baruch, 2008). Biomarkers can also have anti-malignant properties through proliferation inhibition or anti-angiogenetic processes such as CXCL10 and IGFBP-3 (Cardona et al., 2013; Colston et al., 1998; Goldberg-Bittman et al., 2004).

IGF-1 plays an important role in growth processes like cell proliferation and development, and plays an important part in the pathology of diabetes mellitus, adipositas and

hypertriglyceridemia, factors of the metabolic syndrome (Dupont and Le Roith, 2001; Lorincz and Sukumar, 2006). The main transport protein of IGF-1 is IGFBP-3. The estrogen receptor status and the expression of the transport protein IGFBP-3 were reported to correlate with each other (Figueroa et al., 1993; Salahifar et al., 1997). The pro-inflammatory cytokine IL-6 is connected to diseases such as obesity and insulin resistance through its increased expression in adipose tissue. Additionally, IL-6 is involved in the biosynthesis of estrogen by aromatase stimulation (Lorincz and Sukumar, 2006). The cytokine IL-11 acts on the other hand as an adipogenesis inhibitor (Kawashima et al., 1991).

Up- or downregulated secretion of IGF-1, MCP-1, IL-8, VEGF, MMP-9, Rantes, IL-6, and IGFBP-3 could be shown, when exposed to estrogen active substances (Bendrik and Dabrosin, 2009; Chrzan and Bradford, 2007; Dubois et al., 1995; Garvin et al., 2005; Inadera et al., 2000; Kanda and Watanabe, 2003; Nilsson et al., 2007). In general, involvement in reproductive and developmental events such as pregnancy or menstruation was reported for MCP-1, Rantes, IGF-1, and IL-8 (Hull and Harvey, 2014; Kayisli et al., 2002).

Due to their involvement in various biological and pathogenic processes such as reproduction, development, metabolic syndrome and cancer, which are related to endpoints of estrogenic action, the final panel of the biomarkers represents an outstanding tool for the screening of xenoestrogens. In addition, their additive or synergistic action within a molecular and cellular level in food and environmental samples can be pictured. An extension of the system by implementation of new biomarkers can be easily realized on the supposition that high quality antibodies are available.

4.3.1. Biomarker chip development and matrix effects

In order to develop a multiplexed protein microarray for the final biomarker panel of 10 proteins (MCP-1, IGF-1, IGFBP-3, MMP-9, IL-11, IL-6, IL-8, CXCL10, Rantes, VEGF), the assay performance of each antibody pair with protein standards was evaluated and optimized, as well as reagents used for the sandwich immunoassay (Appendix I see: Figure A 6 for the calibration curves). The performance of the biomarker assays established in assay buffer J were compared to the conventional cell medium DMEM with 10% FBS and to the serum-free medium DMEM/F-12 for further protein analysis in cell culture medium. Assays made in the conventional cell medium DMEM with 10% FBS showed similar performance or even an increase in sensitivity (expressed by the limit of detection (LOD), compared to the buffer J (Appendix I see: Figure A 7, Table A 2). A change of sensitivity from 18 pg/mL to 9 pg/mL for IL-6 and from 9834 pg/mL to 224 pg/mL for IL-11 could be detected in DMEM with 10% FBS. However a minimal reduction of the LOD of MCP-1 from 7 pg/mL to 14 pg/mL and IGF-1 from 115 pg/mL to 125 pg/mL in DMEM with 10% FBS was also

observed (Appendix I see: Table A 2). In contrast, performance in the serum-free medium DMEM/F-12 resulted in high losses of sensitivity for MCP-1, IL-6, IL-11, Rantes, and CXCL10. IL-11 for instance revealed in around 50% decrease of signal intensity from 48,000 to 25,000 arbitrary units A.U. and an increase of the LOD from 224 pg/mL to 3653 pg/mL compared to the serum supplemented medium (Appendix I see: Figure A 7, Table A 2). Furthermore, cross-reactivity of VEGF antibodies was determined. This was especially seen against IGF-1 of 58%.

Due to adding of 10 mg/mL BSA solution to the serum-free medium DMEM/F-12 , an up to 10-fold increase in assay sensitivity for IL-11, CXCL10, Rantes and IL-6 and an improvement of signal intensities for Rantes and IL-11 for the highest assay standard concentration by 25 to 36% was observed (See: Figure 32, Table 17). In addition, the cross-reactivity of VEGF against IGF-1 decreased by 77% and the recovery rates improved for IL-6, IL-11, Rantes, VEGF, IGF-1, and MMP-9 when 10 mg/mL BSA supplement was used. Depending on the analysed biomarker, recovery rates within a range of 80-140 % were determined within the working range of the assay (See: Table 18).

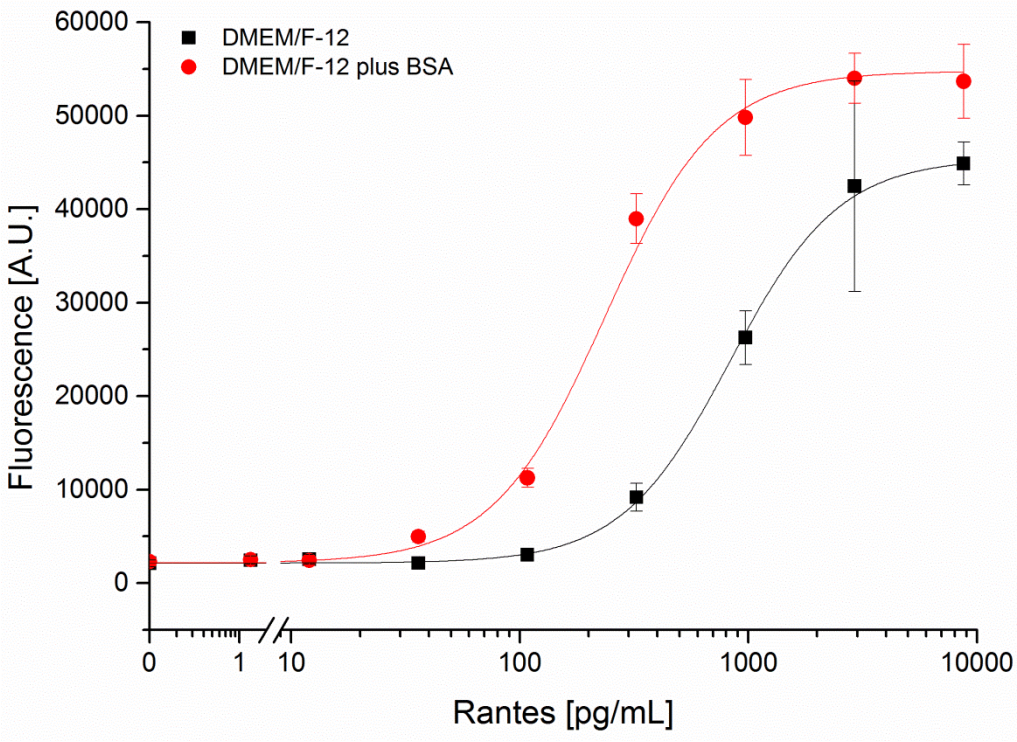

Figure 32: Improvement of the assay performance by 10 mg/mL BSA supplementation shown for the biomarker Rantes. Calibration curves display the assay performance in BSA (10 mg/mL) supplemented (red curve) and BSA free DMEM/F-12 (black curve).

Table 17: Limit of detection (LOD), limit of quantification (LOQ), half maximal effective concentration (EC50) of the multiplexed Rantes sandwich assay performed in serum-free medium DMEM/F-12 with and without BSA supplementation.

Matrix	LOD [pg/mL]	LOQ [pg/mL]	EC50 [pg/mL]
DMEM/F-12	113	227	832
DMEM/F-12 plus BSA	33	65	236

In comparison with commercial single-analyte ELISAs, the multiplexed protein microarray showed similar or increased detection ranges (Appendix I see: Table A 1). However, the values presented in Table A 1 (Appendix I) are based on measurements in assay buffer and not on a complex matrix as cell medium. The choice of a fluorescence based multiplexed approach was made due to the possibility for high throughput screening of various markers in parallel while minimizing size and reagent quantity, which outperform other conventionally used bioanalytical techniques. Next to the quality of the commercial antibodies, the sample matrix can also affect the sensitivity, specificity and reproducibility. In order to do not bias the protein expression and keep a simple setup, the cell supernatant did not undergo extra preparation steps. In addition, dilution of the sample to minimize potential interferences is not possible due to low expression of some proteins used for the assay.

Table 18: The assay parameter limit of detection (LOD), limit of quantification (LOQ), half maximal effective concentration (EC50), recovery rate and coefficient of variation (CV) of the multiplexed IL-6, IL-8, IL-11, MCP-1, CXCL10, Rantes, IGF-1, VEGF, MMP-9 and IGFBP-3 sandwich assays on chip are given. The assay was performed in DMEM/F-12 with 10 mg/mL BSA. LOD-, LOQ- and EC50– values are calculated as mean +/- SEM of three experiments. The CV of three experiments is calculated as mean of eleven standards. Recovery rate data express an added analyte concentration within the linear range of the calibration curves. Table of assay parameter from (Gier et al., 2017).

Biomarker	LOD[pg/mL]	LOQ [pg/mL]	EC50 [pg/mL]	Recovery Rate [%]	CV [%]
MCP-1	4 +/- 2	16 +/- 7	2431+/- 1668	83	14
IL-6	5 +/- 2	16 +/- 6	3916 +/- 1155	132	13
Rantes	16 +/- 7	46 +/- 21	4400 +/- 1841	144	11
VEGF	20 +/- 12	61 +/- 25	3923 +/- 938	131	15
IL-8	53 +/- 17	196 +/- 97	3216 +/- 678	80	22
CXCL10 (IP-	91 +/- 24	321+/- 119	7852 +/- 2275	116	19
IL-11	157 +/- 26	530 +/- 199	26330 +/-13022	105	13
IGFBP-3	581 +/- 254	1630 +/- 477	30644 +/- 3011	104	17
MMP-9	669 +/- 197	2035 +/- 447	49071+/- 7070	118	19
IGF-1	803 +/- 122	2553 +/- 453	39523 +/- 10874	87	15

The decrease in assay performance due to changing the matrix to serum-free DMEM/F-12 can be explained by the absence of blocking reagents such as Tween 20 or serum protein

BSA. These reagents are included in the assay buffer J and in the conventional DMEM with 10% FBS as serum proteins. Blocking reagents are used to suppress non-specific binding, to increase signal intensities and to guarantee assay specificity. In addition, serum proteins are common in the natural environment of antibodies. They reduce protein aggregation and stabilize biomolecules in plasma as well as on assay surfaces (Finn et al., 2012; Gibbs, 2001; Kishore et al., 2014).

4.3.2. Quantification of MCF-7 cell protein secretion in cell medium

In order to successfully quantify the biomarkers on chip, the working range of the assay has to cover the protein expression of the MCF-7 cells (See: Table 18; Appendix I Figure A 6). The biomarker VEGF, MMP-9, IGFBP-3, IL-8, IL-11, Rantes and IGF-1 were secreted in concentrations, sufficient enough for the detection on chip. However, IL-8 and Rantes were difficult to quantify due to low secretion within the low pg/mL range. CXCL10, MCP-1, and IL-6 were secreted in concentrations below the LOD of their corresponding calibration curves. An increase of protein secretion by MCF-7 cells via stimulation with cytokines or growth factors represents a possible option for shifting the secretion in detectable assay ranges. Several stimulants were applied in concentrations mentioned in literature and provided by the supplier (Bronger et al., 2012; Freund et al., 2004; Hollingshead et al., 2008; Mira et al., 2001). The MCF-7 cells were separately stimulated with either 50 ng/mL MCP-1, 10 ng/mL TNF-α, 10 ng/mL IL-1β, 50 ng/mL IL-1α, 10 ng/mL IFN-γ or 50 ng/mL IGF-1 for 24 hours. The measured protein expression corresponds to the working range of the chip. Figure 33 pictures the secretion of marker with low expression for IL-8, Rantes, IL-6, MCP-1, and CXCL10 after stimulation, in comparison to non-stimulated (C0) cells.

The blank value or zero standard (S0) was represented as DMEM/F-12 medium plus BSA. For standard 1 (S1) DMEM/F-12 was spiked with 7.7 ng/mL (concentration within the linear range of the calibration curves) protein standard from each protein presented on the chip. S0 and S1 were applied as negative and positive controls for the protein measurement and for the estimation of the protein expression. The medium control (C0) was introduced in the setup, in order to determine the success of the cell stimulation.

The highest increase in expression was seen after stimulation with IL-1α, IL-1β, and TNF-α, compared to the other stimulants and C0. The stimulation resulted in up to one log higher expression of the biomarkers. Especially for the low abundant and not measured markers without stimulation IL-8, IL-6, Rantes, CXCL10 and MCP-1, stimulation with IL-1ß reached high signal intensities. In consequence, further experiments were performed using IL-1ß as

stimulant over 48 hours, to allow in addition an accumulation of the proteins in the cell supernatant after treatment with ER agonist and antagonists. The medium from untreated MCF-7 cells was further used as negative control. Nine of ten biomarkers could be quantified within the exposure to estrogen active substances in the following experiments. Concentrations of ≥50 pg/mL were detected after 48 hours IL-1ß stimulation. Upon treatment with agonists of the estrogen receptor, IGF-1 could not be quantified within the working range of the assay.

The sensitivity of the protein chip was not satisfactory, for the *in vitro* low expressed markers IL-6, IL-8, Rantes, MCP-1, and CXCL10 by MCF-7 cells (Chiu et al., 1996; Freund et al., 2004; Goldberg-Bittman et al., 2004; Inadera et al., 2000; Mira et al., 2001) and for a reliable quantification in the low pg/mL range (See: Table 18). Secretion promoting stimulants of MCF-7 cells such as growth factors and cytokines, especially the mediator of inflammatory response interleukin-1ß, was highly effective in upregulating the expression of very low abundant biomarkers in a detectable range (See: Figure 33).

The biomarker IGF-1, which normally has a high expression for MCF-7 cells, shows different expression patterns *in vivo* and *in vitro* after treatment with estrogens. An upregulated secretion after estradiol exposure was seen *in vivo*, while it was downregulated *in vitro* (Huff et al., 1986).

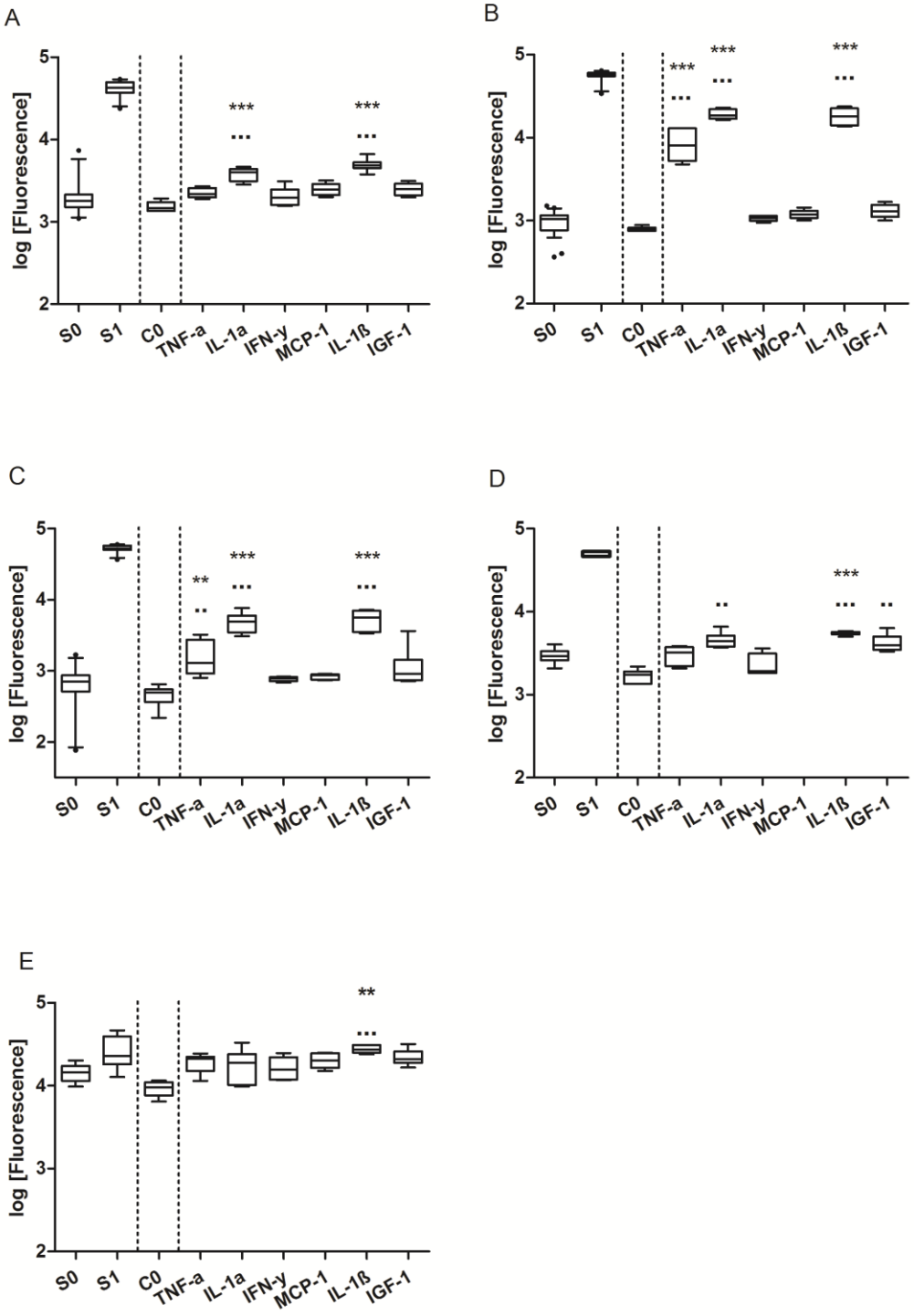

Figure 33: Results of MCF-7 cell secretion after stimulation with IGF-1, MCP-1, IL-1a, IL-1ß, TNF-a, and IFN-y. The box blots display the secretion of IL-8 (A), Rantes (B), IL-6 (C), MCP-1 (D), and CXCL10 (E) after 24 hours in log [fluorescence]. Compared to two standards (without cells) S0 and S1 and the non-stimulated medium control (with cells) C0. Box plots are expressed as 5th and 95th quartiles. One-way-ANOVA and Bonferroni multiple comparison post-hoc test ($p \leq 0.05$ (*), $p \leq 0.01$ (**), $p \leq 0.001$ (***)), for alpha = 0.05 were used for the statistical analysis of n = 6 samples for stimulation against the zero standard S0 (*) and the medium control C0 (▪). Figure was taken from (Gier et al., 2017).

4.3.3. Influences of solvents on protein secretion

Estrogen and estrogen-active substances are hydrophobic compounds, which have to be resolved in organic solvents, due to low solubility in liquids such as water or cell medium. These solvents or vehicles have to be tested in order to do not interfere with experimental outcomes and their interpretation. The most suitable solvents for the used test substances are ethanol (EtOH) and DMSO. A fluorescence based cell proliferation assay grounded on the metabolic conversion of resazurin to the highly fluorescent resofurin was performed in parallel to the measurements on the protein chip (See: Figure 34). The effect of EtOH and DMSO in a concentration of 0.1% was tested for changes in proliferation and protein secretion of MCF-7 cells cultured in DMEM supplemented with 10% FBS and the serum-free medium DMEM/F-12 with BSA.

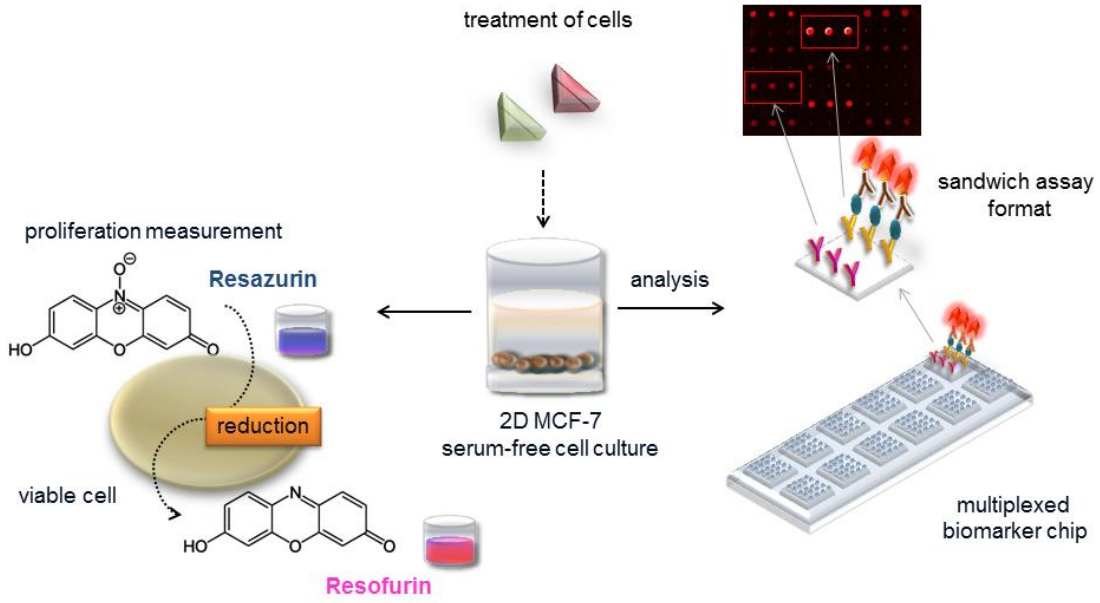

Figure 34: Biomarker chip and proliferation platform shown as experimental setup. First MCF-7 cells are treated with samples containing estrogen receptor agonists and antagonists. Due to the treatment, proteins are secreted and quantified in the cell medium, using the fluorescence based multiplexed protein microarray. The biomarkers are measured on-chip in a sandwich assay format. Analytes are captured by immobilized antibodies. The binding is detected by fluorescently labeled detection antibodies. A proliferation assay based on metabolic reduction of resazurin to resofurin is applied in parallel, to measure the proliferative effect in hormone-sensitive cancer cell line MCF-7. Figure was taken from (Gier et al., 2017).

Upon exposure to 0.1% EtOH, the secretion of VEGF, Rantes, IL-6, and IGFBP-3 was upregulated. The expression of the markers seems to directly affect the stimulation. Other markers showed no increase in expression. The biomarker Rantes showed the highest effect on the treatment. Approximately 34% increase was determined compared to the medium control (See: Figure 35 A and B). In addition, the cell proliferation in DMEM with 10% FBS

increased after 0.1% EtOH treatment compared to the medium control. However, the serum-free cell culture showed no significant effect on treatment. Treatment of cells with 0.1% DMSO, a concentration reported to be non-cytotoxic (Jamalzadeh et al., 2016), showed no significant change in proliferation nor in secretion after 48 hours. Therefore, 0.1% DMSO was applied in following experiments as solvent for the test substances.

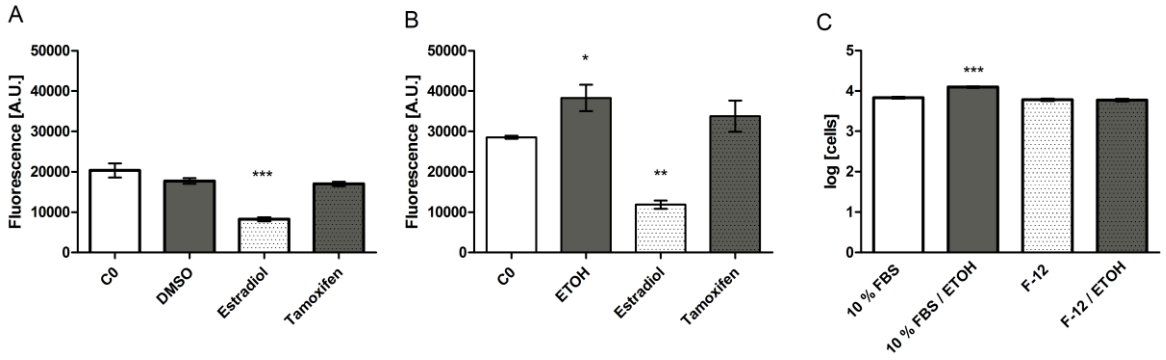

Figure 35 Secretion of the biomarker Rantes in IL-1ß stimulated cells challenged with solvents 0.1% DMSO (A) and 0.1% EtOH (B) compared to untreated cells (C0), and estrogen receptor agonist (estradiol) and antagonist (tamoxifen) treatment. Proliferation of MCF-7 cells in standard medium and serum-free/phenol-red-free medium DMEM/F-12 with and without 0.1% EtOH (C). Proliferation data are log transformed. Bar graphs are plotted as means ±SEM. Significance was tested (n = 5 (A,B); n = 4–8 (C)) against the C0 control with a one-way ANOVA and a Bonferroni multiple comparison test for alpha = 0.05 ($p \leq 0.5$ (*), $p \leq 0.01$ (**), $p \leq 0.001$ (***)).

The proliferation assay and the biomarker chip were used for the determination of effects on the expression of MCF-7 cells and their secretion due to solvent exposure for the further application in cell experiments. Already concentrations above 0.5% DMSO can actually show cytotoxic effects (Jamalzadeh et al., 2016). In comparison to DMSO, EtOH was reported to be cytotoxic in higher concentrations (Jamalzadeh et al., 2016). However, the increase in proliferation in DMEM with 10% FBS due to exposure to 0.1% EtOH in the experiments, can be probably explained by an additive effect through the weak estrogenic phenol red and EtOH. That effect was not observed in the serum- and phenol-red-free cell medium (See: Figure 35). Etique et al., (2004), further supports our findings. They reported an increase in MCF-7 cell proliferation for especially low EtOH concentrations. Furthermore, EtOH was shown to be directly involved in the expression of MMP-9 at concentrations of ≥0.3% (Etique et al., 2006), and dose-dependently stimulates the activity of ER alpha (Fan et al., 2000). Nevertheless, no effects on the secretion of MMP-9 after treatment to 0.1% EtOH were detected in our experiments, only on VEGF, Rantes, IL-6, and IGFBP-3. In conclusion the experimental bias by DMSO is lower compared to EtOH, when compared to our data and the

facts of the literature. For that reason DMSO in concentrations ≤0.1% is the preferred solvent for the test substances.

4.3.4. Specific secretion patterns

MCF-7 cells were treated with 1 µM of the known ER agonists, bisphenol A, genistein and nonylphenol over 48 hours and compared to the most affine endogen ligand 17ß-estradiol (1 nM), as positive control for estrogenic action. As control for anti-estrogenic action, 10 nM fulvestrant and 1 nM tamoxifen (in breast tissue) were applied. The chosen concentrations are shown to be not cytotoxic and correspond to maximal responses in proliferation assays (Payne et al., 2000; Soto et al., 1995; van Meeuwen et al., 2007; Wetherill et al., 2007). The nuclear estrogen receptors trigger the transcription of downstream genes, which can be influenced differently by antagonists and agonistic (See: Figure 36 A, B).

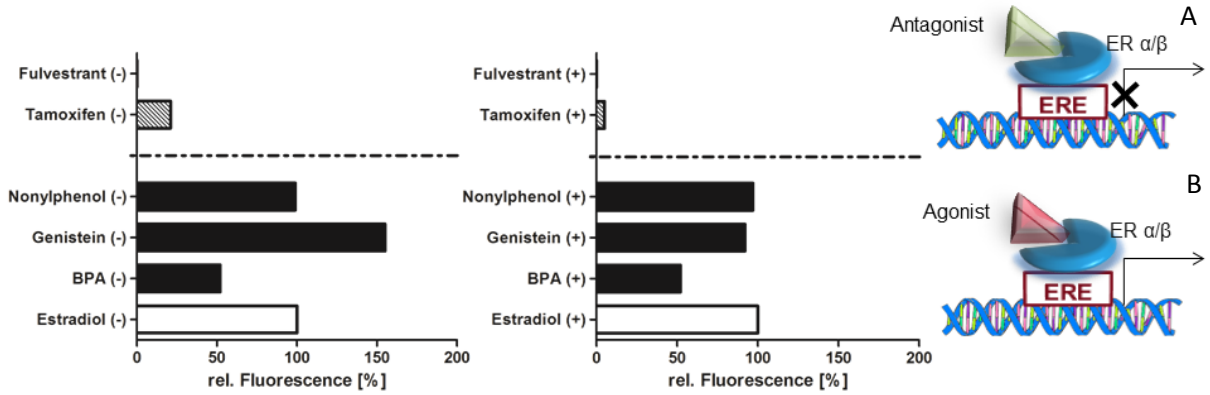

Figure 36: Graphs (left graph without (-) and right graph with IL-1ß stimulation (+)) picture the proliferative effect of MCF-7 cells. The cells were exposed to agonists (estradiol, bisphenol A (BPA), genistein, and nonylphenol) and antagonists (tamoxifen and fulvestrant) of the estrogen receptor. Antagonistically action (A) on the estrogen receptor blocks proliferation signaling, and agonistically (B) triggers proliferation of cells. Baseline-corrected (to estradiol treatment and medium control) data for n = 6, are plotted as relative fluorescence.

An increase in cell proliferation after exposure to ER agonists was expected, especially to its isoform ERα compared to ER antagonists. Nonylphenol treatment resulted in the same proliferative effect as estradiol treatment with and without stimulation. Bisphenol A proliferation was reduced by half, while genistein exposure, resulted in 50% more response without stimulation (See: Figure 36). Due to exposure to the antagonists fulvestrant and tamoxifen proliferation rates below 30% were measured. Like genistein, also the tamoxifen treatment showed a decreased proliferation after stimulation (See: Figure 36).

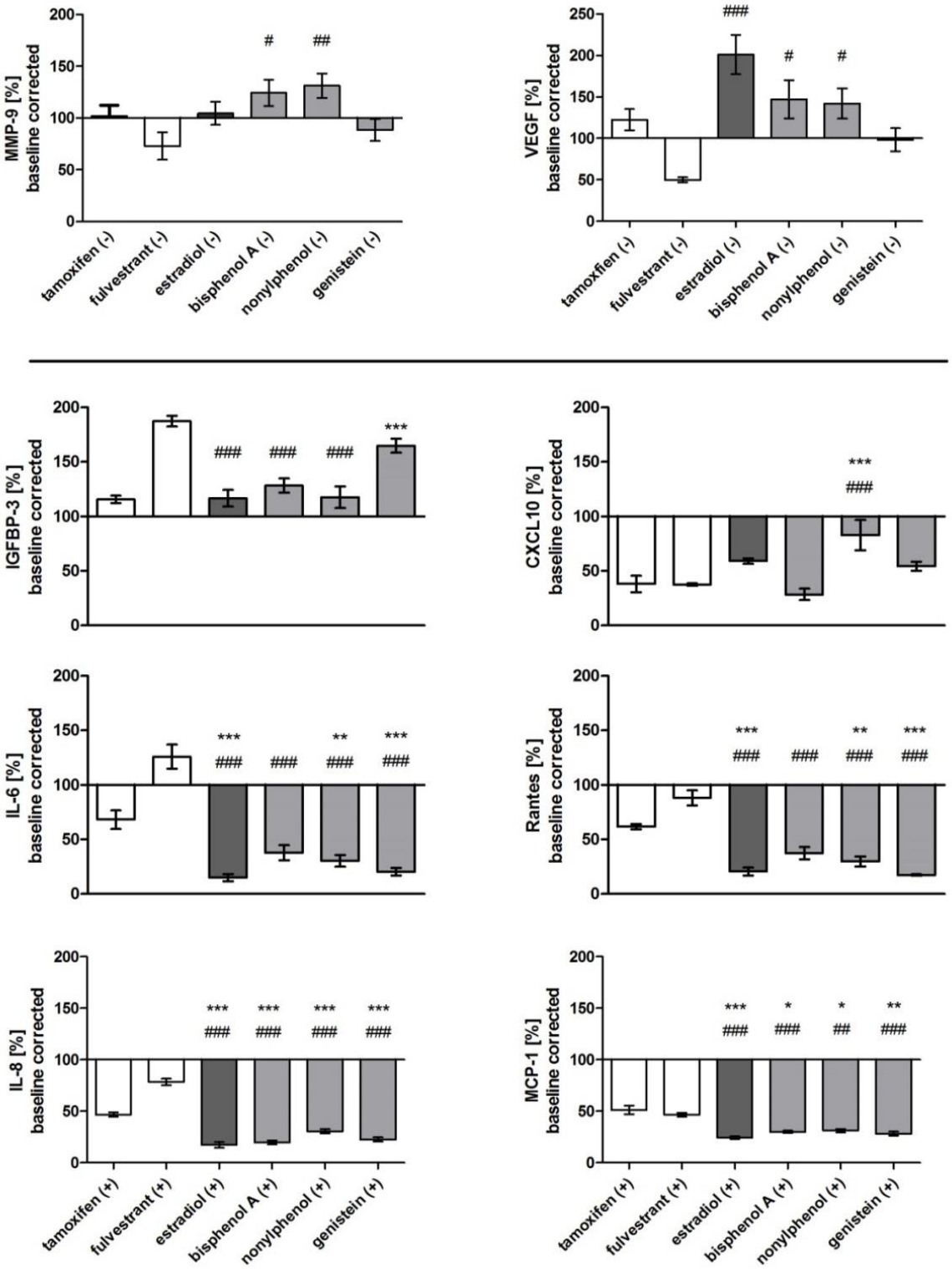

Figure 37: The relative secretion after treatment with ER agonists (estradiol, BPA, nonylphenol, genistein) and ER antagonists (fulvestrant, tamoxifen), without (-) or with (+) IL-1ß stimulation of the markers MMP-9, VEGF, IGFBP-3, CXCL10, IL-6, Rantes, IL-8, and MCP-1 over 48 hours is shown. The mean of baseline-corrected data with SEM is plotted, and shown in percent to the medium control. One-way-ANOVA and a Bonferroni multiple comparison post-hoc test (alpha = 0.05) was applied for significance testing against treatment with tamoxifen (*) and fulvestrant (#) for n = 6 ($p \leq 0.05$ (*), $p \leq 0.01$ (**), $p \leq 0.001$ (***)).

Figure 37 displays the biomarker graphs, which showed a specific estrogenic or anti-estrogenic secretion. VEGF and MMP-9 expression without IL-1ß stimulus was significantly upregulated after treatment with agonist compared to antagonist, while the differences disappear after stimulation. Under IL-1ß stimulation, significant secretion patterns were determined for the other biomarkers. IL-6, IL-8, Rantes, and MCP-1 were significantly downregulated for estradiol, nonylphenol and genistein treatment in comparison to tamoxifen and fulvestrant. BPA treatment showed slightly less expression differences. Downregulation of IGFBP-3 was detected when treated with estradiol, bisphenol A and nonylphenol. Genistein treatment showed under stimulation similar secretion patterns compared to fulvestrant treatment. Only for IGFBP-3, MMP-9 and IL-11, an upregulated expression was seen after agonist exposure in relation to the medium, while all others showed lower expression. Table 19 summarizes the gained results in a color coded translation of expression patterns overview.

Table 19: Color-coded biomarker secretion patterns. MCF-7 cells (stimulated: +, non-stimulated: -) challenged with tamoxifen, fulvestrant, estradiol, genistein, bisphenol A, and nonylphenol, and marker expression quantified with the chip relative to untreated cells (%). Colors are graded in steps of 20 % (Gier et al., 2017).

	Tamoxifen	Fulvestrant	17ß	Genistein	BPA	Nonylphenol
MMP-9 -	102	73	105	89	124	131
VEGF -	122	50	201	98	147	142
IGFBP-3 +	133	213	130	190	145	136
IL-6 +	68	126	15	20	38	30
IL-8 +	47	78	17	23	20	31
MCP-1 +	51	47	24	28	30	31
Rantes +	62	88	21	17	37	30
CXCL-10 +	38	38	59	54	28	83
IL-11 +	139	328	192	268	295	198
IGF-1 +	n.a.	n.a.	n.a.	n.a.	n.a.	n.a.

Colour code: <30 % | 31-50 % | 51-70 % | 71-90 % | 91-110 % | 111-130 % | 131-150 % | >150 %

Validation of the system was performed by exposure of MCF-7 cells with popular estrogen active substances. Similarity in secretion (See: Table 19) and proliferation to estradiol treated cells was noticed. Expression of the markers after exposure to agonists and antagonists, especially fulvestrant are remarkable different. Anti-estrogens, in special selective estrogen receptor modulators (SERMs) such as tamoxifen can show tissue depended agonistic and antagonistic action on the proliferation of MCF-7 cells under deprivation of estrogen.

Agonistic effects of tamoxifen were reported for low concentrations (Katzenellenbogen et al., 1987). Expression patterns gained for tamoxifen treatment support the findings, when compared to the results of fulvestrant treatment. Significant downregulation was seen for IL-6, IL-8, MCP-1 and Rantes after exposure to estrogen active substances compared to fulvestrant. Other markers show more distinct secretion patterns (See: Figure 37, Table 19).

The similar expression of MMP-9, VEGF and IGFBP-3 due to the treatment of genistein and fulvestrant can be explained by the capability of genistein to trigger the downregulation of ERα mRNA and therefore protein levels (Maggiolini et al., 2001), as well as fulvestrant (Scott et al., 2011). The phytoestrogen genistein binds to ERα and ERβ. That could be an explanation for diversity in secretion and proliferation.

IL-1ß stimulation combined with treatment by genistein and fulvestrant showed for IL-11, IGFBP-3, and MMP-9 additive effects. Even synergistic effects were observed due to the treatment of BPA in combination with IL-1ß stimulation for IL-11 (See: Figure 38). The reason could be a positive feedback loop within the MCF-7 cells. Nevertheless, more experiments have to be performed for verification of these effects on MCF-7 cells to the treatment.

MCF-7 cells proliferate in presence of hormones. Due to their sensitivity to hormones and related substances, they are applied in validated toxicological measurements like the E-Screen. The E-Screen determines and verifies estrogen active substances in relation to estradiol using proliferation rates of the MCF-7 cells (Soto et al., 1995). Therefore a resazurin based assay with fluorescence read out was used to evaluate the hormone regulated proliferation of MCF-7 cells, supporting in parallel the measurements on the biomarker chip. Differences seen in our proliferation measurements after treatment with genistein or bisphenol A were also described by Seo et al., (2006) and Soto et al. (1995). Nonylphenol was described as a full estrogen receptor agonist, showing 100% response in the EScreen, whereas bisphenol A exhibit only 85% (Sonnenschein et al., 1995).

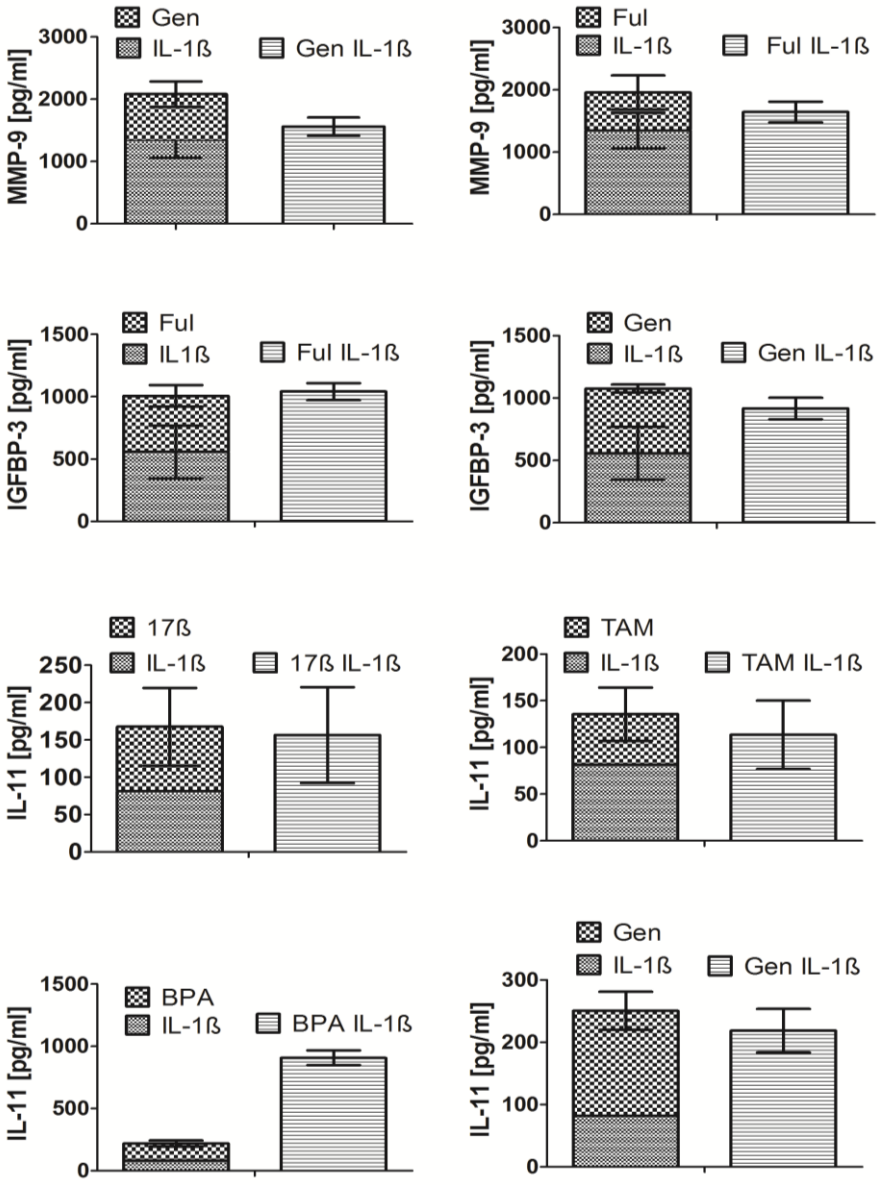

Figure 38: Additive and synergistic effects of the secretion of MMP-9, IGFBP-3 and IL-11 when treated with IL-1ß and receptor agonist bisphenol A (BPA), genistein (Gen), ß-estradiol (17ß) and antagonists fulvestrant (Ful) and tamoxifen (TAM) over 48 hours. Stacked graphs show the addition of the concentration of the single treatments compared to the combi-treatment. Bar graphs are shown as mean of n=6 with SD. Concentrations were calculated via the calibration curves (Appendix I see: Figure A 6).

4.4. Immobilization of Bisphenol A

For the development of an on-chip bisphenol A (BPA) binding inhibition immunoassay, BPA has to be immobilized on the chip surface. However, BPA is a small organic molecule with less reactive functional groups compared to bigger proteins. In order to immobilize BPA, different strategies were tested: 1) immobilization of BPA-protein conjugates and 2) immobilization of the bare molecule BPA in sciPOLY3D gel.

BPA was conjugated to keyhole limped protein (KLH), human serum albumin (HSA), bovine serum albumin (BSA) and horseradish peroxidase (HRP) by the heterobifunctional cross-linker p-maleimidophenyl isocyanate (PMPI), whereas proteins were conjugated in a reduced and a unreduced form. The covalent immobilization of the hapten-protein conjugate was investigated on different functionalized surfaces: poly-L-lysine, ARChip Epoxy, superaldehyde, amine and the ARChip gel. The unconjugated BPA, BPA-PMPI conjugates and BPA-protein conjugates without the PMPI crosslinker were tested on the surfaces. Unconjugated protein carriers were taken as a control for the specific binding of the BPA antibody. The immobilization was tested within a direct binding assay with a concentration of 0.1 to 2 µg/mL of the labeled BPA antibody. High signal intensities up to 50,000 [A.U.] were measured for the BPA-PMPI-BSA conjugates on the ARChip gel (See: Table 20, Figure: 39A), whereas the conjugates with unreduced BSA carriers showed up to 1.25 fold lower intensities. In general, the reduced protein carrier gained an increase in signal compared to the unreduced molecules. HSA, KLH and HRP-conjugates exhibited a poor performance with signal intensities lower than 25,000 [A.U.], independently from the surface. No significant difference in signal was determined between the BPA-protein conjugates and the crosslinked BPA-protein conjugates (See: Figure 39A). The bare Bisphenol A molecule exhibits the best performance on aldehyde and poly-l-lysine surfaces (See: Figure 39B, Table: 20). However, intensities equal or lower than 25,000 [A.U.] were obtained and therefore intensities were similar to the immobilization with KLH-, HSA-, and HRP conjugates. Evaluation of the interaction of the BPA detection antibody with the carrier proteins showed high cross reactivity against BSA on all surfaces compared to signals of the immobilized conjugates. Medium, low or no cross reactivity was seen for the proteins HSA, KLH and HRP depend on the surface (See: Table 20).

Table 20: Comparison of cross reactivity (CR) and fluorescence intensities (I) of the different BPA-protein conjugates, immobilized on different surfaces (high (h) : >30,000 A.U., medium (m): 10,000-30,000 A.U., low (l):<10,000 A.U.). Only the fluorescence intensities of the BPA-conjugates with reduced proteins are displayed.

Surface	**BSA conjugate**		**HSA conjugate**		**HRP conjugate**		**KLH conjugate**		**BPA-PMPI**		**BPA-BSA**		**BPA**	
	CR	**I**	**CR**	**I**	**CR**	**I**	**CR**	**I**	**CR**	**I**	**CR**	**I**	**CR**	**I**
Epoxy	m	m	m	l	-	-	l	l	-	m	m	m	-	-
Gel	h	h	m	m	-	-	-	-	-	-	h	h	-	-
Aldehyd	m	l	l	l	l	m	l	l	-	m	m	l	-	m
Poly- L.	m	m	l	m	l	m	l	m	-	l	m	m	-	l
Amine	m	m	l	m	-	l	-	-	-	-	m	m	-	-

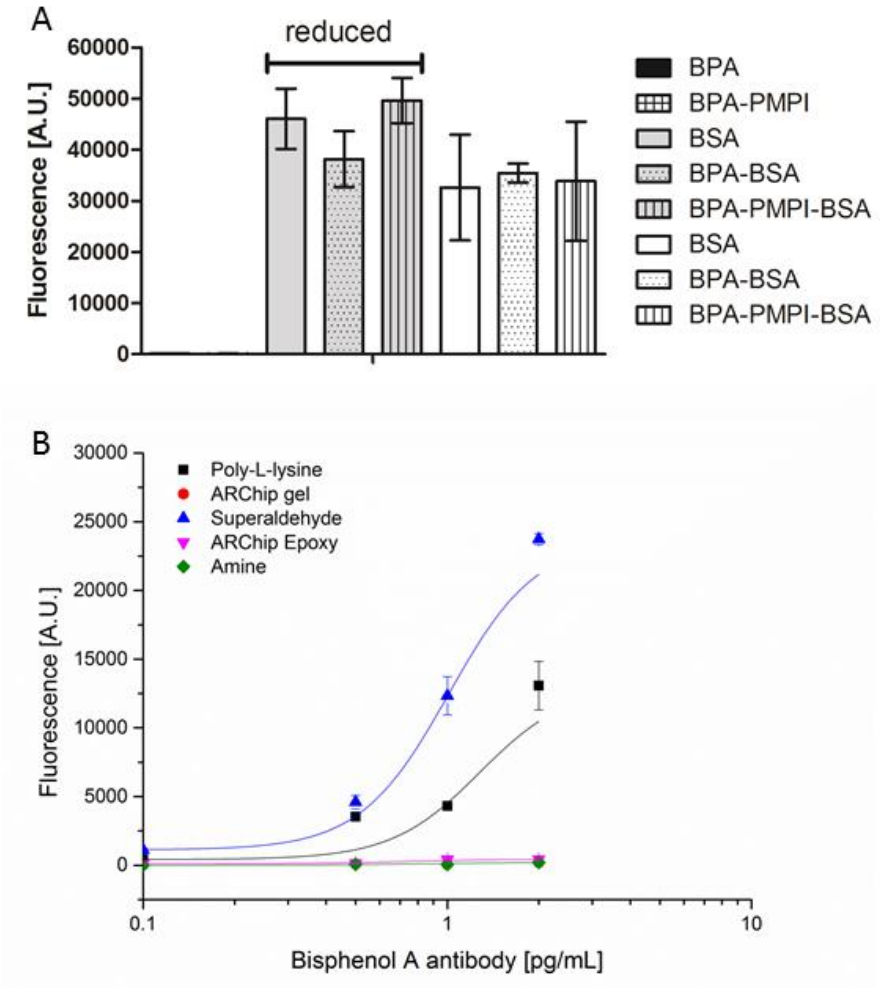

Figure 39: Immobilization of the bare molecule bisphenol A (BPA) (A) and the comparison of BPA-PMPI-BSA-, BPA-BSA-, BPA-PMPI-conjugates (reduced and unreduced BSA) and bare BPA immobilized on ARChip gel surfaces (B). Mean of fluorescence intensities of nine replicates are plotted with standard deviation. The standard curves were made using a 4-parametric-fit.

The immobilization of BPA was further investigated in the hydrogel sciPOLY3D provided by Scienion AG, Berlin, Germany. Therefore, BPA was covalently immobilized via its methyl groups in sciPOLY3D gel onto ARChip epoxy surfaces (See: Figure 40A, B). The BPA immobilization was validated in a direct assay for 0.4 to 3 mg/mL immobilized BPA using a Dy647-labeled BPA antibody in concentrations of 0.1 to 2 µg/mL. The highest signals were detected for 3 mg/mL immobilized BPA with fluorescence intensities of ~ 30,000 [A.U.] for the highest antibody concentration. For lower immobilized BPA concentrations, the intensities decreased stepwise in average 1.2 fold to 10,000 [A.U.] (Appendix I see: Figure A 8). An antibody concentration of 0.75 µg/mL proved to be suitable for the further development of the binding inhibition assay. However, the spot morphology for all BPA concentration was not uniform, what is a sign for uneven molecule distribution in the spot (Mujawar et al., 2013) (See: Figure 40C). In order to improve the spot morphology and thereby the molecule distribution in the spots, 20 µM trehalose was added in the BPA-sciPOLY3D solution. Upon

trehalose addition, the spots became uniform (See: Figure 40 C). For the development of the binding inhibition assay, BPA concentrations of 1 to 4 mg/mL with and without 20 µM trehalose were immobilized for the purpose of difference determination in consequence of trehalose addition. The BPA analytes were incubated with the BPA detection antibody for 10 minutes prior to application on the array. The mixture of BPA analytes and antibodies was incubated for 2 hours on the arrays. The highest signal intensities in the binding inhibition assay were achieved for 3 mg/mL BPA in sciPOLY3D plus 20 mM trehalose. Upon adding of 20 µM trehalose, the sensitivity increased from 7.09 ng/mL for 3mg/mL BPA without trehalose to 3 ng/mL with trehalose addition. Furthermore, the inter slide variation of the signals from 22% to 7% was improved due to trehalose supplementation (Appendix I see: Figure A 8; See: Figure 40D, Table 21). 3 mg/mL proved to be the highest concentration possible for the immobilization in sciPOLY3D.

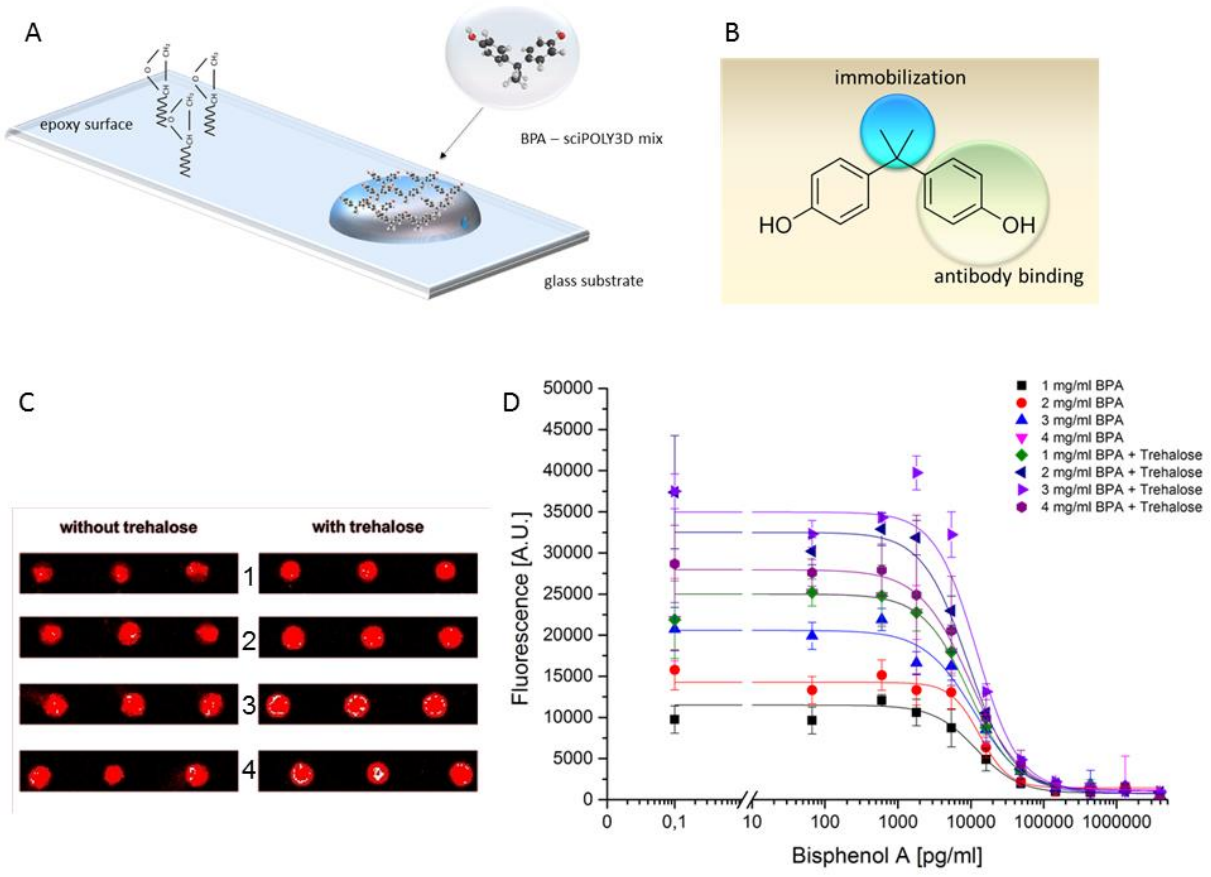

Figure 40: Immobilization of bisphenol A (BPA). BPA was immobilized in sciPOLY3D gel on a ARChip Epoxy surface (A). Immobilization in sciPOLY3D gel via covalent binding to the methyl groups of BPA, therefore antibody recognition of BPAs hydroxyphenyl groups is assumed (B). Spot morphology for the immobilization of 1 to 4 mg/mL (1-4) BPA in sciPOLY3D with and without 20 mM trehalose (C). Comparison of the standard curves of the binding inhibition assay made with different BPA concentrations immobilized and with and without 20 µM trehalose (D). Data of standards are shown as mean with standard deviation of n=6 replicates.

The immobilization of BPA was investigated as hapten-protein-conjugates on different functionalized surfaces and with the bare molecule in a new hydrogel from Scienion AG. The heterobifunctional cross linker PMPI enables conjugation of haptens and peptides with less functional groups such as estradiol, progesterone or digoxigenin to proteins by thiol to hydroxyl coupling via its maleimide and isocyanate groups (Annunziato et al., 1993). The crosslinker PMPI is mostly suitable for small molecules conjugation, because of its solvent limitation (Annunziato et al., 1993). Isocyanates immediately hydrolyze in aqueous solutions and therefore organic solvents such as DMSO or DMF are recommended for the conjugation to the hapten OH-groups. The reaction of maleimide with sulfhydryl groups prefers aqueous buffers with a pH range of 6.5-7.5 for the formation of stable thiol-ether bonds (Thermo Fischer, 2012). However, phenols can also react with the isocyanate group of PMPI under development of aryl carbamates, but with less hydrolytic stability

High cross reactivity of the BPA antibody against the protein BSA or its conjugates was observed. We assume that the cross reactivity occurred due to the production process of the antibody, because bisphenol valeric acid-BSA conjugates were taken as immunogens (Agrisera, 2018). Immunogens produced by hapenation of proteins result in the generation of antibodies against the linkage (Tijssen, 1985; van Weemen et al., 1972). Other BPA-protein conjugates exhibited insufficient assay performance or resulted in lower signal intensities than the bare molecule BPA or the BPA-PMPI-conjugate. We suspected that protein agglomeration and thus prevention of the antibody binding or instability of the conjugate could be an explanation. Feng et al., (2009) achieved better assay performance with direct immobilization of the Bisphenol A derivate 4,4-bis(4-hydroxyphenyl) valeric acid compared to the hapten-protein conjugates. They concluded that conformational changes of the protein are the reason for the poor performance (Feng et al., 2009).

The water-soluble polymer sciPOLY3D enabled a fast forward covalent immobilization of BPA via its methyl groups in a random orientation. The epitope targeted by the antibody is not known, but our results suggest that the antibody binds to the phenols of the molecule (See: Figure 40 B), what would be an additional explanation for the bad assay performance of the phenols conjugated BPA. The supplier did not provide any information about the chemical composition of sciPoly3D gel. However, also Ahn et al., (2012) successfully trapped and immobilized BPA in a porous hydrogel. The addition of trehalose to the BPA-sciPOLY3D gel solution increased the spot morphology, inter-slide variances as well as the signal intensities. The spotting buffer composition (e.g. surfactant concentrations, viscosity and surface tension) strongly influence the spot morphology on surfaces. Higher buffer viscosities ensure compact and uniform spots by achieving more reliable results, higher signal intensities and low background. Buffer supplements such as trehalose were additionally

reported to stabilize proteins and protect them from dehydrating (Kusnezow et al., 2003; Preininger et al., 2005). However, further development of the BPA binding inhibition assay is necessary for possible signal enhancement, definition of the convenient standard concentrations for the standard curve, determination of assay parameters and for the assay performance in real samples.

4.5. Channel assembly of the glass hanging drop system

3D cell culture pictures better the morphological and functional properties of real tissues compared to cells cultured in 2D (Pampaloni et al., 2007). Furthermore, implementation of microfluidics in cell culture applications allows mimicking microenvironments close to *in vivo* conditions by microscale dimensions equals the human body (Gupta et al., 2016; Halldorsson et al., 2015). Therefore, a microfluidic supported hanging droplet device was developed for the generation of MCF-7 cell spheroids.

Different channel assemblies were tested to achieve a stable droplet formation in a glass hanging drop system. In a first approach, a closed serial channel assembly in PDMS bonded to a glass slide was tested. This device consisted of a single channel (diameter: 0.8 mm), which connected four droplet wells to the in- and outlet (See: Figure 41A). Each droplet well had a size of 3 mm in diameter with a well to well pitch of 1 mm. Under flow conditions, we observed an uneven droplet formation. Liquid provided by mechanical filling with a syringe or automatically by a syringe pump resulted in formation of only one droplet, which was closest to the inlet (See: Figure 41B). It was necessary to prefill all wells and connecting channels with liquid, in order to perfuse the whole system by pressure-driven flow. The droplet volume increased evenly in all wells to around 20 µL. Further increase of volume was not possible, due to uneven distribution of the liquid within the wells (See: Figure 41C), which resulted in a final drip off of the droplet closest to the inlet. The other droplets decreased in volume and the whole network failed. However movement of the device in angular positions resulted in backflow of liquid to the outer wells, followed by a dripping off the biggest droplet (See: Figure 41D, E).

A serial channel assembly was tested similar to the devices developed by Frey et al., (2014) and Wu et al., (2016) for the establishment of the glass hanging drop system. The 3 mm diameter of the droplet wells was chosen to enable the transfer of the droplet containing spheroids to a perifusion chamber (See: Chapter 4.5) and to provide higher nutrient supplementation for the spheroids by larger droplet volumes (>20 µL). Furthermore, larger droplet volumes might prevent shear stress on spheroids and so adverse effects on formation processes (Moshksayan et al., 2018; Zuchowska et al., 2017). Zuchowska et al., (2017) reported that more compact spheroids were formed in microwells with 500 µm height

compared to 350 µm high wells, due to lower shear stresses. PDMS was applied in the first line, because of its straight forward production at reasonable cost. The hydrophobic nature of the material complicated the filling with liquid and its distribution in the channel-well network. Due to oxygen plasma treatment, the hydrophobic material PDMS becomes hydrophilic (Tan et al., 2010). This material property can be maintained by immediate application of liquid to the channel system (Maria et al., 2017). Also Wu et al., (2016) had to prefill their device with liquid by flipping to the back side, before they could provide the cell medium. The system failure, due to the droplet drip off in horizontal and angular positions can be explained by exceedance of the droplet volume bigger than the volume of a hemisphere and the introduction of backflow due to hydrostatic pressure differences between the droplets (Frey et al., 2014).

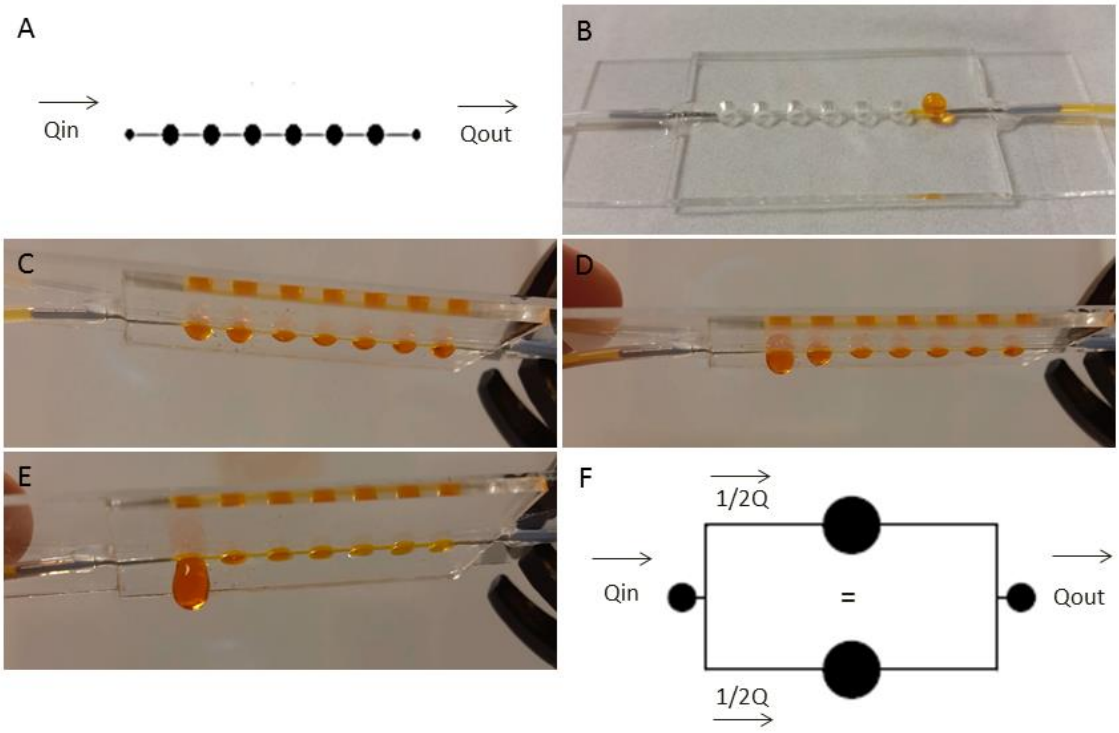

Figure 41: Serial (A) and parallel (F) channel-well assemblies are shown with liquid flow directions and properties of the volumetric flow rate. Drawbacks of the serial channel-well assembly were: no perfusion without prefilling (B and C), backflow of liquid after movement (D and E) and network failure caused by droplet drip off (E).

The failure of the droplet network due to one droplet showed similarity to electrical devices, working with a series circuit like a chain of light. In order to avoid failure of the whole system caused by one component and to increase the droplet stability, we concluded that a parallel well-channel design overcomes the disadvantages of the series design. Under the assumptions of the continuity equation for multiple flow paths for incompressible fluids $\sum Q_{in} = \sum Q_{out}$ (ITACA, 2018) and a parallel circuit from electrical engineering, we designed

a split channel system with an inlet channel positioned in the middle and parallel ordered droplet wells (See: Figure 41F). Due to the design, the volumetric flow rate decreases half at the bifurcation compared to Q_{in} and the droplet wells get filled simultaneously. We hypothesize that the pressure provided by the incoming flow and the resistance of the channels prevent backflow of liquid. In general, the principle of split channels was already successfully applied for microfluidic concentration generators (Dertinger et al., 2001; Frey et al., 2014).

4.5.1. Challenges of the glass hanging drop device fabrication

Prerequisites for an even droplet formation in a glass device are well holes with uniform diameter, equally etched channels and good glass-glass bonding. This requires a good established fabrication protocol. In order to connect the hanging drop platform to an additional spheroid incubation chamber, two 75x25 mm sized glass slides as well as corresponding structure dimensions were used (See: Figure 42). Borosilicate glass was applied for the implementation of the parallel channel-well assembly, due to less oxide content.

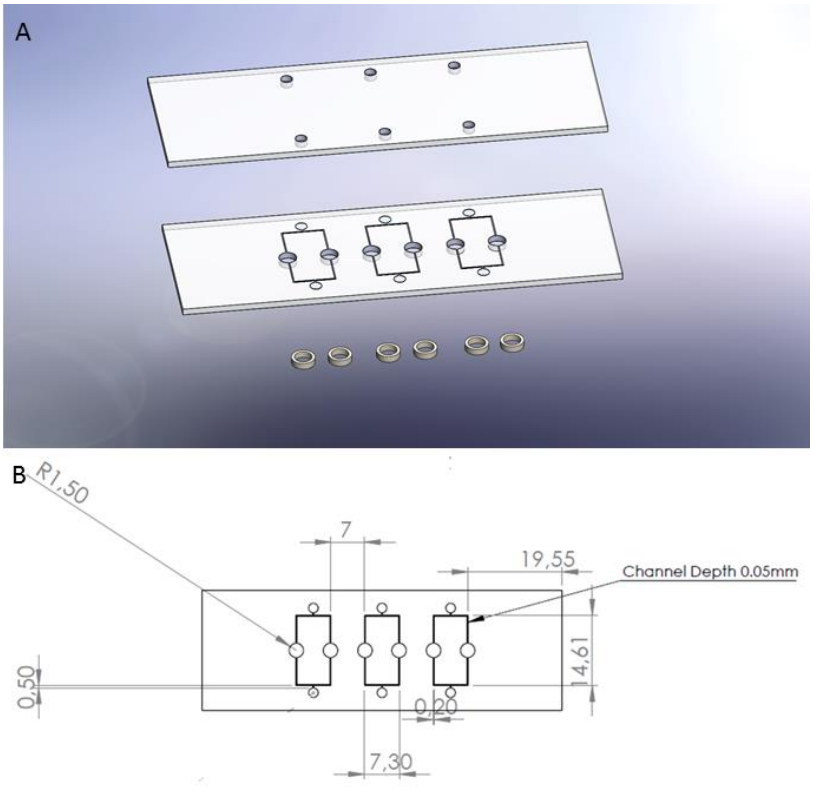

Figure 42: Design of the developed glass hanging drop device (A) with specified dimensions (B).

The introduction of holes for droplet wells and in-/outlets by sandblasting damaged and roughed the glass surface, which complicated the later bonding process (See: Figure 43 A,

B). Protection of the glass and therefore undamaged glass surfaces, were achieved by Scotch tape covering and AZ coating. A metallic mask containing the exact well assembly with corresponding diameters, was used to increase the repeatability of the well diameters and simplify the photomask alignment. Variations in diameter of 0.06 mm (CV; n=18) were achieved.

The coating was challenging, due to the already sandblasted holes. An even thickness of the coating solution on the glass surface for the precise development of the structures was realized by covering the backside of the glass slides with HF paper and adding extra photoresist in the sandblasted holes after spin coating. Therefore backflow of the photoresist in the holes was avoided. After leveling, a thin (approximately 100 µm thick; not measured) and even distributed AZ coating was accomplished, resulting in consisting exposure and development of the structures. The adhesion of the AZ layer was improved by HMDS treatment of the glass slides before coating. After 25 minutes of wet etching with HF, channels with a depth of 0.05 mm and a width of 0.2 mm were achieved (See: Figure 43 D). However, the vertical and horizontal located channels show little size variation (CV: 0.10; n=14) in some devices and partly broken AZ coating, especially at channel parts connected to the droplet wells (See: Figure 43 C, E).

The glass-glass pre-bonding using pressure was challenging. Many newton rings, a sign for trapped air in this area were detected (See: Figure 43F). An improved pre-bonding was gained using ultra clean water wetted glass slides (“Glass Microfluidic Device Fabrication SOP,” 2015; Tan et al., 2010). Most of the water was removed after pressure. A total bonding of the glass slides was determined by the absence of newton rings (See: Figure 43D) in the channel area.

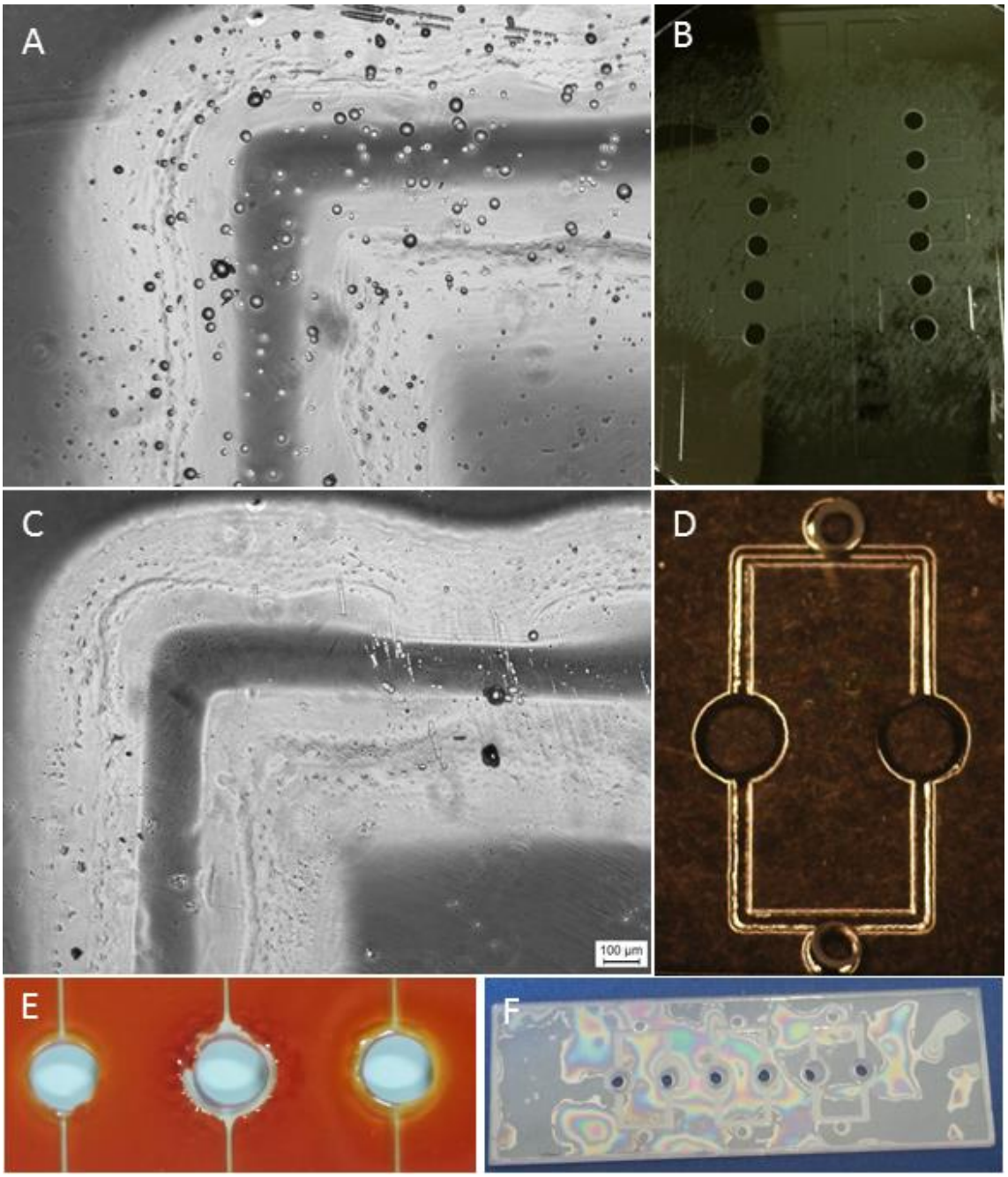

Figure 43: Defects occurred during the production process included: damages due to sandblasting without protection (A, B) in comparison to protected glass slides (C and D), channel dimension variances (C) peeling off of AZ photoresist (E) and newton rings after fusion bonding (F).

The final established glass device fabrication process (See: Figure 44) resulted in a glass hanging drop device, containing an array of three parallel assembled channel-well subarrays (See: Figure 42) in the bottom layer and the in- and outlet holes (diameter: 1.5 mm) in the upper cover layer. Droplet wells (diameter: 3 mm) are connected by channels of 0.2 mm width and 0.05 mm height, which can be filled with a total volume of 21.48 µL (See: Figure 42B).

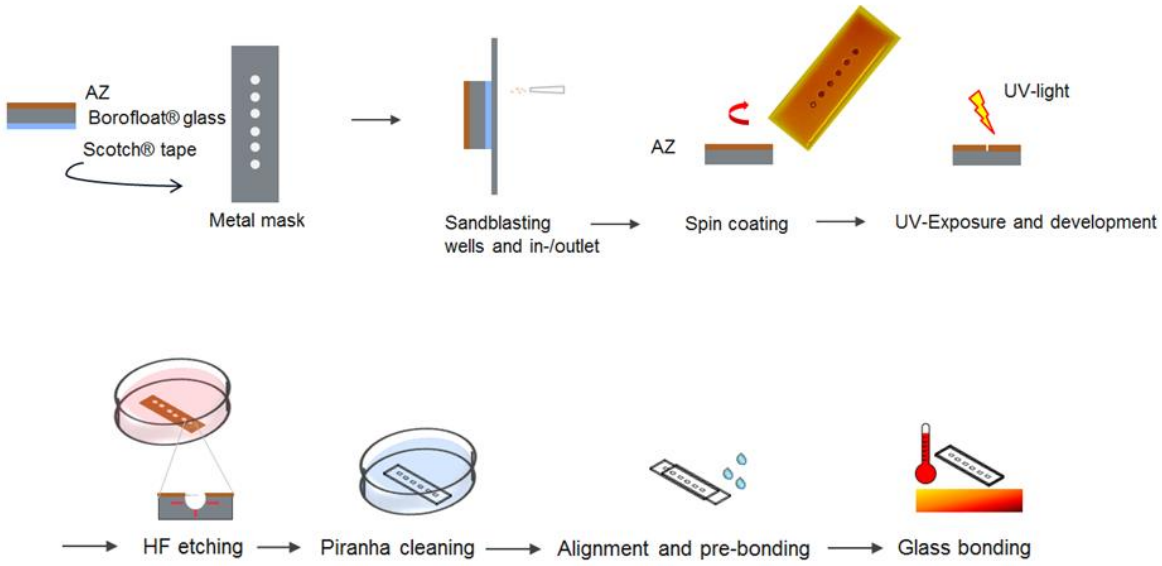

Figure 44: Scheme of the established glass hanging drop device fabrication.

Sandblasting of the holes was performed before wet etching in order to avoid damage on the channels. Defects emerged by sandblasting were near-completely prevented. However, the process is time-consuming and the possibility to introduce damages is high. Alternative techniques for the introduction of holes after etching such as drilling, laser ablation or hybrid techniques could improve the disadvantages (Hof and Ziki, 2017). Furthermore it would simplify the complex coating process and the glass bonding. The wet etching process was already developed in the working group (Jellema et al., 2009). It offers the opportunity for fast processing due to high etching rates, it needs only simple equipment and it shows a high selectivity. Differences measured in channel width can be explained by the isotropic etching, which results in material removal under the coating. Due to longer etching times, the quality of the photoresist coating is affected massively and even results in spalling (Ciprian Iliescu et al., 2008). Improvement of the etching outcome by addition of Cr/Au, silicon or a multilayer under the AZ coating, especially for deeper structures up to 1 mm and longer etching times, is recommended (Bu et al., 2004; Ciprian Iliescu et al., 2007; Iliescu and Tay, 2005). Glass surfaces have to be very cleaned, undamaged and smooth for the fusion bonding (Moriceau et al., 2010). The newton rings, which appear after the fusion bonding, are a result of trapped hydrogen. This is, a product from the reaction of water with silicon crystal substrates, which is unable to diffuse to the edges (Masteika et al., 2014). A water layer between the pre-bonded slides improved the process. The small number of newton rings, which appear in the improved process, can also be a consequence of little damages introduced into the glass substrate during the production process, particle contaminations or insufficient pressure after pre-bonding (Moriceau et al., 2010).

4.5.2. Droplet formation and stability

The stability of the hanging droplets in a humid and warm environment over time is a precondition for the generation of equally formed cell spheroids. Preliminary experiments in the PDMS devices resulted in spreading and fusion of the medium droplets over the device and the other droplet wells after incubation at 37°C, 95% humidity and 5% CO_2 for two days. In agreement with Frey et al., (2014), the spreading of medium was prevented by introducing of a 100 µm deep rim with an inner diameter of 4 mm and an outer of 5 mm in the PDMS device around the droplet wells.

In order to accomplish successful droplet formation of a polar liquid such as cell medium on a hydrophilic glass surface, hydrophobic coatings or nano- or microstructures have to be introduced. In order to change the surface properties of the glass slides, the surface was roughened in a round rim-like structure by a diamond pen and by sandblasting in borosilicate glass and by wet etching with hydrofluoric acid in soda lime glass (See: Figure 45A-D; Appendix I See: Figure A 10). In addition, the borosilicate glass was coated with a water repellent polysiloxane solution Rain-X® and compared to a clued Teflon® ring (See: Figure 45E). The analysis of the droplet formation and stability on the mentioned surfaces was performed by contact - and tilted angle measurements between the surface and the liquid droplet. The contact angle provides a measure for wettability of the surface, whereas angles between 90° and 120° are an expression for incomplete wetting, which is equivalent to droplet formation on a hydrophobic surface (Yuan and Lee, 2013). The tilted angle was used to determine the stability of the droplet on the surface under movement (Eral et al., 2013).

The contact angle of 40 µL DMEM/F-12 cell medium droplets in comparison to water droplets and untreated glass was measured on the different treated surfaces (See: Table 21). The mechanical treatment by sandblasting and by diamond pen scratching did not change the surface properties of the glass slide compared to the untreated glass. The exhibit structures were either quite smooth (sandblasting) or scratched (diamond pen) (Appendix I see: Figure A 10). Contact angles below 90° for both water and medium were determined similar to the untreated glass (See: Table 21). In general, cell medium droplets showed smaller angles for all approaches compared to water with in average 6° variance. The Rain-X® treatment and the chemical etching of the surface exhibited an increase of the contact angle to 95° +/- 1.2° for DMEM/F12 and thereby allowed droplet formation. The motion of the droplet on an inclined plane was tested beginning with a 45° angle under slowly increasing the angle until droplet movement was detected. Cavity-like structures were formed at the inner edge of the wet etched rim (See: Figure 45A-C). The 40 µL droplets started moving at ~ 47° at the HF etched rim. However, a decrease of the droplet volume to 20 µL caught the droplet at the

etched rim, even in a vertical position (90°) of the slide (See: Table 21). In addition, the droplet also slid off at an angle of 47°+/- 3.5° on the Rain-X® coated surfaces (See: Table 21).

Table 21: Contact and roll off angles measurements of 40 µL droplets on glass with different surface treatments. Angels are given as mean of three measurements with standard deviation.

material	chemical properties	surface treatment	contact angle [°]		tilted angle [°]
			H_2O	DMEM/F-12	DMEM/F-12
BOROFLOAT®	hydrophilic	Untreated	35.0 +/- 4.2	27 +/-4.0	-
BOROFLOAT®	hydrophilic	diamond pen	34.0 +/-1.4	33 +/-9.0	-
BOROFLOAT®	hydrophilic	sandblasting	32 +/-3.1	24 +/-1.2	-
BOROFLOAT®	hydrophilic	Rain-X coating	97.0 +/-3.4;	95 +/-1.2	47.0 +/-3.5
Soda lime	hydrophilic	HF etching	95.0 +/-4.4;	86 +/-5.1	- (20 µL droplets)

Glass is a very hydrophilic and inert material and shows good wetting properties for polar liquids such as water with contact angles below 40° (Engländer et al., 1996). The basis of cell culture medium is likewise water supplemented with proteins and growth factors. The addition of proteins and the incubation at 37°C affect the surface tension of a liquid and supports thereby the wetting properties, with contact angles below 30° (Lam et al., 2001; Waghmare and Mitra, 2013). This was also observed in our experiments. The alteration of the glass surface by sandblasting or diamond pen scratching was not efficient enough for the formation of droplets. Roughness of a hydrophilic surface can change the surface characteristics in two directions. It can become hydrophobic or can show even enhanced hydrophilic effects. The hydrophobic behavior of a hydrophilic surface was interpreted by the generation of a rough surface with cavities. In this cavities, air got trapped after depositing of a liquid drop (Patankar, 2009). However, no cavities were formed on the glass by sandblasting or diamond pen, but on HF treated glass. Etching changes the surface topography of glass under creation of micro- and nanoscale structures due to generation of insoluble products, which are deposit on the treated surface (Iliescu et al., 2006; Xiong et al., 2010). The generation of insoluble products is depending on the composition of the glass substrate. The used soda lime glass contains high amounts of CaO and MgO, which react in contact with HF acid to the insoluble products CaF_2 and MgF_2. This causes increased roughness (Iliescu et al., 2005). The motion of a droplet at an inclined plane is introduced by gravity, while the contact angle hysteresis keeps it in position. This yields in an asymmetric shape of the droplet (thin is low angle on top and thick is high contact angle at the bottom), but it will not start immediately to move. After reaching a critical angle, the droplet slipped off the surface keeping the asymmetrical shape. The difference between front and back contact angles is described as contact angle hysteresis (Eral et al., 2013). In consequence of contact

angle hysteresis, change of surface roughness/topography and probably also by the creation of liquid-air interface between the lower edge of the droplet and the rest of the glass surface, the 20 µL droplet on the HF rim did not slip off. However, due to the generation of insoluble products, the etching process for the soda lime glass was not satisfactory for the production of the hanging drop device. Therefore, soda lime glass was replaced by borosilicate glass, which contains only 2% Al_2O_3 and thus results in low concentrations of insoluble products and small surface changes. As a consequence, the hydrophillic surface properties will not change and so prevent droplet formation or stability. The hydrophobic RainX® coating yielded in droplet formation and even so in an immediately droplet slid off from the surface on an inclined plane. In consequence, neither a hydrophobic coating nor changes in surface roughness are enough to keep the droplets stable on the planar glass device.

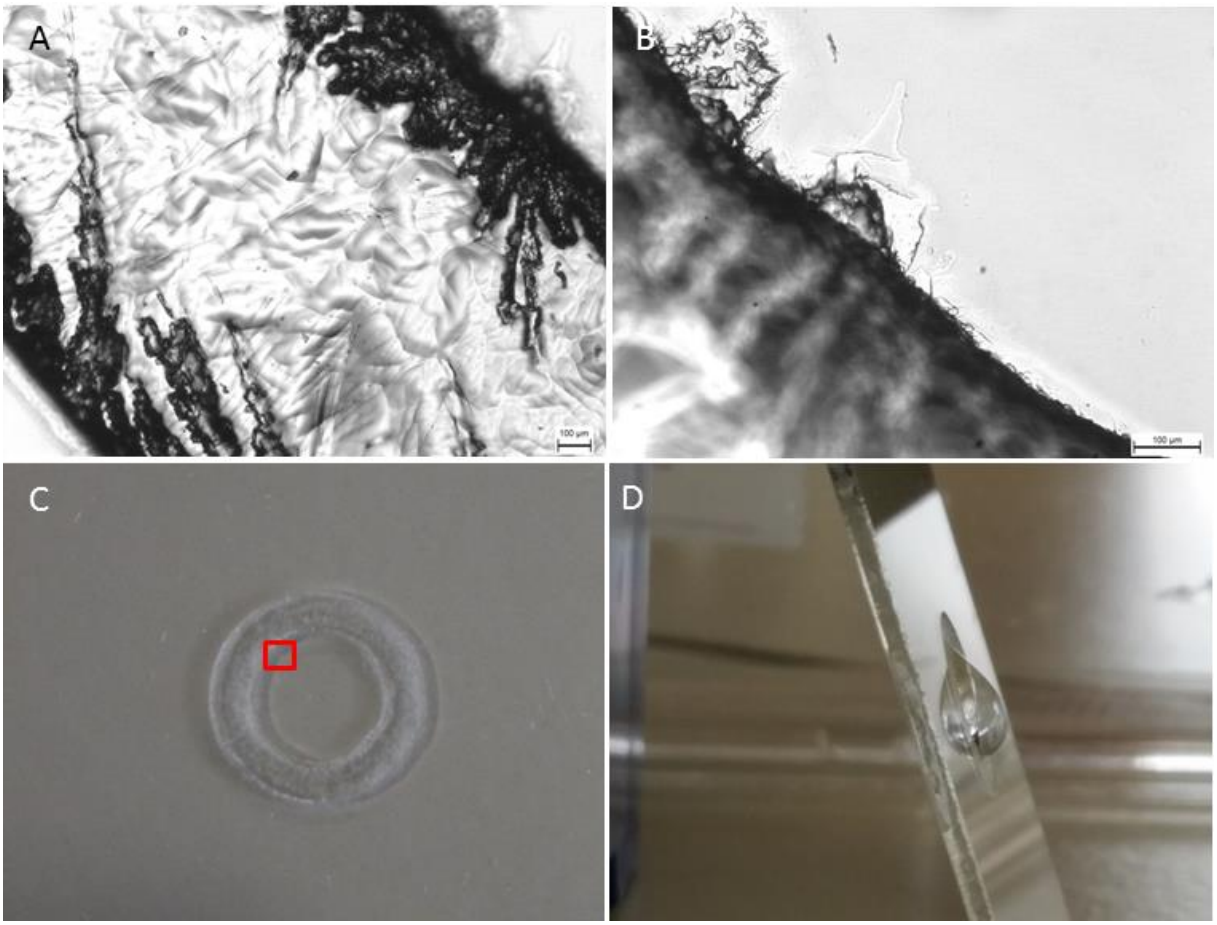

Figure 45: Droplet stability on glass due to surface treatment. The changes of roughness/topography of soda lime glass after treatment with hydrofluoric acid (HF). Surface inside of the HF generated rim (Bar scale = 100 µM) (A). Inner-edge of the HF generated rim (Bar scale = 100 µM) (B). Rim HF generated on soda lime glass (red box shows position of microscopic pictures) (C). Droplet stability was tested at the HF rim and is shown with 20 µL water droplet in a vertical position (D).

4.5.3. Introduction of a hydrophobic PFPE ring

Preliminary experiments showed that changing the glass surface properties was not enough to form a droplet or keep it stable on the glass device. An introduction of a ring structure using an hydrophobic and chemical inert material could improve this. The chemical inert UV-curable material perfluoropolyether (PFPE) was used to form ring-like structures. Tests for droplet stability on an inclined plane and for determination of the ring size was made with different heights (0.5 and 1 mm) and widths (1 and 2 mm) of PDMS rings, which were attached to glass and filled with different volumina of a stained solution. The results showed increased stability for the hanging droplet with increased heigths and widths under enlargement of the droplet volumina from 30 to 65 µL. Rings of 2 mm width and 1 mm height were able to hold up 65 µL droplets stable even under movement (See: Figure 46A). Nethertheless, 2 mm wide rings were more suitable within the production process.

Different PFPE-glass attachment approaches were investigated: direct bonding and adhesive bonding to glass. Direct bonding of uncured PFPE rings with an outer diameter of 6 mm, 2 mm width and a height of 1 mm in PDMS molds with glass resulted in a lot of air bubbles in the cured rings. Pre-curing of the rings in those molds and attachment to the glass slide with liquid PFPE prevented air bubbles in the structures and resulted in strong bonding. However, in a humid atmosphere, the rings delaminated from the glass slide even when treated with oxygen plasma. Silane and epoxy based reagents such as APTES or SU-8 were used to improve bonding to other materials, when plasma activation was not efficient (Aran et al., 2010; Ren et al., 2015; van Dam, 2006). Adhesive bonding with SU-8 and APTES was investigated for the strong attachment of the PFPE rings to glass slides. Glass slides were functionalized with SU-8 and APTES (APTES functionalization according to van Dam, (2006)). SU-8 solutions with different viscosities (from low to high) were tested for the improvement of the bonding: SU-8 2002, 10 and 50. Pre-cured PFPE rings were bonded to the coated surface by UV-light exposure using uncured PFPE as intermediate layer. The SU-8 bonded rings were further treated with heat (95 °C) for 10 minutes. The APTES coating did not improve the bonding. The PFPE rings immediately peel off after incubation under humid conditions (Data not shown). Therefore, SU-8 coating resulted in a strong adhesive bonding of PFPE rings to glass, especially for the SU-8 10 solution. However, under humid conditions the SU-8 was delaminated. Further improvement of the SU-8 bonding was seen after implementation of a prebake step, before the PFPE ring attachment via UV-light and a final post-bake step under pressure after UV-treatment. In order to avoid clogging of the channels by SU-8, the SU-8 10 solution was coated via micro contact printing using rounded and punched PDMS stamps (See: Figure 46B, 47). As a result, the bonding was strengthened and withstood humid conditions over two weeks. Delamination were seen exclusively, when

the bonding between PFPE and SU-8 on the glass slide was insufficient due to non-planar SU-8 layers or uncomplete SU-8 layer covering by PFPE.

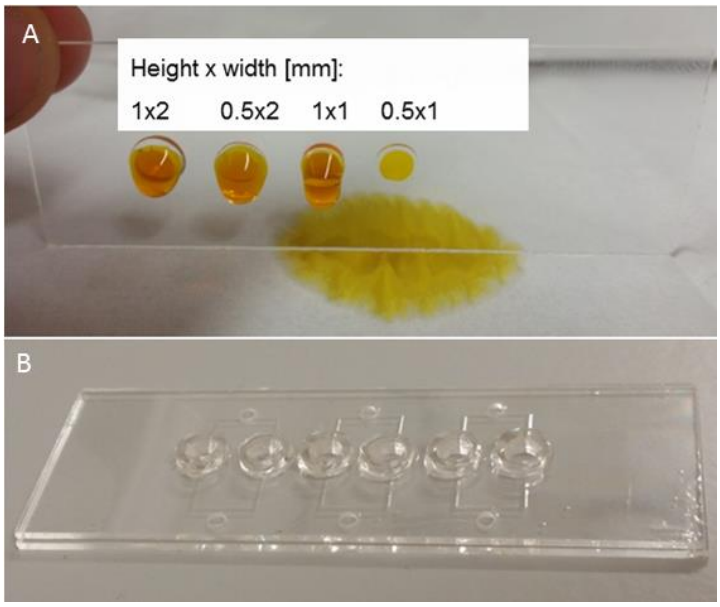

Figure 46: Determination of the ring dimensions on the droplet stability at an inclined plane. Bonded PDMS rings were tested with different heights and widths to keep 65 µL stained liquid droplets (A). Glass hanging drop device with SU-8 bonded PFPE rims (B).

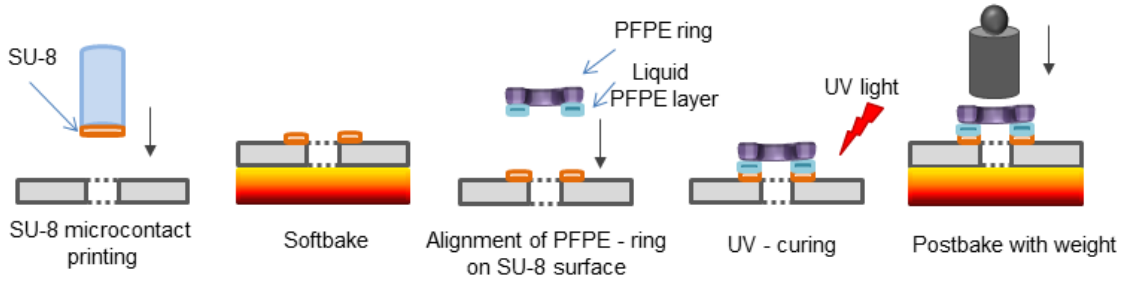

Figure 47: Scheme of the attachment of the pre-cured Fluorolink®-PFPE-ring on the SU-8 coated BOROFLOAT ® glass slide.

Hsiao et al., (2012) introduced micro-ring structure in polystyrene hanging drop plates by injection molding. That stabilized the droplets most effective against environmental perturbations, supported droplet formation and prevented liquid spreading. PFPE was used as material for the ring in our hanging droplet platform because it is chemical inert, non-toxic, hydrophobic, less porous than PDMS and biocompatible, what was already proved within tissue engineering approaches (Schulte et al., 2010). But, PFPE has also a low surface energy and is hardly to polarize. As a result, it complicates the bonding to other materials (PVA TePLA, 2018). In addition, PFPE shows weak bonding to glass or similar materials (Devaraju and Unger, 2011). It was reported that plasma treatment improves the bond

strengths through increase of the PFPE surface energy by addition or substitution of polar surface groups (PVA TePLA, 2018). Especially, for PDMS-PFPE devices, strong bonding by plasma treatment was reached (Rolland et al., 2004). However, it did not improve the binding of PFPE to glass in our experiments. Irreversible attachment was obtained by APTES modification of nanoporous polycarbonate membranes by covalently bonding of NH_2-groups of APTES with OH-groups of plasma activated PDMS (Aran et al., 2010). For the attachment of PFPE to glass, APTES was not sufficient. SU-8 was used for the adhesive bonding of glass wafers or PMMA devices, materials which are normally bonded at high temperatures (Bilenberg et al., 2004; Lima et al., 2015; Serra et al., 2007; Yu et al., 2006b). Introduction of the PFPE rings to glass was also successful for our approach. Interaction of PFPE and SU-8 is probably mediated by an ether bond formation by the –OH terminal groups of the PFPE polymer and the carbo-cations (C+) of SU-8 epoxide rings by linkage under UV (Saravanan et al., 2013). Saravanan et al., (2013), improved significant tri-biological properties such as friction and wear life by using a mixture of SU-8 and PFPE to produce a self-lubricating Lub-tape. The strong binding to SU-8 requires liquid PFPE, what could be an explanation for the partly delamination.

4.5.4. Network stability, simultaneously filling and transfer of droplets

Perfusion experiments made in PDMS and glass applying different (20, 80,150 µL/min) flow rates via pressure-driven flow, resulted in a simultaneously and an even droplet formation in both two droplet wells (See: Figure 48A, B). Limitation for simultaneous filling were seen for unequal glass bonding and slight differences in channel width, occurred by the production process. Polystyrene particles (size: 20 µm) in 30 µL droplets, which mimic the spheroids, were used to determine effects by shear stress through the applied flow. No movement of particles could be observed at flow rates between 10-40 µL/min. Perfusion of the droplets using a stained solution and applying in– and outflow simultaneously, showed that only around 15 µL droplets were completely perfused. The larger the volume of the droplet, the less the droplet was perfused. In order to perfuse the whole droplet, the outflow had to be stopped and only inflow was applied. That resulted in distribution of the stain at the bottom part of the droplet. Old medium was removed by starting the outflow after stopping the inflow (See: Figure 48B, C).

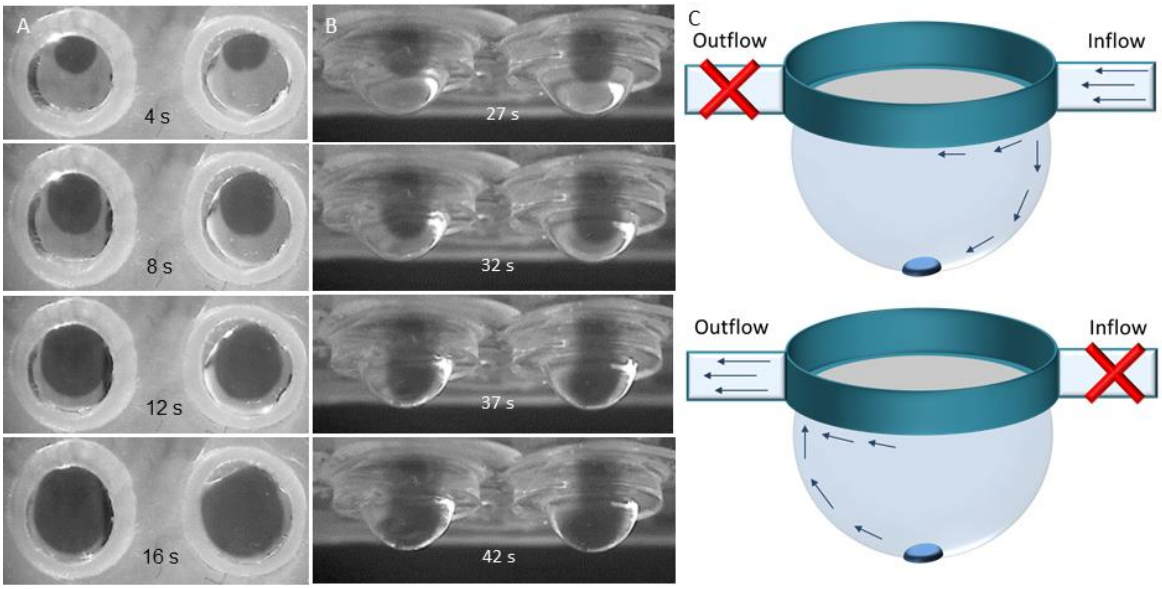

Figure 48: Simultaneously formation and perfusion of the droplet (A). Stained liquid is applied by the inlet and perfused the bottom part of the droplet. (B). A whole droplet can be perfused by lagged perfusion of in-and outlet (C). Images were made at a flow rate of 20 µL/min in ~90° (A) and ~45° (B) angles.

The final design was not sensitive to perturbations, when filled with droplets up to 40 µL at RT or under humid conditions. When tilting the device in 45° or 90° angle, no change in droplet volume and no droplet drip off were detected as seen for the series design (See: Figure 49A). Under humid conditions, 30 µL droplets proved to be more stable. The droplets reached a height of 7.92 mm and a volume of ~ 108 µL until drip off. The drip off of one droplet did not affect the other droplets in the subarray (See: Figure 49B). The droplets were fully automatic transferred by increase of the droplet volume until their drip off, whereas approximately 60 µL was collected in the PDMS chamber (See: Figure 49C). However, smaller volumes can be transferred by pipetting or by touching the droplets on a plane surface.

The new droplet channel assembly provides a simultaneously filling of droplets wells without pre-filling and therefore droplets can be fully automatic transferred to another device. One droplet drip off did not affect other droplets and backflow of the liquid can be avoided as observed and reported for the droplets in series (Frey et al., 2014). Frey et al., (2014) postulated that droplets with a smaller base diameter withstand higher pressures until their drip off, for example a drop with a base diameter of 3.5 mm can hold a water column of 8.5 mm in height, what explains the high droplet volume until drip off for the new glass hanging drop platform. The prevented complete failure of the system can be explained by a parallel circuit from electrical engineering, whereas the current represents the volumetric flow rate, the voltage the droplet volume and the resistor the droplet well (Halliday and Resnick, 2015).

The flow rate splits at the branches and is the same at in and outlet, whereas each droplet well contains the same volume. The failure of one component, so the drip off of a droplet does not affect failure of the whole system, but the volume of the remaining droplet increases. Probably, pressure differences in the whole system, which occur due to channel splitting and droplet holes are responsible for the prevention of backflow. The channel designs of the new device support only the perfusion of approximately 15 µL. Pressure driven flow supports maximal flow velocities in the center of the of closed channel, what could be an explanation for the incomplete perfusion of the droplets (Frey et al., 2014), but has to be proved in a simulation.

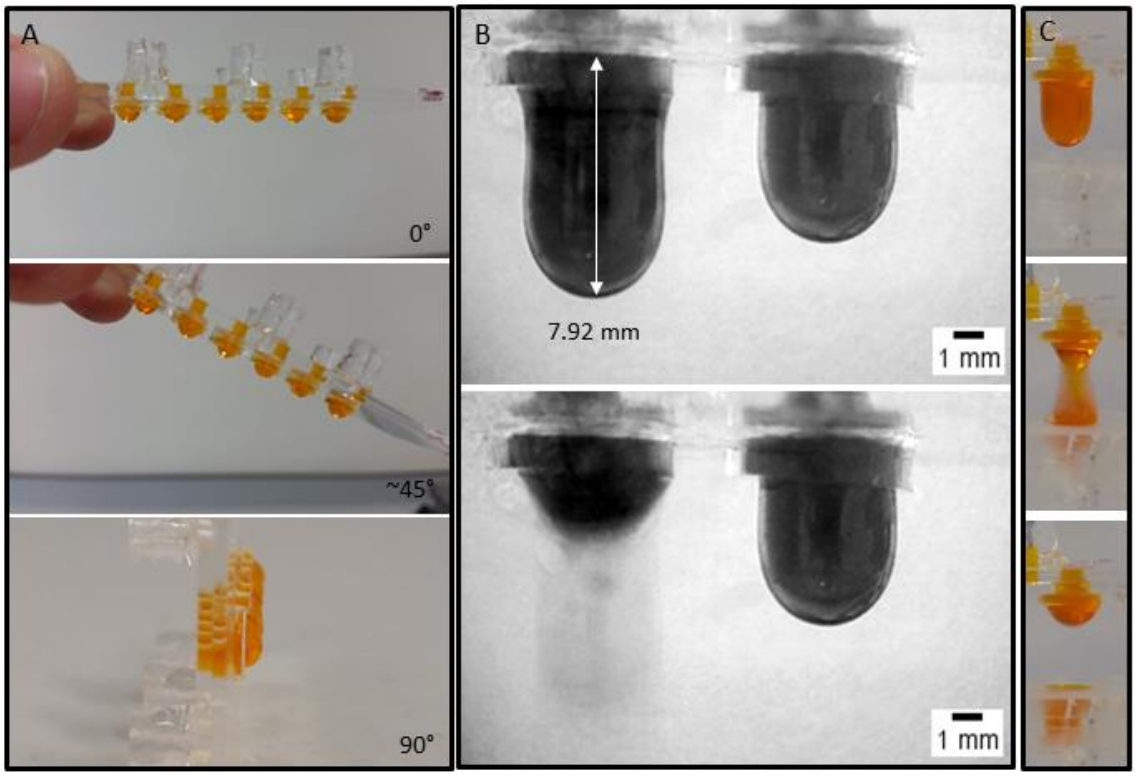

Figure 49: Network stability under movement (A). The stability was tested, when moving the device in different angles (0°, ~45°, 90°). Droplet heights of ~7.92 mm were reached until drip off, without affecting the volume of the second droplet in a subarray without movement (B). Fully automatically transfer of droplets into a PDMS chamber (C).

4.5.5. Incubation chamber against evaporation

The open droplets device provides a permanent gas exchange and a high evaporation, which could lead to an increase in osmolality and therefore effects on the growth conditions of cells (Heo et al., 2007; Vadivelu et al., 2017). Testing the evaporation of 30 µL cell medium droplets under static conditions in a plastic chamber with wetted paper at 37°C, resulted in an evaporation loss of 22.5% over 24 hours. A pre-incubation of the chamber with wetted paper at 37 °C for 30 minutes, before the droplet device was transferred into it,

decreased the loss of liquid from the droplets to 11% (See: Figure 50A). Further reduction of the extensive evaporation was reached with a 3D printed closeable incubation chamber made out of polylactic acid (PLA). The 40x90 mm chamber enables gas exchange through an opening on one side, ensures a horizontal device position and the detection of the droplets through the glass bottom of the device (See: Figure 50B and C). A height of 4.5 mm from the hanging droplet device to the bottom glass was appropriate for the detection of spheroids in 30-65 µL droplets depending on the spheroid size. Evaporation experiments with this chamber, closed with a PDMS slab for a better gas exchange (Halldorsson et al., 2015), showed a further decrease in evaporation to a loss of 7.8%. However an evaporation gradient from 0% at the closed side to 16.7% at the opening side was detected (See: Figure 50A). That is similar to cell culture experiments made under static conditions in 96-well plates, because the outer wells show the highest evaporation (Lundholt et al., 2003; Neeley, 2016). In order to avoid unequal evaporation, wetted paper was added at both ends of the chamber. That resulted in additional improvement of 12.5% to a loss of 7% and droplet volume difference of around 1 µL or 3% per droplet. Pre-incubation of the holder in the incubator for 30 minutes decreased it to 2.77% (See: Figure 50A). Further decrease was not possible.

Microfluidic cell devices with large surface to volume ratios, a minimum of evaporation exhibit significant osmolality shifts, especially in PDMS devices with high water vapor permeability (Heo et al., 2007). The evaporation on the surface of a liquid occurs until the equilibrium between evaporation and condensation is reached, so until the surrounding gas phase is saturated with this liquid. Substance concentration in the surrounding gas phase, temperature of the substance, amount of minerals in a liquid and the surface area are factors which can influence evaporation. Also, surface wettability influences the evaporation of liquids, which increases in microscale with a strong impact in microfluidic applications. Complex fluids such as cell medium have an impact on the evaporation by changing of surface properties, due to protein adsorption on the material (Choi and Kim, 2009). Droplets on hydrophobic surfaces have slower evaporation rates due to a smaller droplet radius compared to hydrophilic surfaces (Shahidzadeh et al., 2015). By implication, high mineral concentrations of the liquid in the surrounding gas phase, high inter-molecular forces, small volume to area ratios, hydrophobic surfaces and lower temperatures of the liquid and so lower kinetic energy of the molecules in the liquid will lead to slower evaporation (Silberberg and Amateis, 2015). Techniques applied for the prevention of excessive evaporation include: high humidity at least 95%, avoiding non-essential opening of the incubator, covering of cell culture devices during incubation, liquid reservoirs surrounding the culture area (Bartosh et al., 2010; Breslin and O'Driscoll, 2013; Neeley, 2016), pre-incubation of freshly seeded cells

at room temperature (Lundholt et al., 2003), wetted filter paper (Frey et al., 2014), PDMS coatings minimizing water vapor permeability (Heo et al., 2007), minimizing the surface area to volume ratio (Mcjannet et al., 2008; Scott Lynn et al., 2009) or by simply compensation of evaporation by adding more medium (Breslin and O'Driscoll, 2013; Frey et al., 2014). Here we showed that a decrease of droplet evaporation was reached by reduction of the incubation area applying the 3D printed incubation chamber and by pre-incubation of the device at 37 °C under ~ 95% humidity. The pre-incubation and the reduced area support a faster saturation of the gas phase with liquid vapor, whereas the fact of using non- or less permeable materials such as glass and PFPE could additionally promote less evaporation. However, the hydrophobic PFPE supports additionally smaller diameter of droplets, which tends to slower the evaporation, compared to materials with good wettability. Furthermore, a decrease of the surface to volume ratio by using droplets as cell culture platform are probably also affect the evaporation of the droplets.

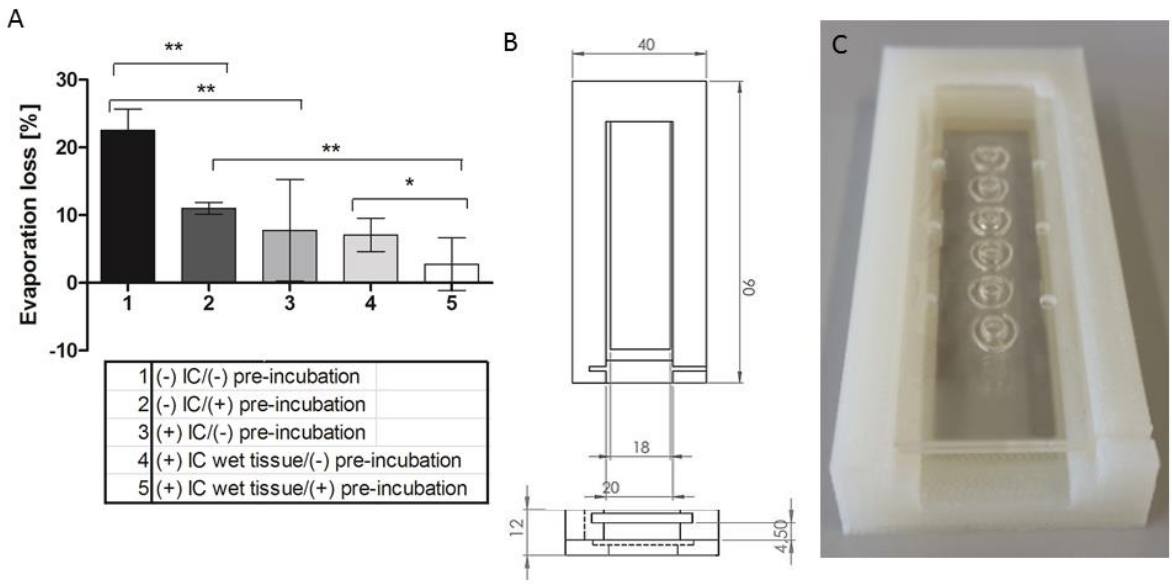

Figure 50: Reduction of evaporation of the hanging droplets in a 3D printed incubation chamber. Graph shows the reduction of evaporation loss with and without incubation chamber (IC), after pre-incubation and wetted conditions. Minus (-) and plus (+) at the front of IC and pre-incubation refer to the absence or presence of it (A). Data are shown as mean with standard deviation for n=6. Statistical significance was tested using the Mann-Whitney test for alpha=0.05. Dimensions of the 3D printed incubation chamber (B). PLA incubation chamber is shown, containing the hanging drop device (C).

4.5.6. Biocompatibility of the glass device materials

Materials applied for cell culture applications can affect cell growth and viability. The biocompatibility of the glass device materials was investigated by growth and viability of MCF-7 cell spheroids under static conditions in serum-free medium over four days in comparison to PDMS. To prevent leaching of uncured PFPE, the glass devices were

incubated in 70% EtOH and were placed into an ultrasonic bath for 20 minutes, a day before application. The diameter of the MCF-7 cell spheroids increased continuously in a daily average of 15.77+/-13.59 µM over the four days in the glass device, resulting in insignificant differences compared to PDMS with 13.22+/-12.22 µM per day (See: Figure 51). No effects on cell viability were observed (See: Figure 52B and C). The cell aggregates in both devices became compact on the third day (See: Figure 51B). The circularity was increasing over time and aspect ratios of in average 1.31+/-0.18 for the glass device and 1.59 +/-0.47 for PDMS on day three with a circularity of 0.79+/-0.11 and 0.77+/-0.04 were measured. When the PFPE rings were not sufficiently bonded to the glass, cells looked stressed and did not form compact spheroids (Appendix I see: Figure A 11). To investigate which material induce this effect on cell growth and spheroid formation, glass devices with SU-8 bonded and silicone sealed PFPE rings were tested against PDMS rings. The rings were clued with silicon sealant at the outer edge to avoid direct contact with the cultured cells. The devices were incubated in 70% EtOH under ultrasound prior to cell culture. No negative influences on cell viability were detected for PFPE (See: Figure 52A). Since the cells grew equal in PDMS and glass devices with silicon clued rings, an impact on cells by SU-8 was concluded.

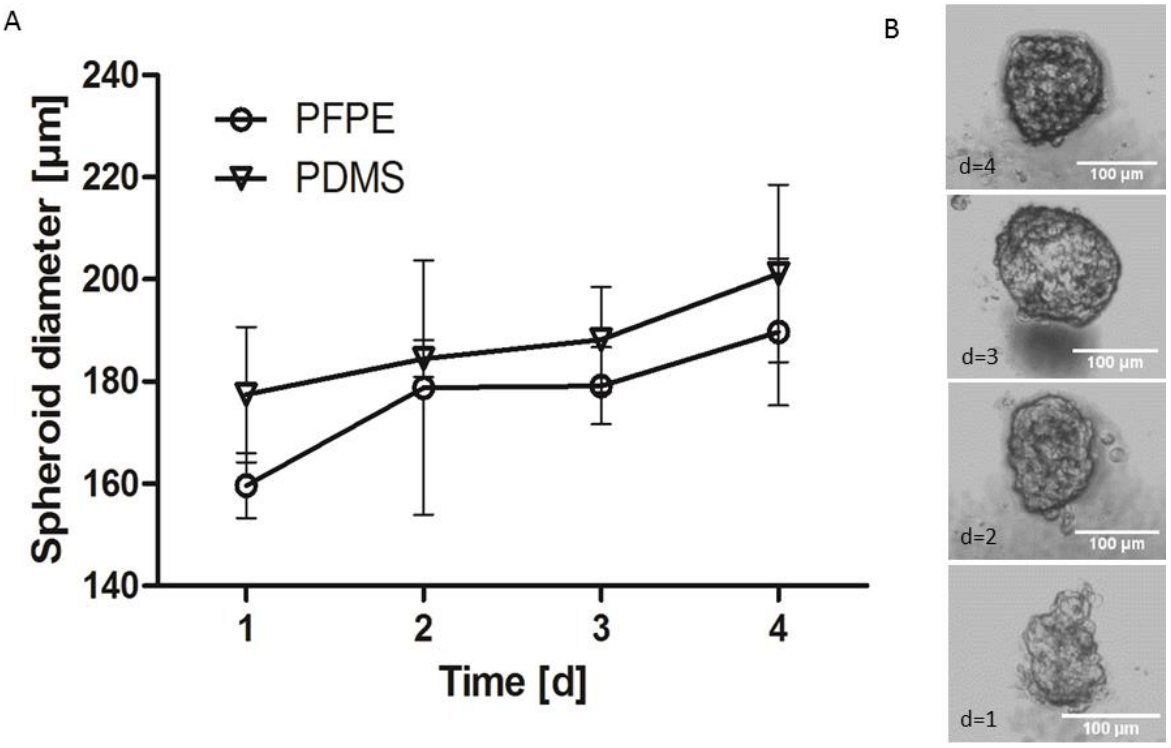

Figure 51: The biocompatibility of the materials used for the glass hanging drop device is shown for MCF-7 cell spheroids, which were grown in serum-free medium DMEM/F-12 over 4 days. The growth in the glass device is compared to the growth in a PDMS device (A). Data are plotted as mean with SD from n= 4. Morphology of MCF-7 spheroids: The spheroids grew in the glass hanging drop device and are represented for the days 1 to 4 of cell culture (B). 300 cells per 30 µL were seeded.

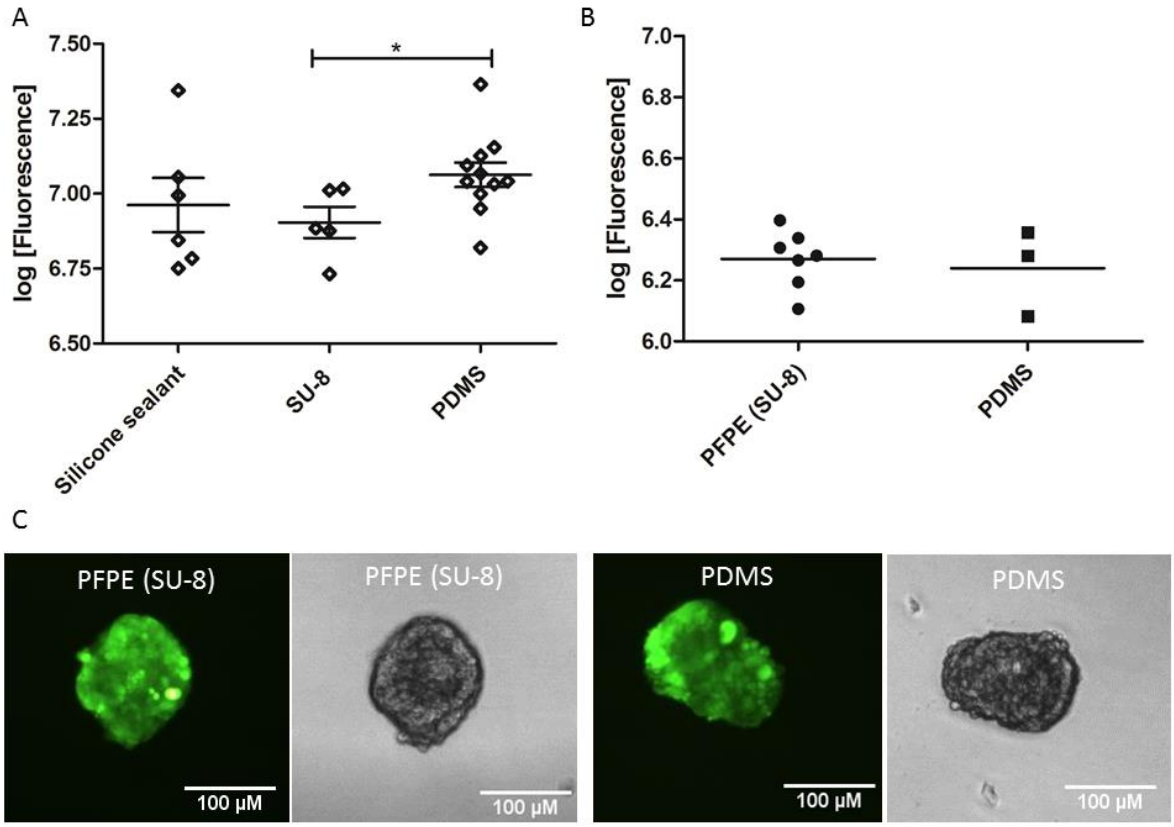

Figure 52: Influences on MCF-7 cell viability through the device material. Viability of cells growing in glass devices with PFPE rings bonded via SU-8 (when not totally covered by PFPE) or silicon sealant compared to PDMS (A). Viability of cells growing in glass devices with PFPE rings bonded via SU-8 (totally covered by PFPE) compared to PDMS (B). Fluorescent viability stain CAAM images with corresponding phase contrast images of MCF-7 cell spheroids grown in the glass hanging drop device with SU-8 attached PFPE rings (left) compared to spheroids grown in PDMS devices (C). Data are given as mean with SEM. Statistical analysis of log transformed fluorescence intensities of CAAM stained spheroids were made with an unpaired t-test for alpha=0.05 n=5-11 (A) or n=3-7 (B). 300 cells per 30 µL were seeded.

Serum-free medium was already used from day one of the cell culture, due to less efficient spheroid formation in conventional cell medium DMEM with 10% FBS. Therefore EGF; FGF, B-27 mix and hydrocortisone were added to the growth medium. All materials used for the new glass hanging drop device and the PDMS device, were already proved to be biocompatible and used successfully for cell culture applications (Arscott, 2014; Ayuso et al., 2015; Nemani et al., 2013; Schulte et al., 2010; P M van Midwoud et al., 2012). However, Nemani et al., (2013) also reported an increase of imunne response *in vivo* for mice, which were exposed to subcutaneous SU-8 implants. Furthermore they suggestesd to treat SU-8 for biological studies. SU-8 was exhibiting cytotoxicity within neuronal cultures. The authors linked the cytotoxic effects on leachates such as antimony salts. However, post-processing of SU-8 by a combined heat, isopropanol sonication and oxygen plasma treatment rendered the material biocompatible (Vernekar et al., 2009). Additionally, during the crosslinking of SU-8, a strong acid is formed after exposure to UV light, which is thermally catalyzed during the

post bake. The extent of residual epoxy groups and antimony salts are determined by UV-dose and baking time (Del Campo and Greiner, 2007). In the developmental stages of the PFPE ring bonding procedure, a pH shift to the acidic range of the conventional cell medium was observed, however it was not seen in later stages. This negative effect on cell growth can be introduced by leaching of acid and thus shifts the pH of the medium or from antimony salts showing direct toxic effects on cells. However, the SU-8 coating is covered by liquid PFPE and the cured PFPE ring during the UV-exposure. The energy dose for the exposure was decreased from 2 to approximately 1 J/ cm², which was still too high for SU-8 exposure. On the other hand, the SU-8 layer did not lift of the glass when the PFPE ring was detached, what would be an argument against insufficient UV-light exposure. Nevertheless, the effect on the viability of MCF-7 cells was only observed when SU-8 was not totally covered by PFPE, therefore SU-8 bonding and silicon bonding was used for further cell experiments.

4.5.7. Effect of material and flow on experimental outcome and spheroid growth

Materials can have a different effect on the outcome of experiments, especially when working with EDCs, which deploy their action already in low concentrations. Furthermore, spheroids can be affected by shear stress provided by the liquid flow, which can result in degradation of the construct.

MCF-7 cell spheroids were exposed to 100 pM and 1 nM estradiol over four days for the investigation of the effects by different device materials. The spheroids were seeded in 30 µL DMEM/F-12 supplemented with EGF, FGF, hydrocortisone, ITS, B-27 mix, L-glutamine and BSA in glass devices with SU-8 and silicone sealed PFPE rings as wells as PDMS devices for 24 hours. Next, the medium was changed to DMEM/F-12 with ITS EGF, FGF, L-glutamine and BSA. After additional 24 hours, insulin was removed. 72 hours after seeding, the spheroids were exposed to estradiol and the medium was changed every second day. The estradiol solvent DMSO was taken in a concentration of 0.01% in the assay. The viability of the spheroids was evaluated using the green-fluorescent calcein-AM stain, which indicates intracellular esterase activity. Since the fluorescence intensity is proportional to the spheroid diameter, the stain can also be used as indicator for growth of the spheroids. Relative fluorescence intensities of treated to untreated spheroids was calculated and compared to the values in the different devices. Significant differences on estradiol treatment was obtained for the MCF-7 spheroids grown in the glass device with the silicone sealed rings compared to the PDMS and the glass device with SU-8 attached rings. Fluorescence signals increased 4 fold for spheroids in the glass device with the silicone clued rings for 1 nM and 2 fold for 100 pM estradiol treatment, whereas the spheroids in the other devices only showed half of the signal (See: Figure 53A). Spheroids grown in the glass device with SU-8 clued

rings and in the PDMS device did not differ in signal (See: Figure 53A). Comparison of untreated, equal sized spheroids in the glass device with SU-8 and the PDMS device exhibit less than half fluorescence intensities for the glass device with SU-8 compared to PDMS, indicating toxic effects on the cells (See: Figure 53B). Furthermore, the molecule adsorption in PDMS and PFPE was investigated using a 50 µM rhodamine solution and incubated overnight at 37 °C, 5% CO_2 and 95% humidity. Rhodamine uptake in PDMS was significantly higher compared to PFPE (See: Figure 54). After 24 hours, the rhodamine molecules diffused through the 2 mm wide PDMS ring, but with higher accumulation in the first half of the ring (See: Figure 54 A). The PFPE ring also exhibits higher accumulation in the first half, however in the rest of the ring, the signal was neglectable.

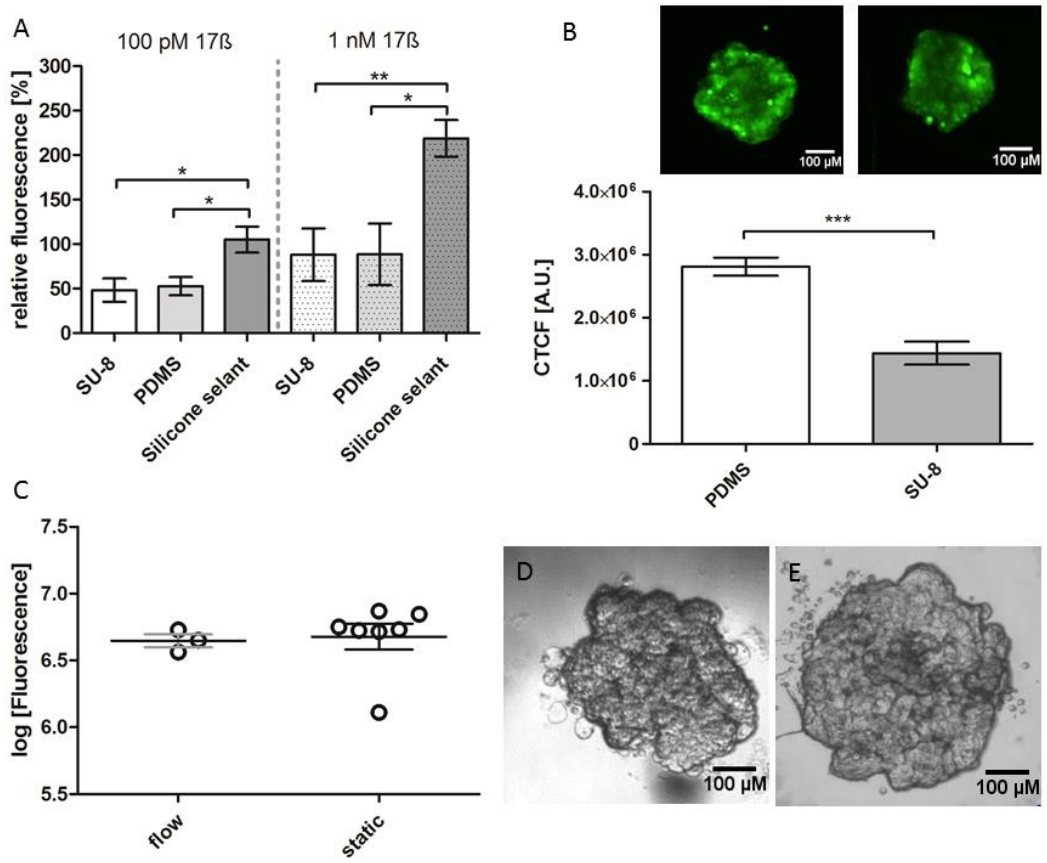

Figure 53: Effect of culture material and flow on MCF-7 spheroids. Influence of culture materials SU-8, PDMS and silicone sealant on cell growth prior to estradiol treatment (A). Effects of SU-8 on viability of MCF-7 cell spheroids (B). Bars are shown with corresponding fluorescent images of the spheroids grown in PDMS or glass device with SU-8 attached PFPE rings. Data are shown as mean of corrected total cell fluorescence (CTCF) with SEM. Viability of MCF-7 spheroids grown under flow (20 µL/min) or static conditions (C). Data are given as mean of log fluorescence values with SEM. Morphology of a MCF-7 spheroid of 1500 cells on day two of cell culture exposed 15 minutes to flow (D). Morphology of a MCF-7 spheroid of 1500 cells on day two of cell culture grown under static conditions is shown (E). Statistical analysis was done with an unpaired t-test for alpha=0.05 (A: n=4-6, B: n=6, C: n=3-7 replicates). Significance was tested group wise for each concentration, material or flow condition.

Effects of flow on the spheroid morphology and viability were investigated. Therefore 325, 750 and 1500 cells were seeded in 30 µL DMEM/F-12 per well, settled down overnight for aggregation before 20 µL/min flow was applied for 15 minutes between the in– and outlet. The spheroids were evaluated for flow and static conditions after 48 hours of growth. The application of flow exhibited no effects on the viability of spheroids (See: Figure 53 C). Spheroids, which were exposed to flow, looked more compact than spheroids under static conditions (See: Figure 53D; E).

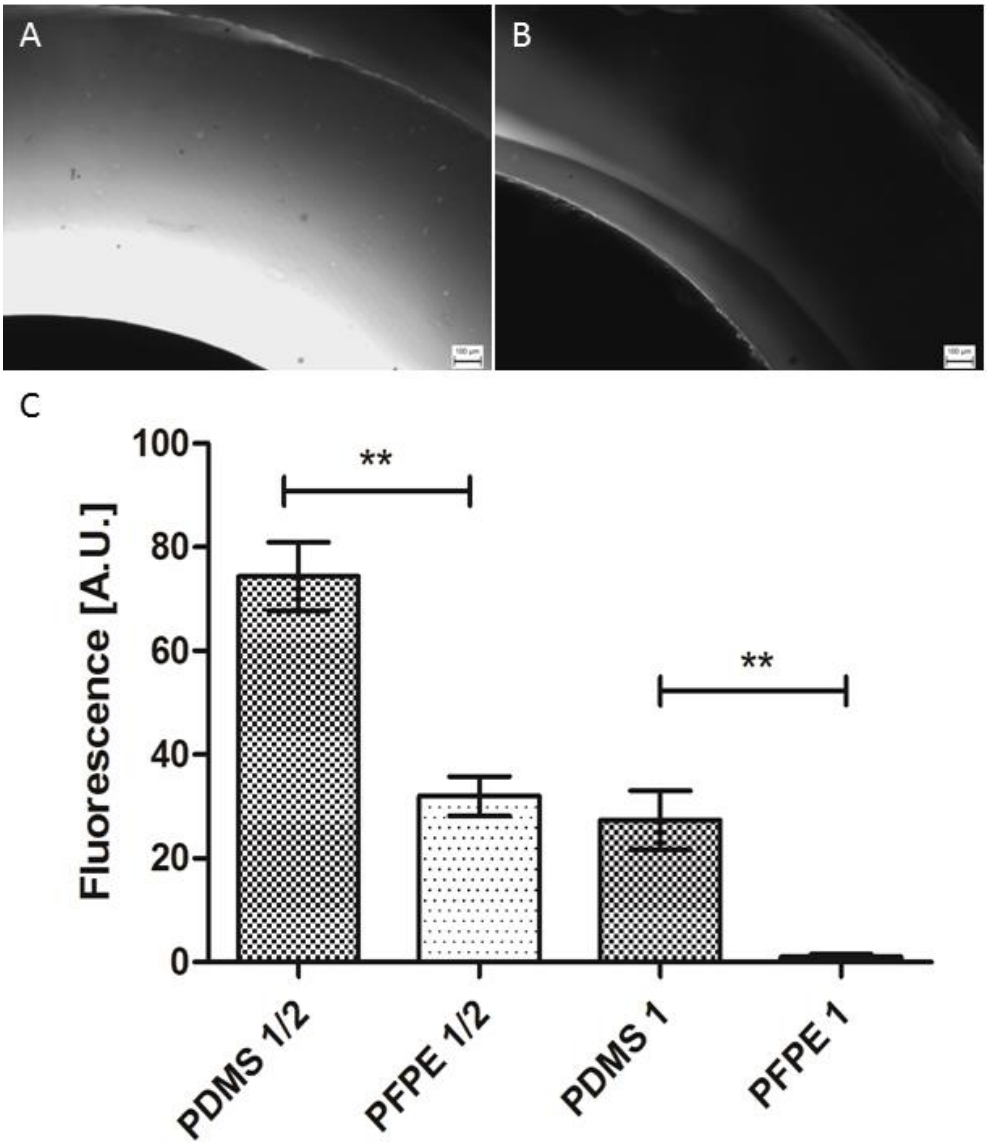

Figure 54: Adsorption of rhodamine. Fluorescence image of a 2 mm wide PDMS ring after 24 hours incubation in 50 µM rhodamine solution (Scale bar=100µM) (A). Fluorescence image of a 2 mm wide PFPE ring after 24 hours incubation in 50 µM rhodamine solution (Scale bar=100µM) (B). Rhodamine adsorption in PFPE and PDMS is expressed as fluorescence intensity (C). Fluorescence was measured for the first half (1/2) and the second half of both rings (1). Bar graphs showing mean values with standard deviation for n=3 replicates. Significance was tested with an unpaired t-test for alpha=0.05

The proportional relationship of intensity increases with the spheroid diameter was seen in our experiments, which was also demonstrated by (Frey et al., 2014). Therefore, the CAAM cell stain can be applied for the indication of direct toxic effects on the viability as well as the growth and thus the proliferation of spheroids. Diffusion of especially small hydrophobic molecules into PDMS was reported manifold (Toepke and Beebe, 2006; van Meer et al., 2017; Wang et al., 2012). Regehr et al., (2009) showed that neither a pre-saturation of the PDMS with the hydrophobic molecule estradiol nor blocking with serum proteins was able to prevent the reduction of estrogen concentration from approximately 1 to 0.1 nM within 24 hours. This features the importance of the careful choice of cell culture materials for biological or toxicological screening, especially for endocrine active substances, which exploit their action within the low concentration ranges and explains our findings. The response of the MCF-7 cells after exposure to 100 pM estradiol in the glass device with silicone clued rings is similar to the 1 nM treatment of spheroids in the other two devices. The low response obtained for the glass device with the SU-8 attached rings seems to be a result of direct effects of SU-8 leachates on the viability of the cells and thus on the response to estradiol treatment. Compared to that, the high responses seen for spheroids in the glass device with the silicone sealed rings could indicate leaching of estrogen active substances from the sealant in the cell culture medium. However, nothing is stated for the substances contained in the sealant, neither in literature nor in the safety data sheet of the manufacturer RS (RS, 2018).

Flow, applied after 24 hours of cell seeding, did not have any influences on cell sedimentation and aggregation. A flow rate of 20 µL/min for 15 minutes did not result in disaggregation or effects on the viability of the spheroids. However, more compactly formed spheroids were observed under flow than under static conditions after 48 hours. Spheroid formation is faster under continuous medium perfusion in microfluidic devices (Gupta et al., 2016; Katt et al., 2016; Mehta et al., 2012; Wu et al., 2008). Wu et al., (2008) showed that especially at higher perfusion rates (e.g. 10 µL/min) the formation time decreases to in average 7 hours. In addition, it has positive effects on the size uniformity (Mehta et al., 2012). However, high flow rates can additionally result in high shear stress for the cells and thereby cause spheroid disaggregation. The maximum shear stress a spheroid can withstand was reported in a range of 0.001 to 10 dyne/cm^2 and is dependent on the cell type. Furthermore, it can influence the cell cycle, differentiation and gene expression (Moshksayan et al., 2018). Zuchowska et al., (2017) obtained more compactly formed spheroids in 500 µm deep microwells compared to 350 µm deep wells. They ascribed it to lower shear stresses in the deeper well (Zuchowska et al., 2017). Due to large droplet volumes with the highest flow

velocities in the upper droplet part, we conclude that the spheroids are less affected by shear stress.

4.6. Spheroid perifusion chamber

The long-term culturing of spheroids requires a sufficient supply of oxygen and nutrients, especially for spheroid diameters of 300 µm and higher, which increases the viability of cells inside the cell aggregate and therefore ensures accurate results (Anada et al., 2012; Cui et al., 2007; Wan et al., 2016). Small hydrophobic molecules tend to diffuse into PDMS devices with the consequence of concentration reduction in applied solutions and affect therefore the accuracy and reliability of experiments. Glass coatings can reduced the absorption of hydrophobic molecules in PDMS devices (Wang et al., 2012). A perifusion chamber integrated in the chip system can provide efficient growth conditions for the MCF-7 cell spheroids over long periods and can serve as an experimental platform for proliferation and protein secretion due to EDC exposure of MCF-7 cell spheroids.

PDMS perifusion chambers provided by the group of Pharmaceutical Analysis of Elizabeth Verpoorte, which were originally made to perifuse tissue samples (liver slices of 4 mm in diameter, 100 µm thickness) (Van Midwoud et al., 2010) and were used as a basis for the further development of the spheroid perifusion system. M. Skolimowski advanced the perifusion system, which consists of two PDMS parts including three chambers with a total height of 4 mm, a chamber diameter of 5 mm and a single chamber volume of ~ 79 µL. Both PDMS slabs contained a non-transparent polycarbonate membrane (8 µm pores), which kept the tissue samples in position during perifusion and ensured equal perifusion. The term ‘‘perifusion’’ was chosen by the authors instead of ‘‘perfusion’’, because the medium flew around the tissue sections (Van Midwoud et al., 2010). The tissue was perifused via a bottom edge inlet and a top edge outlet, which were closed by 2 mm thick PDMS slabs (See: Figure 55D).

In order to attach the hanging drop device to the cell perifusion system and to enable detection of the spheroids, the device had to be reassembled. Two assembling strategies were tested: 1) an open perfusion system (See: Figure 55 A, C) and 2) a closed system with an integrated hanging drop chip (See: Figure 55 B). The chamber parts were new assembled by moving the outlet to the middle and removing the upper polycarbonate membrane, to integrate the hanging drop system on top of the device and to ensure a detection of the inner part of the chambers from above (See: Figure 55A, E). The bottom PDMS slab was replaced by a glass slide, to ensure good bonding and to allow two perifusion chamber devices next to each other for parallel transfer of six spheroids.

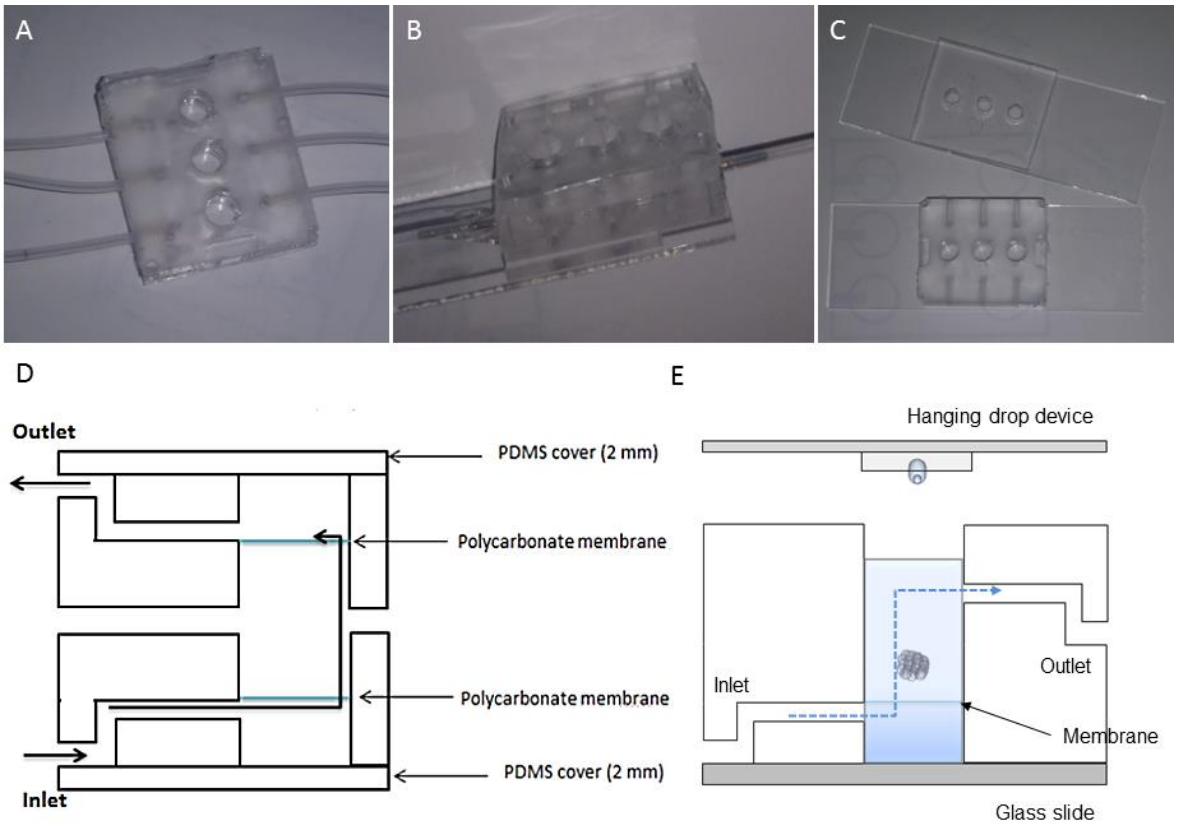

Figure 55: Assembly strategies of the perifusion chamber. The reassembled perifusion chamber is shown, with one polycarbonate membrane in the bottom layer (A). Closed approach with integrated hanging drop system (B). Open approach with extra hanging drop system (C). Scheme of the original perifusion chamber assembly is displayed (D). Scheme of the new perifusion chamber assembly is displayed (E).

For the fabrication of the device, both PDMS parts were bonded after 20 s of oxygen plasma activation. Due to insufficient bonding, applied liquid diffused in between the two PDMS parts. The bonding was further improved by 30 s of oxygen plasma treatment with an additional 30 minutes post-heating step at 70 °C under pressure. The new assembly was tested under flow conditions for leaking. Liquid applied by pressure driven flow via the inlets neither penetrated the parallel located chambers nor overflew at the openings, when aspirated via the outlet (See Figure: 56). However, during the filling of the molds with PDMS, glycerol from the membrane parts was partly dissipated and created thereby areas, which could not be filled with PDMS and resulted in holes in the PDMS device and thereby in leakage. By minimizing the glycerol amount, it could be prevented. Van Midwoud et al., (2010) took aluminum clamps to press the two PMDS parts together to close them tightly.

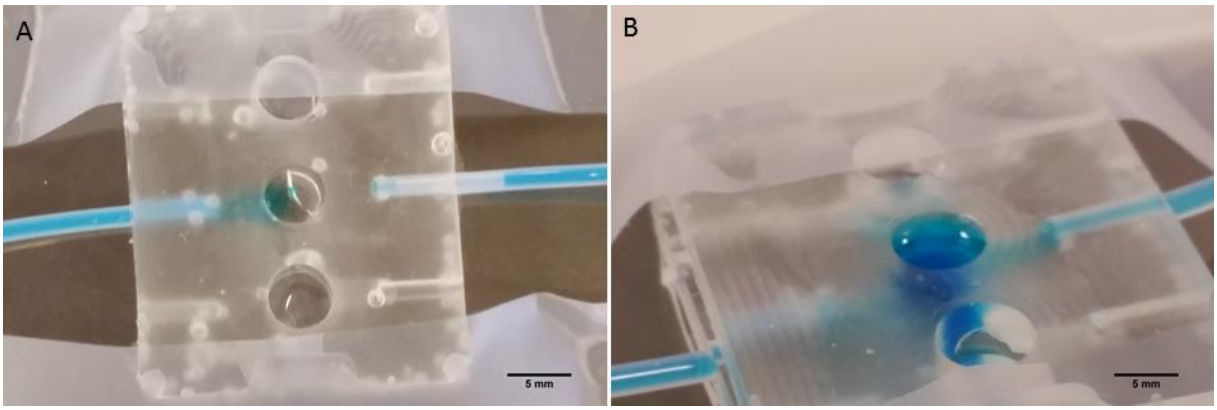

Figure 56: Liquid flow in perifusion chambers. Improvement of PDMS layer bonding prevented leakage of fluid to other chambers (A). Perifusion of the open chamber was possible without overrun of the liquid (B).

Abate et al., (2008) used a 1 : 1 : 1 : 1 ratio of TEOS, MTES, ethanol, and pH 4.5 water to coat channels with a glass layer in a PDMS device. This protocol was used and was further adapted for the glass coating of the perifusion chambers. The mixture was homogenized on a 65 °C hotplate and either placed in a 65 °C oven for 12 hours pre-conversion or stored at room temperature overnight. The total conversion of the mixture was tested at 100 °C heat for both conditions by pipetting a droplet of approximately 1 mL sol-mixture in a petri dish, before it was applied to the PDMS device. Full conversion was observed after 10 minutes. In the droplet of the fast converted mixture, cracks were detected and the droplet seemed to be shrunken (See: Figure 57 A). This was not obtained for the overnight storage at room temperature. The surface of the droplet was very smooth and even (See: Figure 57 B).

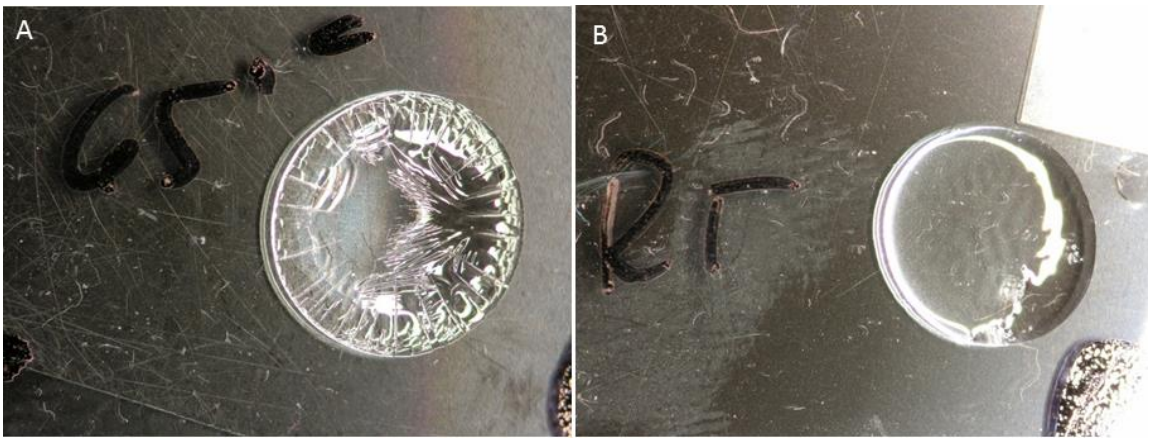

Figure 57: Glass solution preparation with different incubation temperatures. Cured glass solution droplet is shown after overnight incubation at 65 °C (A). Cured glass solution droplet is shown after overnight incubation at RT (B).

The coating of the perifusion chambers were performed with the room temperature incubated solution. The mixture was applied to the PDMS device immediately after oxygen plasma (30 s) and heat (10 min) treatment. Therefore, the whole device was incubated for 30 minutes in

a box filled with the coating solution under movement at 80 °C. The channels were immediately flushed with air after the coating, to prevent channel clogging. The device was stored at 100°C for ensuring total conversion of the sol-mixture.

With the adapted protocol ~10 µM thick glass layer was coated on the PDMS device (Appendix I see: Figure A 12, See: Figure 58A, B). The consistence of the coating was tested by incubation with 50 µM rhodamine solution. Therefore, the rhodamine solution was applied into the chambers and incubated at room temperature for 4 days. The rhodamine permeability was evaluated by fluorescence measurements and compared to uncoated PDMS devices. The coating prevented rhodamine diffusion into the PDMS device, but not into the glass coating (See: Figure 58C, D).

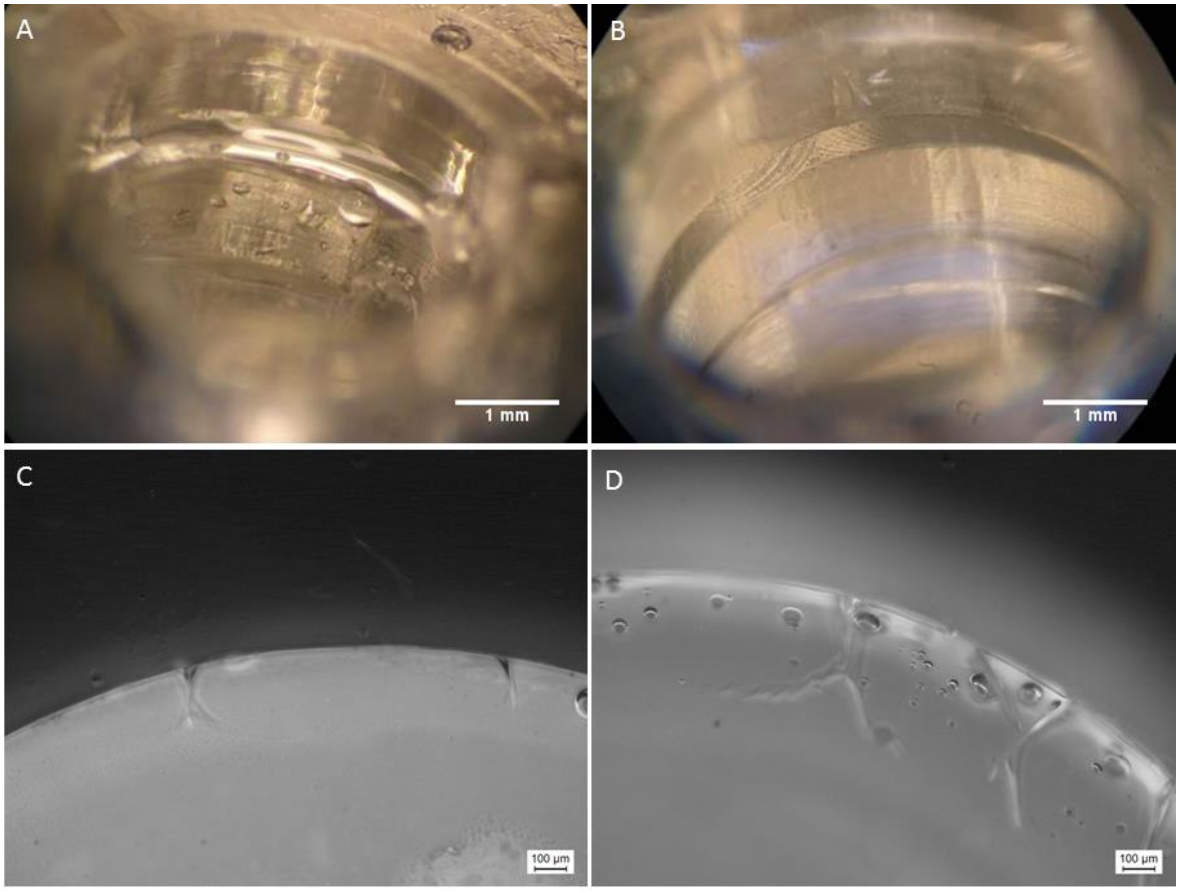

Figure 58: Glass coated perifusion chambers. Glass coated perifusion chamber (A). Uncoated perifusion chamber (B). Fluorescent image of the edge of a glass-coated PDMS perifusion chamber after 4 day incubation in a 50 µM rhodamine solution is shown (C). Fluorescent image of the edge of an uncoated PDMS perifusion chamber after 4 day incubation in a 50 µM rhodamine solution is shown (D).

In order to enable the detection of the spheroids from the bottom part with an inverted microscope, the polycarbonate membrane was replaced by a glass membrane (See: Figure 59A). The 2 x 2 mm G-Flat™ silicone oxide membrane from SimPore Inc. was fixed in a 5.4 x 5.4 mm silicon frame, which has a thickness of 0.3 mm and shows 20% porosity with 3 µM

large pores. The membrane was slightly larger compared to the diameter of the perifusion chamber and prevented therefore a simple click in of the membrane into the device. 3D printed clamps (height: 1.8 mm) were used for the creation of a 6.5 x 6.5 mm area to integrate the membranes into the chamber (See: Figure 59B). The removing of the clamps resulted in PDMS surface irregularities due to the nonplanar 3D print and complicated the perfect fitting of the membranes in the bottom chamber areas. PDMS had to be removed by a scalpel to receive a plane surface and enable membrane integration in the glass coated device (See: Figure 59C). The bottom part of the perifusion system was bonded to a glass slide by oxygen plasma activation to close the system.

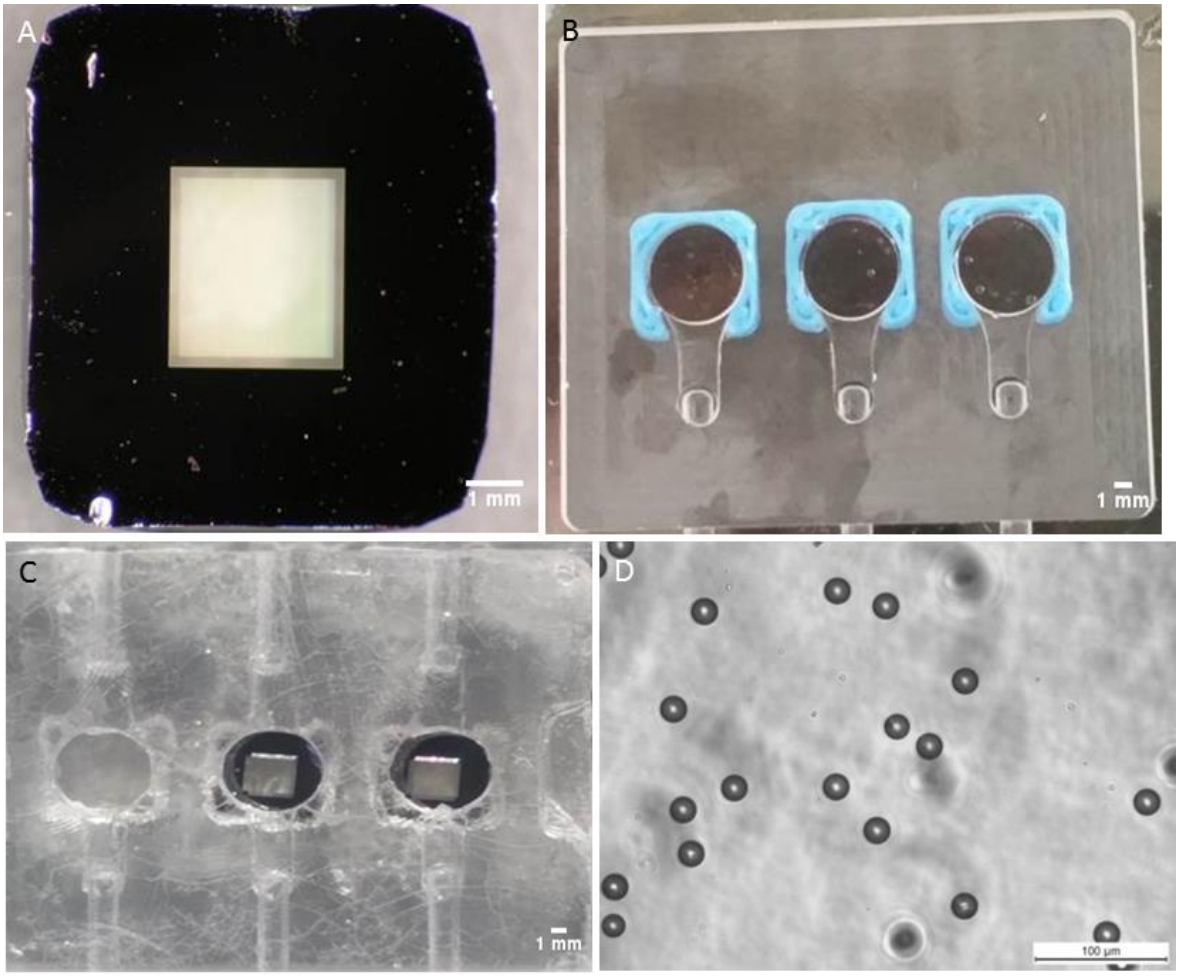

Figure 59: Glass membrane integration in the perifusion device. Glass membrane (A). Perifusion device mold with 3D printed clamps around each chamber mold for the integration of the glass membranes (B). Glass coated perifusion device with integrated glass detection windows (C). A Solution of 15 µM particles (round circles) in the perifusion chamber, was focused through the membrane (D).

A particle solution with 15 µM sized particles was applied for the detection feasibility. Detection of the 15 µM particles was possible through the bottom part of the device over the whole size of the glass membrane (See: Figure 59 D). The detection width of the chamber

was limited by the dimension of the glass membrane. However, cracks in the coated surface were obtained, caused by the pressure applied during the membrane integration and PDMS glass bonding (See: Figure 59C). A test for liquid permeability of the glass membranes showed that the liquid did not perfuse directly through the pores of the membrane, but rather diffused over the outer edges of the membrane into the chambers. Increased pressure during chamber filling resulted in membrane rupture.

The open system would provide better oxygen supply from above, while spheroid culturing will enable direct access to the cell culture for direct screening of proliferation, what would be more difficult in the closed device. The open and the closed system allow an easy spheroid transfer from the hanging drop system into the chambers by increasing the droplet volume until drip off. Higher evaporation and contamination of the cell culture might be more likely in the open system, whereas an early droplet drip off due to mechanical perturbations or humid conditions might occur in the closed design. As a conclusion, the open perifusion system was used for the further development.

The nontransparent polycarbonate membranes in the chambers between the in-and outlet, determined the tissue slice position,an uniform medium distribution and flow across the entire chamber (Van Midwoud et al., 2010). Additional, the membranes generated flow resistances to avoid high flow rates directly at the tissue. By removing of the upper membrane in the new assembled device the outflow will be changed. Furthermore, we expect that the flow will move the spheroids to the medium surface and thus expose them to air. Embedding of the cell aggregates in hydrogel such as collagen-alginate mixtures or matrigel could prevent this, spheroids are protected from direct flow and at the same time an extracellular matrix could be provided (Gupta et al., 2016; Moshksayan et al., 2018; van Duinen et al., 2015). For the detection of cells in the perifusion system, the lower polycarbonate membrane was replaced for a glass membrane. Those membranes were already used within cell interaction and differentiation studies, showing biocompatibility of the materials and the ability to study cell interactions on both sides of the membrane (Mazzocchi et al., 2014). However, they suffered from stability under liquid perfusion. The liquid could not penetrate the membrane, probably due to insufficient permeability or the pore size. Furthermore, the size of the membrane limited the detection area. Exchange of wider membranes containing larger pores and higher porosity could probably improve the perfusion and the detection limitations. Another possibility is the application of the recently developed method for liquid glass printing, which could simplify the production process of the perifusion chamber and overcome the limitations (Klein et al., 2015; Kotz et al., 2017).

PDMS was used by the authors, because of its gas permeability and to obtain sufficient oxygen and carbon dioxide supply for the tissue parts. However, the gas permeability is limited by the thickness of the PDMS layers (Van Midwoud et al., 2010).

Sol-gels based on the alkoxy silanes TEOS and MTES are frequently applied for coating of microfluidic devices, due to low synthesis temperatures, which mediate the formation of strong covalent bonds between elements. The precursor MTES strongly influences the ratio, which depends on mechanical and surface properties such as flexibility, hydrophobicity and the porosity of the aerogels (Abate et al., 2008; Cai et al., 2014; Sinkó, 2010; Wang et al., 2012; Yu et al., 2003; Zhou et al., 2010). 1:1 ratios of TEOS and MTES were described for higher porosity, whereas they are not fully permeable compared to other ratios (Yu et al., 2003). The gels were successfully employed within cell culture applications and reduced drug absorption into the material by preserving transparency and oxygen permeability (Aymerich et al., 2016; Gomez-Sjoberg et al., 2010). Shrinkage of the gel and crack development happened, due to condensation of surface silanol groups driven by capillary pressure during gel drying (Aravind et al., 2010; Yang et al., 2014; Yun et al., 2014). The shrinkage increases with the amount of organo-alkoxysilanes such as MTES (Yang et al., 2014). Ambient pressure drying (APD) was reported to effective remove the pore liquid without shrinkage effects or crack development compared to the other drying methods by using for example temperature gradients (Aravind et al., 2010; Yun et al., 2007). However, we obtained crack-free non-shrunken aerogel after RT incubation.

Further experiments have to be performed under long term flow conditions to ensure the proper bonding of the device without leakage as well as biocompatibility. Additionally, flow simulations and spheroid perifusion experiments have to be evaluated on changes in flow and therefore possibly negative influences on spheroid growth.

5. Summary and conclusions

A new approach for the screening of endocrine active substances and their effects with the focus on estrogen and antiestrogen substances was presented. The detection system consists of three main components: 1) a glass hanging drop platform for the generation of compact MCF-7 cell multicellular spheroids 2) a spheroid perifusion chip supporting the long-term spheroid culture, to ensure sufficient nutrient, oxygen supply and to serve as an experimental platform for proliferation and biomarker measurements after exposure to estrogen and antiestrogen substances, and 3) a protein microarray for the quantification of the biomarker expression. The immobilization of BPA was investigated for the development of an on chip BPA screening in real samples and shall serve as additional pre-screening tool for the detection platform.

The human breast cancer cell line MCF-7 was chosen as a model for the establishment of the system. The hormone sensitive cells proliferate in presence of estrogen or estrogen active substances. In order to avoid interferences by hormones and hormone like substances contained in supplements of cell medium, the cells were cultured under serum-free and phenol-red free conditions. The proliferative response of MCF-7 cells due to exposure to estrogen active substances can be measured in parallel to the quantification of the protein expression with a proliferation assay based on metabolically conversion of resazurin to the highly fluorescent resofurin. The proliferative response of MCF-7 cells was enhanced due to incubation under hormone lacking conditions.

The glass hanging drop device for the generation of MCF-7 cell spheroids, contains six droplet wells assembled in 3 sub-arrays, which can be individually perfused with medium via a parallel assembled well–channel system. The formation and stability of droplets was ensured by hydrophobic and inert PFPE rings around the droplet openings, which were strongly attached to the glass surface by adhesive bonding with SU-8 photoresist or silicone sealant. The system kept droplet volumes up to 65 µL even under humid conditions. The design ensured a simultaneously liquid filling of two wells without pre-treatment of the channels and independently on the flow rate. Droplets can reach a height of 7.92 mm (~100 µL) until they drip off and can be fully automatic transferred to the perifusion chambers by stopping the outflow and providing a continuous inflow until drip off. Neither the droplet drip off nor the tilting of the whole device was affecting the other droplets in the system. In order to completely perfuse droplets larger than ~ 20 µL, in-and outflow of liquid was provided consecutively. High evaporation emerged due to the open system, was reduced by the integration of an incubation chamber. Detection of spheroids was enabled through a glass window in the bottom of the incubation chamber. Compact spheroids were formed after three

days of static cell culture and after two days under flow conditions. 20 µL/min flow was neither affecting the viability of the MCF-7 cell spheroids nor the formation. Effects on the cell viability were obtained for the photoresist SU-8, used for the attachment of the PFPE rings. Due to SU-8 replacement by a silicone sealant, this effect could be prevented. No data were found about potentially estrogenic action of the reagents in the sealant. However, by mechanical integration of the PFPE rings via clicking or tracks, these secondary material- or reagent-based effects can be avoided. Higher response of MCF-7 cells prior to estradiol exposure was seen in the new glass hanging drop device compared to PMDS, confirming the application of less porous and chemically inert materials for toxicological testing of endocrine active substances at the low molar level and displays the importance for the right choice of material.

The new channel design displaced the disadvantages seen for serial systems made of PDMS such as back flow, droplet volume limit, pre-filling or network failure due to drip off. The device can also be applied as experimental platform for toxicological research. The channel-well-network can be further extended on larger glass plates for higher sample numbers and the subarrays can be merged to one array with multi-ports or by integration of additional channel structures connected to the subarrays following the principle of flow for split channels. Limitation for simultaneously filling occurred, due to partial glass bonding and resistance of the channels emerged by the production process. The application of other production methods such as dry etching or laser ablation for the integration of structures and holes in glass may improve this. The device can be further automatized by adding of inlets for the introduction of the cell solution.

The PDMS based perifusion device, based on Van Midwoud et al., (2010), was reassembled to enable the integration of the hanging droplet platform and the biomarker chip. Detection of the spheroids was realized by integration of a glass membrane at the bottom of each perifusion chamber and by opening of the upper part of the device. The opening might allow additionally proliferation measurements in a plate reader. The glass membrane was not permeable for liquids and broke under pressure. Due to removal of the polycarbonate membranes, the flow distribution will be changed. A glass coating of the PDMS device ensures the impermeability for small hydrophobic molecules into the PDMS layers. The single perifusion chambers provide sufficient medium volumes for the processing of protein microarray. However, also the direct integration of a bead based protein immunoassay in the perifusion device is imaginable and thus enables the screening of lower supernatant volumes. A further redesign of the system by for instance increasing the amount of the chambers, decreasing the chamber volume or changing of in- and outlet flow conditions is necessary to ensure the growth of 150-500 µm cell spheroids and to allow high throughput

screening. In order to fasten and simplify the production process, new techniques such as liquid glass printing can be applied.

A biomarker microarray for the fluorescence based detection of 10 proteins (IL-6, IL-8, IL-11, MMP-9, CXCL10, VEGF, IGF-1, IGFBP-3, Rantes, MCP-1) in MCF-7 cell supernatant, which are related to physiological and pathological endpoints of EDCs action in human can be attached to the perifusion chamber. The assay performance was increased for some biomarkers due to the addition of BSA to the sample matrix DMEM/F-12. Upon IL-1ß stimulation of the MCF-7 cells, the secretion of low abundant biomarkers was promoted to measurable levels on one hand, but sometimes masked estrogen dependent secretion variances on the other hand. However, mimicking inflammatory processes by IL-1ß application, allows the screening of estrogen active substances within complex biological responses. The validation of the system was performed by exposure of MCF-7 cells grown in 2D to well-known estrogen and antiestrogen active substances and resulted in distinct secretion patterns. The parallel determination of MCF-7 cell proliferation approved agonistic and antagonistic effects by increase or decrease of proliferation of the hormone sensitive cell line. Further experiments for the protein secretion of the MCF-7 spheroid culture have to be performed to confirm the observed secretion patterns of the 2D cultured cells. However, additional screening of various estrogen receptor ligands in different concentrations, binding affinities to the receptor as well as over different periods is pivotal to assess the secretion patterns seen.

In conclusion the biomarker chip represents an outstanding tool for the evaluation of estrogen and antiestrogen action also for substances which are not assessed for endocrine action by now. The platform can be applied for the evaluation of protein expression within the progress of diseases and involvement in steroid synthesis or reproductive disorders. There are manifold opportunities for the extension of the system, which further support the detection of endocrine action with the new biomarker chip. An extension of the system may include an increase of the biomarker amount, applying of cell lines or primary cells from different tissues and co-cultures with for instance fibroblasts.

The immobilization of bisphenol A (BPA) was investigated for the on-chip BPA detection in applied samples by a binding inhibition assay and shall be integrated as pre-screening tool into the screening platform. Immobilization of BPA conjugates suffered from high cross-reactivity of the bisphenol antibody against the protein carriers BSA, HSA and from low signal intensities for KLH and HRP conjugates on different functionalized surfaces. The unconjugated bisphenol A showed even higher signal intensities on poly-L-lysine surfaces than conjugates without high cross-reactivity to the antibody. BPA was further tested in

sciPOLY3D gel. Application of sciPOLY3D gel allows a fast and straight forward covalent immobilization of especially small molecules owning less functional reactive groups, due to bonding to alkyl groups. The immobilization of BPA in sciPOLY3D was validated within a direct assay format, suggesting immobilization via its methyl groups and detection of its phenyl groups. Spot morphology and inter-assay variances were improved by adding of trehalose. The reached signal intensities were similar to unconjugated BPA on poly-L-lysine surfaces. However, using sciPOLY3D gel as immobilization matrix, detection limits similar to already established competitive formats with conjugated BPA, were analyzed for the binding inhibition format. Further characterization and improvement of the performance of the BPA binding inhibition assay is necessary to quantify BPA accurately in food or environmental samples. The immobilization of other endocrine substances in sciPOLY3D gel has to be tested as further extension of the chip to a multi-analyte platform.

6. List of references

A, M., N, G., HM, W., 1990. Miniaturized total chemical analysis systems: a novel concept for chemical sensing. Sensors actuators B Chem. 1, 244–248.

Abate, A.R., Lee, D., Do, T., Holtze, C., Weitz, D.A., 2008. Glass coating for PDMS microfluidic channels by sol–gel methods. Lab Chip 8, 516. doi:10.1039/b800001h

Abdelgawad, M., Watson, M.W.L., Young, E.W.K., Mudrik, J.M., Ungrin, M.D., Wheeler, A.R., 2008. Soft lithography: masters on demand. Lab Chip 8, 1379. doi:10.1039/b804050h

Abdelgawad, M., Wheeler, A.R., 2009. The Digital Revolution: A New Paradigm for Microfluidics. Adv. Mater. 21, 920–925. doi:10.1002/adma.200802244

Achilli, T.-M., Meyer, J., Morgan, J.R., 2012. Advances in the formation, use and understanding of multi-cellular spheroids. Expert Opin. Biol. Ther. 12, 1347–1360. doi:10.1517/14712598.2012.707181

Agrawal, S., Łuc, M., Ziółkowski, P., Agrawal, A.K., Pielka, E., Walaszek, K., Zduniak, K., Woźniak, M., 2017. Insulin-induced enhancement of MCF-7 breast cancer cell response to 5-fluorouracil and cyclophosphamide. Tumor Biol. 39. doi:10.1177/1010428317702901

Agrisera, 2018. Bisphenol A [WWW Document]. URL http://www.agrisera.com/en/artiklar/bisphenol-a-2.html (accessed 3.5.18).

Ahn, J.Y., Lee, S., Jo, M., Kang, J., Kim, E., Jeong, O.C., Laurell, T., Kim, S., 2012. Sol-Gel derived nanoporous compositions for entrapping small molecules and their outlook toward aptamer screening. Anal. Chem. 84, 2647–2653. doi:10.1021/ac202559w

Aijian, A.P., Garrell, R.L., 2015. Digital Microfluidics for Automated Hanging Drop Cell Spheroid Culture. J. Lab. Autom. 20, 283–295. doi:10.1177/2211068214562002

Akyazi, T., Basabe-Desmonts, L., Benito-Lopez, F., 2018. Review on microfluidic paper-based analytical devices towards commercialisation. Anal. Chim. Acta. doi:10.1016/j.aca.2017.11.010

Al-Bader, M., Ford, C., Al-Ayadhy, B., Francis, I., 2011. Analysis of estrogen receptor isoforms and variants in breast cancer cell lines. Exp. Ther. Med. 2. doi:10.3892/etm.2011.226

Allegra, J.C., Lippman, M.E., 1978. Growth of a Human Breast Cancer Cell Line in Serum-free Hormone-supplemented Medium. Cancer Res. 38, 3823–3829.

Alvarez-Pérez, J., Ballesteros, P., Cerdán, S., 2005. Microscopic images of intraspheroidal pH by 1H magnetic resonance chemical shift imaging of pH sensitive indicators. Magn. Reson. Mater. Physics, Biol. Med. 18, 293–301. doi:10.1007/s10334-005-0013-z

Anada, T., Fukuda, J., Sai, Y., Suzuki, O., 2012. An oxygen-permeable spheroid culture system for the prevention of central hypoxia and necrosis of spheroids. Biomaterials 33, 8430–8441. doi:10.1016/j.biomaterials.2012.08.040

Anderson, G.P., Jacoby, M.A., Ligler, F.S., King, K.D., 1997. Effectiveness of protein A for antibody immobilization for a fiber optic biosensor. Biosens. Bioelectron. 12, 329–336. doi:10.1016/S0956-5663(96)00074-7

Annunziato, M.E., Patel, U.S., Ranade, M., Palumbo, P.S., 1993. P-Maleimidophenyl Isocyanate: A novel Heterobifunctional Linker for Hydroxyl to Thiol Coupling. Bioconjug.

Chem. 4, 212–218. doi:10.1021/bc00021a005

Antibodies-online, n.d. Bisphenol A ELISA Kit [WWW Document]. URL https://www.antibodies-online.com/kit/459330/Bisphenol+A+ELISA+Kit/ (accessed 2.24.18).

Aran, K., Sasso, L.A., Kamdar, N., Zahn, J.D., 2010. Irreversible, direct bonding of nanoporous polymer membranes to PDMS or glass microdevices. Lab Chip 10, 548. doi:10.1039/b924816a

Aravind, P.R., Shajesh, P., Soraru, G.D., Warrier, K.G.K., 2010. Ambient pressure drying: A successful approach for the preparation of silica and silica based mixed oxide aerogels. J. Sol-Gel Sci. Technol. 54, 105–117. doi:10.1007/s10971-010-2164-2

Armbruster, D. a, Pry, T., 2008. Limit of blank, limit of detection and limit of quantitation. Clin. Biochem. Rev. 29 Suppl 1, S49–S52.

Arora, M., 2013. Cell Culture Media: A Review. Mater. Methods 3, 1–27. doi:10.13070/mm.en.3.175

Arscott, S., 2014. SU-8 as a material for lab-on-a-chip-based mass spectrometry. Lab Chip 14, 3668. doi:10.1039/C4LC00617H

Au, S.H., Chamberlain, M.D., Mahesh, S., Sefton, M. V., Wheeler, A.R., 2014. Hepatic organoids for microfluidic drug screening. Lab Chip 14, 3290. doi:10.1039/C4LC00531G

Austin, J., Holway, A.H., 2011. Contact printing of protein microarrays. Methods Mol. Biol. 785, 379–394. doi:10.1007/978-1-61779-286-1_25

Aymerich, M., Gómez-Varela, A.I., Álvarez, E., Flores-Arias, M.T., 2016. Study of different sol-gel coatings to enhance the lifetime of PDMS devices: Evaluation of their biocompatibility. Materials (Basel). 9. doi:10.3390/ma9090728

Ayuso, J.M., Monge, R., Llamazares, G.A., Moreno, M., Agirregabiria, M., Berganzo, J., Doblaré, M., Ochoa, I., Fernández, L.J., 2015. SU-8 Based Microdevices to Study Self-Induced Chemotaxis in 3D Microenvironments. Front. Mater. 2. doi:10.3389/fmats.2015.00037

Badaoui, M., Mimsy-Julienne, C., Saby, C., Van Gulick, L., Peretti, M., Jeannesson, P., Morjani, H., Ouadid-Ahidouch, H., Badaoui, M., Mimsy-Julienne, C., Saby, C., Van Gulick, L., Peretti, M., Jeannesson, P., Morjani, H., Ouadid-Ahidouch, H., 2017. Collagen type 1 promotes survival of human breast cancer cells by overexpressing Kv10.1 potassium and Orai1 calcium channels through DDR1-dependent pathway. Oncotarget 5. doi:10.18632/oncotarget.19065

Baltzer, L., 2011. Crossing borders to bind proteins-a new concept in protein recognition based on the conjugation of small organic molecules or short peptides to polypeptides from a designed set. Anal. Bioanal. Chem. doi:10.1007/s00216-011-4905-7

Baluka, S.A., Rumbeiha, W.K., 2016. Bisphenol A and food safety: Lessons from developed to developing countries. Food Chem. Toxicol. 92, 58–63. doi:10.1016/j.fct.2016.03.025

Barnes, D., Sato, G., 1980a. Methods for growth of cultured cells in serum-free medium. Anal. Biochem. doi:10.1016/0003-2697(80)90151-7

Barnes, D., Sato, G., 1980b. Serum-free cell culture: a unifying approach. Cell. doi:10.1016/0092-8674(80)90540-1

Barnes, D., Sato, G., 1979a. Growth of a human mammary tumour cell line in a serum-free

medium. Nature 281, 388–389. doi:10.1038/281388a0

Barnes, D., Sato, G., 1979b. Growth of a human mammary tumour cell line in a serum-free medium. Nature 281, 388–389.

Bartosh, T.J., Ylöstalo, J.H., Mohammadipoor, A., Bazhanov, N., Coble, K., Claypool, K., Lee, R.H., Choi, H., Prockop, D.J., 2010. Aggregation of human mesenchymal stromal cells (MSCs) into 3D spheroids enhances their antiin fl ammatory properties. Proc. Natl. Acad. Sci. U. S. A. 107, 13724–13729. doi:10.1073/pnas.1008117107/-/DCSupplemental.www.pnas.org/cgi/doi/10.1073/pnas.1008117107

Beebe, D.J., Mensing, G.A., Walker, G.M., 2002. Physics and Applications of Microfluidics in Biology. Annu. Rev. Biomed. Eng. 4, 261–286. doi:10.1146/annurev.bioeng.4.112601.125916

Bendrik, C., Dabrosin, C., 2009. Estradiol increases IL-8 secretion of normal human breast tissue and breast cancer in vivo. J. Immunol. 182, 371–378. doi:182/1/371 [pii]

Berthier, E., Young, E.W.K., Beebe, D., 2012. Engineers are from PDMS-land, Biologists are from Polystyrenia. Lab Chip 12, 1224. doi:10.1039/c2lc20982a

Berthois, Y., Katzenellenbogen, J.A., Katzenellenbogen, B.S., 1986. Phenol red in tissue culture media is a weak estrogen: implications concerning the study of estrogen-responsive cells in culture. Proc. Natl. Acad. Sci. U. S. A. 83, 2496–500. doi:10.1073/pnas.83.8.2496

Berthold, A., Laugere, F., Schellevis, H., De Boer, C.R., Laros, M., Guijt, R.M., Sarro, P.M., Vellekoop, M.J., 2002. Fabrication of a glass-impolemented microcapillary electrophoresis device with integrated contactless conductivity detection. Electrophoresis 23, 3511–3519. doi:10.1002/1522-2683(200210)23:20<3511::AID-ELPS3511>3.0.CO;2-C

Bilenberg, B., Nielsen, T., Clausen, B., Kristensen, A., 2004. PMMA to SU-8 bonding for polymer based lab-on-a-chip systems with integrated optics. J. Micromechanics Microengineering 14, 814–818. doi:10.1088/0960-1317/14/6/008

Blair, R.M., Fang, H., Branham, W.S., Hass, B.S., Dial, S.L., Moland, C.L., Tong, W., Shi, L., Perkins, R., Sheehan, D.M., 2000. The estrogen receptor relative binding affinities of 188 natural and xenochemicals: structural diversity of ligands. Toxicol. Sci. 54, 138–153. doi:10.1093/toxsci/54.1.138

Boellner, S., Becker, K.-F., 2015. Reverse Phase Protein Arrays—Quantitative Assessment of Multiple Biomarkers in Biopsies for Clinical Use. Microarrays 4, 98–114. doi:10.3390/microarrays4020098

Bogojevic, D., Chamberlain, M.D., Barbulovic-Nad, I., Wheeler, A.R., 2012. A digital microfluidic method for multiplexed cell-based apoptosis assays. Lab Chip 12, 627–634. doi:10.1039/C2LC20893H

Borra, R.C., Lotufo, M.A., Gagioti, S.M., Barros, F. de M., Andrade, P.M., 2009. A simple method to measure cell viability in proliferation and cytotoxicity assays. Braz. Oral Res. 23, 255–262. doi:10.1590/S1806-83242009000300006

Bovee, T.F.H., Helsdingen, R.J.R., Koks, P.D., Kuiper, H.A., Hoogenboom, R.L.A.P., Keijer, J., 2004. Development of a rapid yeast estrogen bioassay, based on the expression of green fluorescent protein. Gene 325, 187–200. doi:10.1016/j.gene.2003.10.015

Breslin, S., O'Driscoll, L., 2013. Three-dimensional cell culture: The missing link in drug discovery. Drug Discov. Today. doi:10.1016/j.drudis.2012.10.003

Briand, P., Lykkesfeldt, A.E., 1984. Effect of estrogen and antiestrogen on the human breast cancer cell line MCF-7 adapted to growth at low serum concentration. Cancer Res. 44, 1114–9.

Briand, P., Lykkesfeldt, A.E., 1983. Continuous Growth of a Human Breast Cancer Cell Line (MCF-7) in Serum-Free Medium, in: Fischer G., Wieser R.J. (Eds) Hormonally Defined Media. Proceedings in Life Sciences. Springer, Berlin, Heidelberg, pp. 436–438.

Bronger, H., Kraeft, S., Schwarz-Boeger, U., Cerny, C., Stöckel, A., Avril, S., Kiechle, M., Schmitt, M., 2012. Modulation of CXCR3 ligand secretion by prostaglandin E2 and cyclooxygenase inhibitors in human breast cancer. Breast Cancer Res. 14, R30. doi:10.1186/bcr3115

Bronzert, D.A., Pantazis, P., Antoniades, H.N., Kasid, A., Davidson, N., Dickson, R.B., Lippman, M.E., 1987. Synthesis and secretion of platelet-derived growth factor by human breast cancer cell lines. Proc. Natl. Acad. Sci. U. S. A. 84, 5763–7.

Bu, M., Melvin, T., Ensell, G.J., Wilkinson, J.S., Evans, A.G.R., 2004. A new masking technology for deep glass etching and its microfluidic application, in: Sensors and Actuators, A: Physical. pp. 476–482. doi:10.1016/j.sna.2003.12.013

Cai, S., Zhang, Y., Zhang, H., Yan, H., Lv, H., Jiang, B., 2014. Sol-gel preparation of hydrophobic silica antireflective coatings with low refractive index by base/acid two-step catalysis. ACS Appl. Mater. Interfaces 6, 11470–11475. doi:10.1021/am501972y

Campion, S., Aubrecht, J., Boekelheide, K., Brewster, D.W., Vaidya, V.S., Anderson, L., Burt, D., Dere, E., Hwang, K., Pacheco, S., Saikumar, J., Schomaker, S., Sigman, M., Goodsaid, F., 2013. The current status of biomarkers for predicting toxicity. Expert Opin. Drug Metab. Toxicol. 9, 1391–408. doi:10.1517/17425255.2013.827170

Cardona, S.M., Garcia, J.A., Cardona, A.E., 2013. The fine balance of chemokines during disease: trafficking, inflammation, and homeostasis. Methods Mol. Biol. doi:10.1007/978-1-62703-426-5_1

Chen, C., Mehl, B.T., Munshi, A.S., Townsend, A.D., Spence, D.M., Martin, R.S., 2016. 3D-printed microfluidic devices: fabrication, advantages and limitations—a mini review. Anal. Methods 8, 6005–6012. doi:10.1039/C6AY01671E

Chen, W., Wong, C., Vosburgh, E., Levine, A.J., Foran, D.J., Xu, E.Y., 2014. High-throughput Image Analysis of Tumor Spheroids: A User-friendly Software Application to Measure the Size of Spheroids Automatically and Accurately. J. Vis. Exp. doi:10.3791/51639

Chen, Y., Gao, D., Liu, H., Lin, S., Jiang, Y., 2015. Drug cytotoxicity and signaling pathway analysis with three-dimensional tumor spheroids in a microwell-based microfluidic chip for drug screening. Anal. Chim. Acta 898, 85–92. doi:10.1016/j.aca.2015.10.006

Cheung, V.G., Morley, M., Aguilar, F., Massimi, a, Kucherlapati, R., Childs, G., 1999. Making and reading microarrays. Nat. Genet. 21, 15–19. doi:10.1038/4439

Chiu, J.J., Sgagias, M.K., Cowan, K.H., 1996. Interleukin 6 acts as a paracrine growth factor in human mammary carcinoma cell lines. Clin. Cancer Res. 2, 215–221.

Choi, C.H., Kim, C.J., 2009. Droplet evaporation of pure water and protein solution on nanostructured superhydrophobic surfaces of varying heights. Langmuir 25, 7561–7567. doi:10.1021/la803614h

Choi, D.H., Katakura, Y., Matsuda, R., Hayashi, Y., Ninomiya, K., Shioya, S., 2007. Simulation model for predicting limit of detection and range of quantitation of competitive

enzyme-linked immunosorbent assay. J. Biosci. Bioeng. 103, 427–31. doi:10.1263/jbb.103.427

Choi, K., Ng, A.H.C., Fobel, R., Wheeler, A.R., 2012. Digital Microfluidics. Annu. Rev. Anal. Chem. 5, 413–440. doi:10.1146/annurev-anchem-062011-143028

Choi, Y.S., Lee, C., 2011. Generation of protein and cell microarrays on functionalized surfaces. Methods Mol. Biol. 671, 207–217. doi:10.1007/978-1-59745-551-0_12

Chrzan, B.G., Bradford, P.G., 2007. Phytoestrogens activate estrogen receptor beta1 and estrogenic responses in human breast and bone cancer cell lines. Mol. Nutr. Food Res. 51, 171–177. doi:10.1002/mnfr.200600091

Ciprian Iliescu, Bangtao Chen, Jianmin Miao, 2007. Deep wet etching-through 1mm pyrex glass wafer for microfluidic applications, in: 2007 IEEE 20th International Conference on Micro Electro Mechanical Systems (MEMS). pp. 393–396. doi:10.1109/MEMSYS.2007.4433150

Colston, K.W., Perks, C.M., Xie, S.P., Holly, J.M., 1998. Growth inhibition of both MCF-7 and Hs578T human breast cancer cell lines by vitamin D analogues is associated with increased expression of insulin-like growth factor binding protein-3. J. Mol. Endocrinol. 20, 157–162.

Core Life Science, 2012. Core Life Sciences Microarray White Papers and Guides Series Technical Features to Consider When Purchasing a Microarrayer 1–5.

Cox, K.L., 2012. Immunoassay Methods. Assay Guid. Man. 26–28. doi:NBK92434 [bookaccession]

Cui, X., Hartanto, Y., Zhang, H., 2017. Advances in multicellular spheroids formation. J. R. Soc. Interface 14, 20160877. doi:10.1098/rsif.2016.0877

Cui, Z.F., Xu, X., Trainor, N., Triffitt, J.T., Urban, J.P.G., Tirlapur, U.K., 2007. Application of multiple parallel perfused microbioreactors and three-dimensional stem cell culture for toxicity testing. Toxicol. Vitr. 21, 1318–1324. doi:10.1016/j.tiv.2007.05.015

Damstra, T., Barlow, S., Bergman, A., Kavlock, R., Van Der Kraak, G., 2002. Global assessment of the state-of-the-science of endocrine disruptors. WHOpublication no. WHO/PCS/EDC/02.2 180.

Darbre, P.D., 2014. Hypersensitivity and growth adaptation of oestrogen-deprived MCF-7 human breast cancer cells. Anticancer Res. 34, 99–105.

Darwish, I.A., 2006. Immunoassay Methods and their Applications in Pharmaceutical Analysis : Basic Methodology and Recent Advances. Int. J. Biomed. Sciense 2, 217–235.

Davies, C., 2013. Immunoassay Performance Measures11, in: The Immunoassay Handbook. pp. 11–26. doi:10.1016/B978-0-08-097037-0.00003-8

de Groot, T.E., Veserat, K.S., Berthier, E., Beebe, D.J., Theberge, A.B., 2016. Surface-tension driven open microfluidic platform for hanging droplet culture. Lab Chip 16, 334–344. doi:10.1039/C5LC01353D

De Silva, A.P., Gunaratne, H.Q.N., Gunnlaugsson, T., Huxley, A.J.M., McCoy, C.P., Rademacher, J.T., Rice, T.E., 1997. Signaling recognition events with fluorescent sensors and switches. Chem. Rev. 97, 1515–1566. doi:10.1021/cr960386p

Del Campo, A., Greiner, C., 2007. SU-8: A photoresist for high-aspect-ratio and 3D

submicron lithography. J. Micromechanics Microengineering 17. doi:10.1088/0960-1317/17/6/R01

Delon, A., Wang, I., Lambert, E., Mache, S., Mache, R., Derouard, J., Motto-Ros, V., Galland, R., 2010. Measuring, in solution, multiple-fluorophore labeling by combining fluorescence correlation spectroscopy and photobleaching. J. Phys. Chem. B 114, 2988–2996. doi:10.1021/jp910082h

Dertinger, S.K.W., Chiu, D.T., Noo Li Jeon, Whitesides, G.M., 2001. Generation of gradients having complex shapes using microfluidic networks. Anal. Chem. 73, 1240–1246. doi:10.1021/ac001132d

Devaraju, N.S.G.K., Unger, M.A., 2011. Multilayer soft lithography of perfluoropolyether based elastomer for microfluidic device fabrication. Lab Chip 11, 1962. doi:10.1039/c0lc00274g

Diamanti-Kandarakis, E., Bourguignon, J.P., Giudice, L.C., Hauser, R., Prins, G.S., Soto, A.M., Zoeller, R.T., Gore, A.C., 2009a. Endocrine-Disrupting Chemicals: An Endocrine Society Scientific Statement. Endocr. Rev. 30, 293–342. doi:10.1210/er.2009-0002

Diamanti-Kandarakis, E., Bourguignon, J.P., Giudice, L.C., Hauser, R., Prins, G.S., Soto, a M., Zoeller, R.T., Gore, a C., 2009b. Endocrine-disrupting chemicals: an Endocrine Society scientific statement. Endocr Rev 30, 293–342. doi:10.1210/er.2009-0002

Díez, P., Dasilva, N., González-González, M., Matarraz, S., Casado-Vela, J., Orfao, A., Fuentes, M., 2012. Data Analysis Strategies for Protein Microarrays. Microarrays 1, 64–83. doi:10.3390/microarrays1020064

Dixit, C., Aguirre, G., 2014. Protein Microarrays with Novel Microfluidic Methods: Current Advances. Microarrays 3, 180–202. doi:10.3390/microarrays3030180

Dixon, A.E., Damaskinos, S., 2001. Confocal Scanning of Genetic Microarrays, in: J.B., R. (Ed.), DNA Arrays Methods in Molecular Biology™. Humana Press, pp. 237–246.

Dodson, R.E., Nishioka, M., Standley, L.J., Perovich, L.J., Brody, J.G., Rudel, R.A., 2012. Endocrine disruptors and asthma-associated chemicals in consumer products. Environ. Health Perspect. doi:10.1289/ehp.1104052

Domnanich, P., Sauer, U., Pultar, J., Preininger, C., 2009. Protein microarray for the analysis of human melanoma biomarkers. Sensors Actuators, B Chem. 139, 2–8. doi:10.1016/j.snb.2008.06.043

Dubois, V., Couissi, D., Schonne, E., Remacle, C., Trouet, A., 1995. Intracellular levels and secretion of insulin-like-growth-factor-binding proteins in MCF-7/6, MCF-7/AZ and MDA-MB-231 breast cancer cells. Differential modulation by estrogens in serum-free medium. Eur. J. Biochem. 232, 47–53. doi:10.1111/j.1432-1033.1995.tb20779.x

Duffy, D.C., McDonald, J.C., Schueller, O.J.A., Whitesides, G.M., 1998. Rapid prototyping of microfluidic systems in poly(dimethylsiloxane). Anal. Chem. 70, 4974–4984. doi:10.1021/ac980656z

Dupont, J., Le Roith, D., 2001. Insulin-like growth factor 1 and oestradiol promote cell proliferation of MCF-7 breast cancer cells: new insights into their synergistic effects. Mol. Pathol. 54, 149–54.

Edelstein, A., Amodaj, N., Hoover, K., Vale, R., Stuurman, N., 2010. Computer control of microscopes using manager. Curr. Protoc. Mol. Biol. doi:10.1002/0471142727.mb1420s92

Edelstein, A.D., Tsuchida, M.A., Amodaj, N., Pinkard, H., Vale, R.D., Stuurman, N., 2014. Advanced methods of microscope control using μManager software. J. Biol. Methods 1, 10. doi:10.14440/jbm.2014.36

Ekins, R.P., 1987. An overview of present and future ultrasensitive non-isotopic immuno-assay development. Clin. Biochem. Rev. 8, 12–23.

Ekins, R.P., Chu, F.W., 1991. Multianalyte microspot immunoassay - microanalytical compact disk'' of the future. Clin. Chem. 37, 1955–1967.

Ekwall, B., Silano, V., Zucco, F., 1990. Chapter 7 - Toxicity Tests with Mammalian Cell Cultures. Short-term Toxic. Tests Non-genotoxic Eff. 75–98. doi:10.1155/2014/180549

Engländer, T., Wiegel, D., Naji, L., Arnold, K., 1996. Dehydration of glass surfaces studied by contact angle measurements. J. Colloid Interface Sci. 179, 635–636. doi:10.1006/jcis.1996.0260

EPA, 2011. Aromatase Assay (Human Recombinant) OCSPP Guideline 890.1200 Standard Evaluation Procedure (SEP) ENDOCRINE DISRUPTOR SCREENING PROGRAM U.S. Environmental Protection Agency Washington,.

Eral, H.B., 't Mannetje, D.J.C.M., Oh, J.M., 'T Mannetje, D.J.C.M., Oh, J.M., Mannetje, D.J.C.M., Oh, J.M., 2013. Contact angle hysteresis: a review of fundamentals and applications. Colloid Polym. Sci. 291, 247–260. doi:10.1007/s00396-012-2796-6

Erikstein, B.S., Hagland, H.R., Nikolaisen, J., Kulawiec, M., Singh, K.K., Gjertsen, B.T., Tronstad, K.J., 2010. Cellular stress induced by resazurin leads to autophagy and cell death via production of reactive oxygen species and mitochondrial impairment. J. Cell. Biochem. 111, 574–584. doi:10.1002/jcb.22741

Etique, N., Chardard, D., Chesnel, A., Merlin, J.L., Flament, S., Grillier-Vuissoz, I., 2004. Ethanol stimulates proliferation, ERalpha and aromatase expression in MCF-7 human breast cancer cells. Int. J. Mol. Med. 13, 149–155.

Etique, N., Grillier-Vuissoz, I., Flament, S., 2006. Ethanol stimulates the secretion of matrix metalloproteinases 2 and 9 in MCF-7 human breast cancer cells. Oncol Rep 15, 603–608.

Fagin, D., 2012. The Learning Curve. Nature 490, 462–465. doi:10.1136/bmj.38176.444745.63

Fan, S., Meng, Q., Gao, B., Grossman, J., Yadegari, M., Goldberg, I.D., Rosen, E.M., 2000. Alcohol stimulates estrogen receptor signaling in human breast cancer cell lines. Cancer Res. 60, 5635–5639.

Faustino, V., Catarino, S.O., Lima, R., Minas, G., 2016. Biomedical microfluidic devices by using low-cost fabrication techniques: A review. J. Biomech. 49, 2280–2292. doi:10.1016/j.jbiomech.2015.11.031

Feng, Y., Ning, B., Su, P., Wang, H., Wang, C., Chen, F., Gao, Z., 2009. An immunoassay for bisphenol A based on direct hapten conjugation to the polystyrene surface of microtiter plates. Talanta 80, 803–808. doi:10.1016/j.talanta.2009.07.070

Figueroa, J.A., Jackson, J.G., McGuire, W.L., Krywicki, R.F., Yee, D., 1993. Expression of insulin-like growth factor binding proteins in human breast cancer correlates with estrogen receptor status. J. Cell. Biochem. 52, 196–205. doi:10.1002/jcb.240520211

Findlay, J.W. a, Dillard, R.F., 2007. Appropriate calibration curve fitting in ligand binding assays. AAPS J. 9, E260--7. doi:10.1208/aapsj0902029

Finn, T.E., Nunez, A.C., Sunde, M., Easterbrook-Smith, S.B., 2012. Serum albumin prevents protein aggregation and amyloid formation and retains chaperone-like activity in the presence of physiological ligands. J. Biol. Chem. 287, 21530–21540. doi:10.1074/jbc.M112.372961

Francois, E., Wang, D.Y., Fulthorpe, R., Liss, S.N., Edwards, E. a., 2003. DNA microarrays for detecting endocrine-disrupting compounds. Biotechnol. Adv. 22, 17–26. doi:10.1016/j.biotechadv.2003.08.005

Freshney, I.R., 2010. Culture of Animal Cell; A manual of basic technique and specialized applicaitons, John Wiley & Sons inc. doi:10.1007/s13398-014-0173-7.2

Freund, A., Jolivel, V., Durand, S., Kersual, N., Chalbos, D., Chavey, C., Vignon, F., Lazennec, G., 2004. Mechanisms underlying differential expression of interleukin-8 in breast cancer cells. Oncogene 23, 6105–14. doi:10.1038/sj.onc.1207815

Frey, O., Misun, P.M., Fluri, D. a, Hengstler, J.G., Hierlemann, A., 2014. Reconfigurable microfluidic hanging drop network for multi-tissue interaction and analysis. Nat. Commun. 5, 4250. doi:10.1038/ncomms5250

Fukuda, J., Nakazawa, K., 2005. Orderly arrangement of hepatocyte spheroids on a microfabricated chip. Tissue Eng. 11, 1254–1262. doi:10.1089/ten.2005.11.1254

Gaben, A.M., Sabbah, M., Redeuilh, G., Bedin, M., Mester, J., 2012. Ligand-free estrogen receptor activity complements IGF1R to induce the proliferation of the MCF-7 breast cancer cells. BMC Cancer 12. doi:10.1186/1471-2407-12-291

Gainor, J.F., Longo, D.L., Chabner, B.A., 2014. Pharmacodynamic biomarkers: Falling short of the mark? Clin. Cancer Res. 20, 2587–2594. doi:10.1158/1078-0432.CCR-13-3132

García, A.A., Egatz-Gómez, A., Lindsay, S.A., Domínguez-García, P., Melle, S., Marquez, M., Rubio, M.A., Picraux, S.T., Yang, D., Aella, P., Hayes, M.A., Gust, D., Loyprasert, S., Vazquez-Alvarez, T., Wang, J., 2007. Magnetic movement of biological fluid droplets. J. Magn. Magn. Mater. 311, 238–243. doi:10.1016/j.jmmm.2006.10.1149

Garnier, M., Giamarchi, C., Delrieu, I., Rio, M.C., Chinestra, P., Bayard, F., Poirot, M., Faye, J.C., 2003. Insulin and estrogen receptor ligand influence the FGF-2 activities in MCF-7 breast cancer cells. Biochem. Pharmacol. 65, 629–636. doi:10.1016/S0006-2952(02)01563-0

Garvin, S., Nilsson, U.W., Dabrosin, C., 2005. Effects of oestradiol and tamoxifen on VEGF, soluble VEGFR-1, and VEGFR-2 in breast cancer and endothelial cells. Br. J. Cancer 93, 1005–10. doi:10.1038/sj.bjc.6602824

Gasparri, F., Galvani, A., 2010. Image-based high-content reporter assays: Limitations and advantages. Drug Discov. Today Technol. 7, e21–e30. doi:10.1016/j.ddtec.2010.04.003

Geens, T., Aerts, D., Berthot, C., Bourguignon, J.P., Goeyens, L., Lecomte, P., Maghuin-Rogister, G., Pironnet, A.M., Pussemier, L., Scippo, M.L., Van Loco, J., Covaci, A., 2012. A review of dietary and non-dietary exposure to bisphenol-A. Food Chem. Toxicol. doi:10.1016/j.fct.2012.07.059

Gibbs, J., 2001. Effective Blocking Procedures. ELISA Tech. Bull. Corning Inc. Life Sci. Kennebunk, ME 1–6.

Giepmans, B.N.G., Adams, S.R., Ellisman, M.H., Tsien, R.Y., 2006. The fluorescent toolbox for assessing protein location and function. Science (80-.). doi:10.1126/science.1124618

Gier, K., Preininger, C., Sauer, U., 2017. A chip for estrogen receptor action: Detection of biomarkers released by MCF-7 cells through estrogenic and anti-estrogenic effects. Sensors (Switzerland) 17. doi:10.3390/s17081760

Giridhar, M.S., Seong, K., Schülzgen, A., Khulbe, P., Peyghambarian, N., Mansuripur, M., 2004. Femtosecond pulsed laser micromachining of glass substrates with application to microfluidic devices. Appl. Opt. 43, 4584. doi:10.1364/AO.43.004584

Glass Microfluidic Device Fabrication SOP [WWW Document], 2015. URL https://microfab.ku.edu/sites/microfab.edu/files/docs/SOPs/Glass Microfluidic Device Fabrication SOP.pdf

Goldberg-Bittman, L., Neumark, E., Sagi-Assif, O., Azenshtein, E., Meshel, T., Witz, I.P., Ben-Baruch, A., 2004. The expression of the chemokine receptor CXCR3 and its ligand, CXCL10, in human breast adenocarcinoma cell lines. Immunol. Lett. 92, 171–178. doi:10.1016/j.imlet.2003.10.020

Gomez-Sjoberg, R., Leyrat, A.A., Houseman, B.T., Shokat, K., Quake, S.R., 2010. Biocompatibility and reduced drug absorption of sol-gel-treated poly(dimethyl siloxane) for microfluidic cell culture applications. Anal. Chem. 82, 8954–8960. doi:10.1021/ac101870s

Gong, P., Grainger, D.W., 2007. Nonfouling surfaces A review of principles and applications for microarray capture assay designs. Methods Mol. Biol. 381, 59–92. doi:10.1385/1-59745-303-X:59

Gore, A.C. Crews, D. Doan, L.L. La Merrill, M. Patisaul, H. Zota, A. et al., 2014. Introduction to Endocrine disrupting Chemicals (EDCs)-A Guide for Public interest Organizations and Policy-markers. Endocrine Society., Www.Endocrine.Org.

Greenbaum, D., Baruch, A., Hayrapetian, L., Darula, Z., Burlingame, A., Medzihradszky, K.F., Bogyo, M., 2002. Chemical Approaches for Functionally Probing the Proteome. Mol. Cell. Proteomics 1, 60–68. doi:10.1074/mcp.T100003-MCP200

Grzeskowiak, R., Gerke, N., 2015. Leachables: Minimizing the Influence of Plastic Consumables on the Laboratory Workflows. WHITE Pap. Eppend. No. 26, 1–6.

Gstraunthaler, G., Lindl, T., 2013. Zell- und Gewebekultur: Allgemeine Grundlagen und spezielle Anwendungen, 7th Editio. ed. Springer Spektrum.

Gupta, C., Tikoo, K., 2013. High glucose and insulin differentially modulates proliferation in MCF-7 and MDA-MB-231 cells. J. Mol. Endocrinol. 51, 119–129. doi:10.1530/JME-13-0062

Gupta, N., Liu, J.R., Patel, B., Solomon, D.E., Vaidya, B., Gupta, V., 2016. Microfluidics-based 3D cell culture models: Utility in novel drug discovery and delivery research. Bioeng. Transl. Med. 1, 63–81. doi:10.1002/btm2.10013

Haab, B.B., Dunham, M.J., Brown, P.O., 2001. Protein microarrays for highly parallel detection and quantitation of specific proteins and antibodies in complex solutions. Genome Biol. 2, 4–1. doi:10.1186/gb-2001-2-2-research0004

Habauzit, D., Boudot, A., Kerdivel, G., Flouriot, G., Pakdel, F., 2010. Development and validation of a test for environmental estrogens: Checking xeno-estrogen activity by CXCL12 secretion in Breast Cancer Cell Lines (CXCL-test). Environ. Toxicol. 25, 495–503. doi:10.1002/tox.20594

Hadley, M., Levine, J.E., 2006. Endocrinology, 6 edition. ed. Benjamin Cummings.

Häggström, M., Stannered;, Hoffmeier;, Settersr;, Richfield, D., 2014. Diagram of the pathways of human steroidogenesis. doi:10.15347/wjm/2014.005

Halldorsson, S., Lucumi, E., Gómez-Sjöberg, R., Fleming, R.M.T., 2015. Advantages and challenges of microfluidic cell culture in polydimethylsiloxane devices. Biosens. Bioelectron. doi:10.1016/j.bios.2014.07.029

Halliday, Resnick, 2015. Fundamental of Physics 10th Edition, Wiley. doi:10.1017/CBO9781107415324.004

Hamelers, I.H.L., van Schaik, R.F.M.A., Sussenbach, J.S., Steenbergh, P.H., 2003. 17β-estradiol responsiveness of MCF-7 laboratory strains is dependent on an autocrine signal activating the IGF type I receptor. Cancer Cell Int. 3. doi:10.1186/1475-2867-3-10

Hecker, M., Giesy, J.P., 2008. Novel trends in endocrine disruptor testing: The H295R Steroidogenesis Assay for identification of inducers and inhibitors of hormone production. Anal. Bioanal. Chem. 390, 287–291. doi:10.1007/s00216-007-1657-5

Heegaard, P.M.H., Pedersen, H.G., Jensen, A.L., Boas, U., 2009. A robust quantitative solid phase immunoassay for the acute phase protein C-reactive protein (CRP) based on cytidine 5′-diphosphocholine coupled dendrimers. J. Immunol. Methods 343, 112–118. doi:10.1016/j.jim.2009.02.002

Heo, Y.S., Cabrera, L.M., Song, J.W., Futai, N., Tung, Y.C., Smith, G.D., Takayama, S., 2007. Characterization and resolution of evaporation-mediated osmolality shifts that constrain microfluidic cell culture in poly(dimethylsiloxane) devices. Anal. Chem. 79, 1126–1134. doi:10.1021/ac061990v

Hernandez, K., Fernandez-Lafuente, R., 2011. Control of protein immobilization: Coupling immobilization and site-directed mutagenesis to improve biocatalyst or biosensor performance. Enzyme Microb. Technol. doi:10.1016/j.enzmictec.2010.10.003

Hof, L.A., Ziki, J.A., 2017. Micro-hole drilling on glass substrates-A review. Micromachines. doi:10.3390/mi8020053

Hoff, A., Bagû, A.C., André, T., Roth, G., Wiesmüller, K.H., Gückel, B., Brock, R., 2010. Peptide microarrays for the profiling of cytotoxic T-lymphocyte activity using minimum numbers of cells. Cancer Immunol. Immunother. 59, 1379–1387. doi:10.1007/s00262-010-0867-4

Hollingshead, B.D., Beischlag, T. V., DiNatale, B.C., Ramadoss, P., Perdew, G.H., 2008. Inflammatory signaling and aryl hydrocarbon receptor mediate synergistic induction of interleukin 6 in MCF-7 cells. Cancer Res. 68, 3609–3617. doi:10.1158/0008-5472.CAN-07-6168

Holtfreter, J., 1944. A study of the mechanics of gastrulation. J. Exp. Zool. 95, 171–212. doi:10.1002/jez.1400950203

Hong, H.J., Koom, W.S., Koh, W.G., 2017. Cell microarray technologies for high-throughput cell-based biosensors. Sensors (Switzerland). doi:10.3390/s17061293

Hong, S., Hsu, H.-J., Kaunas, R., Kameoka, J., 2012. Collagen microsphere production on a chip. Lab Chip 12, 3277. doi:10.1039/c2lc40558j

Hou, X., Zhang, Y.S., Santiago, G.T. De, Alvarez, M.M., Ribas, J., Jonas, S.J., Weiss, P.S., Andrews, A.M., Aizenberg, J., Khademhosseini, A., 2017. Interplay between materials and microfluidics. Nat. Rev. Mater. doi:10.1038/natrevmats.2017.16

Hsiao, A.Y., Torisawa, Y. suke, Tung, Y.C., Sud, S., Taichman, R.S., Pienta, K.J.,

Takayama, S., 2009. Microfluidic system for formation of PC-3 prostate cancer co-culture spheroids. Biomaterials 30, 3020–3027. doi:10.1016/j.biomaterials.2009.02.047

Hsiao, A.Y., Tung, Y.C., Kuo, C.H., Mosadegh, B., Bedenis, R., Pienta, K.J., Takayama, S., 2012. Micro-ring structures stabilize microdroplets to enable long term spheroid culture in 384 hanging drop array plates. Biomed. Microdevices 14, 313–323. doi:10.1007/s10544-011-9608-5

Hu, S., Xie, Z., Qian, J., Blackshaw, S., Zhu, H., 2011. Functional protein microarray technology. Wiley Interdiscip. Rev. Syst. Biol. Med. 3, 255–268. doi:10.1002/wsbm.118

Huff, K.K., Kaufman, D., Gabbay, K.H., Spencer, E.M., Lippman, M.E., Dickson, R.B., 1986. Secretion of an insulin-like growth factor-I-related protein by human breast cancer cells. Cancer Res 46, 4613–4619.

Hull, K.L., Harvey, S., 2014. Growth Hormone and Reproduction: A Review of Endocrine and Autocrine/Paracrine Interactions. Int. J. Endocrinol. doi:10.1155/2014/234014

Huy, T.Q., Hanh, N.T.H., Thuy, N.T., Chung, P. Van, Nga, P.T., Tuan, M.A., 2011. A novel biosensor based on serum antibody immobilization for rapid detection of viral antigens. Talanta 86, 271–277. doi:10.1016/j.talanta.2011.09.012

Iliescu, C., Chen, B., Miao, J., 2008. On the wet etching of Pyrex glass. Sensors Actuators, A Phys. 143, 154–161. doi:10.1016/j.sna.2007.11.022

Iliescu, C., Chen, B.T., Tay, F.E.H., Xu, G.L., Miao, J.M., 2006. Characterization of deep wet etching of glass - art. no. 60370A. Device Process Technol. Microelectron. MEMS, Photonics IV 6037, A370–A370. doi:Artn 60370a\rDoi 10.1117/12.638521

Iliescu, C., Jing, J., Tay, F.E.H., Miao, J., Sun, T., 2005. Characterization of masking layers for deep wet etching of glass in an improved HF/HCl solution. Surf. Coatings Technol. 198, 314–318. doi:10.1016/j.surfcoat.2004.10.094

Iliescu, C., Tay, F.E.H., 2005. Wet etching of glass, in: Proceedings of the International Semiconductor Conference, CAS. pp. 35–44. doi:10.1109/SMICND.2005.1558704

Iliescu, C., Taylor, H., Avram, M., Miao, J., Franssila, S., 2012. A practical guide for the fabrication of microfluidic devices using glass and silicon. Biomicrofluidics 6, 16505–1650516. doi:10.1063/1.3689939

Iliescu, C., Xu, G., Barbarini, E., Avram, M., Iliescu, F.S., 2008. Paramagnetic microchip for high-gradient separation of blood cell, in: Proceedings of SPIE - The International Society for Optical Engineering. doi:10.1117/12.810713

Inadera, H., Sekiya, T., Yoshimura, T., Matsushima, K., 2000. Molecular analysis of the inhibition of monocyte chemoattractant protein-1 gene expression by estrogen and xenoestrogens in MCF-7 cells. Endocrinology 141, 50–59.

Inamdar, N.K., Borenstein, J.T., 2011. Microfluidic cell culture models for tissue engineering. Curr. Opin. Biotechnol. 22, 681–689. doi:10.1016/j.copbio.2011.05.512

Inc, M.D., 2010. GenePix®Pro 7 Software User guide [WWW Document]. URL mdc.custhelp.com/euf/assets/content/GPP_7_2_SoftRef.pdf (accessed 2.4.18).

ITACA, 2018. Fluid Mechanics For Gravity – Flow Water Systems and Pumps [WWW Document]. URL http://www.itacanet.org/fluid-mechanics-for-gravity-flow-water-systems-and-pumps/part-4-the-continuity-equation-for-multiple-pipe-system/ (accessed 3.2.18).

JABŁOŃSKI, A., 1933. Efficiency of Anti-Stokes Fluorescence in Dyes. Nature 131, 839–840. doi:10.1038/131839b0

Jamalzadeh, L., Ghafoori, H., Sariri, R., Rabuti, H., Nasirzade, J., Hasani, H., Aghamaali, M.R., 2016. Cytotoxic Effects of Some Common Organic Solvents on MCF-7 , RAW-264.7 and Human Umbilical Vein Endothelial Cells. Avicenna J Med Biochem 4, 1–6. doi:10.17795/ajmb-33453.Research

Jellema, L.C., Mey, T., Koster, S., Verpoorte, E., 2009. Charge-based particle separation in microfluidic devices using combined hydrodynamic and electrokinetic effects. Lab Chip 9, 1914–1925. doi:10.1039/b819054b

Johnstone, C.N., Chand, A., Putoczki, T.L., Ernst, M., 2015. Emerging roles for IL-11 signaling in cancer development and progression: focus on breast cancer. Cytokine Growth Factor Rev. 26, 489–498. doi:10.1016/j.cytogfr.2015.07.015

Ju, C., Xiong, Y., Gao, A., Yang, T., Wang, L., 2011. Development of a direct competitive enzyme-linked immunosorbent assay using a sensitive monoclonal antibody for bisphenol A. Hybridoma (Larchmt). 30, 95–100. doi:10.1089/hyb.2010.0079

Kabir, E.R., Rahman, M.S., Rahman, I., 2015. A review on endocrine disruptors and their possible impacts on human health. Environ. Toxicol. Pharmacol. doi:10.1016/j.etap.2015.06.009

Kanda, N., Watanabe, S., 2003. 17??-estradiol inhibits the production of RANTES in human keratinocytes. J. Invest. Dermatol. 120, 420–427. doi:10.1046/j.1523-1747.2003.12067.x

Karabín, M., Hudcová, T., Jelínek, L., Dostálek, P., 2016. Biologically Active Compounds from Hops and Prospects for Their Use. Compr. Rev. Food Sci. Food Saf. 15, 542–567. doi:10.1111/1541-4337.12201

Karey, K.P., Sirbasku, D.A., 1988. Differential responsiveness of human breast cancer cell lines MCF-7 and T47D to growth factors and 17 beta-estradiol. Cancer Res. 48, 4083–4092.

Katt, M.E., Placone, A.L., Wong, A.D., Xu, Z.S., Searson, P.C., 2016. In Vitro Tumor Models: Advantages, Disadvantages, Variables, and Selecting the Right Platform. Front. Bioeng. Biotechnol. 4. doi:10.3389/fbioe.2016.00012

Katzenellenbogen, B.S., Kendra, K.L., Norman, M.J., Katzenellenbogen, B.S., Rendra, K.L., Norman, M.J., Berthois, Y., 1987. Proliferation , Hormonal Responsiveness , and Estrogen Receptor Content of MCF-7 Human Breast Cancer Cells Grown in the Short-Term and Long-Term Absence of Estrogens Proliferation , Hormonal Responsiveness , and Estrogen Receptor Content of MCF-7 of Estro 4355–4360.

Kawashima, I., Ohsumi, J., Mita-Honjo, K., Shimoda-Takano, K., Ishikawa, H., Sakakibara, S., Miyadai, K., Takiguchi, Y., 1991. Molecular cloning of cDNS encoding adipogenisis inhibitory factor and identity with interleukin-11. FEBS Lett. 283, 199–202.

Kayisli, U.A., Mahutte, N.G., Arici, A., 2002. Uterine chemokines in reproductive physiology and pathology. Am. J. Reprod. Immunol. 47, 213–221. doi:10.1034/j.1600-0897.2002.01075.x

Kelm, J.M., Timmins, N.E., Brown, C.J., Fussenegger, M., Nielsen, L.K., 2003. Method for generation of homogeneous multicellular tumor spheroids applicable to a wide variety of cell types. Biotechnol. Bioeng. 83, 173–180. doi:10.1002/bit.10655

Kerbel, R.S., Blakeslee, D., 2006. Rapid adsorption of a foetal calf serum component by

mammalian cells in culture. A potential source of artifacts in studies of antisera to cell-specific antigens. Immunology 31, 881–91.

Kida, N., Yoshimura, T., Mori, K., Hayashi, K., 1989. Hormonal regulation of synthesis and secretion of pS2 protein relevant to growth of human breast cancer cells (MCF-7). Cancer Res. 49, 3494–3498.

Kidd, K.A., Becher, G., Bergman, Å., Muir, D.C.G., Woodruff, T.J., 2012. Human and wildlife exposures to EDCs. State Sci. Endocr. Disrupting Chem. - 2012 1–261.

Kim, C., Chung, S., Kim, Y.E., Lee, K.S., Lee, S.H., Oh, K.W., Kang, J.Y., 2011. Generation of core-shell microcapsules with three-dimensional focusing device for efficient formation of cell spheroid. Lab Chip 11, 246–252. doi:10.1039/C0LC00036A

Kingsmore, S.F., 2006. Multiplexed protein measurement: Technologies and applications of protein and antibody arrays. Nat. Rev. Drug Discov. doi:10.1038/nrd2006

Kishore, V., R, S.G.K., Krishna, S., Sharma, K., Rashmi, M., Nishita, K.P., 2014. Bovine Serum Albumin a Potential Thermostabilizer : a Study on α -Amylase 2, 37–41. doi:10.12691/jaem-2-2-1

Kiyama, R., Wada-Kiyama, Y., 2015. Estrogenic endocrine disruptors: Molecular mechanisms of action. Env. Int 83, 11–40. doi:10.1016/j.envint.2015.05.012

Kiyama, R., Zhu, Y., 2014. DNA microarray-based gene expression profiling of estrogenic chemicals. Cell. Mol. Life Sci. doi:10.1007/s00018-013-1544-5

Klein, J., Stern, M., Franchin, G., Kayser, M., Inamura, C., Dave, S., Weaver, J.C., Houk, P., Colombo, P., Yang, M., Oxman, N., 2015. Additive Manufacturing of Optically Transparent Glass. 3D Print. Addit. Manuf. 2, 92–105. doi:10.1089/3dp.2015.0021

Kluger, R., Alagic, A., 2004. Chemical cross-linking and protein-protein interactions-a review with illustrative protocols. Bioorg. Chem. doi:10.1016/j.bioorg.2004.08.002

KÖHLER, G., MILSTEIN, C., 1975. Continuous cultures of fused cells secreting antibody of predefined specificity. Nature 256, 495–497. doi:10.1038/256495a0

Köhn, M., Wacker, R., Peters, C., Schröder, H., Soulère, L., Breinbauer, R., Niemeyer, C.M., Waldmann, H., 2003. Staudinger Ligation: A New Immobilization Strategy for the Preparation of Small-Molecule Arrays. Angew. Chemie - Int. Ed. 42, 5830–5834. doi:10.1002/anie.200352877

Kotz, F., Arnold, K., Bauer, W., Schild, D., Keller, N., Sachsenheimer, K., Nargang, T.M., Richter, C., Helmer, D., Rapp, B.E., 2017. Three-dimensional printing of transparent fused silica glass. Nature 544, 337–339. doi:10.1038/nature22061

Kricka, L.J., Master, S.R., Joos, T.O., Fortina, P., 2006. Current perspectives in protein array technology. Ann. Clin. Biochem. doi:10.1258/000456306778904731

Kuo, C. Te, Chiang, C.L., Huang, R.Y.J., Lee, H., Wo, A.M., 2012. Configurable 2D and 3D spheroid tissue cultures on bioengineered surfaces with acquisition of epithelial-mesenchymal transition characteristics. NPG Asia Mater. 4. doi:10.1038/am.2012.50

Kusnezow, W., Jacob, A., Walijew, A., Diehl, F., Hoheisel, J.D., 2003. Antibody microarrays: An evaluation of production parameters. Proteomics 3, 254–264. doi:10.1002/pmic.200390038

Lam, C.N.., Kim, N., Hui, D., Kwok, D.Y., Hair, M.L., Neumann, A.W., 2001. The effect of liquid properties to contact angle hysteresis. Colloids Surfaces A Physicochem. Eng.

Asp. 189, 265–278. doi:10.1016/S0927-7757(01)00589-1

Leca-Bouvier, B., Blum, L.J., 2005. Biosensors for protein detection: A review. Anal. Lett. doi:10.1081/AL-200065780

Lee, C., Kim, B., 2002. Improvement of protein stability in protein microarrays. Biotechnol. Lett. 24, 839–844. doi:10.1023/A:1015554705979

Lee, H.J., Chattopadhyay, S., Gong, E.Y., Ahn, R.S., Lee, K., 2003. Antiandrogenic effects of bisphenol A and nonylphenol on the function of androgen receptor. Toxicol. Sci. doi:10.1093/toxsci/kfg150

Lee, H.J., Wark, A.W., Corn, R.M., 2008. Microarray methods for protein biomarker detection. Analyst 133, 975–983. doi:10.1039/b717527b

Lee, J.N., Park, C., Whitesides, G.M., 2003. Solvent Compatibility of Poly(dimethylsiloxane)-Based Microfluidic Devices. Anal. Chem. 75, 6544–6554. doi:10.1021/ac0346712

Leester-Schädel, M., Lorenz, T., Jürgens, F., Richter, C., 2016. Fabrication of microfluidic devices, in: Microsystems for Pharmatechnology: Manipulation of Fluids, Particles, Droplets, and Cells. pp. 23–57. doi:10.1007/978-3-319-26920-7_2

Lei, Y., Fang, L., Hamid Akash, M.S., Liu, Z., Shi, W., Chen, S., 2013. Development and comparison of two competitive ELISAs for the detection of bisphenol A in human urine. Anal. Methods 5, 6106. doi:10.1039/c3ay41023d

Leskinen, P., Michelini, E., Picard, D., Karp, M., Virta, M., 2005. Bioluminescent yeast assays for detecting estrogenic and androgenic activity in different matrices. Chemosphere 61, 259–266. doi:10.1016/j.chemosphere.2005.01.080

Li, J., Gramatica, P., 2010. QSAR classification of estrogen receptor binders and pre-screening of potential pleiotropic EDCs. SAR QSAR Env. Res 21, 657–669. doi:930321120 [pii]\r10.1080/1062936X.2010.528254

Liao, M.-H., Tai, Y.-T., Cherng, Y.-G., Liu, S.-H., Chang, Y.-A., Lin, P.-I., Chen, R.-M., 2014. Genistein induces oestrogen receptor-α gene expression in osteoblasts through the activation of mitogen-activated protein kinases/NF-κB/ activator protein-1 and promotes cell mineralisation. Br. J. Nutr. 111, 55–63. doi:10.1017/S0007114513002043

Liddel, E., 2005. Antibodies, in: The Immunoassay Handbook. pp. 144–161. doi:10.1016/B978-0-08-097037-0.06001-2

Lima, R.S., Leão, P.A.G.C., Piazzetta, M.H.O., Monteiro, A.M., Shiroma, L.Y., Gobbi, A.L., Carrilho, E., 2015. Sacrificial adhesive bonding: A powerful method for fabrication of glass microchips. Sci. Rep. 5. doi:10.1038/srep13276

Lin, C.-H., Lee, G.-B., Lin, Y.-H., Chang, G.-L., 2001. A fast prototyping process for fabrication of microfluidic systems on soda-lime glass. J. Micromechanics Microengineering 11, 726–732. doi:10.1088/0960-1317/11/6/316

Lin, R.Z., Chang, H.Y., 2008. Recent advances in three-dimensional multicellular spheroid culture for biomedical research. Biotechnol. J. 3, 1172–1184. doi:10.1002/biot.200700228

Lin, R.Z., Chou, L.F., Chien, C.C.M., Chang, H.Y., 2006. Dynamic analysis of hepatoma spheroid formation: Roles of E-cadherin and β1-integrin. Cell Tissue Res. 324, 411–422. doi:10.1007/s00441-005-0148-2

Lorincz, A.M., Sukumar, S., 2006. Molecular links between obesity and breast cancer.

Endocr. Relat. Cancer 13, 279–292. doi:10.1677/erc.1.00729

Lu, Y., Peterson, J.R., Gooding, J.J., Lee, N.A., 2012. Development of sensitive direct and indirect enzyme-linked immunosorbent assays (ELISAs) for monitoring bisphenol-A in canned foods and beverages. Anal. Bioanal. Chem. 403, 1607–1618. doi:10.1007/s00216-012-5969-8

Lundholt, B.K., Scudder, K.M., Pagliaro, L., 2003. A simple technique for reducing edge effect in cell-based assays. J. Biomol. Screen. 8, 566–570. doi:10.1177/1087057103256465

Luo, L.J., Liu, F., Lin, Z.K., Xie, Y.F., Xu, J.L., Tong, Q.C., Shu, R., 2012. Genistein regulates the IL-1 beta induced activation of MAPKs in human periodontal ligament cells through G protein-coupled receptor 30. Arch. Biochem. Biophys. 522, 9–16. doi:10.1016/j.abb.2012.04.007

MacDougall, Daniel, Crummett, W.B., 1980. Guidelines for data acquisition and data quality evaluation in environmental chemistry. Anal. Chem. 52, 2242–2249.

Maggiolini, M., Bonofiglio, D., Marsico, S., Panno, M.L., Cenni, B., Picard, D., Andò, S., 2001. Estrogen receptor alpha mediates the proliferative but not the cytotoxic dose-dependent effects of two major phytoestrogens on human breast cancer cells. Mol. Pharmacol. 60, 595–602. doi:VL - 60

Magnani, E., Bettini, E., 2000. Resazurin detection of energy metabolism changes in serum-starved PC12 cells and of neuroprotective agent effect. Brain Res. Protoc. 5, 266–272. doi:10.1016/S1385-299X(00)00022-2

Maria, M.S., Rakesh, P.E., Chandra, T.S., Sen, A.K., 2017. Capillary flow-driven microfluidic device with wettability gradient and sedimentation effects for blood plasma separation. Sci. Rep. 7. doi:10.1038/srep43457

Marieb, E.N., 2015. Essential of Human Anatomy & Physiology, Pearson. doi:10.1038/nnano.2011.234

Marsden, D.M., Nicholson, R.L., Ladlow, M., Spring, D.R., 2009. 3D small-molecule microarrays. Chem. Commun. (Camb). 7107–7109. doi:10.1039/b913665g

Masteika, V., Kowal, J., Braithwaite, N.S.J., Rogers, T., 2014. A Review of Hydrophilic Silicon Wafer Bonding. ECS J. Solid State Sci. Technol. 3, Q42–Q54. doi:10.1149/2.007403jss

Mateo, C., Abian, O., Fernandez-Lafuente, R., Guisan, J.M., 2000a. Increase in conformational stability of enzymes immobilized on epoxy-activated supports by favoring additional multipoint covalent attachment. Enzyme Microb. Technol. 26, 509–515. doi:10.1016/S0141-0229(99)00188-X

Mateo, C., Fernández-Lorente, G., Abian, O., Fernández-Lafuente, R., Guisán, J.M., 2000b. Multifunctional epoxy supports: A new tool to improve the covalent immobilization of proteins. The promotion of physical adsorptions of proteins on the supports before their covalent linkage. Biomacromolecules 1, 739–745. doi:10.1021/bm000071q

Matthews, J., Celius, T., Halgren, R., Zacharewski, T., 2000. Differential estrogen receptor binding of estrogenic substances: A species comparison. J. Steroid Biochem. Mol. Biol. 74, 223–234. doi:10.1016/S0960-0760(00)00126-6

Maverakis, E., Kim, K., Shimoda, M., Gershwin, M.E., Patel, F., Wilken, R., Raychaudhuri, S., Ruhaak, L.R., Lebrilla, C.B., 2015. Glycans in the immune system and The Altered Glycan Theory of Autoimmunity: A critical review. J. Autoimmun. 57, 1–13.

doi:10.1016/j.jaut.2014.12.002

Mayeux, R., 2004. Biomarkers: potential uses and limitations. NeuroRx 1, 182–8. doi:10.1602/neurorx.1.2.182

Mazzocchi, A.R., Man, A.J., DesOrmeaux, J.P.S., Gaborski, T.R., 2014. Porous membranes promote endothelial differentiation of adipose-derived stem cells and perivascular interactions. Cell. Mol. Bioeng. 7, 369–378. doi:10.1007/s12195-014-0354-7

McCloy, R.A., Rogers, S., Caldon, C.E., Lorca, T., Castro, A., Burgess, A., 2014. Partial inhibition of Cdk1 in G2phase overrides the SAC and decouples mitotic events. Cell Cycle 13, 1400–1412. doi:10.4161/cc.28401

McDonald, G.R., Hudson, A.L., Dunn, S.M.J., You, H., Baker, G.B., Whittal, R.M., Martin, J.W., Jha, A., Edmondson, D.E., Holt, A., 2008. Bioactive Contaminants Leach from Disposable Laboratory Plasticware. Science (80-.). 322, 917–917. doi:10.1126/science.1162395

McDonald, J.C., Whitesides, G.M., 2002. Poly(dimethylsiloxane) as a material for fabricating microfluidic devices. Acc. Chem. Res. 35, 491–499. doi:10.1021/ar010110q

Mcjannet, D., Cook, F., Burn, S., 2008. Evaporation Reduction by Manipulation of Surface Area to Volume Ratios : Overview , Analysis and Effectiveness. Report 28.

McKim Jr., J., 2010. Building a Tiered Approach to In Vitro Predictive Toxicity Screening: A Focus on Assays with In Vivo Relevance. Comb. Chem. High Throughput Screen. 13, 188–206. doi:10.2174/138620710790596736

Mclachlan, M.J., Katzenellenbogen, J.A., Zhao, H., 2011. A new fluorescence complementation biosensor for detection of estrogenic compounds. Biotechnol. Bioeng. 108, 2794–2803. doi:10.1002/bit.23254

Mehta, G., Hsiao, A.Y., Ingram, M., Luker, G.D., Takayama, S., 2012. Opportunities and challenges for use of tumor spheroids as models to test drug delivery and efficacy. J. Control. Release 164, 192–204. doi:10.1016/j.jconrel.2012.04.045

Menger, M., Yarman, A., Erdossy, J., Yildiz, H.B., Gyurcsányi, R.E., Scheller, F.W., 2016. MIPs and aptamers for recognition of proteins in biomimetic sensing. Biosensors. doi:10.3390/bios6030035

Mira, E., Lacalle, R.A., González, M.A., Gómez-Moutón, C., Abad, J.L., Bernad, A., Martínez, C., Santos, M., 2001. A role for chemokine receptor transactivation in growth factor signaling. EMBO Rep. 2, 151–156. doi:10.1093/embo-reports/kve027

Misawa, A., Inoue, S., 2015. Estrogen-related receptors in breast cancer and prostate cancer. Front. Endocrinol. (Lausanne). doi:10.3389/fendo.2015.00083

Moriceau, H., Rieutord, F., Fournel, F., Le Tiec, Y., Di Cioccio, L., Morales, C., Charvet, A.M., Deguet, C., 2010. Overview of recent direct wafer bonding advances and applications. Adv. Nat. Sci. Nanosci. Nanotechnol. 1. doi:10.1088/2043-6262/1/4/043004

Moscona, A., Moscona, H., 1952. The dissociation and aggregation of cells from organ rudiments of the early chick embryo. J. Anat. 86, 287–301.

Moshksayan, K., Kashaninejad, N., Warkiani, M.E., Lock, J.G., Moghadas, H., Firoozabadi, B., Saidi, M.S., Nguyen, N.-T., 2018. Spheroids-on-a-chip: Recent advances and design considerations in microfluidic platforms for spheroid formation and culture. Sensors Actuators B Chem. doi:10.1016/j.snb.2018.01.223

Mujawar, L.H., Norde, W., van Amerongen, A., 2013. Spot morphology of non-contact printed protein molecules on non-porous substrates with a range of hydrophobicities. Analyst 138, 518–524. doi:10.1039/C2AN36104C

Muller, P.Y., Dieterle, F., 2009. Tissue-specific, non-invasive toxicity biomakers: Translation from preclinical safety assessment to clinical safety monitoring. Expert Opin. Drug Metab. Toxicol. 5, 1023–1038. doi:10.1517/17425250903114174

Nahavandi, S., Baratchi, S., Soffe, R., Tang, S.-Y., Nahavandi, S., Mitchell, A., Khoshmanesh, K., 2014. Microfluidic platforms for biomarker analysis. Lab Chip 14, 1496–514. doi:10.1039/c3lc51124c

Narang, U., Anderson, G.P., King, K.D., Liss, H.S., Ligler, F.S., 1997. Maintaining antibody function after immobilization is critical to the performance of a biosensor . The conventional methods to immobilize antibodies onto surfaces are via covalent by the addition of the analyte . Finally , a fluorophore-labeled antibody i, in: Proceedings of SPIE - The International Society for Optical Engineering. pp. 187–194.

NAS, 2015. Application of Modern Toxicology Approaches for Predicting Acute Toxicity for Chemical Defense, National Academies Press. doi:10.17226/21775

Naylor, S., 2003. Biomarkers : current perspectives. Expert Rev. Mol. diagnostics 3, 525–529.

Neave, N., 2007. Hormones and behaviour: A psychological approach, Hormones and Behaviour: A Psychological Approach. doi:10.1017/CBO9780511808203

Neeley, C., 2016. Reducing the edge effect [WWW Document]. URL https://www.thermofisher.com/blog/cellculture/reducing-the-edge-effect/ (accessed 3.4.18).

Nelson, L.R., Bulun, S.E., 2001. Estrogen production and action. J. Am. Acad. Dermatol. 45, S116–S124. doi:10.1067/mjd.2001.117432

Nemani, K. V., Moodie, K.L., Brennick, J.B., Su, A., Gimi, B., 2013. In vitro and in vivo evaluation of SU-8 biocompatibility. Mater. Sci. Eng. C 33, 4453–4459. doi:10.1016/j.msec.2013.07.001

Ng, A.H.C., Li, B.B., Chamberlain, M.D., Wheeler, A.R., 2015. Digital Microfluidic Cell Culture. Annu. Rev. Biomed. Eng. 17, 91–112. doi:10.1146/annurev-bioeng-071114-040808

Niles, A.L., Moravec, R.A., Riss, T.L., 2008. Update on in vitro cytotoxicity assays for drug development. Expert Opin. Drug Discov. 3, 655–669. doi:10.1517/17460441.3.6.655

Nilsson, U.W., Garvin, S., Dabrosin, C., 2007. MMP-2 and MMP-9 activity is regulated by estradiol and tamoxifen in cultured human breast cancer cells. Breast Cancer Res. Treat. 102, 253–261. doi:10.1007/s10549-006-9335-4

Nishikawa, J., Saito, K., Goto, J., Dakeyama, F., Matsuo, M., Nishihara, T., 1999. New screening methods for chemicals with hormonal activities using interaction of nuclear hormone receptor with coactivator. Toxicol. Appl. Pharmacol. 154, 76–83. doi:S0041008X9898557X [pii]

Nordberg, G.F., 2010. Biomarkers of exposure, effects and susceptibility in humans and their application in studies of interactions among metals in China. Toxicol. Lett. 192, 45–49. doi:10.1016/j.toxlet.2009.06.859

O'Brien, J., Wilson, I., Orton, T., Pognan, F., 2000. Investigation of the Alamar Blue

(resazurin) fluorescent dye for the assessment of mammalian cell cytotoxicity. Eur. J. Biochem. 267, 5421–5426. doi:10.1046/j.1432-1327.2000.01606.x

O 'reilly, M.S., Boehm, T., Shing, Y., Fukai, N., Vasios, G., Lane, W.S., Flynn, E., Birkhead, J.R., Olsen, B.R., Folkman, J., 1997. Endostatin: An Endogenous Inhibitor of Angiogenesis and Tumor Growth. Cell 88, 277–285. doi:10.1016/S0092-8674(00)81848-6

Odum, J., Tittensor, S., Ashby, J., 1998. Limitations of the MCF-7 cell proliferation assay for detecting xenobiotic oestrogens. Toxicol. Vitr. 12, 273–278. doi:10.1016/S0887-2333(97)00115-X

OECD, 2017. OECD Guidelines for the Testing of Chemicals, Section 4. doi:http://dx.doi.org/10.1787/20745788

OECD, 2015. Performance-Based Test Guideline for Human Recombinant Estrogen Receptor (hrER) In Vitro Assays to Detect Chemicals with ER Binding Affinity 1–64. doi:10.1787/9789264242623-en

OECD, 2011. Test No. 456: H295R Steroidogenesis Assay, OECD Guidelines for the Testing of Chemicals, Section 4. doi:10.1787/9789264122642-en

Ogawa, M., Kosaka, N., Choyke, P.L., Kobayashi, H., 2009. H-type dimer formation of fluorophores: A mechanism for activatable, in vivo optical molecular imaging. ACS Chem. Biol. 4, 535–546. doi:10.1021/cb900089j

Okuyama, T., Yamazoe, H., Mochizuki, N., Khademhosseini, A., Suzuki, H., Fukuda, J., 2010. Preparation of arrays of cell spheroids and spheroid-monolayer cocultures within a microfluidic device. J. Biosci. Bioeng. 110, 572–576. doi:10.1016/j.jbiosc.2010.05.013

Ota, H., Kodama, T., Miki, N., 2011. Rapid formation of size-controlled three dimensional hetero-cell aggregates using micro-rotation flow for spheroid study. Biomicrofluidics 5. doi:10.1063/1.3609969

Pace, R.T., Burg, K.J.L., 2013. Toxic effects of resazurin on cell cultures. Cytotechnology 67, 13–17. doi:10.1007/s10616-013-9664-1

Pampaloni, F., Reynaud, E.G., Stelzer, E.H.K., 2007. The third dimension bridges the gap between cell culture and live tissue. Nat. Rev. Mol. Cell Biol. doi:10.1038/nrm2236

Pan, C., Kumar, C., Bohl, S., Klingmueller, U., Mann, M., 2009. Comparative Proteomic Phenotyping of Cell Lines and Primary Cells to Assess Preservation of Cell Type-specific Functions. Mol. Cell. Proteomics 8, 443–450. doi:10.1074/mcp.M800258-MCP200

Patankar, N. a, 2009. Hydrophobicity of Surfaces with Cavities: Making Hydrophobic Substrates from Hydrophilic Materials? J. Adhes. Sci. Technol. 23, 413–433. doi:Doi 10.1163/156856108x370073

Patisaul, H.B., Jefferson, W., 2010. The pros and cons of phytoestrogens. Front. Neuroendocrinol. doi:10.1016/j.yfrne.2010.03.003

Patra, B., Peng, C.-C., Liao, W.-H., Lee, C.-H., Tung, Y.-C., 2016. Drug testing and flow cytometry analysis on a large number of uniform sized tumor spheroids using a microfluidic device. Sci. Rep. 6, 21061. doi:10.1038/srep21061

Payne, J., Jones, C., Lakhani, S., Kortenkamp, A., 2000. Improving the reproducibility of the MCF-7 cell proliferation assay for the detection of xenoestrogens. Sci. Total Environ. 248, 51–62. doi:10.1016/S0048-9697(99)00479-9

Perrot, S., Dutertre-Catella, H., Martin, C., Warnet, J.-M., Rat, P., 2003. A new nondestructive cytometric assay based on resazurin metabolism and an organ culture model for the assessment of corneal viability. Cytometry 55A, 7–14. doi:10.1002/cyto.a.10067

Präbst, K., Engelhardt, H., Ringgeler, S., Hübner, H., 2017. Basic colorimetric proliferation assays: MTT, WST, and resazurin, in: Methods in Molecular Biology. pp. 1–17. doi:10.1007/978-1-4939-6960-9_1

Preininger, C., Bodrossy, L., Sauer, U., Pichler, R., Weilharter, A., 2004. ARChip Epoxy and ARChip UV for covalent on-chip immobilization of pmoA gene-specific oligonucleotides. Anal. Biochem. 330, 29–36. doi:10.1016/j.ab.2003.12.037

Preininger, C., Sauer, U., Dayteg, J., Pichler, R., 2005. Optimizing processing parameters for signal enhancement of oligonucleotide and protein arrays on ARChip Epoxy, in: Bioelectrochemistry. pp. 155–162. doi:10.1016/j.bioelechem.2004.06.010

PVA TePLA, 2018. Plasma Surface Treatment of Polymers, Metals, and Ceramics [WWW Document]. URL http://www.pvateplaamerica.com/materials/polymers-Perfluoropolyether.php (accessed 3.2.18).

Ragavan, K. V., Rastogi, N.K., Thakur, M.S., 2013. Sensors and biosensors for analysis of bisphenol-A. TrAC - Trends Anal. Chem. doi:10.1016/j.trac.2013.09.006

Ray, S., Mehta, G., Srivastava, S., 2010. Label-free detection techniques for protein microarrays: Prospects, merits and challenges. Proteomics. doi:10.1002/pmic.200900458

Regehr, K., Domenech, M., Koepsel, J., 2009. Biological implications of polydimethylsiloxane-based microfluidic cell culture. Lab Chip 9, 2132–2139. doi:10.1039/b903043c.Biological

Regehr, K., Domenech, M., Koepsel, J., Carver, K., 2009. Biological implications of polydimethylsiloxane-based microfluidic cell culture. Lab Chip.

Ren, K., Zhao, Y., Su, J., Ryan, D., Wu, H., 2010. Convenient method for modifying poly(dimethylsiloxane) to be airtight and resistive against absorption of small molecules. Anal. Chem. 82, 5965–5971. doi:10.1021/ac100830t

Ren, K., Zhou, J., Wu, H., 2013. Materials for microfluidic chip fabrication. Acc. Chem. Res. 46, 2396–2406. doi:10.1021/ar300314s

Ren, Y., Huang, S.H., Mosser, S., Heuschkel, M.O., Bertsch, A., Fraering, P.C., Chen, J.J.J., Renaud, P., 2015. A Simple and Reliable PDMS and SU-8 Irreversible Bonding Method and Its Application on a Microfluidic-MEA Device for Neuroscience Research. Micromachines 6, 1923–1934. doi:10.3390/mi6121465

Reyes, D.R., Iossifidis, D., 2002. Micro total analysis systems. 1. Introduction, theory, and technology. Anal. ….

Riss, T.L., Moravec, R.A., Niles, A.L., Duellman, S., Benink, H.A., Worzella, T.J., Minor, L., 2013. Cell Viability Assays. Assay Guid. Man. [Internet] 114, 785–796. doi:10.1016/j.acthis.2012.01.006

Roggen, E.L., 2011. In vitro toxicity testing in the twenty-first century. Front. Pharmacol. FEB. doi:10.3389/fphar.2011.00003

Rolland, J.P., Van Dam, R.M., Schorzman, D.A., Quake, S.R., DeSimone, J.M., 2004. Solvent-resistant photocurable liquid fluoropolymers for microfluidic device fabrication

[corrected]. J. Am. Chem. Soc. 126, 2322–3. doi:10.1021/ja031657y

Roomi, M.W., Monterrey, J.C., Kalinovsky, T., Rath, M., Niedzwiecki, A., 2009. Patterns of MMP-2 and MMP-9 expression in human cancer cell lines. Oncol. Rep. 21, 1323–1333. doi:10.3892/or_00000358

Rothbauer, M., Wartmann, D., Charwat, V., Ertl, P., 2015. Recent advances and future applications of microfluidic live-cell microarrays. Biotechnol. Adv. doi:10.1016/j.biotechadv.2015.06.006

Routledge, E.J., Sumpter, J.P., 1996. Estrogenic activity of surfactants and some of their degradation products assessed using a recombinant yeast screen. Environ. Toxicol. Chem. 15, 241–248. doi:10.1002/etc.5620150303

Roy, E., Pallandre, A., Horny, M.C., Delapierre, F.D., Horny, M.C., Delapierre, F.D., Cattoni, A., Gamby, J., Cattoni, A., Gamby, J., Marie, A., Gosnet, H., Marie, A., Gosnet, H., 2016. Overview of Materials for microfluidics, in: Yu, X.-Y. (Ed.), Advances in Microfluidics - New Applications in Biology, Energy, and Materials Sciences. InTech, pp. 335–355. doi:10.5772/60788

RS, 2018. Transparent Silicone Sealant Liquid for Battery Terminal Covering, Conformal Coating, Potting. 90 ml Tube [WWW Document]. URL https://uk.rs-online.com/web/p/silicone-sealants/0692542/ (accessed 3.8.18).

Ru, C., Luo, J., Xie, S., Sun, Y., 2014a. A review of non-contact micro- and nano-printing technologies. J. Micromechanics Microengineering 24, 53001. doi:10.1088/0960-1317/24/5/053001

Ru, C., Luo, J., Xie, S., Sun, Y., 2014b. A review of non-contact micro- and nano-printing technologies. J. Micromechanics Microengineering. doi:10.1088/0960-1317/24/5/053001

Rubin, B.S., 2011. Bisphenol A: An endocrine disruptor with widespread exposure and multiple effects. J. Steroid Biochem. Mol. Biol. 127, 27–34. doi:10.1016/j.jsbmb.2011.05.002

Ruppen, J., Cortes-Dericks, L., Marconi, E., Karoubi, G., Schmid, R.A., Peng, R., Marti, T.M., Guenat, O.T., 2014. A microfluidic platform for chemoresistive testing of multicellular pleural cancer spheroids. Lab Chip 14, 1198–1205. doi:10.1039/C3LC51093J

Rusmini, F., Zhong, Z., Feijen, J., 2007. Protein immobilization strategies for protein biochips. Biomacromolecules. doi:10.1021/bm061197b

Sabhachandani, P., Motwani, V., Cohen, N., Sarkar, S., Torchilin, V., Konry, T., 2016. Generation and functional assessment of 3D multicellular spheroids in droplet based microfluidics platform. Lab Chip 16, 497–505. doi:10.1039/C5LC01139F

Sackmann, E.K., Fulton, A.L., Beebe, D.J., 2014. The present and future role of microfluidics in biomedical research. Nature 507, 181–189. doi:10.1038/nature13118; 10.1038/nature13118

Salahifar, H., Baxter, R.C., Martin, J.L., 1997. Insulin-like growth factor binding protein (IGFBP)-3 protease activity secreted by MCF-7 breast cancer cells: inhibition by IGFs does not require IGF-IGFBP interaction. Endocrinology 138, 1683–90. doi:10.1210/endo.138.4.5064

Saravanan, P., Satyanarayana, N., Siong, P.C., Duong, H.M., Sinha, S.K., 2013. Tribology of self-lubricating SU-8+PFPE composite based Lub-tape, in: Procedia Engineering. pp. 497–504. doi:10.1016/j.proeng.2013.12.212

Sauer, U., Domnanich, P., Preininger, C., 2011. Protein chip for the parallel quantification of high and low abundant biomarkers for sepsis. Anal. Biochem. 419, 46–52. doi:10.1016/j.ab.2011.07.038

Sauer, U., Pultar, J., Preininger, C., 2012. Critical role of the sample matrix in a point-of-care protein chip for sepsis. J. Immunol. Methods 378, 44–50. doi:10.1016/j.jim.2012.02.002

Schafer, Z.T., Brugge, J.S., 2007. IL-6 involvement in epithelial cancers. J. Clin. Invest. doi:10.1172/JCI34237

Schena, M., Shalon, D., Davis, R.W., Brown, P.O., 1995. Quantitative Monitoring of Gene Expression Patterns with a Complementary DNA Microarray. Science (80-.). 270, 467–470. doi:10.1126/science.270.5235.467

Schmitz, C.H.J., Rowat, A.C., Köster, S., Weitz, D.A., 2009. Dropspots: a picoliter array in a microfluidic device. Lab Chip 9, 44–49. doi:10.1039/B809670H

Schroeder, H.W., Cavacini, L., 2010. Structure and function of immunoglobulins. J. Allergy Clin. Immunol. 125, S41-52. doi:10.1016/j.jaci.2009.09.046

Schug, T.T., Abagyan, R., Blumberg, B., Collins, T.J., Crews, D., DeFur, P.L., Dickerson, S.M., Edwards, T.M., Gore, A.C., Guillette, L.J., Hayes, T., Heindel, J.J., Moores, A., Patisaul, H.B., Tal, T.L., Thayer, K.A., Vandenberg, L.N., Warner, J.C., Watson, C.S., vom Saal, F.S., Zoeller, R.T., O'Brien, K.P., Myers, J.P., 2013. Designing endocrine disruption out of the next generation of chemicals. Green Chem. 15, 181–198. doi:10.1039/C2GC35055F

Schulte, V.A., Hu, Y., Diez, M., Bünger, D., Möller, M., Lensen, M.C., 2010. A hydrophobic perfluoropolyether elastomer as a patternable biomaterial for cell culture and tissue engineering. Biomaterials 31, 8583–8595. doi:10.1016/j.biomaterials.2010.07.070

Scott, S.M., Brown, M., Come, S.E., 2011. Emerging data on the efficacy and safety of fulvestrant, a unique antiestrogen therapy for advanced breast cancer. Expert Opin. Drug Saf. 10, 819–826. doi:10.1517/14740338.2011.595560

Scott Lynn, N., Henry, C.S., Dandy, D.S., 2009. Evaporation from microreservoirs. Lab Chip 9, 1780. doi:10.1039/b900556k

Seifert, M., Haindl, S., Hock, B., 1999. Development of an enzyme linked receptor assay (ELRA) for estrogens and xenoestrogens. Anal. Chim. Acta 386, 191–199. doi:10.1016/S0003-2670(99)00044-6

Self, C.H., Thompson, S., Street, T., Lamb, K.J., Duffin, G., Dessi, J.L., Turnbull, M., 2013. Non-competitive Immunoassays for Small Molecules-the Anti-complex and Selective Antibody Systems, in: The Immunoassay Handbook. pp. 61–65. doi:10.1016/B978-0-08-097037-0.00005-1

Serra, S., Schneider, a, Malecki, K., 2007. A simple bonding process of SU-8 to glass to seal a microfluidic device. Proc. 3rd Int. Conf. … 2035, 11–14. doi:10.13140/2.1.2832.2082

Shahidzadeh, N., Schut, M.F.L., Desarnaud, J., Prat, M., Bonn, D., 2015. Salt stains from evaporating droplets. Sci. Rep. 5. doi:10.1038/srep10335

Shin, D.-Y., Yoo, S.-S., Song, H., Tak, H., Byun, D., 2015. Electrostatic-Force-Assisted Dispensing Printing to Construct High-Aspect-Ratio of 0.79 Electrodes on a Textured Surface with Improved Adhesion and Contact Resistivity. Sci. Rep. 5, 16704. doi:10.1038/srep16704

Silberberg, M.S., Amateis, P., 2015. Chemistry: The Molecular Nature of Matter and Change, August 26. doi:10.1007/s13398-014-0173-7.2

Sinkó, K., 2010. Influence of chemical conditions on the nanoporous structure of silicate aerogels. Materials (Basel). doi:10.3390/ma3010704

Sittampalam, G., Coussens, N., Arkin, M., Auld, D., Austin, C., Bejcek, B., Glicksman, M., Inglese, J., Iversen, P., Mcgee, J., Mcmanus, O., Minor, L., Napper, A., Peltier, J.M., Riss, T., Trask, O., Weidner, J., 2016. Assay Guidance Manual, Assay Guidance Manual. doi:PMID:22553881

Skoog, D.A., Holler, F.J., Crouch, S.R., 2007. Principles of Instrumental Analysis, The sections on atomic and molecular spectroscopy serve as excellent introductions to the subject. doi:10.1090/S0002-9904-1936-06390-1

Slagle, K.M., Ghosn, S.J., 1996. Immunoassays: Tools for sensitive, specific, and accurate test results. Lab. Med. doi:10.1093/labmed/27.3.177

Soares, A., Guieysse, B., Jefferson, B., Cartmell, E., Lester, J.N., 2008. Nonylphenol in the environment: A critical review on occurrence, fate, toxicity and treatment in wastewaters. Environ. Int. doi:10.1016/j.envint.2008.01.004

Soltysik, K., Czekaj, P., 2013. Membrane estrogen receptors - is it an alternative way of estrogen action? J. Physiol. Pharmacol.

Sonnenschein, C., Soto, A.M., Fernandez, M.F., Olea, N., Olea-Serrano, M.F., Ruiz- Lopez, M.D., 1995. Development of a marker of estrogenic exposure in human serum, in: Clinical Chemistry. pp. 1888–1895.

Sonneveld, E., Jansen, H.J., Riteco, J.A.C., Brouwer, A., van der Burg, B., 2005. Development of androgen- and estrogen-responsive bioassays members of a panel of human cell line-based highly selective steroid-responsive bioassays. Toxicol. Sci. 83, 136–148. doi:10.1093/toxsci/kfi005

Soria, G., Ben-Baruch, A., 2008. The inflammatory chemokines CCL2 and CCL5 in breast cancer. Cancer Lett. doi:10.1016/j.canlet.2008.03.018

Soto, A.M., Sonnenschein, C., Chung, K.L., Fernandez, M.F., Olea, N., Olea Serrano, F., 1995. The E-SCREEN assay as a tool to identify estrogens: An update on estrogenic environmental pollutants, in: Environmental Health Perspectives. pp. 113–122. doi:10.1289/ehp.95103s7113

Soule, H.D., Vazquez, J., Long, A., Albert, S., Brennan, M., 1973. A Human Cell Line From a Pleural Effusion Derived From a Breast Carcinoma2. JNCI J. Natl. Cancer Inst. 51, 1409–1416.

Squatrito, R.C., Connor, J.P., Buller, R.E., 1995. Comparison of a Novel Redox Dye Cell Growth Assay to the ATP Bioluminescence Assay. Gynecol. Oncol. 58, 101–105. doi:10.1006/gyno.1995.1190

Stewart, a J., Johnson, M.D., May, F.E., Westley, B.R., 1990. Role of insulin-like growth factors and the type I insulin-like growth factor receptor in the estrogen-stimulated proliferation of human breast cancer cells. J. Biol. Chem. 265, 21172–8.

Stillman, B.A., Tonkinson, J.L., 2000. FAST(TM) slides: A novel surface for microarrays. Biotechniques 29, 630–635.

Stoevesandt, O., Taussig, M.J., He, M., 2009. Protein microarrays: High-throughput tools for proteomics. Expert Rev. Proteomics. doi:10.1586/epr.09.2

Strimbu, K., Tavel, J.A., 2010. What are biomarkers? Curr.Opin.HIV.AIDS 5, 463–466. doi:10.1097/COH.0b013e32833ed177

Sugioka, K., Cheng, Y., 2011. Integrated microchips for biological analysis fabricated by femtosecond laser direct writing. MRS Bull. doi:10.1557/mrs.2011.274

Sumpter, J.P., Jobling, S., 1995. Vitellogenesis as a biomarker for estrogenic contamination of the aquatic environment. Environ. Health Perspect. 103, 173–178. doi:10.1289/ehp.95103s7173

Sun, F., Kang, L., Xiang, X., Li, H., Luo, X., Luo, R., Lu, C., Peng, X., 2016. Recent advances and progress in the detection of bisphenol A. Anal. Bioanal. Chem. doi:10.1007/s00216-016-9791-6

Sun, Y.S., Landry, J.P., Fei, Y.Y., Zhu, X.D., Luo, J.T., Wang, X.B., Lam, K.S., 2009. Macromolecular scaffolds for immobilizing small molecule microarrays in label-free detection of protein-ligand interactions on solid support. Anal. Chem. 81, 5373–5380. doi:10.1021/ac900889p

Sutandy, F.X.R., Qian, J., Chen, C.S., Zhu, H., 2013. Overview of protein microarrays. Curr. Protoc. Protein Sci. doi:10.1002/0471140864.ps2701s72

Swenberg, J.A., Fryar-Tita, E., Jeong, Y.C., Boysen, G., Starr, T., Walker, V.E., Albertini, R.J., 2008. Biomarkers in toxicology and risk assessment: Informing critical dose-response relationships. Chem. Res. Toxicol. doi:10.1021/tx700408t

Syahir, A., Usui, K., Tomizaki, K., Kajikawa, K., Mihara, H., 2015. Label and Label-Free Detection Techniques for Protein Microarrays. Microarrays 4, 228–244. doi:10.3390/microarrays4020228

Takashimizu, Y., Iiyoshi, M., 2016. New parameter of roundness R: circularity corrected by aspect ratio. Prog. Earth Planet. Sci. 3, 2. doi:10.1186/s40645-015-0078-x

Tan, S.H., Nguyen, N.T., Chua, Y.C., Kang, T.G., 2010. Oxygen plasma treatment for reducing hydrophobicity of a sealed polydimethylsiloxane microchannel. Biomicrofluidics 4. doi:10.1063/1.3466882

Tao, S.C., Chen, C.S., Zhu, H., 2007. Applications of protein microarray technology. Comb Chem High Throughput Screen 10, 706–718.

Terranova, V.P., Rao, C.N., Kalebic, T., Margulies, I.M., Liotta, L. a, 1983. Laminin receptor on human breast carcinoma cells. Proc. Natl. Acad. Sci. USA 80, 444–448. doi:10.1073/pnas.80.2.444

Thermo Fischer, 2012. Guide PMPI [WWW Document]. URL https://www.thermofisher.com/order/catalog/product/28100 (accessed 3.5.18).

Thermo Fischer, 2009. Chemistry of Crosslinking [WWW Document]. URL https://www.thermofisher.com/nl/en/home/life-science/protein-biology/protein-biology-learning-center/protein-biology-resource-library/pierce-protein-methods/chemistry-crosslinking.html#/legacy=www.piercenet.com (accessed 2.4.18).

Thiantanawat, A., Long, B.J., Brodie, A.M., 2003. Signaling Pathways of Apoptosis Activated by Aromatase Inhibitors and Antiestrogens. Cancer Res. 63, 8037–8050.

Tiggelaar, R.M., Benito-López, F., Hermes, D.C., Rathgen, H., Egberink, R.J.M., Mugele, F.G., Reinhoudt, D.N., van den Berg, A., Verboom, W., Gardeniers, H.J.G.E., 2007. Fabrication, mechanical testing and application of high-pressure glass microreactor chips. Chem. Eng. J. 131, 163–170. doi:10.1016/j.cej.2006.12.036

Tijssen, P., 1985. Conjugation of haptens. Lab. Tech. Biochem. Mol. Biol. 15, 279–296. doi:10.1016/S0075-7535(08)70142-6

Toepke, M.W., Beebe, D.J., 2006. PDMS absorption of small molecules and consequences in microfluidic applications. Lab Chip 6, 1484. doi:10.1039/b612140c

Tomasi, R., Amselem, G., Baroud, C., 2013. High Density Hydrogel Arrays for 3D Cell Colonies With Dynamically Controlled External Stimuli. Rsc.Org 1069–1071.

Torisawa, Y., Chueh, B., Huh, D., Ramamurthy, P., Roth, T.M., Barald, K.F., Takayama, S., 2007. Efficient formation of uniform-sized embryoid bodies using a compartmentalized microchannel device. Lab Chip 7, 770. doi:10.1039/b618439a

Totta, P., Acconcia, F., Leone, S., Cardillo, I., Marino, M., 2004. Mechanisms of naringenin-induced apoptotic cascade in cancer cells: involvement of estrogen receptor alpha and beta signalling. IUBMB Life 56, 491–499. doi:10.1080/15216540400010792

Tourovskaia, A., Figueroa-Masot, X., Folch, A., 2005. Differentiation-on-a-chip: A microfluidic platform for long-term cell culture studies. Lab Chip 5, 14. doi:10.1039/b405719h

Uttamchandani, M., Walsh, D.P., Yao, S.Q., Chang, Y.T., 2005. Small molecule microarrays: recent advances and applications. Curr. Opin. Chem. Biol. 9, 4–13. doi:DOI 10.1016/j.cpba.2004.12.005

Uzarski, J.S., DiVito, M.D., Wertheim, J.A., Miller, W.M., 2017. Essential design considerations for the resazurin reduction assay to noninvasively quantify cell expansion within perfused extracellular matrix scaffolds. Biomaterials 129, 163–175. doi:10.1016/j.biomaterials.2017.02.015

Uzunoglu, S., Karaca, B., Atmaca, H., Kisim, A., Sezgin, C., Karabulut, B., Uslu, R., 2010. Comparison of XTT and Alamar blue assays in the assessment of the viability of various human cancer cell lines by AT-101 (-/- gossypol). Toxicol. Mech. Methods 20, 482–486. doi:10.3109/15376516.2010.508080

Vadivelu, R.K., Kamble, H., Shiddiky, M.J.A., Nguyen, N.T., 2017. Microfluidic technology for the generation of cell spheroids and their applications. Micromachines. doi:10.3390/mi8040094

van Dam, R.M., 2006. Solvent-resistant elastomeric microfluidic devices and applications. California Institute of Technology. doi:4796

van Duinen, V., Trietsch, S.J., Joore, J., Vulto, P., Hankemeier, T., 2015. Microfluidic 3D cell culture: From tools to tissue models. Curr. Opin. Biotechnol. doi:10.1016/j.copbio.2015.05.002

van Meer, B.J., de Vries, H., Firth, K.S.A., van Weerd, J., Tertoolen, L.G.J., Karperien, H.B.J., Jonkheijm, P., Denning, C., IJzerman, A.P., Mummery, C.L., 2017. Small molecule absorption by PDMS in the context of drug response bioassays. Biochem. Biophys. Res. Commun. 482, 323–328. doi:10.1016/j.bbrc.2016.11.062

van Meeuwen, J.A., ter Burg, W., Piersma, A.H., van den Berg, M., Sanderson, J.T., 2007. Mixture effects of estrogenic compounds on proliferation and pS2 expression of MCF-7 human breast cancer cells. Food Chem. Toxicol. 45, 2319–2330. doi:10.1016/j.fct.2007.06.011

Van Midwoud, P.M., Groothuis, G.M.M., Merema, M.T., Verpoorte, E., 2010. Microfluidic biochip for the perifusion of precision-cut rat liver slices for metabolism and toxicology studies. Biotechnol. Bioeng. 105, 184–194. doi:10.1002/bit.22516

van Midwoud, P.M., Janse, A., Merema, M.T., Groothuis, G.M.M., Verpoorte, E., 2012. Comparison of Biocompatibility and Adsorption Properties of Different Plastics for Advanced Microfluidic Cell and Tissue Culture Models. Anal. Chem. 84, 3938–3944. doi:10.1021/ac300771z

van Midwoud, P.M., Janse, A., Merema, M.T., Groothuis, G.M.M., Verpoorte, E., 2012. Comparison of biocompatibility and adsorption properties of different plastics for advanced microfluidic cell and tissue culture models. Anal. Chem. 84, 3938–44. doi:10.1021/ac300771z

Van Weemen, B.K., Schuurs, A.H.W.M., 1975. The influence of heterologous combinations of antiserum and enzyme-labeled estrogen on the characteristics of estrogen enzyme-immunoassays. Immunochemistry 12, 667–670. doi:10.1016/0019-2791(75)90213-X

van Weemen, B.K., Schuurs, A.H.W.M., Raymakers, H.H.T., Oostermeyer, M.W., 1972. Immunoassay using hapten-enzyme conjugates. FEBS Lett. 24, 77–81. doi:10.1016/0014-5793(72)80830-5

Vandenberg, L.N., Maffini, M. V., Sonnenschein, C., Rubin, B.S., Soto, A.M., 2009. Bisphenol-a and the great divide: A review of controversies in the field of endocrine disruption. Endocr. Rev. doi:10.1210/er.2008-0021

Vega-Avila, E., Pugsley, M.K., 2011. An overview of colorimetric assay methods used to assess survival or proliferation of mammalian cells. Proc. West. Pharmacol. Soc. 54, 10–4.

Vernekar, V.N., Cullen, D.K., Fogleman, N., Choi, Y., García, A.J., Allen, M.G., Brewer, G.J., Laplaca, M.C., 2009. SU-8 2000 rendered cytocompatible for neuronal bioMEMS applications. J. Biomed. Mater. Res. - Part A 89, 138–151. doi:10.1002/jbm.a.31839

Villalobos, M., Olea, N., Brotons, J.A., Olea-Serrano, M.F., Ruiz de Almodovar, J.M., Pedraza, V., 1995. The E-screen assay: A comparison of different MCF7 cell stocks. Environ. Health Perspect. 103, 844–850. doi:10.1289/ehp.95103844

Vogel, C., Marcotte, E.M., 2012. Insights into the regulation of protein abundance from proteomic\nand transcriptomic analyses. Nat. Rev. Genet. 13, 227–232.

Volkmer, E., Otto, S., Polzer, H., Saller, M., Trappendreher, D., Zagar, D., Hamisch, S., Ziegler, G., Wilhelmi, A., Mutschler, W., Schieker, M., 2012. Overcoming hypoxia in 3D culture systems for tissue engineering of bone in vitro using an automated, oxygen-triggered feedback loop. J. Mater. Sci. Mater. Med. 23, 2793–2801. doi:10.1007/s10856-012-4725-0

Waghmare, P.R., Mitra, S.K., 2013. Contact angle hysteresis of bovine serum albumin (BSA) solution/metal (Au-Cr) coated glass substrate. Colloid Polym. Sci. 291, 375–381. doi:10.1007/s00396-012-2756-1

Wan, X., Li, Z., Ye, H., Cui, Z., 2016. Three-dimensional perfused tumour spheroid model for anti-cancer drug screening. Biotechnol. Lett. 38, 1389–1395. doi:10.1007/s10529-016-2035-1

Wang, C.C., Huang, R.P., Sommer, M., Lisoukov, H., Huang, R., Lin, Y., Miller, T., Burke, J., 2002. Array-based multiplexed screening and quantitation of human cytokines and chemokines. J. Proteome Res. 1, 337–343. doi:10.1021/pr0255203

Wang, J.D., Douville, N.J., Takayama, S., Elsayed, M., 2012. Quantitative analysis of molecular absorption into PDMS microfluidic channels. Ann. Biomed. Eng. 40, 1862–1873. doi:10.1007/s10439-012-0562-z

Wang, Y., Wang, J., 2014. Mixed hydrogel bead-based tumor spheroid formation and anticancer drug testing. Analyst 139, 2449–2458. doi:10.1039/C4AN00015C

Watson, J., Greenough, E.B., Leet, J.E., Ford, M.J., Drexler, D.M., Belcastro, J. V., Herbst, J.J., Chatterjee, M., Banks, M., 2009. Extraction, identification, and functional characterization of a bioactive substance from automated compound-handling plastic tips. J. Biomol. Screen. 14, 566–572. doi:10.1177/1087057109336594

Wetherill, Y.B., Akingbemi, B.T., Kanno, J., McLachlan, J.A., Nadal, A., Sonnenschein, C., Watson, C.S., Zoeller, R.T., Belcher, S.M., 2007. In vitro molecular mechanisms of bisphenol A action. Reprod. Toxicol. doi:10.1016/j.reprotox.2007.05.010

Whitesides, G.M., 2006. The origins and the future of microfluidics. Nature. doi:10.1038/nature05058

Whitesides, G.M., Ostuni, E., Takayama, S., Jiang, X., Ingber, D.E., 2001. Soft Lithography in Biology and Biochemistry. Annu. Rev. Biomed. Eng. 3, 335–373. doi:10.1146/annurev.bioeng.3.1.335

Williams, K.R., Gupta, K., Wasilik, M., 2003. Etch rates for micromachining processing - Part II. J. Microelectromechanical Syst. 12, 761–778. doi:10.1109/JMEMS.2003.820936

Williams, R.T., Bridges, J.W., 1964. Fluorescence of solutions: A review. J. Clin. Pathol. 17, 371–394. doi:10.1136/jcp.17.4.371

Witt, M., Walter, J.-G., Stahl, F., 2015. Aptamer Microarrays—Current Status and Future Prospects. Microarrays 4, 115–132. doi:10.3390/microarrays4020115

Wolfe, D.B., Whitesides, G.M., 2005. Rapid prototyping of functional microfabricated devices by soft lithography, in: Nanolithography and Patterning Techniques in Microelectronics. pp. 76–119. doi:10.1533/9781845690908.76

Wood, W.G., 1991. “matrix effects” in immunoassays. Scand. J. Clin. Lab. Invest. 51, 105–112. doi:10.3109/00365519109104608

Woodruff, T.J., Zota, A.R., Schwartz, J.M., 2012. Environmental chemicals in pregnant women in the United States: NHANES 2003-2004. Environ. Health Perspect. 119, 878–85. doi:10.1289/ehp.1002727

Wu, H.W., Hsiao, Y.H., Chen, C.C., Yet, S.F., Hsu, C.H., 2016. A pdms-based microfluidic hanging drop chip for embryoid body formation. Molecules 21, 1–11. doi:10.3390/molecules21070882

Wu, L.Y., Di Carlo, D., Lee, L.P., 2008. Microfluidic self-assembly of tumor spheroids for anticancer drug discovery. Biomed. Microdevices 10, 197–202. doi:10.1007/s10544-007-9125-8

Wu, P., Grainger, D.W., 2006. Comparison of hydroxylated print additives on antibody microarray performance. J. Proteome Res. 5, 2956–2965. doi:10.1021/pr060217d

Würth, C., Grabolle, M., Pauli, J., Spieles, M., Resch-Genger, U., 2013. Relative and absolute determination of fluorescence quantum yields of transparent samples. Nat. Protoc. 8, 1535–1550. doi:10.1038/nprot.2013.087

Xiong, J., Das, S.N., Kar, J.P., Choi, J.-H., Myoung, J.-M., 2010. A multifunctional nanoporous layer created on glass through a simple alkali corrosion process. J. Mater. Chem. 20, 10246. doi:10.1039/c0jm01695k

Xu, Q., Lam, K.S., 2003. Protein and Chemical Microarrays—Powerful Tools for Proteomics.

J. Biomed. Biotechnol. 2003, 257–266. doi:10.1155/S1110724303209220

Yang, H., Kong, X., Zhang, Y., Wu, C., Cao, E., 2014. Mechanical properties of silica aerogels prepared from a mixture of TEOS and organo-alkoxysilanes of type R1SiX3. J. Wuhan Univ. Technol. Mater. Sci. Ed. 29, 201–207. doi:10.1007/s11595-014-0893-8

Yang, O., Kim, H.L., Weon, J.-I., Seo, Y.R., 2015. Endocrine-disrupting Chemicals: Review of Toxicological Mechanisms Using Molecular Pathway Analysis. J. cancer Prev. 20, 12–24. doi:10.15430/JCP.2015.20.1.12

Yazdi, S.R., Shadmani, A., Bürgel, S.C., Misun, P.M., Hierlemann, A., Frey, O., 2015. Adding the “heart” to hanging drop networks for microphysiological multi-tissue experiments. Lab Chip 15, 4138–4147. doi:10.1039/C5LC01000D

Yazdi, S.R., Shadmani, A., Hierlemann, A., Frey, O., Milano, P., Engineering, D.M., 2015. Microfluidic Hanging-Drop Platform for Parallel Closed-Loop Multi-Tissue Experiments 535–538. doi:10.1109/MEMSYS.2015.7051010

Yedjou, C., Cameron, J., Mbemi, A.T., Tchounwou, P., 2015. β-ESTRADIOL INDUCES CYTOTOXIC EFFECTS TO HUMAN T-LYMPHOMA (JURKAT) CELLS THROUGH OXIDATIVE STRESS. J. Miss. Acad. Sci. 60, 279–283.

Yoon, S., Kim, J.A., Lee, S.H., Kim, M., Park, T.H., 2013. Droplet-based microfluidic system to form and separate multicellular spheroids using magnetic nanoparticles. Lab Chip 13, 1522. doi:10.1039/c3lc41322e

Yu, L., Tay, F.E.H., Xu, G., Chen, B., Avram, M., Iliescu, C., 2006a. Adhesive bonding with SU-8 at wafer level for microfluidic devices. J. Phys. Conf. Ser. 34, 776–781. doi:10.1088/1742-6596/34/1/128

Yu, L., Tay, F.E.H., Xu, G., Chen, B., Avram, M., Iliescu, C., 2006b. Adhesive bonding with SU-8 at wafer level for microfluidic devices. J. Phys. Conf. Ser. 34, 776–781. doi:10.1088/1742-6596/34/1/128

Yu, S., Wong, T., Hu, X., Pita, K., 2003. The effect of TEOS/MTES ratio on the structural and dielectric properties of porous silica films. J. Electrochem. Soc.

Yuan, Y., Lee, T.R., 2013. Contact angle and wetting properties. Springer Ser. Surf. Sci. 51, 3–34. doi:10.1007/978-3-642-34243-1_1

Yun, S., Luo, H., Gao, Y., 2014. Superhydrophobic silica aerogel microspheres from methyltrimethoxysilane: rapid synthesis via ambient pressure drying and excellent absorption properties. RSC Adv. 4, 4535–4542. doi:10.1039/C3RA46911E

Yun, S.H., Cabrera, L.M., Song, J.W., Futai, N., Tung, Y.C., Smith, G.D., Takayama, S., 2007. Characterization and resolution of evaporation-mediated osmolality shifts that constrain microfluidic cell culture in poly(dimethylsiloxane) devices. Anal. Chem. 79, 1126–1134. doi:10.1021/ac061990v

Zhou, J., Ellis, A.V., Voelcker, N.H., 2010. Recent developments in PDMS surface modification for microfluidic devices. Electrophoresis. doi:10.1002/elps.200900475

Zhou, S.-F., 2009. Polymorphism of Human Cytochrome P450 2D6 and Its Clinical Significance. Clin. Pharmacokinet. 48, 761–804. doi:10.2165/11318070-000000000-00000

Zuchowska, A., Kwapiszewska, K., Chudy, M., Dybko, A., Brzozka, Z., 2017. Studies of anticancer drug cytotoxicity based on long-term HepG2 spheroid culture in a microfluidic system. Electrophoresis 38, 1206–1216. doi:10.1002/elps.201600417

Zuo, P., Ye, B.C., 2008. A novel immobilization strategy using oligonucleotide as linker for small molecule microarrays construction. Biosens. Bioelectron. 23, 1694–1700. doi:10.1016/j.bios.2008.02.007

7. Table index

Table 1: Sources of exposure to EDCs and EDCs applications and characterizations (Dodson et al., 2012; Gore, A.C. et al., 2014). Abbreviations see: Table of abbreviations. .. 13
Table 2: Human estrogen receptors (ER), half maximal inhibitory concentration (IC50), relative binding affinities (RBA) and Log RBA values of selected ER agonists and antagonists arrived from a competitive ER binding assay. Binding affinities are relative to 17ß-estradiol and calculated by division of the IC50 of 17ß-estradiol by the one of the competitor (Blair et al., 2000). 17
Table 3: Examples of endogenous and exogenous estrogenic and antiestrogenic compounds and their involvement in signaling pathways (See: table of abbreviations) (Kiyama and Wada-Kiyama, 2015). 20
Table 4: Overview of test battery for estrogenic substances with assay principles, advantages and limitations 25
Table 5: Functional groups of amino acids with interaction partner for probe immobilization (Rusmini et al., 2007). 32
Table 6: Overview of indirect competitive ELISAs for the detection of bisphenol A with immobilized conjugates, LODs and detection range of the assay (indirect refers to detection via primary and secondary antibody)..... 39
Table 7: Parameter for the evaluation of assay performance with description and equations (Armbruster and Pry, 2008; Davies, 2013). 41
Table 8: Advantages and disadvantages of serum-supplemented cell culture (Arora, 2013).51
Table 9: Microfluidic device fabrication methods with appropriate materials for each technique (Beebe et al., 2002; Chen et al., 2016; Faustino et al., 2016). 54
Table 10: Microfluidic spheroid culture techniques (Achilli et al., 2012; Cui et al., 2017; Lin and Chang, 2008). 62
Table 11: Overview of microfluidic hanging drop platforms and their characteristics. 64
Table 12: Reagents with provider used in the protein microarray. 70
Table 13 Chemicals and their provider applied in the protein microarray. 71
Table 14: Hapten-protein conjugates, proteins (reduce/unreduced) and reagents were tested. 73
Table 15: Mastermix printing solution. 73
Table 16: Recovery rates of the established resazurin proliferations assay for serum-free and serum supplemented cell culture. 88
Table 17: Limit of detection (LOD), limit of quantification (LOQ), half maximal effective concentration (EC50) of the multiplexed Rantes sandwich assay performed in serum-free medium DMEM/F-12 with and without BSA supplementation. 95
Table 18: The assay parameter limit of detection (LOD), limit of quantification (LOQ), half maximal effective concentration (EC50), recovery rate and coefficient of variation (CV) of the multiplexed IL-6, IL-8, IL-11, MCP-1, CXCL10, Rantes, IGF-1, VEGF, MMP-9 and IGFBP-3 sandwich assays on chip are given. The assay was performed in DMEM/F-12 with 10 mg/mL BSA. LOD-, LOQ- and EC50– values are calculated as mean +/- SEM of three experiments. The CV of three experiments is calculated as mean of eleven standards. Recovery rate data express an added analyte concentration within the linear range of the calibration curves. Table of assay parameter from (Gier et al., 2017). 95
Table 19: Color-coded biomarker secretion patterns. MCF-7 cells (stimulated: +, non-stimulated: -) challenged with tamoxifen, fulvestrant, estradiol, genistein, bisphenol A, and

nonylphenol, and marker expression quantified with the chip relative to untreated cells (%). Colors are graded in steps of 20 % (Gier et al., 2017). 103
Table 20: Comparison of cross reactivity (CR) and fluorescence intensities (I) of the different BPA-protein conjugates, immobilized on different surfaces (high (h) : >30,000 A.U., medium (m): 10,000-30,000 A.U., low (l):<10,000 A.U.). Only the fluorescence intensities of the BPA-conjugates with reduced proteins are displayed. 106
Table 21: Contact and roll off angles measurements of 40 µL droplets on glass with different surface treatments. Angels are given as mean of three measurements with standard deviation. 117

8. Figure index

Figure 1: Section of the human endocrine system with the main endocrine glands (pituary, pineal, thyroid, parathyroid and adrenal glands), organs containing endocrine cells (pancreas, thymus, gonads (ovaries and testicles) and hypothalamus) and hormone targets (adipose tissue, bone, muscle, heart) (Hadley and Levine, 2006). Pictures of the endocrine system, liver and adipose tissue arrived from the clip art gallery of Microsoft Office Professional Plus PowerPoint 2010. 11
Figure 2: Exposure sources for humans and environment and major exposure routes of EDCs for humans. The exposure by EDCs can be direct (→) by the raw chemical or indirect (-->) by treatments or manufacture processes (Kidd et al., 2012; Yang et al., 2015). Free Stock Image 3D Human Character arrived from cute-pictures.blogspot.ro. 12
Figure 3: Endocrine relevant chemicals accumulated and measured in pregnant woman in the United States of America in the years 2003-2004 within the National health and Nutrition Examination Survey (NHANES) Data from Woodruff et al., (2012) (See: Table of abbreviations). 14
Figure 4: Overview of the human steroidogenesis. Major classes and subclasses of steroid hormones inclusive their enzymatically conversion are shown. Chemical changes are highlighted in white and estrogens in red (Häggström et al., 2014). 15
Figure 5: Chemical structures of some natural and synthesized estrogenic (A) and antiestrogenic (B) compounds and their structural similarity to the endogen steroid hormone 17ß-estradiol. 16
Figure 6: Estrogenic and antiestrogenic action. 1. Direct action via nuclear ER. Binding of antagonists can inhibit the transcription of downstream genes of the ER receptors, while agonists activate it. 2. Suppression of hormone synthesis, which result in no binding to the receptors. 18
Figure 7: Genomic, non-genomic pathways and autocrine/paracrine signaling of estrogenic active substances. Adapted from Kiyama and Wada-Kiyama, 2015. 19
Figure 8: Comparison of monotonic and non-monotonic dose-response curves. Monotonic curves show a proportional increase or inversely proportional decrease of response with the dose. Non-monotonic curves are U-shaped, inverted U-shaped, or even more complex and characterized by different responses for intermediate or low and high doses, but with potential higher effects for low doses. Figure adapted from Fagin, 2012. 21
Figure 9: Overview of methods used to detect estrogenic activity by determination of the signaling network of estrogen and estrogen like chemicals. The red letters indicate the methods used to evaluate the corresponding action. Adapted from Kiyama and Wada-Kiyama, 2015. 22

Figure 10: Direct, sandwich competitive and binding inhibition immunoassay formats with corresponding calibration curves are shown (1 and 2). Direct and sandwich formats show a direct proportional relationship of analyte concentration and signal (1), and competitive and binding inhibition formats an inversely proportional analyte-signal correlation (2) (Cox, 2012). 29
Figure 11: Scheme of the five main steps of a protein microarray. From fabrication to analysis. 30
Figure 12: Principles of non-contact and contact printing. Non-contact printers dispense the probes without contact to the surface using nozzles. The dispensing of the probe is supported by a piezoelement contained in the nozzle (A). Contact printers despose the probe via contact to the surface using solid, split or quilled pins (B) (Austin and Holway, 2011; Ru et al., 2014b). 34
Figure 13: Structure of an IgG antibody. In general antibody monomers are divided into a Fab (fragment antigen binding) (orange) region with antigen binding sites and FC (fragment, crystallizable) region (blue) for cell interactions. They build of heavy (blue) and light (orange) chains, whereas the heavy chain defines the antibody class. Both consist of a variable (upper part) and a constant region (Schroeder and Cavacini, 2010). 36
Figure 14: Sigmoidal calibration curve using the 4-parameter logistic fit is shown. Here the curve of a sandwich immunoassay is pictured and is characterized by a positive correlation between fluorescence signal and concentration (Davies, 2013). 40
Figure 15: Accuracy versus precision. Accuracy describes how close the measured value to the spiked value is. Precision how reducible the measurement is. Pictured adapted from https://apchemcyhs.wikispaces.com. 41
Figure 16: Ways of cross-reactivity in sandwich immunoassays. 1) Binding of cross-reactant to capture antibody blocks detection antibody binding. Decrease of signal intensities. 2) Binding of cross-reactant to the detection antibody blocks binding to endogenous analyte on capture antibody which result in a decrease of signal intensities. 3) Binding of cross-reactant to capture and detection antibody shows an increase of signal intensities. 42
Figure 17: Jablonski diagram ((Jabłoński, 1933) picture adapeted) of fluorescence pictures the shift of an electron from the ground to an excited state due to absorption. The electron loses energy due to vibrational relaxation in the excited state and returns back to the ground state. There it emits photons (Fluorescence) with lower energy and longer wavelengths (A). The shift is called Stokes shift (B). 44
Figure 18: Principles of confocal (right) and non-confocal (left) laser designs. Confocal systems reject signals from out of plane, whereas non-confocal all signals get captured. Therefore non-confocal images contain more information from outside the focus plane. Picture adapted from (Core Life Science, 2012). 45
Figure 19: Alignment and spot segmentation of a protein microarray using GenePix®. Each spot can be evaluated with different flags (white surroundings, stripes or crosses). Flags decsribe the quality (presence, absence, bad) of the spot signal and are consequently used for analysis. 46
Figure 20: Intracellular reduction of the sodium salt resazurin to resofurin and finally hydroresofurin. Picture adapted and changed from Gier et al., (2017). 49
Figure 21: Scheme of production of a microfluidic device out of PDMS using soft-lithography. 55
Figure 22: Production process of microfluidic devices made of glass using a positive photoresist, wet etching and fusion bonding. 56
Figure 23: Spheroid formation process proceeds in three steps (Lin and Chang, 2008). 58

Figure 24: Microenvironments inside a spheroid according Lin and Chang, (2008). The layer like structure results in insufficient transport of CO_2 and waste out of the MCS and an inadequate supply of O_2, nutrients and growth factors.....59
Figure 25: Cell morphology of MCF-7 cells after inner adaption of serum-free medium on day four. Comparison of cell growth in DMEM supplemented with 10 % FBS (A) to DMEM/F-12 serum-free cell culture conditions with collagen coating (B) as well as to ITS lacking conditions (C), no collagen I coating (D) or both (E). 83
Figure 26: Total cell numbers after inner adaption of serum-free medium by MCF-7 cells on day four. Comparison of cell growth in serum-free DMEM/F-12 with collagen I coating compared to DMEM with 10% FBS. Additionally under lacking of ITS, collagen I or both. Total cell numbers were counted for n=2 and given as mean. ITS omission is coded by minus (-) and adding by plus (+). $1x10^4$ cells were seeded on day 0. 84
Figure 27: Morphology of MCF-7 cells after three days of growth in the conventional FBS supplemented medium (A) or in serum-free medium (B) on collagen I coated surfaces.....84
Figure 28: MCF-7 cell growth in the serum-free medium DMEM/F-12 supplemented with Hepes, L-glutamine, insulin/transferrin/selenium and 1 mg/mL BSA over seven days compared to the conventional DMEM with 10% FBS. $5x10^4$ cells were seeded on day 0. Cells in serum-free medium were grown on collagen I (10 µg/cm²) coated surfaces. Data are shown as mean of triplicates with standard deviation. 85
Figure 29: Dependency of incubation time at the single cell densitiy on resazurin conversion in DMEM with 10% FBS. Cells were incubated in 120 µM resazurin solution for 1 to 6 hours. Data are background corrected and shown as mean with SD for n=3.....87
Figure 30: Comparison of resazurin reduction in serum-free cultured cells (red) and conventionally cultured cells (black). Cells were incubated for 4 hours in 120 µM resazurin solution. Data are background corrected and shown as mean with SEM for n=4.....88
Figure 31: Influence of insulin omission (A) and incubation time in estrogen-free medium (B) on the proliferative response of $1x10^4$ MCF-7 cells prior to and during treatment with estradiol (estradiol concentrations: 10^{-12}-10^{-9} M). Timeline for the insulin omission approach (C). Timeline for incubation under estrogen lacking conditions (D). Data are corrected to the fluorescence signals of the untreated cells and shown as mean of relative fluorescence intensities with SEM for n=3. Significance was tested for matching concentrations and treatments with an unpaired t-test for alpha=0.05. Estradiol was solved in DMSO (0.1 % was used in the assay). 90
Figure 32: Improvement of the assay performance by 10 mg/mL BSA supplementation shown for the biomarker Rantes. Calibration curves display the assay performance in BSA (10 mg/mL) supplemented (red curve) and BSA free DMEM/F-12 (black curve).....94
Figure 33: Results of MCF-7 cell secretion after stimulation with IGF-1, MCP-1, IL-1a, IL-1ß, TNF-a, and IFN-y. The box blots display the secretion of IL-8 (A), Rantes (B), IL-6 (C), MCP-1 (D), and CXCL10 (E) after 24 hours in log [fluorescence]. Compared to two standards (without cells) S0 and S1 and the non-stimulated medium control (with cells) C0. Box plots are expressed as 5th and 95th quartiles. One-way-ANOVA and Bonferroni multiple comparison post-hoc test ($p \leq 0.05$ (*), $p \leq 0.01$ (**), $p \leq 0.001$ (***)), for alpha = 0.05 were used for the statistical analysis of n = 6 samples for stimulation against the zero standard S0 (*) and the medium control C0 (▪). Figure was taken from (Gier et al., 2017). 98
Figure 34: Biomarker chip and proliferation platform shown as experimental setup. First MCF-7 cells are treated with samples containing estrogen receptor agonists and antagonists. Due to the treatment, proteins are secreted and quantified in the cell medium, using the fluorescence based multiplexed protein microarray. The biomarkers are measured on-chip in

a sandwich assay format. Analytes are captured by immobilized antibodies. The binding is detected by fluorescently labeled detection antibodies. A proliferation assay based on metabolic reduction of resazurin to resofurin is applied in parallel, to measure the proliferative effect in hormone-sensitive cancer cell line MCF-7. Figure was taken from (Gier et al., 2017). 99
Figure 35 Secretion of the biomarker Rantes in IL-1ß stimulated cells challenged with solvents 0.1% DMSO (A) and 0.1% EtOH (B) compared to untreated cells (C0), and estrogen receptor agonist (estradiol) and antagonist (tamoxifen) treatment. Proliferation of MCF-7 cells in standard medium and serum-free/phenol-red-free medium DMEM/F-12 with and without 0.1% EtOH (C). Proliferation data are log transformed. Bar graphs are plotted as means ±SEM. Significance was tested (n = 5 (A,B); n = 4–8 (C)) against the C0 control with a one-way ANOVA and a Bonferroni multiple comparison test for alpha = 0.05 ($p \leq 0.5$ (*), $p \leq 0.01$ (**), $p \leq 0.001$ (***)).....100
Figure 36: Graphs (left graph without (-) and right graph with IL-1ß stimulation (+)) picture the proliferative effect of MCF-7 cells. The cells were exposed to agonists (estradiol, bisphenol A (BPA), genistein, and nonylphenol) and antagonists (tamoxifen and fulvestrant) of the estrogen receptor. Antagonistically action (A) on the estrogen receptor blocks proliferation signaling, and agonistically (B) triggers proliferation of cells. Baseline-corrected (to estradiol treatment and medium control) data for n = 6, are plotted as relative fluorescence. 101
Figure 37: The relative secretion after treatment with ER agonists (estradiol, BPA, nonylphenol, genistein) and ER antagonists (fulvestrant, tamoxifen), without (-) or with (+) IL-1ß stimulation of the markers MMP-9, VEGF, IGFBP-3, CXCL10, IL-6, Rantes, IL-8, and MCP-1 over 48 hours is shown. The mean of baseline-corrected data with SEM is plotted, and shown in percent to the medium control. One-way-ANOVA and a Bonferroni multiple comparison post-hoc test (alpha = 0.05) was applied for significance testing against treatment with tamoxifen (*) and fulvestrant (#) for n = 6 ($p \leq 0.05$ (*), $p \leq 0.01$ (**), $p \leq 0.001$ (***)). 102
Figure 38: Additive and synergistic effects of the secretion of MMP-9, IGFBP-3 and IL-11 when treated with IL-1ß and receptor agonist bisphenol A (BPA), genistein (Gen), ß-estradiol (17ß) and antagonists fulvestrant (Ful) and tamoxifen (TAM) over 48 hours. Stacked graphs show the addition of the concentration of the single treatments compared to the combi-treatment. Bar graphs are shown as mean of n=6 with SD. Concentrations were calculated via the calibration curves (Appendix I see: Figure A 6). 105
Figure 39: Immobilization of the bare molecule bisphenol A (BPA) (A) and the comparison of BPA-PMPI-BSA-, BPA-BSA-, BPA-PMPI-conjugates (reduced and unreduced BSA) and bare BPA immobilized on ARChip gel surfaces (B). Mean of fluorescence intensities of nine replicates are plotted with standard deviation. The standard curves were made using a 4-parametric-fit. 107
Figure 40: Immobilization of bisphenol A (BPA). BPA was immobilized in sciPOLY3D gel on a ARChip Epoxy surface (A). Immobilization in sciPOLY3D gel via covalent binding to the methyl groups of BPA, therefore antibody recognition of BPAs hydroxyphenyl groups is assumed (B). Spot morphology for the immobilization of 1 to 4 mg/mL (1-4) BPA in sciPOLY3D with and without 20 mM trehalose (C). Comparison of the standard curves of the binding inhibition assay made with different BPA concentrations immobilized and with and without 20 µM trehalose (D). Data of standards are shown as mean with standard deviation of n=6 replicates. ……..108
Figure 41: Serial (A) and parallel (F) channel-well assemblies are shown with liquid flow directions and properties of the volumetric flow rate. Drawbacks of the serial channel-well

assembly were: no perfusion without prefilling (B and C), backflow of liquid after movement (D and E) and network failure caused by droplet drip off (E). 111
Figure 42: Design of the developed glass hanging drop device (A) with specified dimensions (B). 112
Figure 43: Defects occurred during the production process included: damages due to sandblasting without protection (A, B) in comparison to protected glass slides (C and D), channel dimension variances (C) peeling off of AZ photoresist (E) and newton rings after fusion bonding (F). 114
Figure 44: Scheme of the established glass hanging drop device fabrication. 115
Figure 45: Droplet stability on glass due to surface treatment. The changes of roughness/topography of soda lime glass after treatment with hydrofluoric acid (HF). Surface inside of the HF generated rim (Bar scale = 100 µM) (A). Inner-edge of the HF generated rim (Bar scale = 100 µM) (B). Rim HF generated on soda lime glass (red box shows position of microscopic pictures) (C). Droplet stability was tested at the HF rim and is shown with 20 µL water droplet in a vertical position (D). 118
Figure 46: Determination of the ring dimensions on the droplet stability at an inclined plane. Bonded PDMS rings were tested with different heights and widths to keep 65 µL stained liquid droplets (A). Glass hanging drop device with SU-8 bonded PFPE rims (B). 120
Figure 47: Scheme of the attachment of the pre-cured Fluorolink®-PFPE-ring on the SU-8 coated BOROFLOAT ® glass slide. 120
Figure 48: Simultaneously formation and perfusion of the droplet (A). Stained liquid is applied by the inlet and perfused the bottom part of the droplet. (B). A whole droplet can be perfused by lagged perfusion of in-and outlet (C). Images were made at a flow rate of 20 µL/min in ~90° (A) and ~45° (B) angles. 122
Figure 49: Network stability under movement (A). The stability was tested, when moving the device in different angles (0°, ~45°, 90°). Droplet heights of ~7.92 mm were reached until drip off, without affecting the volume of the second droplet in a subarray without movement (B). Fully automatically transfer of droplets into a PDMS chamber (C). 123
Figure 50: Reduction of evaporation of the hanging droplets in a 3D printed incubation chamber. Graph shows the reduction of evaporation loss with and without incubation chamber (IC), after pre-incubation and wetted conditions. Minus (-) and plus (+) at the front of IC and pre-incubation refer to the absence or presence of it (A). Data are shown as mean with standard deviation for n=6. Statistical significance was tested using the Mann-Whitney test for alpha=0.05. Dimensions of the 3D printed incubation chamber (B). PLA incubation chamber is shown, containing the hanging drop device (C). 125
Figure 51: The biocompatibility of the materials used for the glass hanging drop device is shown for MCF-7 cell spheroids, which were grown in serum-free medium DMEM/F-12 over 4 days. The growth in the glass device is compared to the growth in a PDMS device (A). Data are plotted as mean with SD from n= 4. Morphology of MCF-7 spheroids: The spheroids grew in the glass hanging drop device and are represented for the days 1 to 4 of cell culture (B). 300 cells per 30 µL were seeded. 126
Figure 52: Influences on MCF-7 cell viability through the device material. Viability of cells growing in glass devices with PFPE rings bonded via SU-8 (when not totally covered by PFPE) or silicon sealant compared to PDMS (A). Viability of cells growing in glass devices with PFPE rings bonded via SU-8 (totally covered by PFPE) compared to PDMS (B). Fluorescent viability stain CAAM images with corresponding phase contrast images of MCF-7 cell spheroids grown in the glass hanging drop device with SU-8 attached PFPE rings (left) compared to spheroids grown in PDMS devices (C). Data are given as mean with SEM.

Statistical analysis of log transformed fluorescence intensities of CAAM stained spheroids were made with an unpaired t-test for alpha=0.05 n=5-11 (A) or n=3-7 (B). 300 cells per 30 µL were seeded.....127
Figure 53: Effect of culture material and flow on MCF-7 spheroids. Influence of culture materials SU-8, PDMS and silicone sealant on cell growth prior to estradiol treatment (A). Effects of SU-8 on viability of MCF-7 cell spheroids (B). Bars are shown with corresponding fluorescent images of the spheroids grown in PDMS or glass device with SU-8 attached PFPE rings. Data are shown as mean of corrected total cell fluorescence (CTCF) with SEM. Viability of MCF-7 spheroids grown under flow (20 µL/min) or static conditions (C). Data are given as mean of log fluorescence values with SEM. Morphology of a MCF-7 spheroid of 1500 cells on day two of cell culture exposed 15 minutes to flow (D). Morphology of a MCF-7 spheroid of 1500 cells on day two of cell culture grown under static conditions is shown (E). Statistical analysis was done with an unpaired t-test for alpha=0.05 (A: n=4-6, B: n=6, C: n=3-7 replicates). Significance was tested group wise for each concentration, material or flow condition.....129
Figure 60: Adsorption of rhodamine. Fluorescence image of a 2 mm wide PDMS ring after 24 hours incubation in 50 µM rhodamine solution (Scale bar=100µM) (A). Fluorescence image of a 2 mm wide PFPE ring after 24 hours incubation in 50 µM rhodamine solution (Scale bar=100µM) (B). Rhodamine adsorption in PFPE and PDMS is expressed as fluorescence intensity (C). Fluorescence was measured for the first half (1/2) and the second half of both rings (1). Bar graphs showing mean values with standard deviation for n=3 replicates. Significance was tested with an unpaired t-test for alpha=0.05. ……..130
Figure 55: Assembly strategies of the perifusion chamber. The reassembled perifusion chamber is shown, with one polycarbonate membrane in the bottom layer (A). Closed approach with integrated hanging drop system (B). Open approach with extra hanging drop system (C). Scheme of the original perifusion chamber assembly is displayed (D). Scheme of the new perifusion chamber assembly is displayed (E).....133
Figure 56: Liquid flow in perifusion chambers. Improvement of PDMS layer bonding prevented leakage of fluid to other chambers (A). Perifusion of the open chamber was possible without overrun of the liquid (B). 134
Figure 57: Glass solution preparation with different incubation temperatures. Cured glass solution droplet is shown after overnight incubation at 65 °C (A). Cured glass solution droplet is shown after overnight incubation at RT (B). ……134
Figure 58: Glass coated perifusion chambers. Glass coated perifusion chamber (A). Uncoated perifusion chamber (B). Fluorescent image of the edge of a glass-coated PDMS perifusion chamber after 4 day incubation in a 50 µM rhodamine solution is shown (C). Fluorescent image of the edge of an uncoated PDMS perifusion chamber after 4 day incubation in a 50 µM rhodamine solution is shown (D). 135
Figure 59: Glass membrane integration in the perifusion device. Glass membrane (A). Perifusion device mold with 3D printed clamps around each chamber mold for the integration of the glass membranes (B). Glass coated perifusion device with integrated glass detection windows (C). A Solution of 15 µM particles (round circles) in the perifusion chamber, was focused through the membrane (D). 136
Figure A 1: Cell morphology of MCF-7 cells after step-wise decrease of FBS to 0% in serum-free media and serum supplemented medium cells on day four. Comparison of cell growth in DMEM supplemented with 10% FBS (A), to serum-free cell culture conditions (B), and under omission of ITS (C), collagen I (D) or both (E). Total cell numbers counted after 100% adaption to serum-free medium on day four (F). Comparison of cell growth in DMEM

supplemented with 10% FBS (DMEM 10%) to serum-free cell culture conditions (DMEM/F-12) and under lacking of ITS, collagen I or both. Total cell numbers were counted for n=2 and given as mean. ITS omission is coded by minus (-) and adding by plus (+).1*10^4 cells were seeded on day 0.....179
Figure A 2: Cell morphology of MCF-7 cells after sequential media change of serum-free medium and serum supplemented medium cells on day four. Comparison of cell growth in DMEM supplemented with 10% FBS (A) to serum-free cell culture conditions (B) and under lacking of ITS (C), collagen I (D) or both (E). Total cell numbers counted after 100% adaption to serum-free medium on day four (F). Comparison of cell growth in DMEM supplemented with 10% FBS to serum-free cell culture conditions (DMEM/F-12) and under lacking of ITS, collagen I or both. Total cell numbers were counted for n=2 and given as mean. ITS omission is coded by minus (-) and adding by plus (+).1*10^4 cells were seeded on day 0……180
Figure A 3: Growth curve of MCF-7 cells grown in DMEM medium supplemented with 10% FBS (red) and serum-free DMEM/F-12 medium supplemented with Hepes, L-glutamine, insulin/transferrin, sodium selenite (black). Cells under serum-free conditions grew on collagen I coated surfaces. Cells grew over 7 days. Data are shown as mean of triplicates with standard deviation.....181
Figure A 4: Effects of 2 mM Resazurin solution on MCF-7 cells cultured in DMEM with 10% FBS and serum-free DMEM/F-12 medium after 1.5, 3 and 4.5 hours of incubation. Data (n=4) are shown as mean of background corrected fluorescence intensities with SEM.....181
Figure A 5: Standard curves of the excluded biomarkers pS2, endostatin and IGFBP-4 showing a bad assay performance. The sandwich assays were performed in DMEM/F-12 (red), DMEM with 10% FBS (blue) and compared to the assay buffer J (black).....182
Figure A 6: Calibration curves of VEGF, Rantes, MMP-9, MCP-1, IL-11, IL-8, IL-6, IGFBP-3, IGF-1, and CXCL10 are shown. The curves are generated with 11 standards in DMEM/F-12 supplemented with 10 mg/mL BSA as sample buffer. The average of the signals is background corrected and shown with standard deviation in the graph. The mean was calculated for n=9 technical replicates. A four-parametric fit was chosen. Figure from (Gier et al., 2017). ……..…….184
Figure A 7: Comparison of the assay performance in different matrices. The calibration curves of IL-6 (A), IL-11 (B), MCP-1 (C) and IGF-1 (D) are displayed. The assays were made in buffer J (black), and the cell culture media DMEM 10% FBS (red) and the serum-free DMEM/F-12 (blue). Data are shown as mean of n=9 with standard deviation.....185
Figure A 8: Standard curves of bisphenol A antibody titration for different concentration of BPA immobilized in SciPOLY3D. Data are shown as mean with standard deviation for n=9 replicates for each antibody concentration.....186
Figure A 9: Inter slide variance of bisphenol A (BPA) binding inhibition assay. Comparison of BPA-sciPOLY3D spots with and without 20 mM trehalose. Coefficient of variation of three different slides with n=9 replicates each is shown. 186
Figure A 10: Introduction of micro structures in glass. Structure in BOROFLOAT® glass generated with a diamond pen (A). Structure in BOROFLOAT® glass generated with sandblasting (B). ……..187
Figure A 11: MCF-7 cell spheroid grown in the glass hanging drop device with SU-8 attached PFPE rings 24 hours after seeding.....187
Figure A 12: Fluorescence image of a coated perifusion chamber section. Thickness of the coating approximately 10 µm. Incubation with a 50 µM rhodamine solution stained the coating. 187

9. Appendix I

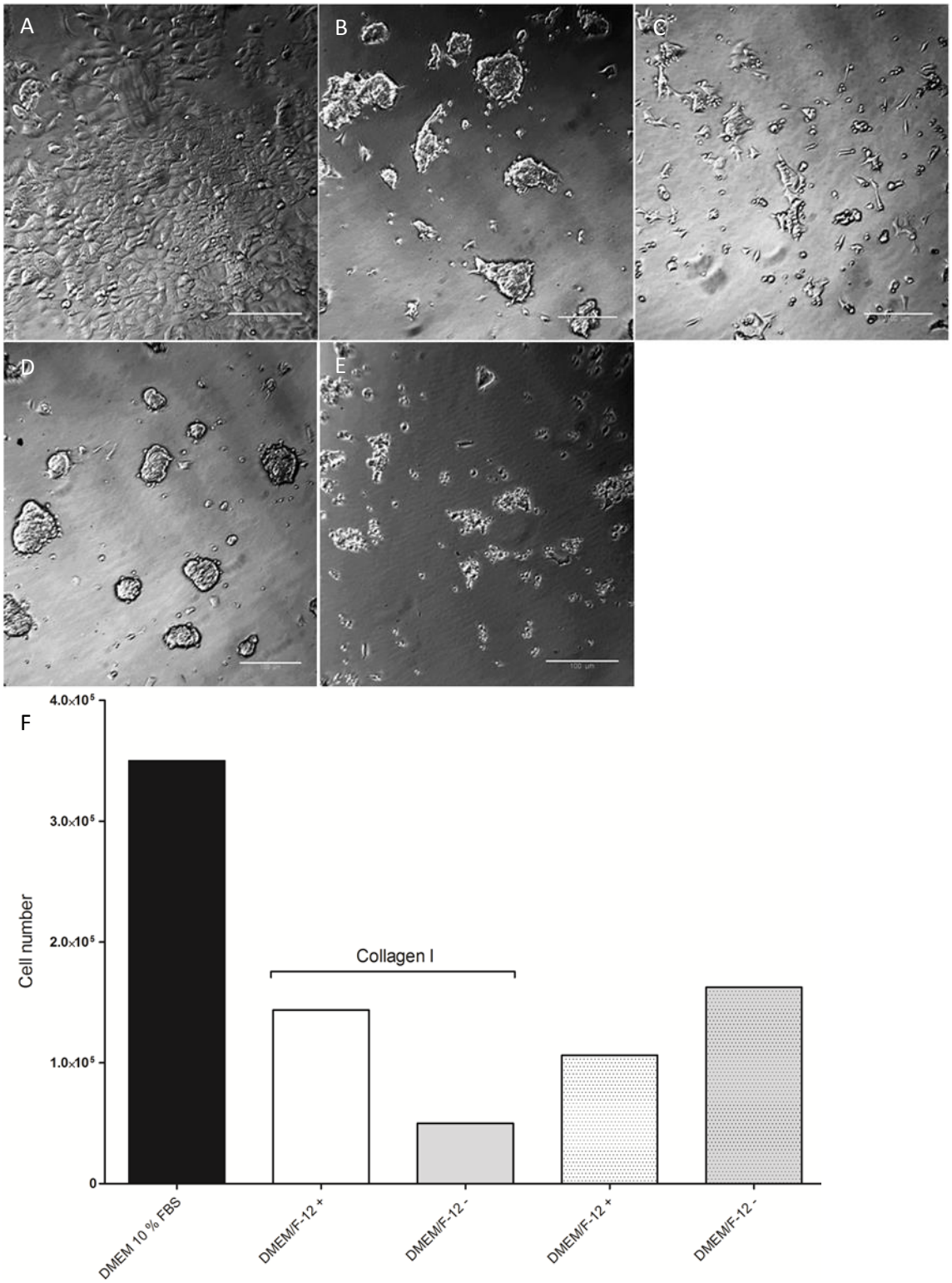

Figure A 1: Cell morphology of MCF-7 cells after step-wise decrease of FBS to 0% in serum-free media and serum supplemented medium cells on day four. Comparison of cell growth in DMEM supplemented with 10% FBS (A), to serum-free cell culture conditions (B), and under omission of ITS (C), collagen I (D) or both (E). Total cell numbers counted after 100% adaption to serum-free medium on day four (F). Comparison of cell growth in DMEM supplemented with 10% FBS (DMEM 10%) to serum-free cell culture conditions (DMEM/F-12) and under lacking of ITS, collagen I or both. Total cell numbers were counted for n=2 and given as mean. ITS omission is coded by minus (-) and adding by plus (+).1*10^4 cells were seeded on day 0.

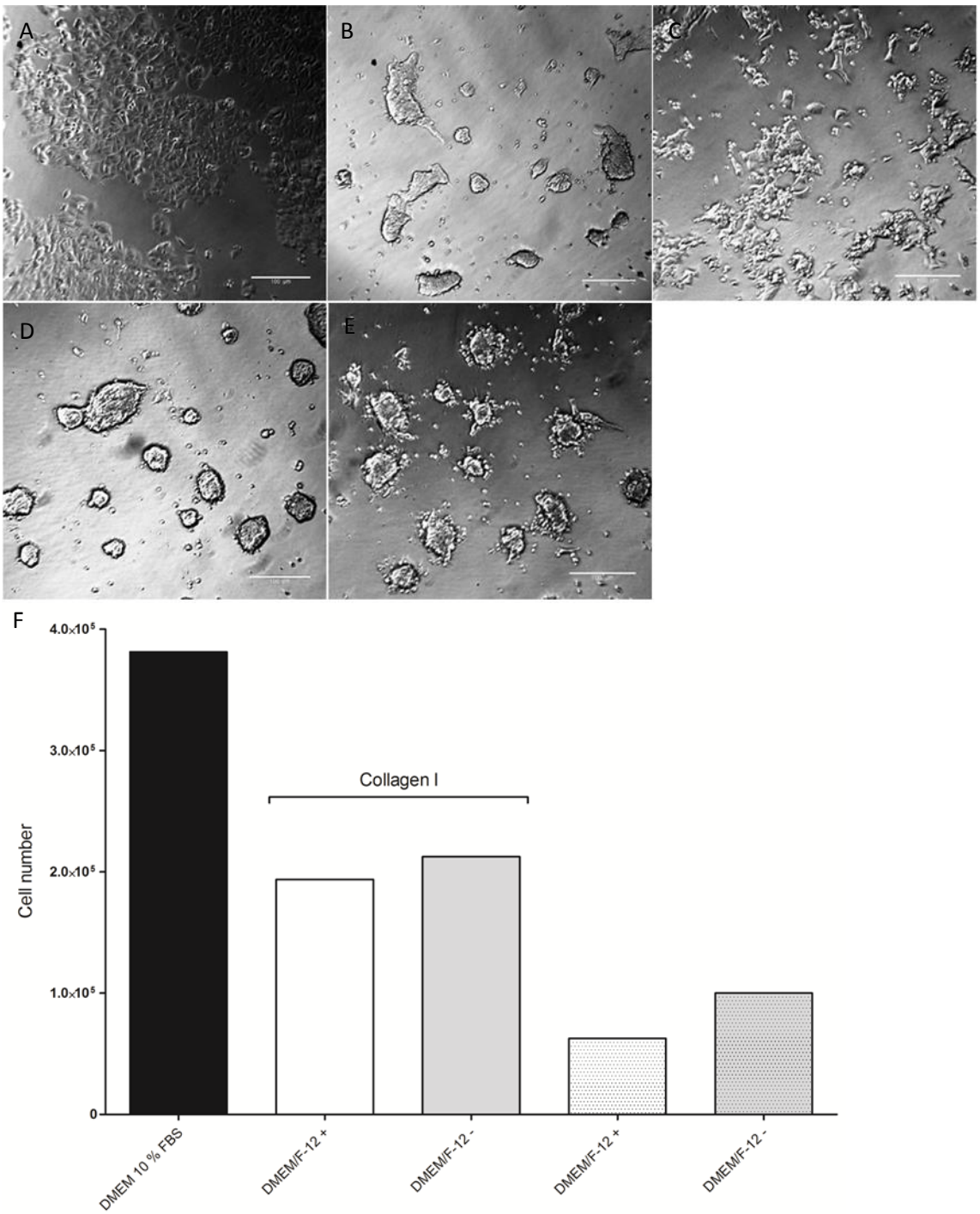

Figure A 2: Cell morphology of MCF-7 cells after sequential media change of serum-free medium and serum supplemented medium cells on day four. Comparison of cell growth in DMEM supplemented with 10% FBS (A) to serum-free cell culture conditions (B) and under lacking of ITS (C), collagen I (D) or both (E). Total cell numbers counted after 100% adaption to serum-free medium on day four (F). Comparison of cell growth in DMEM supplemented with 10% FBS to serum-free cell culture conditions (DMEM/F-12) and under lacking of ITS, collagen I or both. Total cell numbers were counted for n=2 and given as mean. ITS omission is coded by minus (-) and adding by plus (+).1*10^4 cells were seeded on day 0.

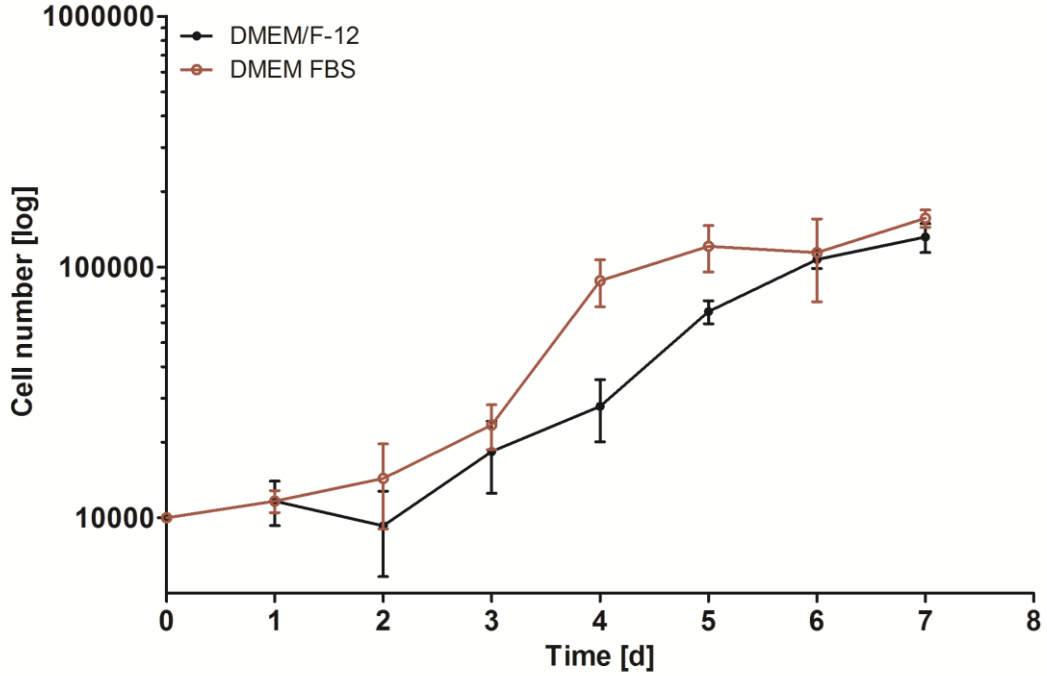

Figure A 3: Growth curve of MCF-7 cells grown in DMEM medium supplemented with 10% FBS (red) and serum-free DMEM/F-12 medium supplemented with Hepes, L-glutamine, insulin/transferrin, sodium selenite (black). Cells under serum-free conditions grew on collagen I coated surfaces. Cells grew over 7 days. Data are shown as mean of triplicates with standard deviation.

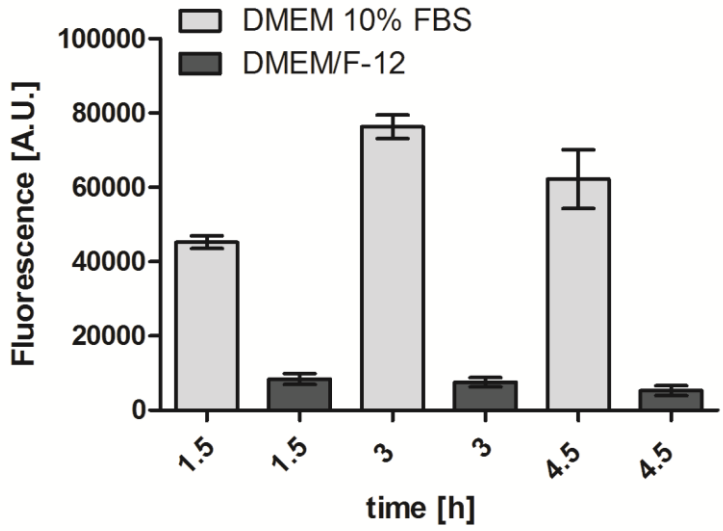

Figure A 4: Effects of 2 mM Resazurin solution on MCF-7 cells cultured in DMEM with 10% FBS and serum-free DMEM/F-12 medium after 1.5, 3 and 4.5 hours of incubation. Data (n=4) are shown as mean of background corrected fluorescence intensities with SEM.

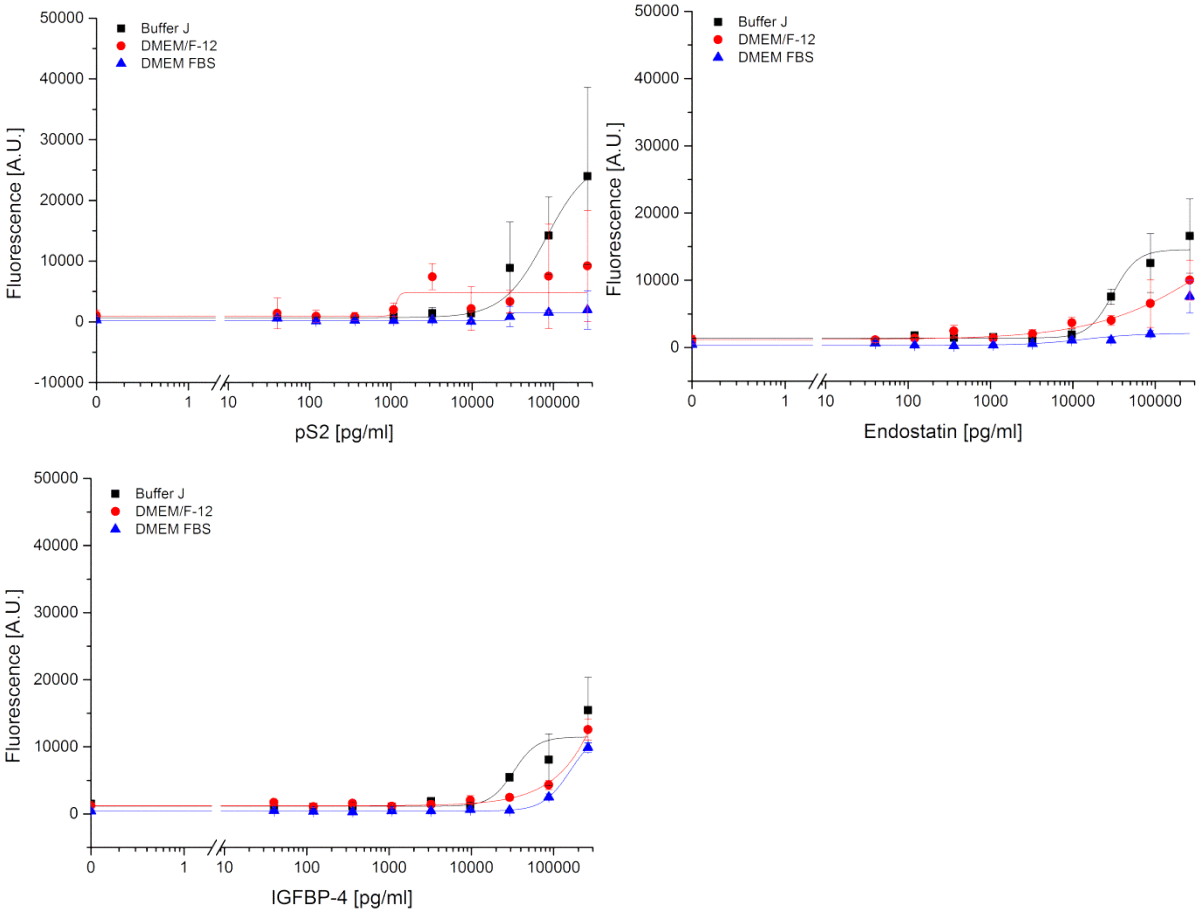

Figure A 5: Standard curves of the excluded biomarkers pS2, endostatin and IGFBP-4 showing a bad assay performance. The sandwich assays were performed in DMEM/F-12 (red), DMEM with 10% FBS (blue) and compared to the assay buffer J (black).

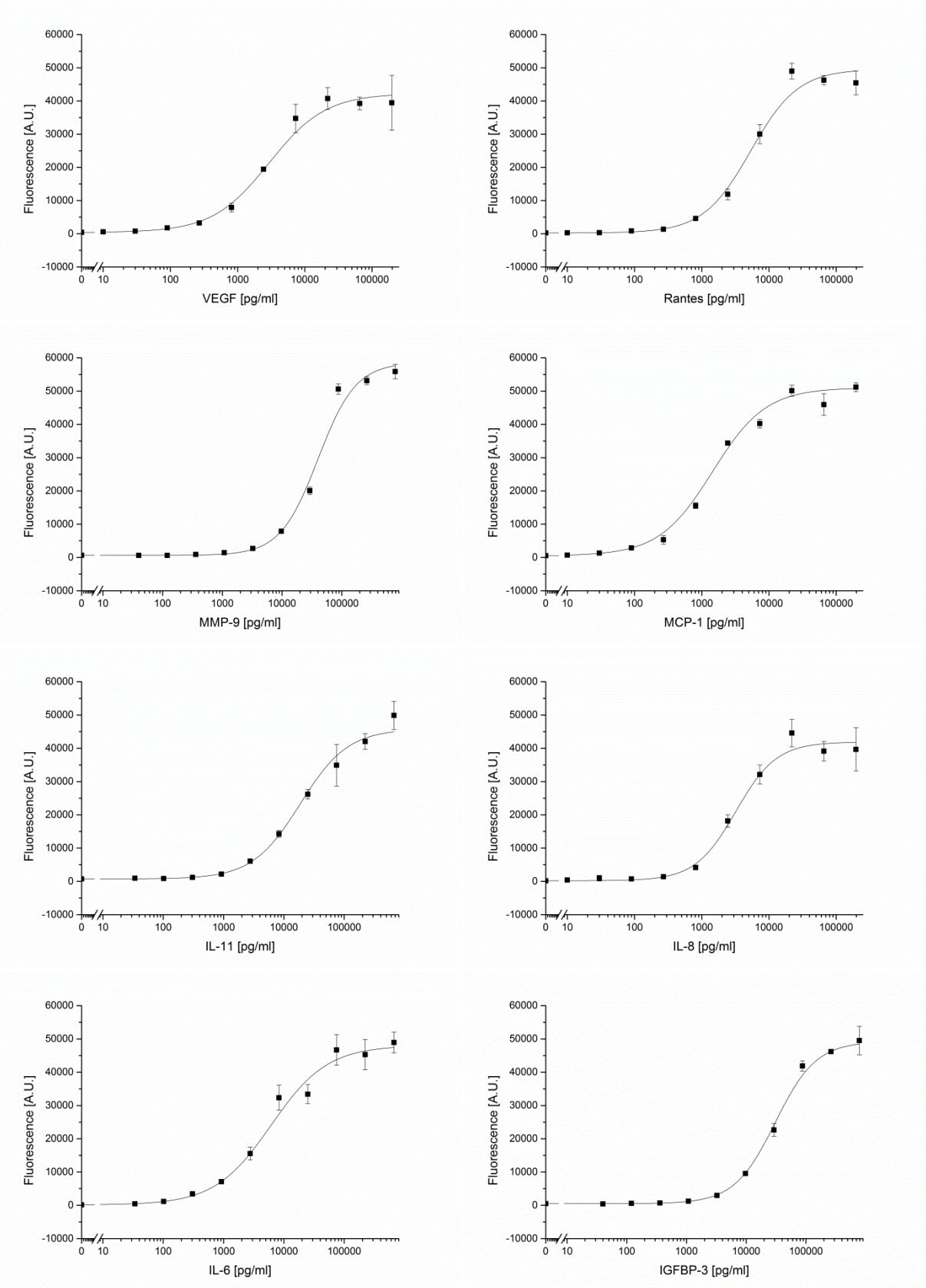
Fluorescence [A.U.]
VEGF [pg/ml]
Rantes [pg/ml]
MMP-9 [pg/ml]
MCP-1 [pg/ml]
IL-11 [pg/ml]
IL-8 [pg/ml]
IL-6 [pg/ml]
IGFBP-3 [pg/ml]

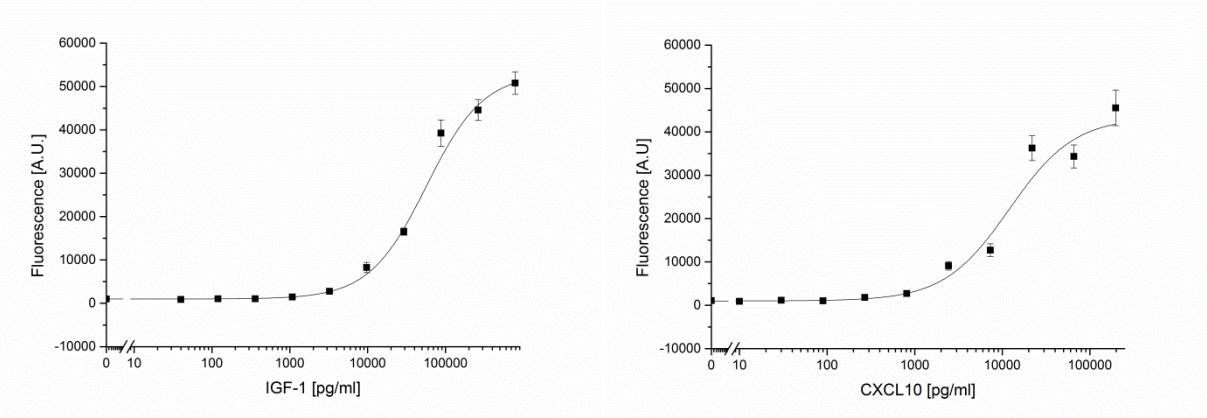

Figure A 6: Calibration curves of VEGF, Rantes, MMP-9, MCP-1, IL-11, IL-8, IL-6, IGFBP-3, IGF-1, and CXCL10 are shown. The curves are generated with 11 standards in DMEM/F-12 supplemented with 10 mg/mL BSA as sample buffer. The average of the signals is background corrected and shown with standard deviation in the graph. The mean was calculated for n=9 technical replicates. A four-parametric fit was chosen. Figure from (Gier et al., 2017).

Table A 1: Working ranges of commercially available standard ELISA kits measuring single biomarkers in well plate formats. Table from (Gier et al., 2017).

Biomarker	Range Comm. ELISA [pg/mL]	Supplier
MCP-1 (CCL2)	15.6–1000	eBioscience, San Diego, USA
IL-6	3.1–200	eBioscience, San Diego, USA
Rantes (CCL5)	31.2–2000	RnD Systems, Minneapolis, USA
VEGF	15.6–1000	RnD Systems, Minneapolis, USA
IL-8	31.2–2000	Biolegend, San Diego, USA
CXCL10 (IP-10)	15.6–1000	Biolegend, San Diego, USA
IL-11	15.6–1000	RnD Systems, Minneapolis, USA
IGFBP-3	800–50,000	RnD Systems, Minneapolis, USA
MMP-9	300–20,000	RnD Systems, Minneapolis, USA
IGF-1	100–6000	RnD Systems, Minneapolis, USA

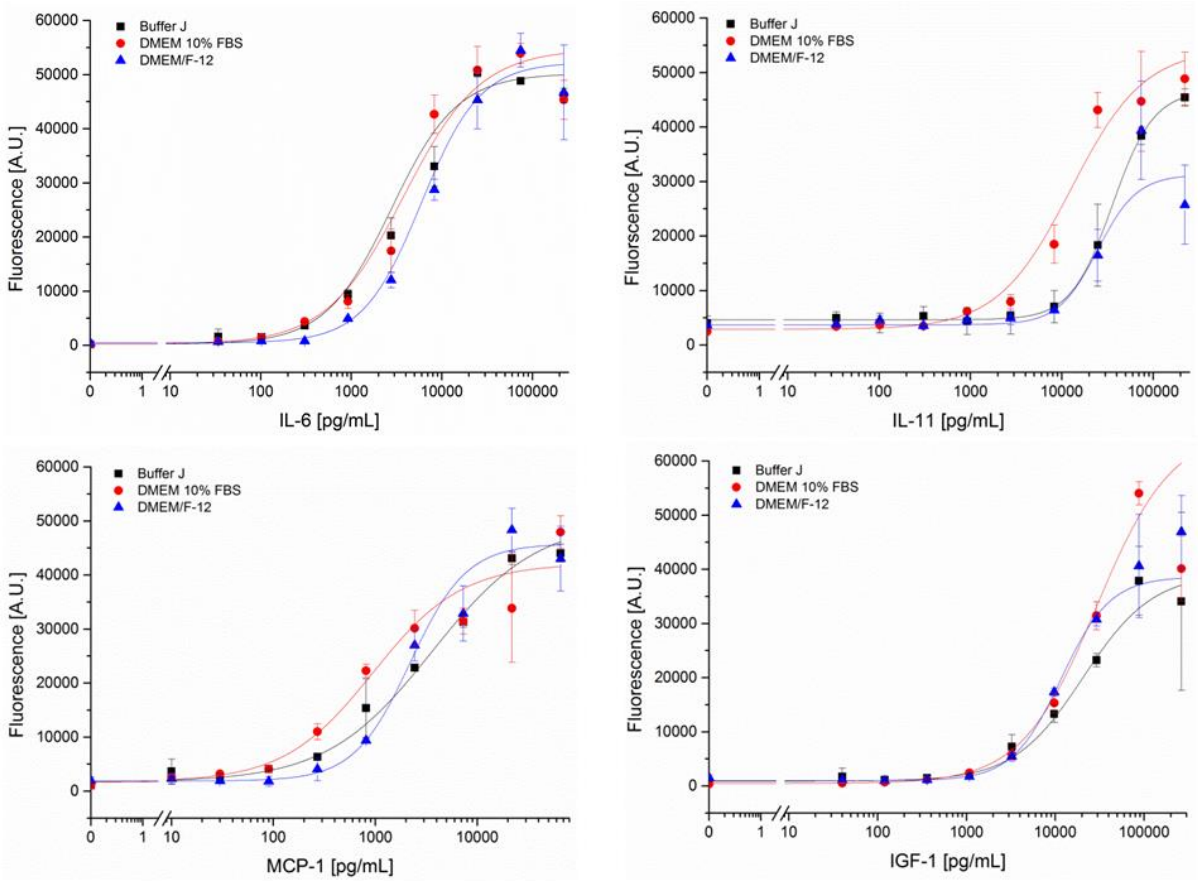

Figure A 7: Comparison of the assay performance in different matrices. The calibration curves of IL-6 (A), IL-11 (B), MCP-1 (C) and IGF-1 (D) are displayed. The assays were made in buffer J (black), and the cell culture media DMEM 10% FBS (red) and the serum-free DMEM/F-12 (blue). Data are shown as mean of n=9 with standard deviation.

Table A 2: LOD-, LOQ-, and EC50-values of IL-6, IL-11, MCP-1 and IGF-1 assays made in assay buffer J, in serum-supplemented medium DMEM 10% FBS and serum-free medium DMEM/F-12.

Biomarker & Matrix	LOD [pg/mL]	LOQ [pg/mL]	EC50 [pg/mL]
IL-6			
Buffer J	18	55	2769
DMEM 10% FBS	9	29	3768
DMEM/F-12	230	664	9413
IL-11			
Buffer J	9834	22657	35743
DMEM 10% FBS	224	1000	12630
DMEM/F-12	3653	6979	24711
MCP-1			
Buffer J	7	102	3609
DMEM 10% FBS	14	90	945
DMEM/F-12	21	62	1297
IGF-1			
Buffer J	115	345	20615
DMEM 10% FBS	125	480	29232
DMEM/F-12	1809	3561	11642

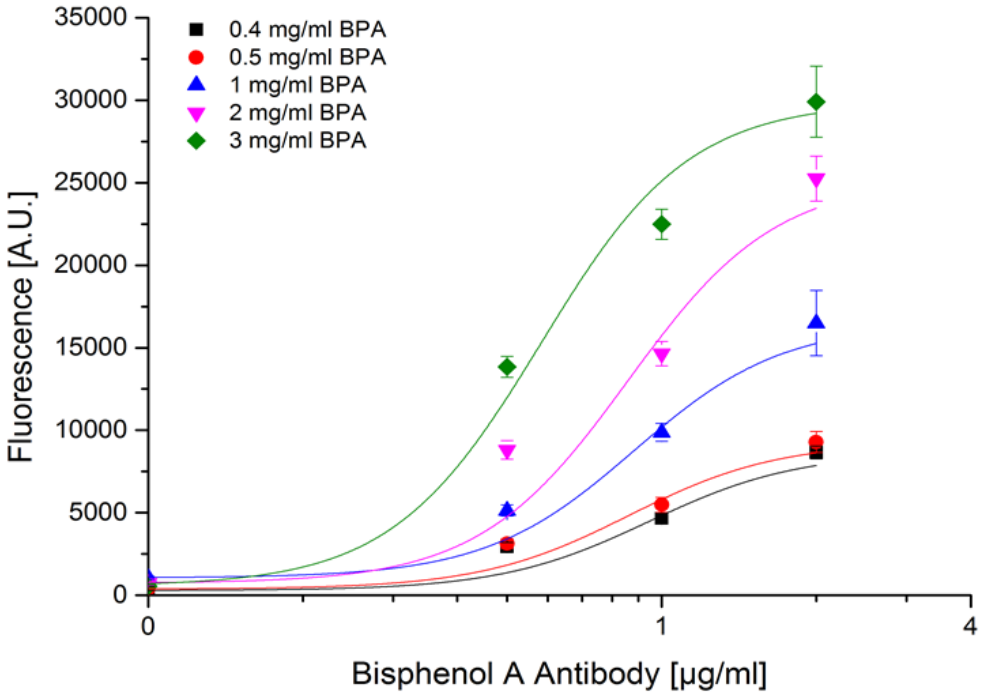

Figure A 8: Standard curves of bisphenol A antibody titration for different concentration of BPA immobilized in SciPOLY3D. Data are shown as mean with standard deviation for n=9 replicates for each antibody concentration.

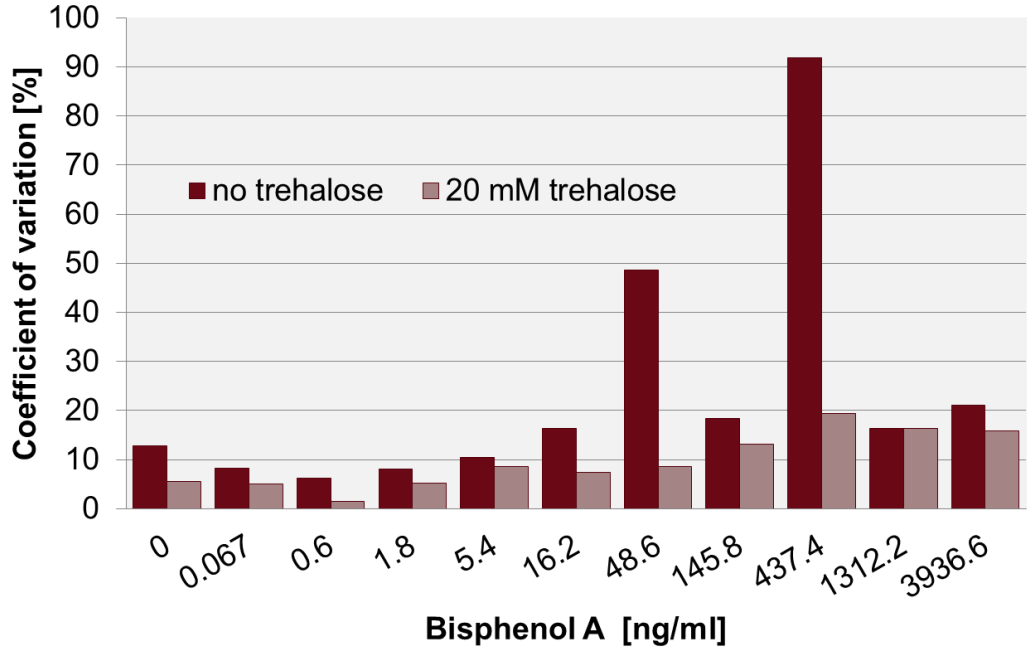

Figure A 9: Inter slide variance of bisphenol A (BPA) binding inhibition assay. Comparison of BPA-sciPOLY3D spots with and without 20 mM trehalose. Coefficient of variation of three different slides with n=9 replicates each is shown.

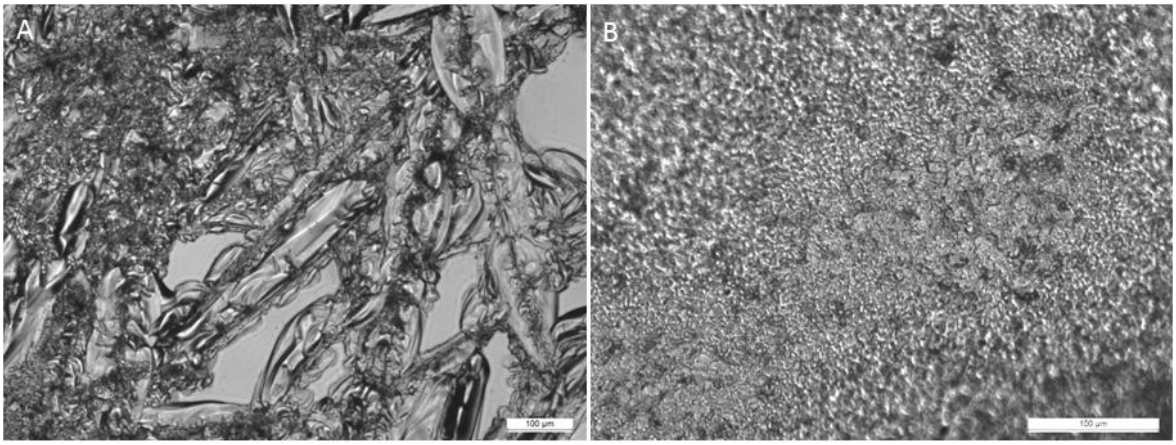

Figure A 10: Introduction of micro structures in glass. Structure in BOROFLOAT® glass generated with a diamond pen (A). Structure in BOROFLOAT® glass generated with sandblasting (B).

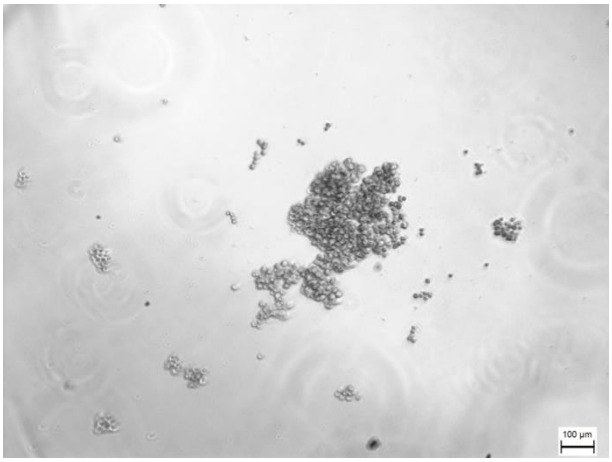

Figure A 11: MCF-7 cell spheroid grown in the glass hanging drop device with SU-8 attached PFPE rings 24 hours after seeding.

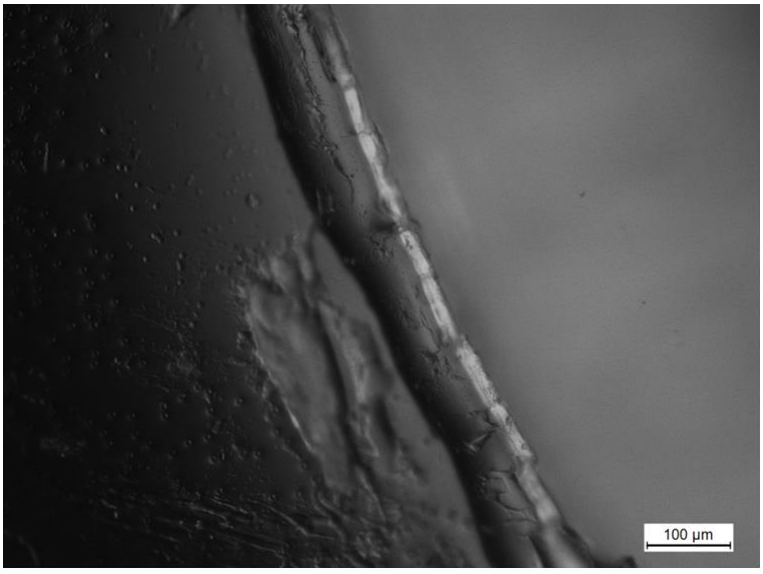

Figure A 12: Fluorescence image of a coated perifusion chamber section. Thickness of the coating approximately 10 µm. Incubation with a 50 µM rhodamine solution stained the coating.

10. Appendix II

10.1. Conference contributions

Microarray System for Toxicity and Bioavailability Studies for Endocrine Disruptors in Food

[1] Gier, K.; [1] Sauer, U. **Konstanze.Gier@ait.ac.at**

[1] AIT Austrian Institute of Technology GmbH, Health and Environment, Bioresources, Tulln, Austria.

Endocrine disrupting chemicals (EDCs) stand in the center of attention in food safety agencies in the European Union. The World Health Organization has defined endocrine disruptors as exogenous substances or mixtures that alters functions of the endocrine system and consequently causes adverse health effects in an intact organism, its progeny, or (sub)populations [1].

There is a lack of high-throughput platforms for identification and characterization of EDC related hazards in food. Therefor we develop a microfluidic chip that combines human 3D- cell- and a multi- analyte protein microarray allowing the rapid analysis of specific EDCs, their toxicity and bioavailability in food samples.

CHIP DESIGN

To evaluate endocrine disrupting processes, the chip includes assay formats like culture cell responses, reporter gene assays and immunoassays (binding inhibition, sandwich). On one hand antibodies, human transport proteins and synthetic or biomimetic receptors are used as capture probes on the protein chip for detection of EDCs in food samples and on the other hand secreted proteins from cell culture supernatant are utilized. Due to the complexity of EDCs action, cells from different tissues are immobilized on the chip in a 3D-culture. The cells are supplied by medium through a microfluidic system.

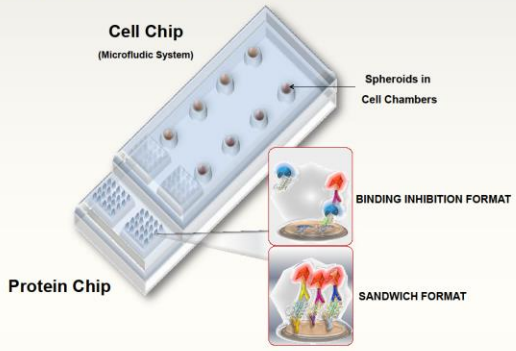

Figure 1: Model of a combined microarray system with serum free 3D-cell culture in a microfluidic system and a multi-analyte protein microarray. The protein chip includes binding inhibition and sandwich assay formats.

METHODS

Cell Culture: Hormone active substances in cell culture media like phenol red and hormones of fetal calf serum can affect the outcomes of the future experiments. Therefore was established a serum-free cell culture media. In a first setup the hormone sensitive breast adenocarcinoma cell line MCF-7 was utilized. For the serum-free cell culture DMEM/F12 HAM supplemented with insulin, transferrin and selenium were taken. The cells grew on a collagen type I coated surface.

Protein Microarray: The insulin growth like factor (IGF)-1 as a biomarker for disrupting of steroid hormone signaling and effects on reproduction was employed. As assay format a sandwich immunoassay was chosen. The capture probes were spotted by a contact printer on an ARChip epoxy glass slide [2] and the samples were spiked in different matrices. Detection occured via fluorophor labled antibodies which were recorded using a non-confocal scanner.

RESULTS & CONCLUSION

We established a serum-free MCF-7 cell culture. The MCF-7 cells grow without an adaption phase and the DMEM/F12 medium supplemented with insulin, transferrin and selenium will support a growth rate identical to the FCS supplemented medium, if the cells grow on a collagen type I coated surface.

First experiments for the protein chip in different cell culture media compositions showed a slight decrease in sensitivity and fluorescence intensity against the assay buffer for the IGF-1 sandwich immunoassay. Optimizing the assay performance will be the aim of further research.

MEASUREMENT ENDPOINTS

The chip will enable detection of toxicological endpoints like cytotoxicity, reproductive toxicity and carcinogenicity and pathological endpoints of cancer and metabolic syndrome by measuring of secreted proteins (biomarkers) and cell proliferation. There will also be a focus on effects of hormone signaling, bioavailability and quantitative and qualitative detection of EDCs themselves.

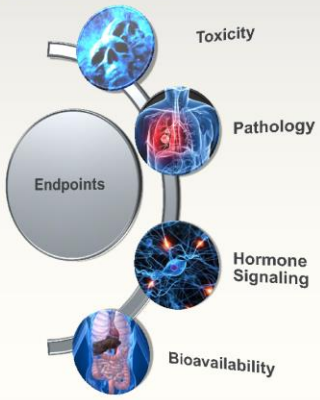

Figure 2: The measurement endpoints on the chip will be toxicity (cytotoxicity, reproductive toxicity and carcinogenicity), pathology of metabolic syndrome and cancer by detection of specific biomarkers in the cell culture supernatant, hormone signaling and bioavailability.

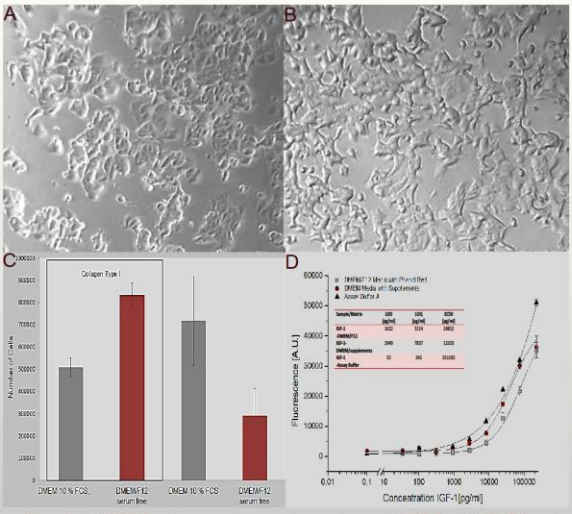

Figure 3: A-C) MCF-7 cells grow under serum free conditions . A) MCF-7 cells in DMEM media with 10 % FCS (day 2); B) MCF-7 cells in DMEM/F12 media supplemented with insulin, transferrin and selenium on a collagen type I- coated surface (day 2) - Magnification: 10x C) Total number of MCF-7 cells on day 7 of cell culture: MCF-7 cells in DMEM/F12 medium with collagen showed a growth rate identical to the cells grown with FCS supplemented medium without collagen D) Protein Microarray: The graph shows the standard curves of the immunoassay for IGF-1 in assay buffer J, DMEM/F12 medium (phenol red) and DMEM supplemented medium (without phenol red); Table 1: Calculated LOD-, LOQ- and EC50- values of the standard curves

References:

[1] Damstra, T et al. 2002. Global assessment of the state-of-the science of endocrine disruptors. World Health Organization, WHO/PCS/EDC.02.2

[2] Sauer U., Domnanich P., Preininger C. Protein chip for the parallel quantification of high and low abundant biomarkers for sepsis. Anal. Biochem. 2011;419:46–52

ACKNOWLEDGEMENTS

This work has been financially supported by the European Union Marie Curie Initial Training Network SAMOSS.

Multiplexed binding inhibition assays for the screening of food contaminants

Konstanze Gier[1], T. Kosch[2], A. Mader[2], G. Bared[2], K. Haupt [3], C. Preininger[1], U. Sauer[1]

Konstanze.Gier@ait.ac.at, Ursula.Sauer@ait.ac.at, bared@scienion.de

[1] AIT Austrian Institute of Technology GmbH, Center for Health & Bioresources, Tulln, Austria
[2] Scienion AG, Volmerstraße 7, 12489 Johannisthal, Germany
[3] UTC Universite de Technologie de Compiegne, Centre de Recherches, Compiegne cedex, France

Residues of bisphenol A (BPA), nonylphenol, atrazine and 2,4-Dichlorophenoxyacetic acid (2,4-D) arrive in food via food contact materials, application of pesticides in agriculture or bioaccumulation in the food chain. These chemicals belong to the group of endocrine disrupting chemicals (EDCs) which are able to interfere with the endocrine system of organisms. Thus there is a strong need for a sensitive detection platform measuring several analytes at the same time and in different matrices. Here we present our first results for the development of a biochip using biological and artificial recognition elements for the rapid detection of endocrine disrupters in food. The chemicals are small molecules and difficult to immobilize because of only few reactive functional groups. Two different immobilization and detection strategies are discussed. On one hand conjugates of either 2,4-D or an amino-modified derivative which were detected with molecular imprinted polymers (MIPs) and on the other hand we immobilized BPA in sciPOLY3D without further modification and used labeled antibodies as recognition elements.

Immobilization strategies

The analytes BPA and 2,4-D were immobilized onto functionalized glass surfaces as conjugates with proteins (bovine serum albumin, horseradish peroxidase) or in the hydrogel sciPOLY3D without further modification (Figure 1). The water-soluble polymer enables a covalent immobilization of analytes in a random orientation.

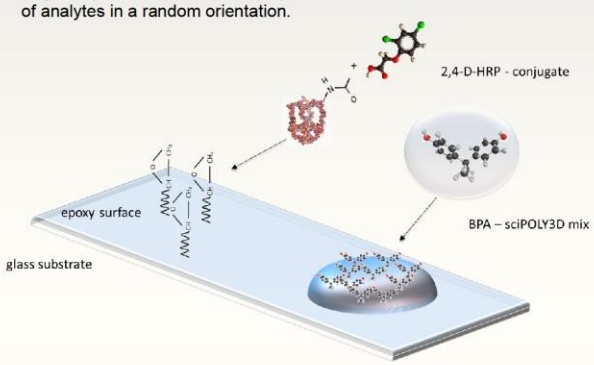

Figure 1: Immobilization strategies for the development of the chip. The scheme shows the immobilization of BPA in sciPOLY3D hydrogel (right) and the immobilization of a 2,4-D-HRP conjugate on ARChip Epoxy.

Assay format and detection with different recognition elements

For small toxins high quality antibodies are often not available, as an alternative labelled MIPs may be used in binding inhibition assays. Our chip will combine natural and artificial recognition elements, namely fluorescently-labeled human antibodies for BPA, nonylphenol and atrazine and MIPs for 2,4D detection (Figure 2).

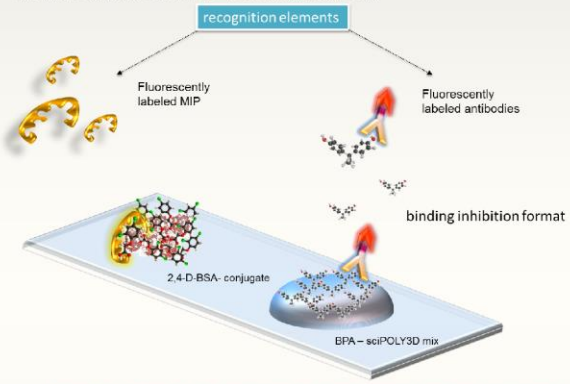

Figure 2: Scheme of the combination of different detection methods. Conventional human antibodies will be used as well as moleculary imprinted polymers.

METHODS

ARChip Epoxy and ARChip Gel were used as immoblization matrix. Mixtures of sciPOLY3D and 1-4 mg/mL BPA in different concentrations and with or without 20 mM trehalose were printed with the sciFLEXARRAYER non-contact spotter and crosslinked under UV light. Successful immobilization was tested in a direct binding assay with labeled BPA antibodies. For binding inhibition assays 0 - 3936.60 ng/mL BPA was incubated with 0.75 µg/mL labelled antibody. 0 – 5 mg/mL 2,4D –HRP conjugates were printed in PBS/0.1% chitosan and in PBS/0.005%CHAPS/0.1% BSA. Binding studies with fluorescently labelled 2,4D MIPs were performed.

RESULTS & CONCLUSIONS

Previous experiments with BPA-PMPI-BSA conjugates showed promising results on ARChip Gel and ARChip Epoxy, but also high cross reactivity of the detection antibody with BSA. Therefore we investigated the immobilization of the small molecule BPA in sciPOLY3D gel. Bisphenol A was immobilized via its methyl groups. The epitope targeted by the antibody is not known but our results suggest that the antibody binds to the hydroxyl groups of the molecule (Figure 3A). The highest signal intensities in the binding inhibition assay were achieved for 3 mg/mL BPA in sciPOLY3D plus 20 mM trehalose in the printing solution. Trehalose improved the spot morphology, the sensitivity and also the inter slide variation of the signals (CV: 1-19% for different concentrations of BPA) (Figure 3 B, C). In the binding inhibition assay a LOD of 3 ng/mL was achieved (Figure 3 D+E). Binding studies with 0-5 mg/mL 2,4 D-HRP and 2-(4-aminopenoxy)acetic acid-HRP conjugates in different print buffers with the labeled 2,4-D MIP demonstrated firstly successful immobilization of the small ligand and secondly sufficient affinity of both, the original molecule and the derivative to the MIP.

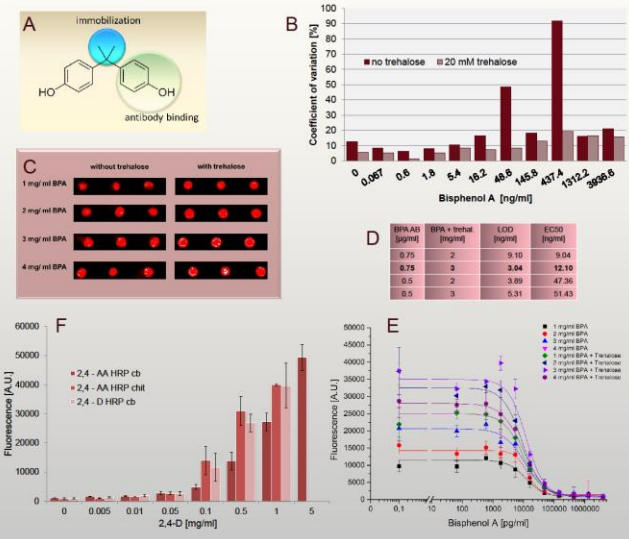

Figure 3: (A) Immobilization and antibody binding site of bisphenol A. (B) Inter slide variance of BPA binding inhibition assay. Comparison of BPA-sciPOLY3D spots with and without trehalose. (C) Spot morphology of BPA printed in sciPOLY3D and with and without trehalose. (D) Limit of detection (LOD) and half maximal effective concentration (EC50) for two different antibody (AB) concentrations and two immobilization concentrations. (E) Binding inhibition assay for BPA. Comparison of different concentrations of immobilized BPA with and without trehalose. (F) Binding study of fluorescently labeled 2,4 D with 2,4 D- HRP conjugate immobilized on ARChip Gel in PBS/Chaps/BSA (cb); or 2-(4-aminophenoxy)acetic acid conjugated in PBS/chitosan or cb printing buffer.

ACKNOWLEDGEMENTS

This project is part of the MARIE CURIE INITIAL TRAINING NETWORK (FP7-PEOPLE-2013-ITN) SAMOSS "SAMPLE IN – ANSWER OUT OPTOCHEMICAL SENSING SYSTEMS".

Establishment of a high-throughput detection system for endocrine disrupting chemicals in food

Konstanze Gier, Ursula Sauer

(AIT – Austrian Institute of Technology GmbH, Health and Environment Department, Konrad-Lorenz-Strasse 24, 3430 Tulln, Austria)

Endocrine disrupting chemicals (EDCs) in food arise either from natural or anthropogenic origin. Plasticizers and other plastic additives from food packaging or pestizides as residues on fruits and vegetables belong to the most focused substances within these chemicals or mixtures. There is still a lack of high-throughput platforms for identification and characterization of EDC related hazards in food. Existing analyzing platforms for endocrine activity are mostly insufficient because they do not reflect the complex interactions of bioactive chemicals and hormones. Therefor we aim at developing a microfluidic device that combines a cell- and protein- microarray allowing the rapid analysis of specific EDC´s, their toxicity and bioavailability in food samples. The protein chip quantifies 13 biomarkers related to various endpoints in a sandwich immunoassay format in the cell culture supernatant of EDC exposed MCF-7 cells cultured in serum free media.

The human breast adenocarcinoma cell line MCF-7 is hormone sensitive and retained a number of properties expressed by breast epithelium in vivo and features receptors for estrogen, androgen, progesterone, glucocorticoid, insulin and L-3, 3´, 5-triiodothyronine. Estrogen, specifically estradiol and even estrogen active substances are capable of modulating the expression and secretion of insulin-like growth factor binding proteins (IGFBPs), insulin-like growth factor (IGF)-1, vascular epidermal growth factor (VEGF), interleukin (IL)-8, matrix metallopeptidase (MMP)-9, estrogen-induced pS2 and endotstatin.

It was reported that the proteins IGF-1, IGFBP-3 and endostatin decreased after estradiol exposure while IGFBP-4, VEGF, pS2, MMP-9 showed an increased protein secretion. The addition of the antiestrogen tamoxifen opposed these effects. Furthermore the expression of e.g. IGFBP-4 is also positively correlated with estrogen receptor (ER) status in mammary tumors.

Steroid hormones like estradiol promote the development and maintenance of primary and secondary female reproductive tissues. After estrogen exposure MCF-7 cells proliferate. Including this effect the detection of the estrogen regulated proteins and the parallel measurement of the proliferation of the cells will be part of the whole system. In ongoing experiments biomarker secretion following exposure to endogen hormones (as control for an ER agonists), EDC´s and ER receptor antagonists like tamoxifen is compared and used for validation of the biomarker chip.

Acknowledgement:
This project is part of the MARIE CURIE INITIAL TRAINING NETWORK (FP7-PEOPLE-2013-ITN) SAMOSS "SAMPLE IN – ANSWER OUT OPTOCHEMICAL SENSING SYSTEMS".

Oral Presentation: 26th Anniversary World Congress on Biosensors (BIOSENSORS)

Gothenburg, Sweden, 25th- 27th May 2016

A microfluidic double chip system for high-throughput detection of endocrine disruptors in food

K. Gier[1], P.P.M.F.A Mulder[2], M.D. Skolimowski[2, 3], E. Verpoorte[2], U. Sauer[1], C. Preininger[1]

[1)]AIT – Austrian Institute of Technology GmbH, Health and Environment Department, Konrad-Lorenz- Strasse 24, 3430 Tulln, Austria
[2)]RUG - University of Groningen, Pharmaceutical Analysis, Groningen Research Institute of Pharmacy, Antonius Deusinglaan 1, 9713 AV Groningen, The Netherlands
[3)]Present address: Micronit Microfluidics B.V., Colosseum 15, 7521 PV Enschede, The Netherlands

Existing analysis platforms for endocrine activity are generally inadequate, as they either require several sensors to detect this activity, or cannot assess the complex interactions of hormone-active chemicals at all. We are therefore developing a double chip system connected to a microfluidic device. This double chip combines a cell- and a protein-microarray allowing the rapid analysis of specific endocrine disrupting chemicals (EDCs), their toxicity and bioavailability in food samples. The protein chip quantifies 13 biomarkers related to various endpoints of EDC action in a sandwich immunoassay format via fluorescently labeled antibodies. The biomarkers for estrogen-related expression, cancer, metabolic syndrome or disorders in reproduction and development will be measured in the cell culture supernatant of hormone sensitive MCF-7 cells cultured in serum free media and exposed to EDCs. The fully developed cell microarray will consist of different cell lines and primary cells to cover different targets of EDC action. The cells will be integrated as multi-cellular spheroids in a hanging drop microfluidic perfusion system coupled to the protein- microarray.

Estradiol but also hormone active substances are capable of modulating the expression and secretion of secreted proteins. We could show that the secretion of vascular endothelial growth factor, chemokine ligand 5 and matrix metallopeptidase 9 is modulated via estrogen receptor alpha agonists and antagonists. We can confirm that 80 % of the biomarkers were secreted and could be detected on the biomarker chip in a pg/ml -range. After estrogen exposure MCF-7 cells proliferate. Therefore a resazurin based cell proliferation assay was established. In ongoing experiments biomarker secretion following exposure to endogen hormones (as control for an estrogen receptor agonists), EDC´s and estrogen receptor antagonists like tamoxifen and cell proliferation measurement are compared and used for validation of the platform.

Acknowledgement: This project is part of the MARIE CURIE ITN (FP7-PEOPLE-2013-ITN) SAMOSS.

Microfluidic spheroid-generation glass platform for integration in a screening system for endocrine disruptors

Konstanze Gier[a,b], *Patty P.M.F.A. Mulder*[b], *Jean-Paul S.H. Mulder*[b],

Ursula Sauer[a], *Elisabeth M.J. Verpoorte*[b]

[a] Center for Health & Bioresources, AIT- Austrian Institute of Technology GmbH, Tulln, Austria

[b] Groningen Research Institute of Pharmacy - University of Groningen, Groningen, The Netherlands

Contact: Konstanze.Gier@ait.ac.at (presenting author), e.m.j.verpoorte@rug.nl (corresponding author)

Abstract

Endocrine disrupting chemicals (EDCs) are substances which affect the hormone system in organisms through interference with different signalling pathways. They can act as agonists or antagonists on nuclear receptors at concentrations in the picomolar range, and are associated with diseases such as cancer, Type 2 diabetes, obesity and developmental disorders. Existing analysis platforms for endocrine activity are generally inadequate, as they either require several sensors to detect this activity, or cannot assess the complex interactions of hormone-active chemicals at all. We are therefore developing a microfluidic screening system to better assess the adverse effects of EDCs on organisms by using hormone-sensitive MCF-7 cells.

The screening platform includes a microfluidic hanging-drop component to generate multi-cellular spheroids, which, once formed, can be automatically transferred to integrated perfusion microchambers for further cultivation. After incubation with medium containing EDCs, the system allows a protein-microarray to be coupled to it, to quantify ten biomarkers which are related to various endpoints of EDC action in organisms. In this way, the effect of potential endocrine disrupting substances on the protein secretion of the cells can be assessed.

The hormone-sensitive epithelial breast cancer cell line, MCF-7, was chosen as the biological model at the heart of the sensing platform. We decided to use 3D-cell culture to better mimic *in vivo* tissue conditions and thus improve the *in vivo* predictability of our assay. The cells are cultured in serum-free, phenol red-free medium to ensure that no hormones or hormone-active substances are present, thus circumventing possible interferences by these compounds on experimental results. In order to avoid leaching of potential hormone-active components or additives from the plastics conventionally used in cell culture, we have developed the microfluidic spheroid-generation platform in glass.

The hanging-drop system (Figure 1) consists of two thermally bonded BOROFLOAT ® glass slides (75.6 x 25 mm). Six hanging drops are formed in the row of 6 holes (wells) in the lower chip. Each pair of holes is connected by parallel channels to a single inlet and outlet for medium and cell introduction, which guarantees a more stable and even drop formation than if six holes were connected to one in- and outlet via one channel. The 6 hanging-drop wells have a diameter of 3 mm for the generation of 3D spheroids in droplets having volumes up to 45 µL drops. For stable drop formation in a hydrophilic glass device, a hydrophobic rim or ring is required around the lower edge of each well, to avoid spreading of the liquid. We have introduced a microfabricated ring made of the inert material, perfluoropolyether (PFPE), to the system. Once cured, using UV light, each ring is attached to the well chip using the epoxy, NANO™ SU-8.

During static operation in a simplified device with drop wells and without channels, we observed up to 40 % evaporation of the hanging drops after 24 hours, especially for the outer wells. An incubation chamber with an integrated glass window was thus designed and constructed by 3D printing for operation of the hanging-drop system. The hanging-drop chip system can be inserted and positioned in this chamber to minimize evaporation and detect the spheroids under the microscope. Polystyrene beads (ø 15 µm) were used to mimic cells in the droplets and look at direct effects of the flow on the beads at different flow rates. No effect could be detected at flow rates from 1 to10 µL/min. Ongoing experiments focus on the generation and cultivation of MCF-7 spheroids in the glass device and effects on the cells through exposure by EDCs.

This contribution will describe the developed glass hanging drop device and its integration in the screening system as well as the latest results gained for generation and testing of MCF-7 spheroids with EDC.

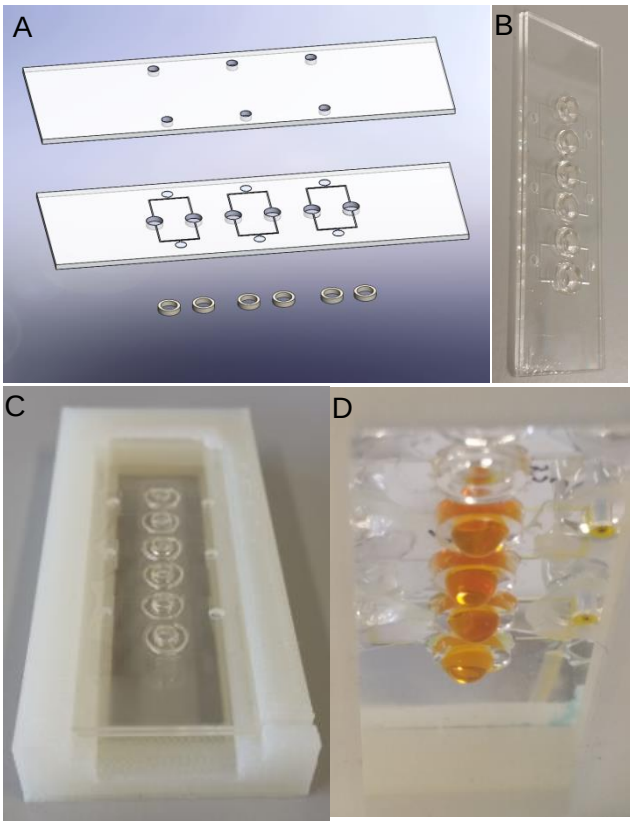

Figure 1: Microfluidic hanging drop system made of glass with integrated PFPE rings for a better stability of the droplet. A) Single sections of the hanging drop device. B) Prototype of the microfluidic spheroid-generation glass platform. C) Hanging drop incubation chamber with glass device. D) Droplet generation in the glass hanging drop device using stained water.

Acknowledgements: This project is part of the MARIE CURIE ITN (FP7-PEOPLE-2013-ITN) SAMOSS. Additional, we like to thank M.D. Skolimowski for sharing his pre-work for a cell perfusion system.

10.2. Publications

sensors

MDPI

Article

A Chip for Estrogen Receptor Action: Detection of biomarkers released by MCF-7 cells through estrogenic and anti-estrogenic effects

Konstanze Gier [1], Claudia Preininger [1] and Ursula Sauer [1,*]

1 Center for Health & Bioresources, AIT Austrian Institute of Technology GmbH, Konrad Lorenz Str 24, 3430 Tulln, Austria; konstanze.gier@ait.ac.at; claudia.preininger@ait.ac.at

* Correspondence: ursula.sauer@ait.ac.at; Tel.: +43-50550-3527

Received: 27 June 2017; Accepted: 28 July 2017date; Published: 1 August 2017

Abstract: The fluorescence based multi-analyte chip platform for the analysis of estrogenic and anti-estrogenic substances is a new *in vitro* tool for high throughput screening of environmental samples. In contrast to existing tools the chip investigates the complex action of xenoestrogens in a human cell model by characterizing protein expression. It allows quantification of 10 proteins secreted by MCF-7 cells, representing various biological and pathological endpoints of endocrine action and distinguishing estrogen or anti-estrogen dependent secretion of proteins. Distinct protein secretion patterns of the cancer cell line after exposure to known estrogen receptor agonists ß-estradiol, bisphenol A, genistein and nonylphenol as well as antagonists fulvestrant and tamoxifen demonstrate the potential of the chip. Stimulation of cells with Interleukin-1ß shifts concentrations of low abundant biomarkers towards the working range of the chip. In the non-stimulated cell culture Matrix Metalloproteinase 9 (MMP-9) and Vascular Endothelial Growth Factor (VEGF) show differences upon treatment with antagonists and agonists of the estrogen receptor. In stimulated MCF-7 cells challenged with receptor agonists secretion of Monocyte Chemoattractant Protein (MCP-1), Interleukin-6 (IL-6), Rantes and Interleukin-8 (IL-8) significantly decreases. In parallel, the proliferating effect of endocrine disrupting substances in MCF-7 cells is assessed in a proliferation assay based on resazurin. Using ethanol as solvent for test substances increases the background of proliferation and secretion experiments while using dimethyl sulfoxide (DMSO) does not show any adverse effects. The role of the selected biomarkers in different physiological processes such as cell development, reproduction, cancer and metabolic syndrome makes the chip an excellent tool for either indicating endocrine disrupting effects in food and environmental samples or for screening the effect of xenoestrogens on a cellular and molecular level.

Keywords: endocrine disrupting chemicals; protein microarray; bisphenol A; cell proliferation

1. Introduction

The World Health Organization defined endocrine disrupting chemicals (EDCs) as "exogenous substances or mixtures that alter functions of the endocrine system and consequently cause adverse health effects in an intact organism, or its progeny, or (sub) populations" [1]. EDCs are from natural sources as for instance phytoestrogens from soy bean, or from anthropogenic sources, e.g. food packaging material like bisphenol A, pesticide residues in food like atrazine or environmental pollutants like alkylphenols [2–6]. Screening of several endocrine active substances showed that they interact with different nuclear receptors such as the estrogen receptors, androgen receptor, or peroxisome proliferative receptors. EDCs are able to inhibit or activate these receptors and to disrupt the normal endocrine function by altering circulating hormone levels. They act together with endogen hormones and show low dose, additive and synergistic effects [7–10]. Since EDCs interfere with the endocrine system of an organism their action may result in symptoms of metabolic syndrome, reproductive dysfunction, and cancer [11].

Thus there is a strong need for test procedures characterizing estrogenic and anti-estrogenic action of chemicals and their involvement in biological processes. Existing in vitro platforms examine the interaction with or activation of nuclear receptors (e.g. Calux® assay, YES/YAS yeast based, ELRA) [12–14], the hormone responsive cell proliferation (e.g. E-Screen) [15], gene products and gene activity (e.g. DNA microarrays) [16], the secretion of single biomarkers (e.g. Vitellogenin) [17] or the enzyme activity within the steroidogenesis [18]. The hormone like activity of substances is often evaluated with several methods in parallel in order to minimize the chance of false positive and especially false negative results [19]. The strong cell wall of yeast for instance can prevent the penetration of lipophilic substances to the target location and cause false negative results of the YES test. Moreover, transferability of yeast data for the risk assessment for different species, especially humans, is questionable. Commonly used cell based receptor assays such as Calux®, show an interference of estrogenic and anti-estrogenic activity which complicates substance dependent assignment to the effect itself [20]. In addition there are no methods characterizing the cell proteome after exposure to EDC´s [19]. Therefore we aimed at the development of an *in vitro* tool which is apt for a) high throughput screening of environmental samples for endocrine disrupting effects in a human cell model and b) providing information on their complex cellular effects at the protein level.

Biomarker panels are used in medical diagnostics where single markers cannot achieve the required accuracy [21]. Multiparameter panels are especially meaningful for fast and highly specific diagnosis [22-24], disease and targeted therapy monitoring, as well as patient stratification [25], because they are drawing a picture of the metabolism of individuals. Furthermore, biomarker panels can be used to detect exposure to xenobiotics and the related metabolic processes, both, on a cell and on an organism level. In consequence of this we developed a fluorescence based multiplexed protein microarray showing the complex action of estrogenic and anti-estrogenic substances based on human MCF-7 cell culture and a parallel proliferation measurement (see Figure 1).

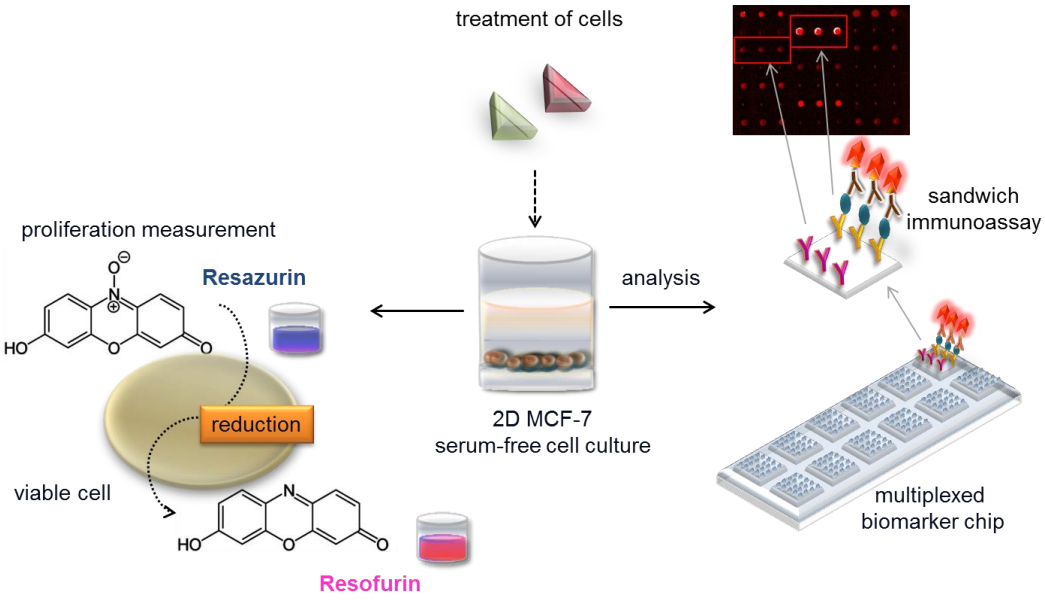

Figure 1. Experimental setup of the biomarker chip and proliferation platform. MCF-7 cells in serum-free cell culture are exposed to e.g. food samples containing estrogen receptor agonists and antagonist; biomarkers released are quantified in supernatant with a multiplexed protein microarray based on fluorescence detection. The on-chip sandwich immunoassay employs immobilized antibodies for capturing the biomarker and a fluorescently labeled detection antibody for read out. In parallel the proliferative effect in hormone sensitive cancer cell line MCF-7 is measured with a resazurin assay.

Sensors **2017**, 17, 1760; doi:10.3390/s17081760

Supernatant of serum-free MCF-7 cell culture, exposed to estrogen receptor agonists and antagonist present in environmental samples, is used for biomarker detection with the protein microarray. In parallel, the proliferative effect of test substances on hormone sensitive cancer cell line MCF-7 is assessed with a resazurin proliferation assay. The microarray shows secretion patterns of ten biomarkers after exposure to estrogen receptor agonists and antagonists and provides indications for their involvement in: estrogen receptor interaction, steroid synthesis, cancer, metabolic syndrome and reproductive and developmental processes. The tool overcomes penetration problems by using a human cancer cell line and avoids interference of different effects by measuring the protein expression of whole cells as an endpoint after exposure to EDCs in comparison to well-known agonists and antagonists of the estrogen receptor.

2. Materials and Methods

2.1. Cell line and cultivation

The hormone sensitive breast cancer cell line MCF-7 was obtained from American Type Culture Collection (ATCC, Manassas, VA, USA). The cells were cultivated routinely in Dulbecco´s modified Eagle´s Medium (DMEM) (Sigma Aldrich, St. Louis, MO, USA) supplemented with 10 % heat inactivated fetal bovine serum (FBS), 1 % non-essential amino acid (NEAA), 2 mM L-glutamine and penicillin/streptomycin (Thermo Fischer Scientific, Waltham, MA, USA) at 37 °C, 5 % CO2 and a humidity of 95 % in cell culture flasks (Falcon® Corning Inc., Corning, NY, USA). Cells were grown for five days to confluence of 80 % and then trypsinated by a 10 % dilution of a 0.5 % trypsin-ethylenediaminetetraacetic acid (EDTA) mixture (Thermo Fischer Scientific, Waltham, MA, USA) in phosphate buffered saline (PBS) without magnesium and calcium (Sigma Aldrich, St. Louis, MO, USA).

2.2. Cell cultivation in serum- /phenol red- free medium

For biomarker secretion and proliferation assays cells were cultured in serum free medium which was introduced by the following adaption phase. MCF-7 cells were seeded at a density of $5x10^4$ cells per well in Costar® cell culture plates, 96 well, flat bottom (Corning Incorporated, Corning, NY, USA) in 200 µl DMEM supplemented with 10 % FBS, 1 % NEAA, 2 mM L-glutamine and pen/step for one day at 37 °C, 95 % humidity and 5 % CO2. Cells were allowed to attach on the well surface for 24 hrs before changing to Gibco™. Dulbecco's Modified Eagle Medium/Nutrient Mixture F-12 (DMEM/F-12) with Hepes, L-glutamine supplemented with pen/strep, bovine serum albumin (BSA) solution and insulin/transferrin/selenium (ITS) mixture (Thermo Fischer Scientific, Waltham, MA, USA) but without phenol red. After 24 hrs the medium was removed and DMEM/F-12 without insulin was added for increasing the proliferative effect 33 and for acclimatization of cells in the changed environment. Transferrin (Thermo Fischer Scientific, Waltham, MA), sodium selenite (Sigma- Aldrich, St. Louis, MO), BSA solution and pen/strep were added. The cell layers were washed with 300 µL PBS (-Ca/-Mg) before changing the medium.

2.3. Cell treatment for biomarker and proliferation assays

After 72 hrs the cells were treated with 1 nM ß-estradiol, 1 nM tamoxifen, 10 nM fulvestrant, 1 µM nonylphenol, 1 µM bisphenol A (BPA) and 1 µM genistein (Sigma- Aldrich, St. Louis, MO, USA) with and without stimulation by 10 ng/mL human recombinant IL-1ß (eBioscience, San Diego, CA, USA) in 200 µL DMEM/F-12 without insulin for 48 hrs. After 48 hrs of treatment 200 µL of each sample was transferred in a 96 well plate and centrifuged for 1 min at 0.3 (x 1000) rpm to get rid of cell particles. The samples were stored on ice while preparing the sampling step for the protein microarray. Test substances were dissolved in dimethyl sulfoxide (DMSO) (Sigma- Aldrich, St. Louis, MO, USA) or 99.9 % ethanol absolute (ETOH) (Emsure® Merck Millipore, Darmstadt, Germany). The final solvent concentration in cell culture medium was 0.1 %. A sterile stock concentration of 100 mM

Sensors **2017**, 17, 1760; doi:10.3390/s17081760

for each test-substance was made and diluted to the desired concentrations with the solvents. The different dilutions were stored in dark glass jars at 4°C or − 20°C for genistein. After supernatant removal the cells were washed with 300 µL PBS (-Mg/-Ca) for the resazurin proliferation assay.

2.4. Resazurin proliferation assay

1x10^4 cells (in the linear range of the standard curve) were seeded per well to determine the proliferation of the cells in microtiter plates with 200 µL medium. After acclimatization, cells were treated with estradiol, tamoxifen, fulvestrant and three different EDCs. After 48 hrs of exposure the medium was aspirated and the cells were washed with 300 µL of PBS (-Mg/-Ca). 200 µL of fresh medium containing 2 mM Resazurin (Sigma- Aldrich, St. Louis, MO, USA) were added to the wells and incubated for five hrs. No-cell controls were included. The plates were wrapped in aluminium foil and incubated for 4 hrs in cell incubator at 37°C, 5 % CO2, 95 % humidity. Afterwards 150 µL aliquots of each sample and controls were transferred into white fluorescence measurement plates Falcon™ White Opaque 96-Well Tissue Culture Plates (Corning, Corning, NY, USA). Fluorescence signals were read at λex= 560 nm and λem= 590 nm on a plate reader.

2.5. Materials and reagents for the protein microarray

The proprietary ARChip Epoxy [26] was used as a protein microarray immobilization platform. Anti-human IL-6 (MQ2-13A5), recombinant IL-6 protein, biotinylated anti-human IL-6 (MQ2-39C3), as well as anti-human MCP-1 (5D3-F7), recombinant MCP-1, biotinylated anti-human MCP-1 (2H5) and recombinant IL-1ß for the stimulation of the cells were purchased from eBioscience (San Diego, CA, USA). Anti-human IL-8 (H8A5), anti-human CXCL10 (IP-10) (J036G3), anti-human Rantes (J047C5), recombinant protein IL-8, recombinant protein CXCL10 (IP-10), recombinant protein Rantes and the biotinylated anti-human IL-8 (E8N1), biotinylated anti-human CXCL10 (IP-10) (Poly5194), biotinylated anti-human Rantes (Poly5197) were obtained from Biolegend (San Diego, CA, USA). Human IGFBP-3 Antibody (E8N1), Recombinant Human IGFBP-3, Biotinylated Antihuman IGFBP-3, Antibody Human IGF-I, Mouse IgG1 (MAb56408), Recombinant Human IGF-I, CF Recombinant Human IL-11, Human IGF-I Biotinylated Affinity Purified PAb, Goat IgG, Monoclonal Anti-human IL-11 Antibody, Biotinylated Anti-human IL-11(22616), Anti hVEGF 165 (26503), Recombinant Human VEGF 165, VEGF Antibody anti-hVEGF biotinylated, Human Anti-hMMP-9 (36020), Recombinant Human MMP-9, Biotinylated Anti-human MMP-9 Antibody were obtained from R&D Systems (Minneapolis, MN, USA). Labelled streptavidin Dy647 was from Dyomics (Jena, TH, Germany). Polysorbate 20 (Tween 20), sodium deoxycholate, sodium chloride (NaCl), calcium chloride (CaCl) were purchased from Sigma (St. Louis, MO, USA). Phosphate buffered saline (PBS, pH 7.2, 10X) was from Thermo Fischer Scientific (Waltham, MA, USA) and Tris(hydroxymethyl)aminomethane (Tris) from AMRESCO (Cleveland, OH, USA).

2.6. Protein microarray fabrication, processing and scanning

The probes were diluted for spotting in sterile 1x PBS (pH 7.2) /0.01 % sodium deoxycholate to concentrations of 0.4 mg/mL for IL-6, IL-8, IL-11, CXCL10, Rantes, MCP-1, IGF-1, IGFBP-3, MMP-9 and 0.5 mg/mL for VEGF. The capture antibodies were arrayed in triplicates onto ARChip Epoxy with the Arrayit Nanoprint™ contact spotter (Arrayit corporation, Sunnyvale, CA, USA). Twelve identical arrays were spotted on each slide with a SMP3 pin at a relative humidity of 50 %. The spot-to-spot distance was 350 µm. To achieve immobilization of the probes, slides were stored at 4 °C for at least three days. The appropriate spotting conditions such as composition of print buffer, humidity during spotting and antibody concentration were established previously [27]. The blocking was performed in1× PBS (pH 7.2)/0.1 % Tween 20 for half an hour. After washing two times in 1x PBS (pH 7.2) the slides were dried with compressed air and mounted into the hybridization cassette (Arrayit Corporation, Sunnyvale, CA, USA) holding four slides and generating 4 × 12 separated arrays. For

Sensors **2017**, 17, 1760; doi:10.3390/s17081760

setting up calibration curves with at least ten standards for the quantitative assays, a dilution series of mixtures of all analytes in DMEM F12-BSA (minus insulin) was prepared. For an abbreviated procedure, only two to three calibration standards in the linear range and the zero standards were used. Nine replicates for each calibration point (three arrays with three replicate spots) were made which were distributed on different array fields on three slides. The standards and the cell culture samples (six biological each with three technical replicates) were incubated for 2.5 hrs. After washing three times with 1× PBS (pH 7.2)/0.1% Tween-20, slides were incubated for 45 min with 50 µL of biotinylated antibody mixtures in buffer J (100 mM TRIS, 100 mM NaCl, 10 mM $CaCl_2$ and 0.1 % Tween 20; pH 7.4) with final concentrations of 1 µg/mL each. Succeeding another washing cycle 2 µg/mL Dy647 streptavidin (in buffer J) was added. Slides were incubates for 45 min and washed two times with PBS-T, 2 times with 1x PBS, dried with compressed air and stored in the dark until scanning. All incubation steps were made at room temperature on a rotary shaker. The slides were measured at λex= 635 nm, λem= 670 nm at optimal photomultiplier tube (PMTs) voltages for each analyte with a confocal laser scanner (LS100, Tecan Group Ltd, Switzerland).

The cross reactivity of each single biomarker with all non-specific capture antibodies of the panel was analysed and calculated as ratio of unspecific to specific fluorescence signal in percent of concentration well within the linear range.

2.7. Statistical data analysis

Spot segmentation and data analysis of the arrays were made using GenePix® Pro 7.0 software (Molecular Devices, LLC Sunnyvale, CA, USA). Background corrected means signals were calculated from nine technical and six biological replicates for the cell culture samples. Data points that were out of mean signal values ± standard deviation (SD) were excluded. Standard curves were set up with OriginPro 8G using a four parameter fit; and bar graphs with Graph Pad Prism 5.0. Data were plotted with mean +/- standard error of mean (SEM). The limit of detection (LOD) was calculated mean zero concentration plus three SD for the limit of quantification (LOQ) plus ten SDs of the blank of the measured fluorescence intensities [28]. Recovery rates were calculated displaying the %-relation between calculated concentrations and expected concentrations. The proliferation values were calculated by averaging fluorescence signals of the non-cell control and subtract these values from each sample value. The fluorescent values of the samples were averaged and plotted as mean with SEM. Normal distribution of the data was tested with the Kolmogorov-Smirnov test. The data (stimulation experiment, proliferation) were log transformed (Y=Log(Y)) or baseline corrected (treatment dependent secretion experiments) to the medium control (C0) and statistical analyses were made using a one way ANOVA and Bonferroni multiple comparison test for alpha=0.05.

3. Results

3.1. Compilation of the biomarker panel

Based on literature we made an initial selection of 26 potentially interesting biomarkers with known estrogen dependent secretion, representing clues for reproductive and developmental toxicity or links to cancer and metabolic syndrome (as for instance: amphiregulin; ET-1; GCDFP-24 (PBCP); GCDFP-15 (PIP); MMP-2; PGE2; pS2 protein; SCF; TGF-ß; IL-18; Platelet-Derived Growth Factor (PDGF); EGF; endostatin; IGFBP-4). Markers such as endostatin, PDGF and human estrogen-induced protein pS2 had to be excluded as antibodies were either not commercially available or did not show activity in our assays. Ten biomarkers entered the final panel, including the cytokines Interleukin-6 (IL-6), IL-8 and IL-11, Vascular Endothelial Growth Factor (VEGF), Matrix Metalloproteinase-9 (MMP-9), Monocyte Chemotactic Protein-1 (MCP-1), Chemokine (C-C motif) Ligand 5 (CCL5, Rantes), C-X-C Motif Chemokine 10 (CXCL10, IP-10), Insulin-like Growth Factor-1 (IGF-1) and Insulin-like Growth Factor Binding Protein (IGFBP)-3.

Sensors **2017**, 17, 1760; doi:10.3390/s17081760

3.2. Assay performance in serum free cell culture medium

For the resulting panel of 10 biomarkers (IL-11, IL-6, IL-8, MCP-1, IGF-1, IGFBP-3, CXCL10, Rantes, MMP-9, VEGF) a multiplexed protein chip was developed, evaluating and optimizing the performance of antibody pairs, protein standards and assay reagents of the sandwich immunoassay (Calibration curves see Figure S1 in supplementary data). Sensitivity and specificity of assays processed in buffer were compared to those transferred to standard medium of MCF-7 cell culture, DMEM supplemented with 10 % FBS, and serum free/phenol-red free medium DMEM F-12. Sensitivity as expressed by the limit of detection was as good or even better in the standard cell culture medium compared to assay buffer. LOD of IL-6 for instance changed from 18 pg/mL in buffer to 9 pg/mL in DMEM/ 10 % FBS, whereas MCP-1 and IGF-1 showed only little impairment of the detection limit from 7 pg/mL and 115 pg/mL in buffer to 14 pg/mL and 125 pg/mL in DMEM/ 10 % FBS, respectively. Interestingly, processing the biomarker arrays in serum free cell culture medium revealed severe losses in sensitivity for IL-6, IL-11, MCP-1, Rantes and CXCL10. The signal intensities for IL-11 decreased by around 50 % from 48000 to 25000 A.U. and the LOD increased from 224 pg/mL to 3653 pg/mL compared to DMEM/ 10 % FBS. In addition, cross reactivity of VEGF antibodies, primarily against IGF-1 (58 %), occurred. Upon adding BSA solution in a final concentration of 10 mg/mL to the serum free medium we detected an up to 10 fold increase in sensitivity for IL-11, Rantes, CXCL10, and IL-6. In addition signal intensities for IL-11 and Rantes were improved by 25 to 36 % for the highest standard concentration in the assay. The cross reactivity seen for the biomarker VEGF to IGF-1 decreased by 77 %. Also recovery rates of IL-6, IL-11, Rantes, VEGF, IGF-1 and MMP-9 were improved (see Table 1). The system recovered the analytes within a range of 80 - 144 %, depending on the biomarker measured, for relevant concentrations within the working range of the assay. Typical working ranges of commercial ELISA kits for single biomarkers are reported in supplementary Table S1.

Table 1. Limit of detection (LOD), limit of quantification (LOQ), half maximal effective concentration (EC50), recovery rates, and coefficient of variation (CV) of sandwich assays for IL-6, IL-8, IL-11, MCP-1, CXCL10, Rantes, IGF-1, VEGF, MMP-9 and IGFBP-3 on the multiplexed chip platform in DMEM/F-12 cell culture medium supplemented with 10 mg/mL BSA. Data of LOD, LOQ and EC50 are shown as mean +/- SEM of three experiments. The coefficient of variation is calculated as mean of eleven standards of three experiments. The recovery rate is given for a spiked concentration within the linear range of the curves.

Biomarker	LOD [pg/mL]	LOQ [pg/mL]	EC50 [pg/mL]	Recovery Rate [%]	CV [%]
MCP-1 (CCL2)	4 +/- 2	16 +/- 7	2431+/- 1668	83	14
IL-6	5 +/- 2	16 +/- 6	3916 +/- 1155	132	13
Rantes (CCL5)	16 +/- 7	46 +/- 21	4400 +/- 1841	144	11
VEGF	20 +/- 12	61 +/- 25	3923 +/- 938	131	15
IL-8	53 +/- 17	196 +/- 97	3216 +/- 678	80	22
CXCL10 (IP-10)	91 +/- 24	321+/- 119	7852 +/- 2275	116	19
IL-11	157 +/- 26	530 +/- 199	26330 +/-13022	105	13
IGFBP-3	581 +/- 254	1630 +/- 477	30644 +/- 3011	104	17
MMP-9	669 +/- 197	2035 +/- 447	49071+/- 7070	118	19
IGF-1	803 +/- 122	2553 +/- 453	39523 +/- 10874	87	15

3.3. Quantification of biomarker secretion in cell culture supernatant

For a successful quantification, the working range of the chip (see Table 1 and Figure S1 in supplementary data) needs to cover the biomarker concentrations secreted by MCF-7 cells. MMP-9, VEGF, IGFBP-3, IL-8, IL-11, IGF-1 and Rantes could be detected with sufficient sensitivity with the chip, albeit IL-8 and Rantes were secreted only in the low pg/mL range and hence difficult to quantify. Secretion of CXCL10, MCP-1 and IL-6 was below the LOD of their respective standard curves. Since it

Sensors **2017**, 17, 1760; doi:10.3390/s17081760

is known that MCF-7 cells are able to increase secretion of proteins by stimulation with cytokines or growth factors, we tested various stimulants in order to shift secretion of biomarkers to higher concentration levels, fitting better the sensitivity of the chip. The concentrations considered for stimulation were deduced from literature and from specifications on the biological activity provided by the supplier [29–32]. After separate stimulation of MCF-7 cells with either 10 ng/mL TNF-α, 50 ng/mL IL-1α, 10 ng/mL IL-1β, 50 ng/mL IGF-1, 10 ng/mL IFN-γ or 50 ng/mL MCP-1 for 24 to 48 hours all biomarkers were secreted at levels matching the measuring range of the chip. In Figure 2 secretion of low abundant markers is shown without (C0) and with stimulation. Fresh medium without cells and devoid of proteins of the panel was used as zero standard (S0), medium spiked with a 7.7 ng/mL (a concentration in the linear range of the standard curves) biomarker standard as positive control (S1), and medium with cells (C0) as control for a successful stimulation. Particularly stimulation with IL-1α, IL-1β and TNF-α resulted in up to one log higher expression of the analytes compared to the other stimulants and no stimulation. Especially IL-1ß stimulation yielded highest signals, notably for IL-6, IL-8, Rantes, MCP-1 and CXCL10, markers which could not be detected or only in low quantities without stimulation. Consequently, for the experimental set up, in parallel to untreated MCF-7 cells, stimulation with IL-1ß and accumulation of the secretion products over 48 hours was chosen. In following experiments we could quantify nine of the ten biomarkers at concentrations ≥ 50 pg/mL after 48 hrs of cell culture stimulation. Only IGF-1 secretion was falling below the detection limit upon treatment with receptor agonists.

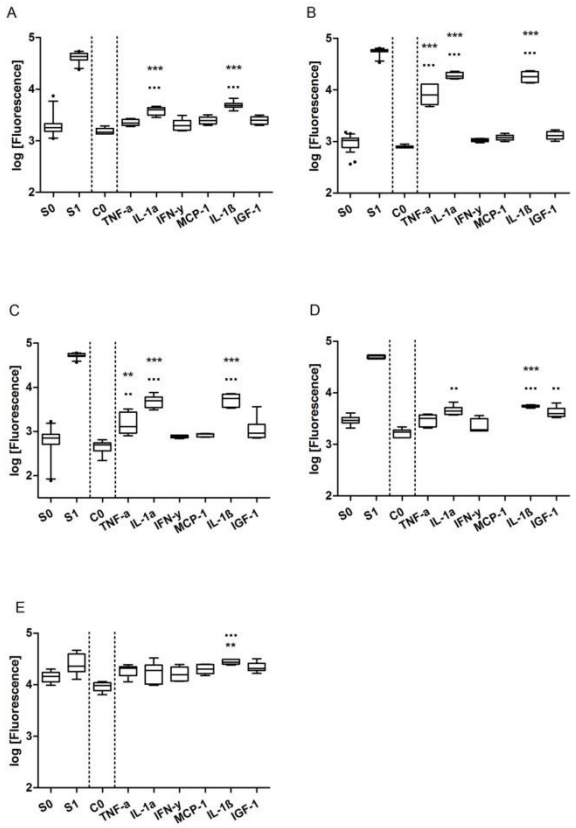

Figure 2. Secretion of IL-8 (A), Rantes (B), IL-6 (C), MCP-1 (D) and CXCL10 (E) after stimulation with IGF-1, MCP-1, IL-1a, IL-1ß, TNF-a and IFN-y. Log of the fluorescence intensities [A.U.] of two standards (without cells) S0 and S1 and the medium control (with cells) C0 without stimulation as well as stimulated cells. Box plots are shown with 5 and 95 quartile. Significance was tested for stimulation (n = 6) against the zero standard S0 (*) and the medium control C0 (▪) for alpha=0.05 using a 1-way-ANOVA and Bonferroni multiple comparison post-hoc test (p≤=0.05(*), p≤=0.01(**), p≤=0.001(***)).

Sensors **2017**, 17, 1760; doi:10.3390/s17081760

3.4. Effect of solvents on biomarker secretion and cell proliferation

Hormones such as estradiol and estrogen like substances are hydrophobic compounds and hence ask for an organic solvent rather than water or cell medium. Clearly, it has to be tested if the vehicles in which the substances are dissolved have an influence on outcome and interpretation of cell experiments. For hormones and xenobiotics tested herein, ethanol (EtOH) and DMSO are suitable solvents. We used the evaluation of those two solvents as a first show case for the utility of the biomarker chip. As reference a proliferation assay was employed, based on fluorescence detection through the biochemical conversion of resazurin to the fluorescent resofurin.

Effects of 0.1% EtOH and 0.1% DMSO on MCF-7 proliferation and biomarker expression were tested in both, DMEM/ 10 % FBS and DMEM F-12. The secretion of biomarkers VEGF, Rantes, IL-6 and IGFBP-3 increased after treatment with 0.1 % EtOH, suggesting direct stimulation of their expression, while neither MMP-9 expression nor the other markers were affected. The strongest upregulation was seen for Rantes of about 34 % compared to the medium control (see Figure 3 B). Also cell proliferation in serum-supplemented cell culture with 0.1 % EtOH compared to medium control increased, while serum free cell cultures were not significantly affected. Experiments with 0.1 % DMSO, a concentration also reported in literature as not cytotoxic [(Jamalzadeh et al., 2016)], showed no significant effect on the proliferation and secretion compared to the medium control after 48 hours and was used in the following experiments for dissolving test substances.

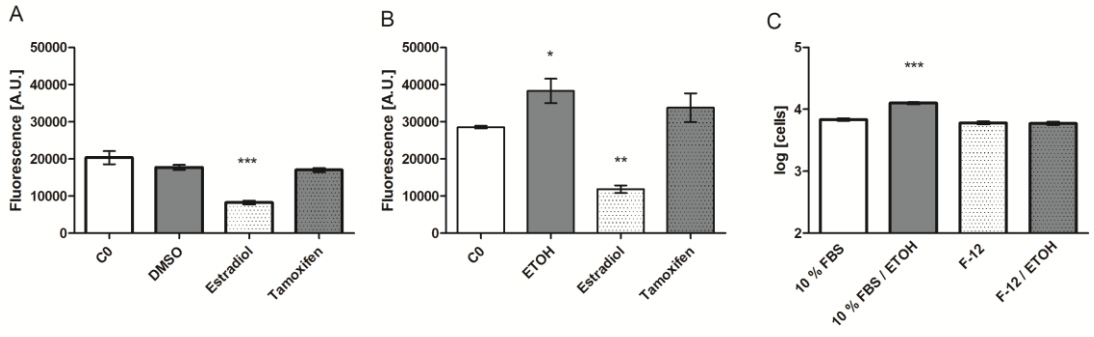

Figure 3. Secretion of the biomarker Rantes in IL-1ß stimulated cells challenged with solvents (A) 0.1% DMSO and (B) 0.1% EtOH compared to untreated cells (C0), and estrogen receptor agonist (estradiol) and antagonist (tamoxifen) treatment. (C) Proliferation of MCF-7 cells in standard medium and serum free/phenol red free medium with and without 0.1% EtOH. Proliferation data are log transformed. Bar graphs are plotted as mean with +/- SEM. Significance was tested (n= 5 (A, B); n= 4-8 (C)) against the C0 control with a one way ANOVA and a Bonferroni multiple comparison test for alpha=0.05 ($p \leq 0.5$ (*), $p \leq 0.01$ (**), $p \leq 0.001$ (***)).

3.5. Specific biomarker secretion patterns and proliferative effect of ER agonists and antagonists

MCF-7 cells were exposed to 1 µM nonylphenol, bisphenol A and genistein, known estrogen receptor agonists, for 48 hours. As positive controls for estrogenic action 1 nM 17ß-estradiol, the most affine endogen ligand of the estrogen receptor, and for anti-estrogenic action 1 nM tamoxifen (in breast tissue) and 10 nM fulvestrant were employed. These concentrations were chosen according to maximal response they showed in proliferative assays without being cytotoxic [(Payne et al., 2000; Soto et al., 1995; van Meeuwen et al., 2007; Wetherill et al., 2007)]. Nuclear receptors act as transcription factors and are switched on and off by agonistic and antagonistic ligands, respectively (Figure 4(A) and (B)). An increase in proliferation after treatment with estrogen receptor agonists, particularly agonists to the receptor isoform ERα, was expected compared to the antagonists. With and without IL-1ß stimulation nonylphenol showed the same proliferative effect as estradiol, bisphenol A reduced it by half, while genistein evoked 50 % more response without stimulation (Figure 4).

Sensors **2017**, 17, 1760; doi:10.3390/s17081760

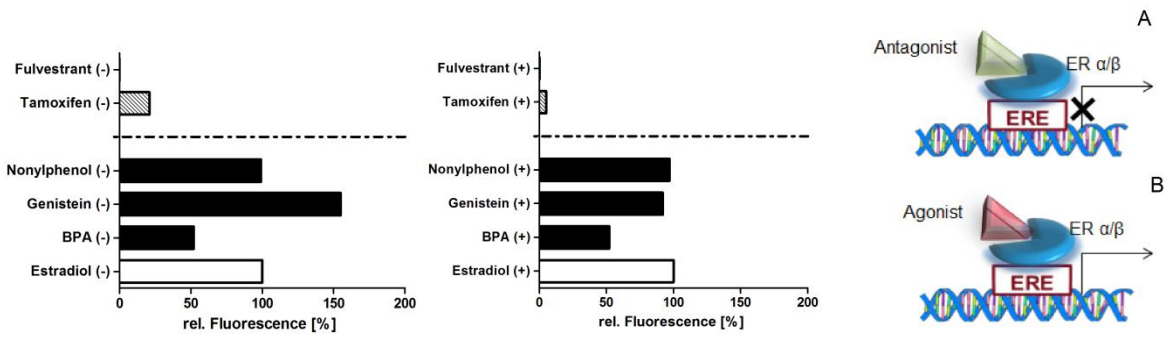

Figure 4. Proliferative effect of MCF-7 cells after treatment with the agonists estradiol, bisphenol A (BPA), genistein and nonylphenol and the antagonists tamoxifen and fulvestrant of the estrogen receptor left graph without (-) and right graph with IL-1ß stimulation (+). The binding of agonists (B) to the estrogen receptor results in proliferation of the cells while the antagonistic (A) action inhibits the proliferation. Data (n = 6) are baseline corrected to the estradiol treatment and the medium control and plotted as relative fluorescence.

Figure 5 depicts the biomarkers which resulted in a specific secretion upon exposure to tested estrogens and anti-estrogens. Without stimulation VEGF and MMP-9 exhibited significant differences in cells challenged with fulvestrant compared to estrogen receptor agonists, however no differential response to agonists and antagonists with stimulation was found. Other biomarkers showed distinct expression patterns upon treatment with agonists and antagonists also when cells were grown in presence of IL-1ß. Relative expression of IL-6, IL-8, Rantes and MCP-1 was significantly lower for estradiol, nonylphenol and genistein compared to tamoxifen and fulvestrant, the effect of bisphenol A was less prominent. IGFBP-3 was downregulated after estradiol, bisphenol A and nonylphenol exposure while genistein treatment resulted in similar secretion like fulvestrant after IL-1ß stimulation. Next to IGFBP-3 only MMP-9 and IL-11 were upregulated compared to the medium control when challenged with endocrine active substances while the other biomarkers were expressed in lower levels. Table 2. summarizes these results, showing the relative expression of markers translated into a colour code.

Table 2. Colour coded biomarker secretion patterns. MCF-7 cells (stimulated + , non-stimulated -) challenged with tamoxifen, fulvestrant, estradiol, genistein, bisphenol A, and nonylphenol and marker expression quantified with the chip relative to untreated cells (%). Colours are graded in steps of 20%.

	Tamoxifen	Fulvestrant	Estradiol	Genistein	BPA	Nonylphenol
MMP-9 -	102	73	105	89	124	131
VEGF -	122	50	201	98	147	142
IGFBP-3	133	213	130	190	145	136
IL-6 +	68	126	15	20	38	30
IL-8 +	47	78	17	23	20	31
MCP-1 +	51	47	24	28	30	31
Rantes +	62	88	21	17	37	30
CXCL-10	38	38	59	54	28	83
IL-11 +	139	328	192	268	295	198
IGF-1 +	n.a.	n.a.	n.a.	n.a.	n.a.	n.a.

Colour code

<30 %	31-50 %	51-70 %	71-90 %	91-110 %	111-130 %	131-150 %	>150 %

Sensors **2017**, 17, 1760; doi:10.3390/s17081760

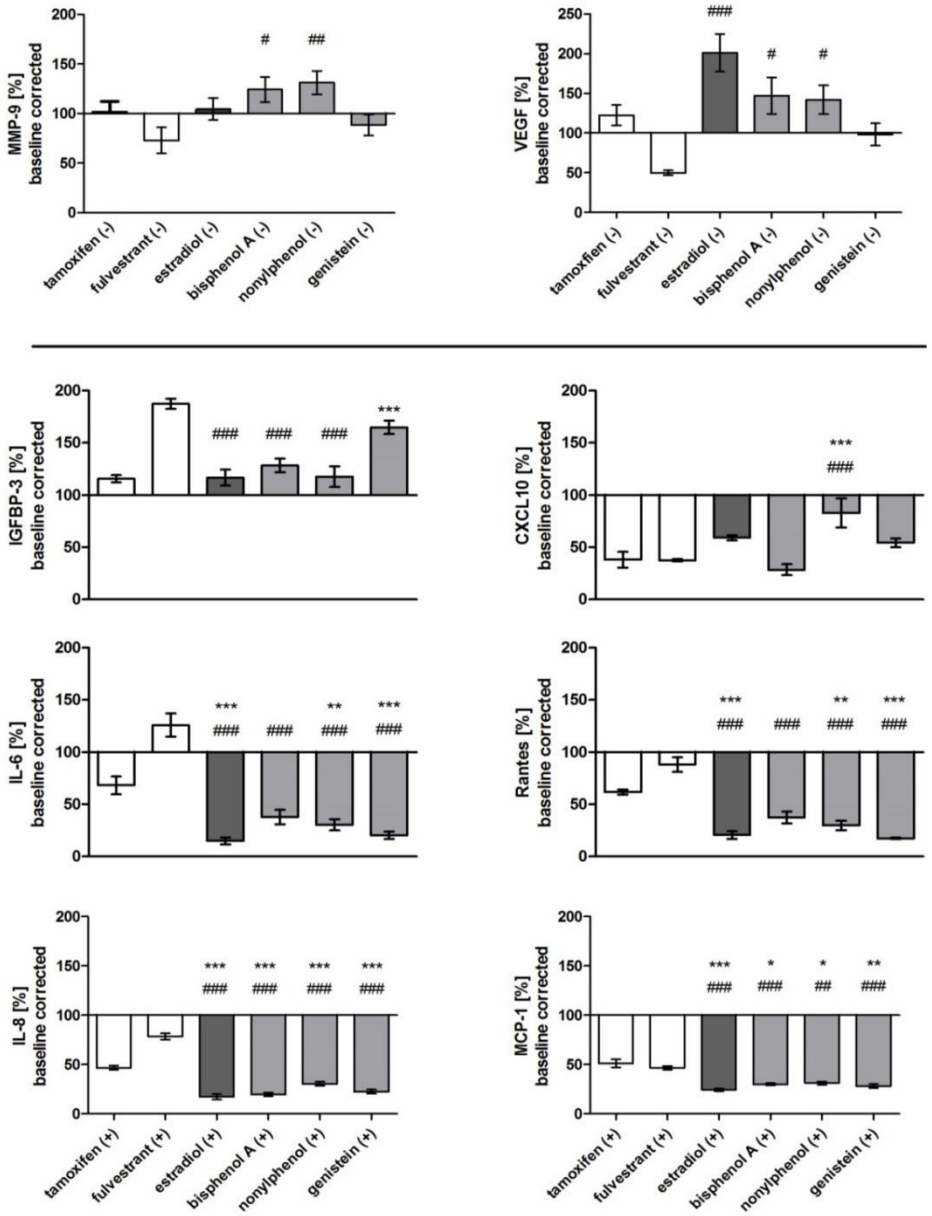

Figure 5. Relative secretion of MMP-9, VEGF, IGFBP-3, CXCL10, IL-6, Rantes, IL-8 and MCP-1 after exposure to estrogen receptor agonists (estradiol, BPA, nonylphenol, genistein) and antagonists (fulvestrant, tamoxifen) without (-) or with (+) stimulation by IL-1ß after 48 hours. Data are baseline corrected and plotted as mean +/- SEM in percent to the C0 control. Significance against tamoxifen (*) and fulvestrant (#) was tested for n= 6 using a 1-way-ANOVA and a Bonferroni multiple comparison post-hoc test for alpha=0.05 (($p \leq 0.05$(*), $p \leq 0.01$(**), $p \leq 0.001$(***)).

4. Discussion

The fluorescence based multi-analyte chip platform for the analysis of estrogenic and anti-estrogenic substances is a new *in vitro* tool for high throughput screening of environmental samples. In contrast to existing tools the chip investigates the complex action of xenoestrogens in a human cell model by characterizing protein expression. It allows quantification of 10 proteins secreted by MCF-7 cells, representing various biological and pathological endpoints of endocrine action and distinguishing estrogen or anti-estrogen dependent secretion of proteins. Biomarkers IL-6 and IL-8,

Sensors **2017**, 17, 1760; doi:10.3390/s17081760

VEGF, MMP-9, MCP-1, IL-11, IGF-1 and Rantes are associated with different stages of cancer. MCP-1 and IL-11 are stimulators within the development and progression of breast cancer while IL-6 takes part in survival, proliferation and cell migration processes [(Chiu et al., 1996; Johnstone et al., 2015; Schafer and Brugge, 2007; Soria and Ben-Baruch, 2008)]. IL-8 as well as VEGF are involved in tumour angiogenesis, metastasis in breast cancer, MMP-9 is related to degradation of the extracellular matrix and tumour cell invasion [41-44]. Co-expression of Rantes, the main inducer of cell invasion, and MCP-1 is related to advanced stages of cancer [38]. In contrast, CXCL10 and IGFBP-3 were shown to have anti-malignant properties by anti-angiogenic action or inhibition of breast cancer cell proliferation [(Cardona et al., 2013; Colston et al., 1998; Goldberg-Bittman et al., 2004)7]. IGF-1 has a main role in cell proliferation and development and is additionally involved in the pathology of adipositas, diabetes mellitus and hypertriglyceridemia, factors of the metabolic syndrome; secretion is stimulated via growth hormones like estradiol [(Dupont and Le Roith, 2001; Lorincz and Sukumar, 2006)9]. IGFBP-3 is the main IGF transport protein and its expression correlates with the estrogen receptor status [50,51]. The biomarker IL-6 is able to stimulate the aromatase secretion and thereby the estrogen biosynthesis. In addition elevated expression was seen for IL-6 in adipose tissue in connection to obesity and insulin resistance [48]. In contrast the multifunctional cytokine IL-11 acts as an effective inhibitor of adipogenesis, one of the factors of the metabolic syndrome [52]. Next to IGF-1 also MCP-1, IL-8, VEGF, MMP-9, Rantes, IL-6 and IGFBP-3 are up- or down-regulated after treatment with estrogen or estrogen like substances [(Bendrik and Dabrosin, 2009; Chrzan and Bradford, 2007; Dubois et al., 1995; Garvin et al., 2005; Inadera et al., 2000; Kanda and Watanabe, 2003; Nilsson et al., 2007)6]. MCP-1, Rantes, IGF-1 and IL-8 are additionally involved in developmental or reproductive processes such as menstruation, pregnancy and endometriosis [(Hull and Harvey, 2014; Kayisli et al., 2002)8]. The role of the selected biomarkers in different physiological processes such as cell development, reproduction, cancer and metabolic syndrome makes the chip an excellent tool for either indicating endocrine disrupting effects in food and environmental samples or for screening new xenoestrogens and their additive or synergistic effects on a cellular and molecular level. Further, the microarray can easily be extended with additional markers, if reagents of adequate quality become available.

Multiplexed on-chip sandwich immunoassays with fluorescent read-out were chosen because the highly parallel, miniaturized format of the chip outperforms conventional bioanalytical techniques in screening applications. Apart from antibody quality, interferences from the sample matrix are likely to affect sensitivity, specificity and reproducibility of immunoassays. In our biomarker chip no sample preparation step of cell supernatants is intended in order to keep the experimental set-up simple and protein expression unbiased. Due to the generally low abundance of the targeted proteins, dilution of the sample is not an option. The drop in assay performance upon changing the matrix from DMEM/ 10% FBS to DMEM F-12 can be explained by the absence of serum proteins from fetal serum in the latter one. Serum albumins such as BSA or HSA, as part of the natural environment of antibodies, are known to minimize or even prevent non-specific binding, to increase signal intensities, to ensure specificity and to stabilize the biomolecules immobilized to the surface [59,60]. Nevertheless, for markers IL-6, IL-8, Rantes, MCP-1 and CXCL10, known to be secreted in vitro in low quantities by MCF-7 cells [29,32,39,45,54] sensitivity of the chip was not sufficient for a reliable detection in the low pg/mL range (see Table 1). Stimulation of MCF-7 cells with cytokines and growth factors, most effectively with interleukin-1ß, mimicking biological processes such as inflammation, promoted secretion to measureable levels for very low abundant biomarkers (Figure 2). There is evidence suggesting that IL-1ß in combination with genistein and fulvestrant showed additive effects for IL-11, IGFBP-3 and MMP-9 and that treatment with BPA and IL-1ß even resulted in synergistic effects, probably due to positive feedback loops within the cells. Further experiments would be needed to decide whether there are additive or synergistic effects of IL-1ß and the estrogen receptor agonists and antagonists.

Sensors **2017**, 17, 1760; doi:10.3390/s17081760

The proliferation of MCF-7 cells is regulated via hormones. Therefore they are used in validated toxicological methods such as the E-Screen to detect estrogen like activity of xenobiotics compared to estradiol via proliferation measurements [15]. Hormone regulated proliferation of MCF-7 cells evaluated by means of fluorescence measurements using the conversion of resazurin to resofurin was therefore used as a reference for our chip experiments. We found more prominent differences in proliferation without IL-1ß stimulation, especially with genistein. Increased proliferation upon challenging cells with genistein was also found in [61]. Bisphenol A showed only half of the effect compared to estradiol. Such differences in proliferation were also detected with the EScreen developed by Soto et al. [15]. They described nonylphenol with a relative proliferative effect of 100 % as a full agonist of the estrogen receptor while Bisphenol A showed only 85 % [62]. Antagonists, fulvestrant and tamoxifen were below 30 % compared to estradiol, but still showed a proliferative response. After stimulation with IL-1ß not only the proliferative effect of genistein was decreased to the level of estradiol, also tamoxifen showed a drop in proliferation (Figure 4).

Both tools, the proliferation assay and the chip, were employed for testing the effects of organic solvents, which may be a necessary vehicle to introduce the test substances in the cell culture medium. Ethanol was described as less cytotoxic compared to DMSO, which showed low cytotoxicity in concentrations above 0.5 % [33]. Nevertheless we detected an increase of cell proliferation in serum-supplemented cell culture with 0.1 % EtOH compared to the medium control, but not in the serum-free and phenol-red free medium (see Figure 3C). A possible explanation might be an additive effect of weak estrogenic phenol red and ethanol. Our results are supported by Etique et al. [63], showing an enhanced proliferation of MCF-7 cells especially in the presence of low concentrations of EtOH. EtOH was described to directly affect the expression of MMP-9 especially at concentrations ≥ 0.3 % [64] and it significantly stimulated the ER alpha activity in a dose dependent manner [65]. However, we did not detect any effects on the secretion of MMP-9 related to 0.1 % EtOH, but on VEGF, Rantes, IL-6 and IGFBP-3. Based on literature and our own data we concluded that the experimental background error by EtOH is higher compared to DMSO at low concentrations and that ≤ 0.1 % DMSO should be the preferred solvent for sample preparation. The system was validated by exposing MCF-7 cells to well-known estrogen like endocrine disruptors resulting in obviously related secretion patterns (Table 2) and proliferation as estradiol treated cells. The biomarker patterns resulting from treatments with the antagonist fulvestrant and with estradiol were clearly distinctive. Anti-estrogens can have agonistic as well as antagonistic effects on MCF-7 cell proliferation in estrogen lacking conditions. Especially tamoxifen was mentioned to show agonistic effects in low concentrations [66]. The biomarker expression pattern of tamoxifen stands out from the one of fulvestrant treated cells and supports this finding.

Especially IL-6, IL-8, MCP-1, and Rantes, showed significantly downregulated expression for all estrogen active substances compared to the full antagonist fulvestrant while the other biomarkers featured a more diverse secretion (Figure 5 and Table 2). Genistein is able to induce the downregulation of the ERα mRNA and protein levels which would explain a similar secretion especially of MMP-9, VEGF and IGFBP-3 following fulvestrant treatment [67]. The selective estrogen receptor antagonist fulvestrant accelerates the degradation of the estrogen receptor too [68]. Furthermore it is reported that the phytoestrogen genistein can bind to both isoforms of the estrogen receptor ERα and ERβ with a high affinity, which also could explain differences in secretion and proliferation.

Additional screening of estrogen receptor agonists and antagonists with graded binding affinities, in varied concentrations and treatments, for different time periods, will be necessary to refine the specific secretion patterns and gain a comprehensive and differentiated understanding of EDCs mode of action. Further, the chip can be employed for elucidating protein secretion within disease development or involvement in processes such as steroid synthesis. An extension of the system offers various options, which can further promote the biomarker chip as new tool for the detection and

Sensors **2017**, 17, 1760; doi:10.3390/s17081760

characterization of endocrine action: adding more biomarkers; integration of other human cell lines; applying 3D cell culture in order to be closer to in vivo conditions; co-cultures with e.g. fibroblasts; or the use of primary cells.

Supplementary Materials: The following are available online at www.mdpi.com/link, Figure S1: Standard curves of CXCL10, IGF-1, IL-6, VEGF, IL-8, Rantes, IL-11, MCP-1, IGFBP-3 and MMP-9 generated with 11 standards using serum free cell culture medium as matrix. Table S1. Typical working ranges of standard ELISA kits for single biomarkers in microtiter plate format.

Acknowledgments: This work has been financially supported by the FP7 European Commission Marie Curie Initial Training Network SAMOSS (FP7-PEOPLE-2013-ITN, 607590). We thank P.P.F.M.A. Mulder from the University of Groningen for proofreading of the manuscript.

Author Contributions: U.S. C.P. and K.G. conceived and designed the experiments; K.G. performed the experiments and analyzed the data; K.G. and U.S. wrote the paper.

Conflicts of Interest: "The authors declare no conflict of interest."

References

1. Damstra, T.; Barlow, S.; Bergman, A.; Kavlock, R.; Van Der Kraak, G. Global assessment of the state-of-the-science of endocrine disruptors. *WHOpublication* **2002,** no. WHO/PCS/EDC/02.2 180.
2. Rochester, J.R. Bisphenol A and human health: A review of the literature. *Reprod Toxicol* **2013,** *42*, 132-155, doi:10.1016/j.reprotox.2013.08.008.
3. Casals-Casas, C.; Desvergne, B. Endocrine Disruptors: From Endocrine to Metabolic Disruption. *Annu Rev Physiol* **2011**, *73*, 135–62, doi:10.1146/annurev-physiol-012110-142200.
4. Mnif, W.; Hassine, A.I.H.; Bouaziz, A.; Bartegi, A.; Thomas, O.; Roig, B. Effect of endocrine disruptor pesticides: A review. *Int J Environ Res Public Health* **2011**, *8*, 2265-2303, doi:10.3390/ijerph8062265.
5. Patisaul, H.B.; Adewale, H.B. Long-term effects of environmental endocrine disruptors on reproductive physiology and behavior. *Front Behav Neurosci* **2009**, *3*, 10, doi:10.3389/neuro.08.010.2009
6. Yang, O.; Kim, H.L.; Weon, J.-I.; Seo, Y.R. Endocrine-disrupting Chemicals: Review of Toxicological Mechanisms Using Molecular Pathway Analysis. *J Cancer Prev* **2015**, *20*, 12–24, doi:10.15430/JCP.2015.20.1.12.
7. Melnick, R.; Lucier, G.; Wolfe, M.; Hall, R.; Stancel, G.; Prins, G.; Gallo, M.; Reuhl, K.; Ho, S.M.; Brown, T.; Moore, J.; Leakey, J.; Haseman, J.; Kohn, M. Summary of the National Toxicology Program's report of the endocrine disruptors low-dose peer review. *Environ Health Perspect* **2002**, *110*, 427–431, doi:sc271_5_1835 [pii].
8. Vandenberg, L.N.; Colborn, T.; Hayes, T.B.; Heindel, J.J.; Jacobs, D.R.; Lee, D.H.; Soto, A.M.; Saal, F.S.; Welshons, W.V.; Zoeller, R.T.; Myers, J.P.; Hormones and Endocrine - Disrupting Chemicals : Low - Dose Effects and Nonmonotonic Dose Responses. *Endocr Rev* **2014**, *33*, 378–455, doi:10.1210/er.2011.
9. Payne, J.; Rajapakse, N.; Wilkins, M.; Kortenkamp, A. Prediction and assessment of the effects of mixtures of four xenoestrogens. *Environ Health Perspect* **2000**, *108*, 983–987. doi:10.1289/ehp.00108983.
10. Rajapakse, N.; Silva, E.; Kortenkamp, A. Combining xenoestrogens at levels below individual no-observed-effect concentrations dramatically enhances steroid hormone action. *Environ Health Perspect* **2002**, *110*, 917–921, doi:10.1289/ehp.02110917.
11. Gore, A.C.; Chappell, V.A.; Fenton, S.E.; Flaws, J.A.; Nadal, A.; Prins, G.S.; Toppari, J.; Zoeller, R.T. Executive Summary to EDC-2: The Endocrine Society's second Scientific Statement on endocrine-disrupting chemicals. *Endocr Rev* **2015**, *36*, E1-E150, doi:10.1210/er.2015-1093.
12. Routledge, E.J.; Sumpter, J.P. Estrogenic activity of surfactants and some of their degradation products assessed using a recombinant yeast screen. *Environ Toxicol Chem* **1996**, *15*, 241–248, doi:10.1002/etc.5620150303.
13. Seifert, M.; Haindl, S.; Hock, B. Development of an enzyme linked receptor assay (ELRA) for estrogens and xenoestrogens. *Anal Chim Acta* **1999**, *386*, 191–199, doi:10.1016/S0003-2670(99)00044-6.
14. van der Burg, B.; Winter, R.; Weimer, M.; Berckmans, P.; Suzuki, G.; Gijsbers, L.; Jonas, A.; van der Linden, S.; Witters, H.; Aarts, J.; Legler, J.; Kopp-Schneider, A.; Bremer, S. Optimization and prevalidation of the in

vitro ERα CALUX method to test estrogenic and antiestrogenic activity of compounds. *Reprod Toxicol* **2010**, *30*, 73–80. doi:10.1016/j.reprotox.2010.04.007.

15. Soto, A.M.; Sonnenschein, C.; Chung, K.L.; Fernandez, M.F.; Olea, N.; Olea Serrano, F. The E-SCREEN assay as a tool to identify estrogens: An update on estrogenic environmental pollutants. *Environ Health Perspect* **1995**, *103(Suppl 7)*, 113–122, doi:10.1289/ehp.95103s7113
16. Francois, E.; Wang, D.Y.; Fulthorpe, R.; Liss, S.N.; Edwards, E.A. DNA microarrays for detecting endocrine-disrupting compounds. *Biotechnol Adv* **2003**, *22*, 17–26, doi:10.1016/j.biotechadv.2003.08.005.
17. Sumpter, J.P.; Jobling, S. Vitellogenesis as a biomarker for estrogenic contamination of the aquatic environment. *Environ Health Perspect* **1995**, *103*, 173–178, doi:10.1289/ehp.95103s7173.
18. Hecker, M.; Giesy, J.P. Novel trends in endocrine disruptor testing: The H295R Steroidogenesis Assay for identification of inducers and inhibitors of hormone production. *Anal Bioanal Chem* **2008**, *390*, 287–291, doi:10.1007/s00216-007-1657-5.
19. Kiyama, R.; Wada-Kiyama, Y. Estrogenic endocrine disruptors: Molecular mechanisms of action. *Env Int* **2015**, *83*, 11–40. doi:10.1016/j.envint.2015.05.012.
20. Bovee, T.F.H.; Hoogenboom, L.A.P.; Thomson, B.M. Bioassays for the detection of hormonal activities. In *Endocrine-Disrupting Chemicals in Food*; Shaw, I, ed.; Publisher: Woodhead Publishing Limited, UK, 2009; pp. 259-280, ISBN 9781845692186.
21. De Paoli, M.; Gogalic, S.; Sauer, U.; Preininger, C.; Pandha, H.; Simpson, G.; Horvath, A.; Marquette, C. Multiplatform Biomarker Discovery for Bladder Cancer Recurrence Diagnosis. *Dis Markers* **2016**, 2016:4591910, doi:10.1155/2016/4591910.
22. Buchegger, P.; Sauer, U.; Toth-Székély, H.; Preininger, C. Miniaturized protein microarray with internal calibration as point-of-care device for diagnosis of neonatal sepsis. *Sensors* **2012**, *12*, 1494–1508, doi:10.3390/s120201494.
23. Sanjay, S.T.; Fu, G.; Dou, M.; Xu, F.; Liu, R.; Qi, H.; Li, XJ. Biomarker detection for disease diagnosis using cost-effective microfluidic platforms, *Analyst* **2015**, *140*, 7062-7081, doi: 10.1021/acsnano.5b07939.
24. Piraino, F.; Volpetti, F.; Watson, C.; Maerkl, S.J. A digital-analog microfluidic platform for patient-centric multiplexed biomarker diagnostics of ultralow volume samples. *ACSnano*, **2016**, *10*, 1699-1710, doi: 10.1021/acsnano.5b07939.
25. Gogalic, S.; Sauer, U.; Doppler, S.; Heinzel, A.; Perco, P.; Lukas, A.; Simpson, G.; Pandha, H.; Horvath, A.; Preininger, C. Validation of a protein panel for the non-invasive detection of recurrent non-muscle invasive bladder cancer. *Biomarkers* **2017**, Jan 19: 1-8, doi:10.1080/1354750X.2016.1276628.
26. Preininger, C.;Bodrossy, L.; Sauer, U.; Pichler, R.; Weilharter, A. ARChip Epoxy and ARChip UV for covalent on-chip immobilization of pmoA gene-specific oligonucleotides. *Anal Biochem* **2004**, *330*, 29–36, doi:10.1016/j.ab.2003.12.037.
27. Domnanich, P.; Sauer, U.; Pultar, J.; Preininger, C. Protein microarray for the analysis of human melanoma biomarkers. *Sensor Actuator, B Chem* **2009**, *139*, 2–8, doi:10.1016/j.snb.2008.06.043.
28. MacDougall, D.; Crummett, W.B. Guidelines for data acquisition and data quality evaluation in environmental chemistry. *Anal Chem* **1980**, *52*, 2242–2249, doi:10.1021/ac50064a004.
29. Freund, A.; Jolivel, V.; Durand, S.; Kersual, N.; Chalbos, D.; Chavey, C.; Vignon, F.; Lazennec, G. Mechanisms underlying differential expression of interleukin-8 in breast cancer cells. *Oncogene* **2004**, *23*, 6105–14, doi:10.1038/sj.onc.1207815.
30. Hollingshead, B.D.; Beischlag, T.V.; DiNatale, B.C.; Ramadoss, P.; Perdew, G.H. Inflammatory signaling and aryl hydrocarbon receptor mediate synergistic induction of interleukin 6 in MCF-7 cells. *Cancer Res* **2008**, *68*, 3609–3617, doi:10.1158/0008-5472.CAN-07-6168.
31. Bronger, H.; Kraeft, S.; Schwarz-Boeger, U.; Cerny, C.; Stöckel, A.; Avril, S.; Kiechle, M.; Schmitt, M. Modulation of CXCR3 ligand secretion by prostaglandin E2 and cyclooxygenase inhibitors in human breast cancer. *Breast Cancer Res* **2012**, *14*, R30, doi:10.1186/bcr3115.
32. Mira, E.; Lacalle, R.A.; González, M.A.; Gómez-Moutón, C.; Abad, J.L.; Bernad, A.; Martínez, C.; Santos, M. A role for chemokine receptor transactivation in growth factor signaling. *EMBO Rep* **2001,** *2*, 151–156, doi:10.1093/embo-reports/kve027.

33. Jamalzadeh, L.; Ghafoori, H.; Sariri, R.; Rabuti, H.; Nasirzade, J.; Hasani, H.; Aghamaali, M.R. Cytotoxic Effects of Some Common Organic Solvents on MCF-7, RAW-264.7 and Human Umbilical Vein Endothelial Cells. *Avicenna J Med Biochem* **2016,** *4*, 1–6, doi:10.17795/ajmb-33453.Research.
34. Wetherill, Y.B.; Akingbemi, B.T.; Kanno, J.; McLachlan, J.A.; Nadal, A.; Sonnenschein, C.; Watson, C.S.; Zoeller, R.T.; Belcher, S.M. *In vitro* molecular mechanisms of bisphenol A action. *Reprod Toxicol* **2007,** *24*, 178-98, doi:10.1016/j.reprotox.2007.05.010
35. Payne, J.; Jones, C.; Lakhani, S.; Kortenkamp, A. Improving the reproducibility of the MCF-7 cell proliferation assay for the detection of xenoestrogens. *Sci Total Environ* **2000**, *248*, 51–62, doi:10.1016/S0048-9697(99)00479-9.
36. van Meeuwen, J.A.; ter Burg, W.; Piersma, A.H.; van den Berg, M.; Sanderson, J.T. Mixture effects of estrogenic compounds on proliferation and pS2 expression of MCF-7 human breast cancer cells. *Food Chem Toxicol* **2007**, *45*, 2319–2330, doi:10.1016/j.fct.2007.06.011.
37. Johnstone, C.N.; Chand, A.; Putoczki, T.L.; Ernst, M. Emerging roles for IL-11 signaling in cancer development and progression: focus on breast cancer. *Cytokine Growth Factor Rev* **2015**, *26*, 489–498, doi:10.1016/j.cytogfr.2015.07.015.
38. Soria, G.; Ben-Baruch, A. The inflammatory chemokines CCL2 and CCL5 in breast cancer. *Cancer Lett* **2008**, *267*, 271-85, doi:10.1016/j.canlet.2008.03.018
39. Chiu, J.J.; Sgagias, M.K.; Cowan, K.H. Interleukin 6 acts as a paracrine growth factor in human mammary carcinoma cell lines. *Clin Cancer Res* **1996**, *2*, 215–221, doi: 10.1016/j.canlet.2008.03.018.
40. Schafer, Z.T.; Brugge, J.S. IL-6 involvement in epithelial cancers. *J Clin Invest* **2007,** *117*, 3660–3663, doi:10.1172/JCI34237.
41. Bendrik, C.; Dabrosin, C. Estradiol increases IL-8 secretion of normal human breast tissue and breast cancer in vivo. *J Immunol* **2009,** *182*, 371–378. doi:182/1/371 [pii].
42. Garvin, S.; Nilsson, U.W.; Dabrosin, C. Effects of oestradiol and tamoxifen on VEGF, soluble VEGFR-1, and VEGFR-2 in breast cancer and endothelial cells. *Br J Cancer* **2005**, *93*, 1005–1010, doi:10.1038/sj.bjc.6602824.
43. Nilsson, U.W.; Garvin, S.; Dabrosin, C.; MMP-2 and MMP-9 activity is regulated by estradiol and tamoxifen in cultured human breast cancer cells. *Breast Cancer Res Treat* **200**7, *102*, 253–261, doi:10.1007/s10549-006-9335-4.
44. Roomi, M.W.; Monterrey, J.C.; Kalinovsky, T.; Rath, M.; Niedzwiecki, A. Patterns of MMP-2 and MMP-9 expression in human cancer cell lines. *Oncol Rep* **2009**, *21*, 1323–1333, doi:10.3892/or_00000358.
45. Goldberg-Bittman, L.; Neumark, E.; Sagi-Assif, O.; Azenshtein, E.; Meshel, T.; Witz, I.P.; Ben-Baruch, A.; The expression of the chemokine receptor CXCR3 and its ligand, CXCL10, in human breast adenocarcinoma cell lines. *Immunol Lett* **2004**, *92*, 171–178, doi:10.1016/j.imlet.2003.10.020.
46. Cardona, S.M.; Garcia, J.A.; Cardona, A.E. The fine balance of chemokines during disease: trafficking, inflammation, and homeostasis. *Methods Mol Biol* **2013**, *1013*, 1-16, doi:10.1007/978-1-62703-426-5_1.
47. Colston, K.W.; Perks, C.M.; Xie, S.P.; Holly, J.M. Growth inhibition of both MCF-7 and Hs578T human breast cancer cell lines by vitamin D analogues is associated with increased expression of insulin-like growth factor binding protein-3. *J Mol Endocrinol* **1998**, *20*, 157–162, doi: 10.1677/jme.0.0200157.
48. Lorincz, A.M.; Sukumar, S. Molecular links between obesity and breast cancer. *Endocr Relat Cancer* **2006**, *13*, 279–292, doi:10.1677/erc.1.00729.
49. Dupont, J.; Le Roith, D. Insulin-like growth factor 1 and oestradiol promote cell proliferation of MCF-7 breast cancer cells: new insights into their synergistic effects. *Mol Pathol* **2001**, *54*, 149–54.
50. Figueroa, J.A.; Jackson, J.G.; McGuire, W.L.; Krywicki, R.F.; Yee, D. Expression of insulin-like growth factor binding proteins in human breast cancer correlates with estrogen receptor status. *J Cell Biochem* **1993**, *52*, 196–205, doi:10.1002/jcb.240520211.
51. Salahifar, H.; Baxter, R.C.; Martin, J.L. Insulin-like growth factor binding protein (IGFBP)-3 protease activity secreted by MCF-7 breast cancer cells: inhibition by IGFs does not require IGF-IGFBP interaction. *Endocrinology* **1997,** *138*, 1683–90, doi:10.1210/endo.138.4.5064.
52. Kawashima, I.; Ohsumi, J.; Mita-Honjo, K.; Shimoda-Takano, K.; Ishikawa, H.; Sakakibara, S.; Miyadai, K.; Takiguchi, Y. Molecular cloning of cDNS encoding adipogenisis inhibitory factor and identity with interleukin-11. *FEBS Lett* **1991**, *283*, 199–202, doi: 10.1016/0014-5793(91)80587-S.

53. Dubois, V.; Couissi, D.; Schonne, E.; Remacle, C.; Trouet, A. Intracellular levels and secretion of insulin-like-growth-factor-binding proteins in MCF-7/6, MCF-7/AZ and MDA-MB-231 breast cancer cells. Differential modulation by estrogens in serum-free medium. *Eur J Biochem* **1995**, *232*, 47–53, doi:10.1111/j.1432-1033.1995.tb20779.x.
54. Inadera, H.; Sekiya, T.; Yoshimura, T.; Matsushima, K. Molecular analysis of the inhibition of monocyte chemoattractant protein-1 gene expression by estrogen and xenoestrogens in MCF-7 cells. *Endocrinology* **2000**, *141*, 50–59, doi: 10.1210/endo.141.1.7233.
55. Kanda, N.; Watanabe, S. 17β-estradiol inhibits the production of RANTES in human keratinocytes. *J Invest Dermatol* **2003**,*120*, 420–427. doi:10.1046/j.1523-1747.2003.12067.x.
56. Chrzan, B.G.; Bradford, P.G. Phytoestrogens activate estrogen receptor beta1 and estrogenic responses in human breast and bone cancer cell lines. *Mol Nutr Food Res* **2007**, *51*, 171–177, doi:10.1002/mnfr.200600091.
57. Kayisli, U.A.; Mahutte, N.G.; Arici, A. Uterine chemokines in reproductive physiology and pathology. *Am J Reprod Immunol* **2002**, 47, 213–221, doi:10.1034/j.1600-0897.2002.01075.x.
58. Hull, K.L.; Harvey, S.; Growth Hormone and Reproduction: A Review of Endocrine and Autocrine/Paracrine Interactions. *Int J Endocrinol* **2014**, doi:10.1155/2014/234014.
59. Gibbs, J. Effective Blocking Procedures. ELISA Tech Bull (Corning Inc. Life Sci. Kennebunk) **2001**, ME 1–6.
60. Kishore, V.; Sangeetha Gowda, K.R.; Krishna, S.; Sharma, K.; Rashmi, M.; Nishita, K.P. Bovine Serum Albumin a Potential Thermostabilizer: a Study on α –Amylase. *J Appl Environ Microbiol* **2014**, *2.2*, 37–41, doi:10.12691/jaem-2-2-1.
61. Seo, H.S.; DeNardo, D.G.; Jacquot, Y.; Laïos, I.; Vidal, D.S.; Zambrana, C.R.; Leclercq, G.; Brown, P.H.; Stimulatory effect of genistein and apigenin on the growth of breast cancer cells correlates with their ability to activate ER alpha. *Breast Cancer Res Treat* **2006**, *99*, 121–134, doi:10.1007/s10549-006-9191-2.
62. Sonnenschein, C.; Soto, A.M.; Fernandez, M.F.; Olea, N.; Olea-Serrano, M.F.; Ruiz-Lopez, M.D. Development of a marker of estrogenic exposure in human serum. *Clin Chem* **1995**, *41*, 1888–1895.
63. Etique, N.; Chardard, D.; Chesnel, A.; Merlin, J.L.; Flament, S.; Grillier-Vuissoz, I. Ethanol stimulates proliferation, ERalpha and aromatase expression in MCF-7 human breast cancer cells. *Int J Mol Med* **2004**, *13*, 149–155.
64. Etique, N.; Grillier-Vuissoz, I.; Flament, S. Ethanol stimulates the secretion of matrix metalloproteinases 2 and 9 in MCF-7 human breast cancer cells. *Oncol Rep* **2006**, *15*, 603–608.
65. Fan, S.; Meng, Q.; Gao, B.; Grossman, J.; Yadegari, M.; Goldberg, I.D.; Rosen, E.M. Alcohol stimulates estrogen receptor signaling in human breast cancer cell lines. *Cancer Res* **2000**, *60*, 5635–5639.
66. Katzenellenbogen, B.S.; Kendra, K.L.; Norman, M.J.; Katzenellenbogen, B.S.; Rendra, K.L.; Norman, M.J.; Berthois, Y. Proliferation, Hormonal Responsiveness, and Estrogen Receptor Content of MCF-7 Human Breast Cancer Cells Grown in the Short-Term and Long-Term Absence of Estrogens Proliferation. *Cancer Res* **1987**, *47*, 4355–4360.
67. Maggiolini, M.; Bonofiglio, D.; Marsico, S.; Panno, M.L.; Cenni, B.; Picard, D.; Andò, S. Estrogen receptor alpha mediates the proliferative but not the cytotoxic dose-dependent effects of two major phytoestrogens on human breast cancer cells. *Mol Pharmacol* **2001**, *60*, 595–602.
68. Scott, S.M.; Brown, M.; Come, S.E. Emerging data on the efficacy and safety of fulvestrant, a unique antiestrogen therapy for advanced breast cancer. *Expert Opin Drug Saf* **2011**, *10*, 819–826, doi:10.1517/14740338.2011.595560.

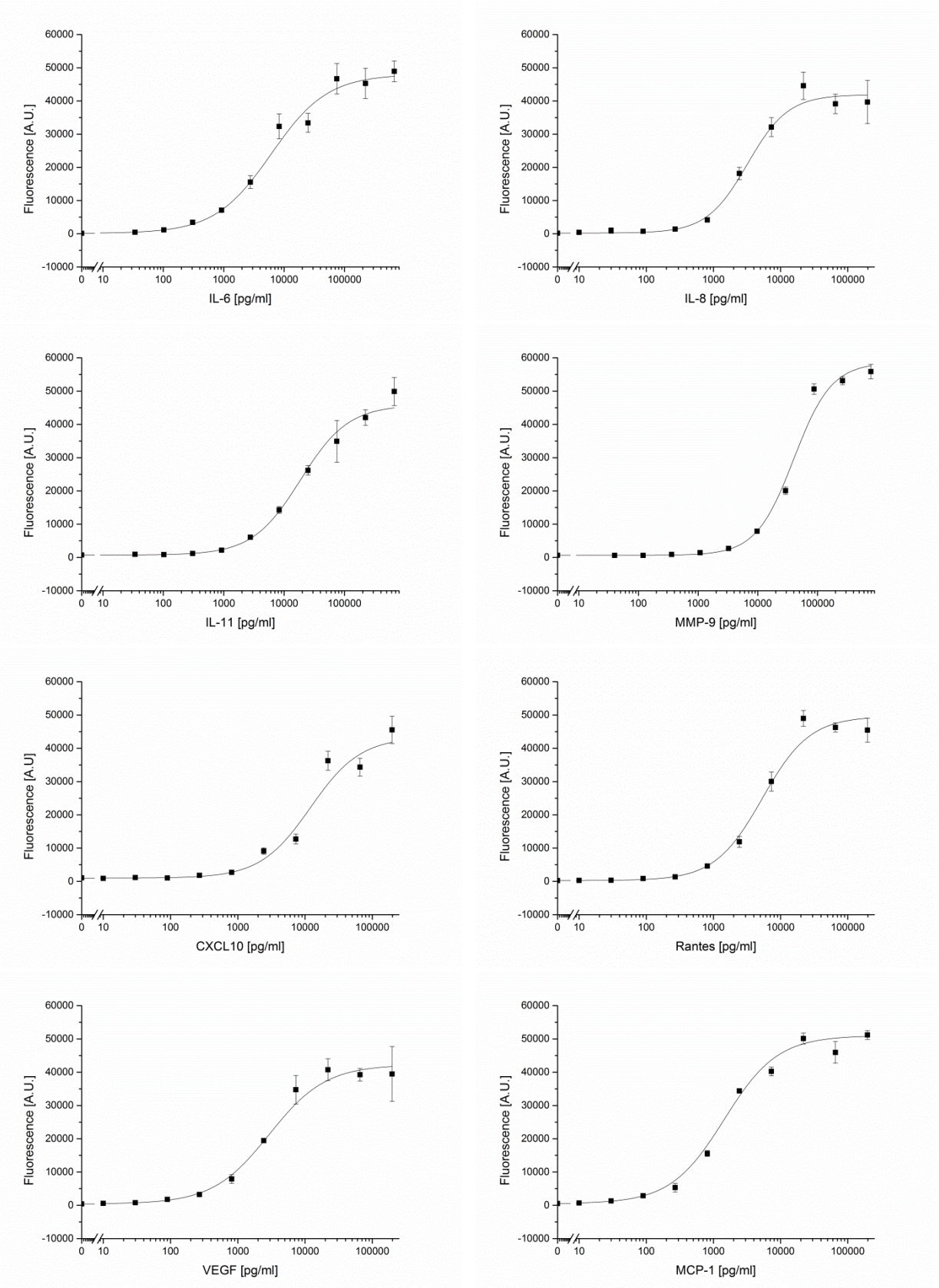

Sensors **2017**, 17, 1760; doi:10.3390/s17081760

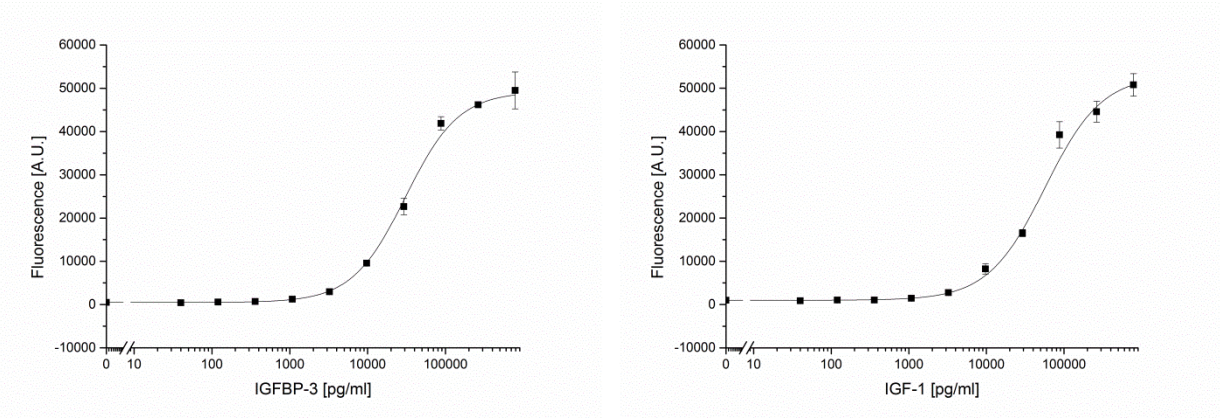

Figure S1. Standard curves of IL-6, IL-8, IL-11, MMP-9, CXCL10, Rantes, VEGF, MCP-1, IGFBP-3, and IGF-1 generated with 11 standards using serum free cell culture medium as matrix. Background-corrected mean signals were calculated from nine technical replicates and plotted as mean +/- SD. Curves were fitted using a four parametric model.

Table S1. Typical working ranges of standard ELISA kits for single biomarkers in microtiter plate format.

Biomarker	range comm. ELISA [pg/mL]	Supplier
MCP-1 (CCL2)	15.6 - 1000	eBioscience, San Diego, USA
IL-6	3.1 - 200	eBioscience, San Diego, USA
Rantes (CCL5)	31.2 - 2000	RnD Systems, Minneapolis, USA
VEGF	15.6. - 1000	RnD Systems, Minneapolis, USA
IL-8	31.2 - 2000	Biolegend, San Diego, USA
CXCL10 (IP-10)	15.6 - 1000	Biolegend, San Diego, USA
IL-11	15.6 - 1000	RnD Systems, Minneapolis, USA
IGFBP-3	800 - 50 000	RnD Systems, Minneapolis, USA
MMP-9	300 - 20 000	RnD Systems, Minneapolis, USA
IGF-1	100 - 6000	RnD Systems, Minneapolis, USA

Sensors **2017**, 17, 1760; doi:10.3390/s17081760

11. Table of abbreviations

EGFR	Epidermal growth factor receptor
Wnt3A	Protein Wnt-3a
c-Fos	Proto-oncogene c-Fos
IL-1β	Interleukin-1 β
IGF-1R	Insulin-like growth factor 1 receptor
IRS-1	Insulin receptor substrate-1
Akt	Protein kinase B
NF-κB	Nuclear factor kappa-light-chain-enhancer of activated B cells)
AP-1	Activator protein 1
ERK	Extracellular signal-regulated kinase
Ca	Calcium
ERRα	Estrogen related receptor alpha
GPER	G-protein-coupled estrogen receptor
PKA	Protein kinase A
CREB	cAMP response element-binding protein
HER	Human epidermal growth factor receptor
c-Src	Proto-oncogene tyrosine-protein kinase Src
TGF-β1	Transforming growth factor β
Smad	Smad signaling pathway
NO	Nitrogen oxide
Wnt	Wnt signaling pathway
DDT	Dichlorodiphenyltrichloroethane
DEHP	Bis(2-ethylhexyl) phthalate (di-2-ethylhexyl phthalate
DINP	Diisononyl phthalate
DIDP	Diisodecyl phthalate
BBP	*N*-butyl benzyl phthalate
PAH	Polycyclic aromatic hydrocarbon
PFC	Perfluorinated compound
PBDE	Polybrominated diphenyl ethers

12. Curriculum Vitae

Konstanze Gier (born: 09th September 1978, Berlin, Germany)

Education

2014–2018 **Doctorate study/Marie Curie ITN ESR-biotechnology**

Austrian Institute of Technology & University of

Natural Resources and Life Sciences, Vienna, Austria

2010–2013 **Master of Science-toxicology**; Charite, Germany

Thesis field: immunotoxicology at ZAUM/Helmholtz Institute Munich

2006–2010 **Bachelor of Science-biology**; Humboldt University of Berlin, Germany

Thesis field: molecular plant physiology at Humboldt University

Professional Experience:

2011-2012 in.vent Diagnostica GmbH, Heinersdorf, Germany/**student assistant**

2009–2010 Humboldt University of Berlin, Germany/**student assistant**

2015-2017 University of Groningen (RUG), Department of Pharmacy, Groningen,

The Netherlands/ **internship (microfluidics)**

2016 SCIENION AG, Berlin, Germany/ **internship (immobilization)**

Advanced Education

2011-2012 consultant toxicologist DGPT Immunotoxicology and reproductive toxicology

Peer reviewed Papers:

Gier, K. et al.,(2017). A Chip for Estrogen Receptor Action: Detection of Biomarkers Released by MCF-7 Cells through Estrogenic and Anti-Estrogenic Effects. *Sensors* 2017, *17*(8), 1760; doi:10.3390/s17081760

Eggert, E. et al.,(2016). A sucrose transporter-interacting protein disulphide isomerase affects redox homeostasis and links sucrose partitioning with abiotic stress tolerance. Plant Cell Environ. 39(6):1366-80.

Chincinska, I. et al.,(2013). Photoperiodic regulation of the sucrose transporter StSUT4 affects the expression of flowering genes and ethylene production. Front Plant Sci. 20; 4:26.

Krügel, U. et al.,(2011). The Potato Sucrose Transporter StSUT1 Interacts with a DRM-Associated Protein Disulfide Isomerase. Mol Plant. 5(1):43-62.